

Imaging of Coronary Atherosclerosis
with Computed Tomography
Coronary Angiography

Stella-Lida Papadopoulou

Financial support for the publication of this thesis was kindly provided by:
Department of Radiology, Erasmus MC, Rotterdam, The Netherlands
Cardialysis BV, Rotterdam

Layout and design: S.L. Papadopoulou
Cover (front): illustration based on Rotterdam Metro map
Cover (back): abstract image of 3D volume rendering of the heart
ISBN: 9789090299020

Printed by: UNIVERSITY STUDIO PRESS publications, Thessaloniki, Greece

Copyright © 2016 S.L. Papadopoulou
All rights reserved. No part of this thesis may be reproduced, stored in a retrieval system or transmitted in any form or by any means, without written permission of the author or, when appropriate, of the scientific journal in which parts of this thesis may have been published.

Imaging of Coronary Atherosclerosis with Computed Tomography Coronary Angiography

**Beeldvorming van coronaire atherosclerose
met Computed Tomography
coronaire angiografie**

Proefschrift

ter verkrijging van de graad van doctor aan de
Erasmus Universiteit Rotterdam
op gezag van de rector magnificus

Prof. dr. J. Verweij

en volgens besluit van het College voor Promoties.

De openbare verdediging zal plaatsvinden op
woensdag 26 oktober 2016 om 9:30 uur

door

Stella Lida Papadopoulou

geboren te Thessaloniki, Griekenland

PROMOTIECOMMISSIE

Promotoren: Prof.dr. F. Zijlstra
Prof.dr. G.P. Krestin

Overige leden: Prof.dr. M. Prokop
Prof.dr. W.J. Niessen
Dr. K. Nieman

Copromotor: Dr. H.M. Garcia-Garcia

To my family

You have to see the bigger picture.
And for that, you need sophisticated tools.

Table of contents

PART I: Preface

Chapter 1	General introduction and outline of the thesis	13
------------------	---	-----------

PART II: CT coronary angiography for the assessment of atherosclerotic plaque

Chapter 2	Detection and quantification of coronary atherosclerotic plaque by 64-slice multidetector CT: A systematic head-to-head comparison with intravascular ultrasound.	23
------------------	--	-----------

Atherosclerosis 2011; 219(1):163-170.

S.L. Papadopoulou, L.A. Neefjes, M. Schaap, H.L. Li, E. Capuano, A.G. van der Giessen, J.C. Schuurbijs, F.J. Gijsen, A.S. Dharampal, K. Nieman, R.J. van Geuns, N.R. Mollet, P.J. de Feyter

Chapter 3	Reproducibility of computed tomography angiography data analysis using semiautomatic plaque quantification software: implications for the design of longitudinal studies.	35
------------------	--	-----------

International Journal of Cardiovascular Imaging. 2013 Jun;29(5):1095-104.

S.L. Papadopoulou, H.M. Garcia-Garcia, A. Rossi, C. Girasis, A.S. Dharampal, P.H. Kitslaar, G.P. Krestin, P.J. de Feyter

Chapter 4	Natural History of Coronary Atherosclerosis by Multislice Computed Tomography: the PROSPECT study.	49
------------------	---	-----------

JACC Cardiovasc Imaging. 2012 Mar;5(3 Suppl):S28-37.

S.L. Papadopoulou, L.A. Neefjes, H.M. Garcia-Garcia, W-J Flu, A. Rossi, A.S. Dharampal, P.H. Kitslaar, N.R. Mollet, S. Veldhof, K. Nieman, G.W. Stone, P.W. Serruys, G.P. Krestin, P.J. de Feyter

Chapter 5	Quantitative CT coronary angiography: does it predict functionally significant coronary stenoses?	63
------------------	--	-----------

Circulation Cardiovascular Imaging 2014 Jan;7(1):43-51.

A. Rossi, **S.L. Papadopoulou**, F. Pugliese, B. Russo, A.S. Dharampal, A. Dedic, P.H. Kitslaar, A. Broersen, W.B. Meijboom, R.J. van Geuns, A. Wragg, J. Ligthart, C. Schultz, S.E. Petersen, K. Nieman, G.P. Krestin, P.J. de Feyter

PART III: CT coronary angiography for the assessment of coronary bifurcations

Chapter 6 Assessment of Atherosclerotic Plaques at Coronary Bifurcations with Multidetector Computed Tomography Angiography and Intravascular Ultrasound – Virtual Histology 77

European Heart Journal – Cardiovascular Imaging. 2012 Aug;13(8):635-42.
S.L. Papadopoulou, S. Brugaletta, H.M. Garcia-Garcia, A. Rossi, C. Girasis, A. S. Dharampal, L. A. Neefjes, J. Ligthart, K. Nieman, G.P. Krestin, P.W. Serruys, P. J. de Feyter

Chapter 7 A CT-based Medina classification in coronary bifurcations: does the lumen assessment provide sufficient information? 89

Catheterization and Cardiovascular Interventions. 2014 Sep 1;84(3):445-52.
S.L. Papadopoulou, C. Girasis, F.J. Gijzen, A. Rossi, J. Ottama, A. van der Giessen, J.C. Schuurbijs, H.M. Garcia-Garcia, P.J. de Feyter, J.J. Wentzel

PART IV: CT coronary angiography for risk stratification of coronary atherosclerotic disease

Chapter 8 The CT-SYNTAX Score: a feasibility and reproducibility study 103

JACC Cardiovascular Imaging. 2013 Mar;6(3):413-5.
S.L. Papadopoulou, C. Girasis, A.S. Dharampal, V. Farooq, Y. Onuma, A. Rossi, M-A Morel, G.P. Krestin, P.W. Serruys, P.J. de Feyter, H.M. Garcia-Garcia

Chapter 9 Diagnostic performance of computed tomography coronary angiography to detect and exclude left main and/or three-vessel coronary artery disease. 133

European Radiology. 2013 Nov;23(11):2934-43.
A.S. Dharampal, **S.L. Papadopoulou**, A. Rossi, W.B. Meijboom, A.C. Weustink, M. Dijkshoorn, K. Nieman, E.H. Boersma, P.J. de Feijter, G.P. Krestin

Chapter 10 CT Coronary Angiography Accuracy in Women and Men at Low to Intermediate Risk of Coronary Artery Disease 147

European Radiology. 2012 Nov;22(11):2415-23.

A.S. Dharampal, **S.L. Papadopoulou**, A. Rossi, A.C. Weustink, N.R.A. Mollet, W.B. Meijboom, L.A. Neefjes, K. Nieman, E. Boersma, P.J de Feijter, G.P. Krestin

Chapter 11 Is there a difference in the diagnostic accuracy of computed tomography coronary angiography between women and men? 159

Coronary Artery Disease. 22(6):421-7 (2011)

A.S. Dharampal, A. Rossi, **S.L. Papadopoulou**, A.C. Weustink, E. Boersma, K. Nieman, C-H Chen, M. Dijkshoorn, N.R. Mollet, G.P. Krestin, P.J. de Feyter

PART V: Summary and conclusions

Chapter 12 171

Summary and conclusions

Samenvatting en conclusies

General discussion and future directions

PhD Portfolio

List of publications

Acknowledgements

About the author

PART I

Preface

Chapter 1

General introduction and
outline of the thesis

General Introduction

Coronary atherosclerosis is a worldwide pandemic disease and accounts for almost 17 million deaths annually (1). Common systemic risk factors for atherosclerosis include high cholesterol levels, hypertension, smoking, obesity, diabetes mellitus and family history for coronary artery disease. Furthermore, in patients with an atherogenic profile, plaque does not develop evenly across the entire coronary tree, but shows a predilection for sites where the laminar blood flow gets disturbed, such as the vicinity of coronary artery bifurcations (2).

The detection and accurate quantification of coronary plaque may potentially improve individualized risk stratification and allow the monitoring of patient's response to pharmacological treatment. Although quantitative coronary angiography (QCA) has been used in the past to study the extent and progression of the disease (3), this technique can only depict the contrast-enhanced lumen, whereas atherosclerotic disease of the arterial wall does not necessarily result in narrowing of the vessel lumen. Currently, the preferred method to study atherosclerosis is by intracoronary, cross-sectional imaging methods, such as intravascular ultrasound (IVUS) (4). However, both QCA and IVUS are expensive, invasive and involve certain, albeit minimal risks, thus they are unsuitable for preventive plaque detection in asymptomatic individuals or routine serial assessment of atherosclerosis.

Computed tomography coronary angiography (CTCA) has rapidly emerged as a noninvasive imaging modality for visualisation of the coronary arteries. Following the advances in multidetector CT technology and the improvement of spatial and temporal resolution with the introduction of 64-slice CT scanners, numerous studies have confirmed the ability of the technique to reliably detect and exclude significant coronary disease against invasive angiography (5-7). Similarly to IVUS, CTCA goes beyond lumenography and enables the assessment of atherosclerotic plaque burden, remodeling, eccentricity, and calcified and noncalcified plaque in both stable and unstable patients (8-10).

It is envisioned that the ability of CTCA to provide information not currently available from invasive angiography (i.e. plaque burden and calcium score) may change the way patients with atherosclerotic cardiovascular disease are stratified and managed (11). IVUS studies (12) have demonstrated that there is a direct association between the burden of coronary atherosclerosis, its progression and the presence of clinical events at follow-up. The use of CTCA to non-invasively quantify and monitor atherosclerotic plaque could contribute to the potential development of prediction models based on atherosclerotic plaque burden.

Moreover, the complex three-dimensional (3D) geometry of coronary artery bifurcations can be better visualized by means of CTCA which can provide a 3D reconstruction of the bifurcation, without the limitations of vessel foreshortening and overlap that exist in conventional angiography. Percutaneous treatment of coronary bifurcation lesions has been associated with worse acute and late outcomes due to higher restenosis and stent thrombosis rates (13-15). Comprehensive pre-interventional assessment of atherosclerosis at coronary bifurcation sites may be important to better plan a percutaneous treatment strategy.

Similar to any other imaging modality, CTCA has certain inherent limitations. Extensive coronary calcifications create blooming artifacts and still hamper the accurate evaluation of coronary vessels. Insufficient spatial resolution does not yet allow for precise detection of very small plaques and discrimination of the atherosclerotic plaque components. Presence of arrhythmias remains a contraindication for CTCA. The radiation exposure during CTCA is still an issue, although current scan protocols can considerably decrease the radiation dose. Anatomical information derived by CTCA can not accurately predict the hemodynamic significance of coronary lesions; however there is extensive research ongoing towards the direction of non-invasive functional assessment.

Outline of the thesis

In Part 2, the potential of CTCA to assess coronary atherosclerotic disease is discussed. The ability of 64-slice CTCA to detect and quantify coronary atherosclerotic plaque using intravascular ultrasound as a reference standard is evaluated (Chapter 2). The reproducibility of CTCA data analysis using semiautomatic plaque quantification software is investigated and the implications for the design of longitudinal studies are discussed (Chapter 3). The natural history of coronary atherosclerosis in patients receiving contemporary medical treatment was studied by CTCA and the serial changes in coronary plaque burden, lumen dimensions and arterial remodeling were assessed (Chapter 4). Also, the potential of CTCA derived cross-sectional parameters to predict functional significance of lesions as indicated by fractional flow reserve was examined (Chapter 5).

Two manuscripts are provided in Part 3 which describe the ability of CTCA to comprehensively assess coronary bifurcations. Using CTCA and intravascular ultrasound-virtual histology, the distribution and composition of atherosclerotic plaques at bifurcations in relation to the bifurcation angle were evaluated (Chapter 6). In the following chapter, a novel CT-Medina classification for bifurcation lesions combining lumen narrowing and plaque distribution is proposed (Chapter 7).

In Part 4, the use of CT coronary angiography for risk stratification of coronary atherosclerotic disease is discussed. The feasibility and reproducibility of a CTCA derived SYNTAX Score compared to the widely used conventional angiography SYNTAX Score was investigated (Chapter 8). The diagnostic performance of CTCA to detect high risk (3-vessel and/or left main) coronary artery disease was evaluated (Chapter 9). The CTCA accuracy was further studied in women and men at low to intermediate risk of coronary artery disease (Chapter 10). Finally, the influence of gender on the diagnostic accuracy of CTCA was investigated (Chapter 11).

References

1. Smith SC, Jr., Jackson R, Pearson TA, et al. Principles for national and regional guidelines on cardiovascular disease prevention: a scientific statement from the World Heart and Stroke Forum. *Circulation* 2004;109:3112-21.
2. Malek AM, Alper SL, Izumo S. Hemodynamic shear stress and its role in atherosclerosis. *JAMA* 1999;282:2035-42.
3. de Feyter PJ, Serruys PW, Davies MJ, Richardson P, Lubsen J, Oliver MF. Quantitative coronary angiography to measure progression and regression of coronary atherosclerosis. Value, limitations, and implications for clinical trials. *Circulation* 1991;84:412-23.
4. Mintz GS, Garcia-Garcia HM, Nicholls SJ, et al. Clinical expert consensus document on standards for acquisition, measurement and reporting of intravascular ultrasound regression/progression studies. *EuroIntervention* 2011;6:1123-30, 9.
5. Meijboom WB, Meijs MF, Schuijf JD, et al. Diagnostic accuracy of 64-slice computed tomography coronary angiography: a prospective, multicenter, multivendor study. *J Am Coll Cardiol* 2008;52:2135-44.
6. Miller JM, Rochitte CE, Dewey M, et al. Diagnostic performance of coronary angiography by 64-row CT. *N Engl J Med* 2008;359:2324-36.
7. Weustink AC, Mollet NR, Neefjes LA, et al. Diagnostic accuracy and clinical utility of noninvasive testing for coronary artery disease. *Ann Intern Med* 2010;152:630-9.
8. Hoffmann U, Moselewski F, Nieman K, et al. Noninvasive assessment of plaque morphology and composition in culprit and stable lesions in acute coronary syndrome and stable lesions in stable angina by multidetector computed tomography. *J Am Coll Cardiol* 2006;47:1655-62.
9. Otsuka M, Bruining N, Van Pelt NC, et al. Quantification of coronary plaque by 64-slice computed tomography: a comparison with quantitative intracoronary ultrasound. *Invest Radiol* 2008;43:314-21.
10. Voros S, Rinehart S, Qian Z, et al. Prospective Validation of Standardized, 3-Dimensional, Quantitative Coronary Computed Tomographic Plaque Measurements Using Radiofrequency Backscatter Intravascular Ultrasound as Reference Standard in Intermediate Coronary Arterial Lesions Results From the ATLANTA (Assessment of Tissue Characteristics, Lesion Morphology, and Hemodynamics by Angiography With Fractional Flow Reserve, Intravascular Ultrasound and Virtual Histology, and Noninvasive Computed Tomography in Atherosclerotic Plaques) I Study. *JACC Cardiovasc Interv* 2011;4:198-208.
11. Mark DB, Berman DS, Budoff MJ, et al. ACCF/ACR/AHA/NASCI/SAIP/SCAI/SCCT 2010 expert consensus document on coronary computed tomographic angiography: a report of the American College of Cardiology Foundation Task Force on Expert Consensus Documents. *J Am Coll Cardiol* 2010;55:2663-99.
12. Nicholls SJ, Hsu A, Wolski K, et al. Intravascular ultrasound-derived measures of coronary atherosclerotic plaque burden and clinical outcome. *J Am Coll Cardiol* 2010;55:2399-407.
13. Colombo A, Moses JW, Morice MC, et al. Randomized study to evaluate sirolimus-eluting stents implanted at coronary bifurcation lesions. *Circulation* 2004;109:1244-9.

14. Ge L, Airoidi F, Iakovou I, et al. Clinical and angiographic outcome after implantation of drug-eluting stents in bifurcation lesions with the crush stent technique: importance of final kissing balloon post-dilation. *J Am Coll Cardiol* 2005;46:613-20.
15. Routledge HC, Lefevre T, Colombo A, et al. Three-year clinical outcome of percutaneous treatment of bifurcation lesions in multivessel coronary artery disease with the sirolimus-eluting stent: insights from the Arterial Revascularisation Therapies Study, part II (ARTS II). *EuroIntervention* 2009;5:190-6.

PART II

CT coronary angiography
for the assessment of
atherosclerotic plaque

Chapter 2

Detection and quantification of coronary atherosclerotic plaque by 64-slice multidetector CT: A systematic head-to-head comparison with intravascular ultrasound.

Atherosclerosis 2011; 219(1):163-170.

S.L. Papadopoulou, L.A. Neefjes, M. Schaap, H.L. Li, E. Capuano, A.G. van der Giessen, J.C. Schuurbijs, F.J. Gijsen, A.S. Dharampal, K. Nieman, R.J. van Geuns, N.R. Mollet, P.J. de Feyter

Detection and quantification of coronary atherosclerotic plaque by 64-slice multidetector CT: A systematic head-to-head comparison with intravascular ultrasound

Stella-Lida Papadopoulou^{a,b,*}, Lisan A. Neefjes^{a,b}, Michiel Schaap^c, Hui-Ling Li^{a,b,1}, Ermanno Capuano^b, Alina G. van der Giessen^d, Johan C.H. Schuurbijs^d, Frank J.H. Gijzen^d, Anoeska S. Dharampal^{a,b}, Koen Nieman^{a,b}, Robert Jan van Geuns^{a,b}, Nico R. Mollet^{a,b}, Pim J. de Feyter^{a,b}

^a Department of Cardiology, Erasmus University Medical Center, PO Box 2040, 3000 CA, Rotterdam, The Netherlands

^b Department of Radiology, Erasmus University Medical Center, PO Box 2040, 3000 CA, Rotterdam, The Netherlands

^c Biomedical Imaging Group, Departments of Radiology and Medical Informatics, Erasmus University Medical Center, PO Box 2040, 3000 CA, Rotterdam, The Netherlands

^d Biomedical Engineering, Department of Cardiology, Erasmus University Medical Center, PO Box 2040, 3000 CA, Rotterdam, The Netherlands

ARTICLE INFO

Article history:

Received 4 April 2011

Received in revised form 8 June 2011

Accepted 2 July 2011

Available online 14 July 2011

Keywords:

Non-invasive imaging

Computed tomography

Intravascular ultrasound

Atherosclerotic plaque

ABSTRACT

Objective: We evaluated the ability of 64-slice multidetector computed tomography (MDCT)-derived plaque parameters to detect and quantify coronary atherosclerosis, using intravascular ultrasound (IVUS) as the reference standard.

Methods: In 32 patients, IVUS and 64-MDCT was performed. The MDCT and IVUS datasets of 44 coronary arteries were co-registered using a newly developed fusion technique and quantitative parameters were derived from both imaging modalities. The threshold of >0.5 mm of maximum wall thickness was used to establish plaque presence on MDCT and IVUS.

Results: We analyzed 1364 coregistered 1-mm coronary cross-sections and 255 segments of 5-mm length. Compared with IVUS, 64-MDCT enabled correct detection in 957 of 1109 cross-sections containing plaque (sensitivity 86%). In 180 of 255 cross-sections atherosclerosis was correctly excluded (specificity 71%). On the segmental level, MDCT detected 213 of 220 segments with any atherosclerotic plaque (sensitivity 96%), whereas the presence of any plaque was correctly ruled out in 28 of 32 segments (specificity 88%). Interobserver agreement for the detection of atherosclerotic cross-sections was moderate (Cohen's kappa coefficient $K=0.51$), but excellent for the atherosclerotic segments ($K=1.0$). Pearson's correlation coefficient for vessel plaque volumes measured by MDCT and IVUS was $r=0.91$ ($p<0.001$). Bland-Altman analysis showed a slight non-significant underestimation of any plaque volume by MDCT ($p=0.5$), with a trend to underestimate noncalcified and overestimate mixed/calcified plaque volumes ($p=0.22$ and $p=0.87$ respectively).

Conclusion: MDCT is able to detect and quantify atherosclerotic plaque. Further improvement in CT resolution is necessary for more reliable assessment of very small and distal coronary plaques.

© 2011 Elsevier Ireland Ltd. All rights reserved.

1. Introduction

The detection and accurate quantification of coronary plaque may potentially improve individualized risk stratification and allow the monitoring of patient's response to pharmacological treatment. Currently, intravascular ultrasound (IVUS) is considered the

reference method to quantify coronary atherosclerosis [1]. However, the method is expensive, invasive and involves certain, albeit minimal risks, which makes it unsuitable for preventive plaque detection in asymptomatic individuals or routine serial assessment of atherosclerosis. Consequently, the ideal alternative to IVUS would be a non-invasive method of coronary imaging that enables accurate assessment of atherosclerotic plaque. Multidetector computed tomography (MDCT) has rapidly emerged as a noninvasive imaging modality for visualisation of the coronary arteries. Following the advances in MDCT technology and the improvement of spatial and temporal resolution with the introduction of 64-slice MDCT scanners, numerous studies have confirmed the ability of the technique to reliably detect and exclude significant coronary disease against invasive angiography [2–7]. The accuracy of detec-

* Corresponding author at: Erasmus Medical Center, Departments of Radiology and Cardiology, Room Ca 207, 's-Gravendijkwal 230, 3015 CE Rotterdam, The Netherlands. Tel.: +31 623726545; fax: +31 107035482.

E-mail address: elpa98@gmail.com (S.-L. Papadopoulou).

¹ Present address: Division of Cardiology, Department of Medicine, Showa University School of Medicine, 1-5-8 Hatanodai, Shinagawa-ku, Tokyo 142-8666, Japan.

tion and quantification of coronary plaque using MDCT compared to IVUS has been less extensively investigated and has been based mainly on qualitative visual plaque detection on MDCT. The aim of this study was to evaluate the ability of 64-slice CT to detect and quantify coronary atherosclerosis compared to IVUS, using similar quantitative parameters on MDCT and IVUS. For this systematic approach we applied a fusion technique recently developed in our institution [8], which allows us to co-register IVUS and MDCT images such that cross-sectional images can be compared head-to-head.

2. Materials and methods

2.1. Patients

Our study comprised patients who were treated in our institution for acute coronary syndromes between May 2005 and January 2006. Acute coronary syndrome (ACS) was defined as ST segment elevation myocardial infarction, non-ST-segment elevation myocardial infarction (troponin positive) or unstable angina (troponin negative). Immediately after initial management of the culprit lesions, these patients were asked to participate in the MDCT study. They were considered for inclusion only if an IVUS pullback was performed in one or more of their coronary arteries other than the treated vessel, if they had a heart rate lower than 70 bpm during the MDCT acquisition and had no prior coronary bypass surgery. Exclusion criteria included renal dysfunction (serum creatinine >120 mmol/L), contrast allergy and irregular heart rhythm. The institutional review board of our hospital approved the study, and all patients provided written informed consent before study participation.

2.2. MDCT acquisition

All patients underwent CT coronary angiography with a 64-slice scanner (Sensation 64, Siemens, Forchheim, Germany), according to a previously published protocol [4]. Because patients having an ACS were already treated with intravenous nitrates and β -blockers, additional medication prior to CT scan was not necessary. Scan parameters were: gantry rotation time of 0.33 s; 32×2 slices per rotation; 0.6 mm detector collimation; table feed of 3.8 mm per rotation; tube voltage of 120 kV; and tube current of 900 mAs. Prospective X-ray tube modulation was not applied. A bolus of 100 mL of contrast material (400 mgI/mL; Iomeron, Bracco, Milan, Italy) was injected intravenously at flow rate of 5 mL/s. The initiation of the scan was synchronized to the arrival of contrast in the coronary arteries by a bolus-tracking technique (threshold of 100 Hounsfield units). The estimated mean effective radiation dose was 17.0 ± 1.1 mSv, using the dose-length product and the conversion factor k (0.017 mSv/mGy/cm). Axial CT images were reconstructed with a slice thickness of 0.75 mm and 0.4 mm increments using a retrospectively ECG gating algorithm to obtain optimal, motion-free image quality, resulting in a temporal resolution of approximately 165 ms and a spatial resolution of 0.4 mm. Optimal data sets with the best image quality were reconstructed mainly in the mid- to end-diastolic phase, using a medium-smooth convolution kernel, and were uploaded to an MDCT Picture Archiving and Communication System.

2.3. IVUS acquisition

The IVUS was performed using standard methodology. One or more of the coronary arteries of these patients were imaged by IVUS with commercially available catheter (40 MHz, Atlantis SR Pro, Boston Scientific, Boston, Massachusetts). After the intracoronary administration of 100–200 μ g of nitroglycerine, IVUS

images were acquired using automatic mechanical pullback devices operating at a continuous pullback speed of 0.5 mm/s [1]. Data were stored on DVD, transformed into the Digital Imaging and Communication in Medicine image standard, and archived for offline analysis with retrospective image-based gating [9] (axial spacing of gated IVUS images approximately 0.5 mm).

2.4. MDCT and IVUS co-registration

Datasets were transferred to an offline workstation for further analysis using an in-house developed tool, based on MeVisLab software (MeVisLab, Mevis, Bremen, Germany, <http://www.mevislab.de>). The registration procedure was performed by an independent investigator not involved in the later comparative analysis, and has been previously described in detail [8]. Briefly, the process was performed as follows: for each vessel of interest, the stack of ECG-gated IVUS images (axial distance of approximately 0.5 mm) was examined to identify bifurcations, which were used as landmarks. In order to register the MDCT to the IVUS images, a vessel centreline was manually drawn in the MDCT dataset starting from the ostium. Cross-sectional images, perpendicular to the centreline, were equidistantly generated at every 0.2 mm. The corresponding IVUS-derived landmarks were identified on this MDCT image set. After manual registration of the side branches, cross-sectional MDCT images perpendicular to the centreline were generated again, but now such that the number of MDCT images between the landmarks was equal to the number of IVUS images between the landmarks. For each IVUS image the position and rotation of the corresponding MDCT image between the manually registered side branches was determined by linear interpolation. Therefore, only vessels with at least two bifurcations identifiable on both imaging modalities were co-registered. The goal of the registration process was to reconstruct cross-sectional MDCT images of the coronary artery at the same axial position where the IVUS images were obtained, enabling a head-to-head comparison between these images.

2.5. MDCT image analysis

For each vessel, the co-registered region of interest (ROI) was considered for plaque analysis. Both the inner lumen and the outer vessel boundaries were identified and manually annotated following a stepwise approach. Multiplanar reformatted images were generated and the lumen and vessel borders were traced longitudinally on at least 3 different vessel views; the intersections between these longitudinal contours and cross-sectional images at 1 mm intervals were calculated in order to create cross-sectional contours, which were examined and, if necessary, adjusted by an experienced observer. The settings for window level and width were previously optimized by an independent investigator and fixed at 740 HU and 220 HU respectively [10] (Rengo M., et al. Optimization of window-level settings in CT coronary angiography for the quantification of coronary lumen and plaque; submitted for publication). The annotation of lumen and the vessel wall boundaries was also facilitated by gradient magnitude images, which are derived from the MDCT images (Fig. 1A and B). They represent the magnitude of the image intensity gradient vector; the amount of local change in image intensity. The transition from high intensity lumen to the low intensity epicardial tissue is depicted in these images as a bright ridge. The plaque area was calculated by subtracting lumen area from vessel area. Plaques in which $\geq 50\%$ of the plaque area was occupied by calcified tissue (in the respective cross-section) were classified as calcified, plaques with calcified tissue occupying $< 50\%$ as mixed and plaques without any calcium as non-calcified. Typical example of non-calcified plaque visu-

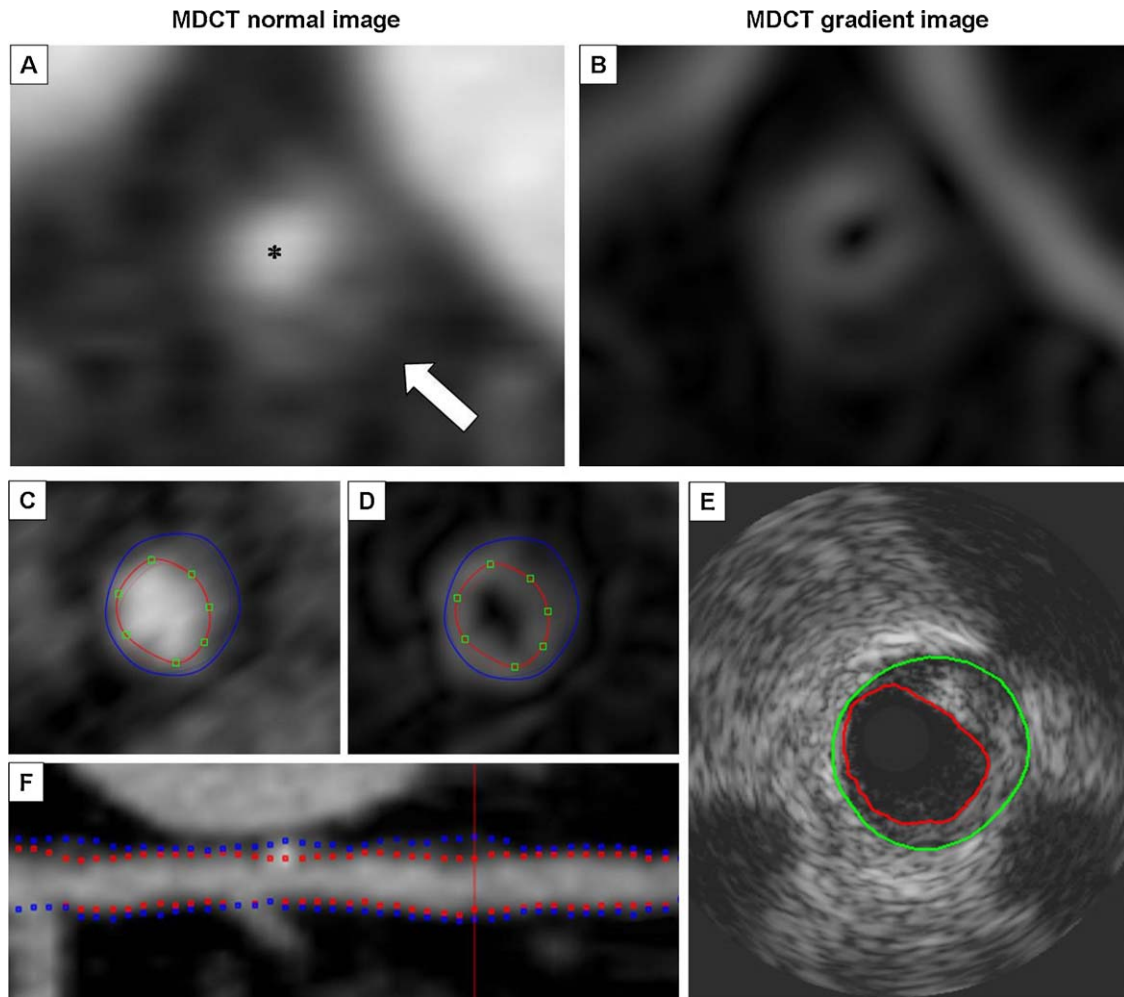


Fig. 1. Example of generated cross-sectional MDCT images (1 mm interval). Panel (A): in the normal MDCT image, the vessel lumen is brightly enhanced (asterisk), and a non-calcified, eccentric plaque is visible (arrow). Panel (B): in the gradient MDCT image, the bigger change in image intensity is depicted brighter, which facilitates the discrimination of borders between tissues with different intensities. Panels (C and D): analyzed normal and gradient image respectively; panel (E): corresponding IVUS cross-section; panel (F): longitudinal vessel view.

alised by MDCT and IVUS is shown in Fig. 1(C–F). The threshold of >0.5 mm plaque thickness on MDCT was used to consider plaque present, similarly to IVUS. Plaque area and % plaque burden (plaque area/vessel area) measured by MDCT were also examined as potential quantitative parameters to detect plaque. A second investigator also blinded to the IVUS results, performed the same analysis independently on 22 randomly selected ROIs.

2.6. IVUS image analysis

IVUS analysis was performed off-line by an experienced cardiologist, blinded to the MDCT scans. Lumen and external elastic membrane (EEM) contours were manually traced to determine lumen area and vessel area using dedicated software (QCU-CMS, version 4.5, Leiden, the Netherlands). The measurements were performed according to the American College of Cardiology recommendations [1] and atherosclerotic plaques were defined as structures located between the media and the intima with a thickness of at least 0.5 mm.

2.7. Comparison between IVUS and 64-MDCT

The MDCT and IVUS annotated contours on the co-registered ROIs were compared at corresponding positions. The software determined the lumen area, vessel area and maximum wall thick-

ness for the annotated MDCT contours at 1 mm increments and for the corresponding IVUS contours, which were obtained by interpolating the IVUS contours with cubic B-spline interpolation, at the position derived from the registration. Plaque volumes on MDCT and IVUS were calculated for the entire ROI by adding plaque volumes of all respective cross-sections, according to Simpson's rule. The co-registered ROIs were further divided into 5-mm segments for the purpose of evaluating diagnostic accuracy of MDCT to detect plaque on a segmental level, apart from the cross-sectional level.

2.8. Statistical analysis

Continuous variables were presented as means \pm standard deviation, unless otherwise indicated, and categorical variables were reported as frequencies. Differences in baseline characteristics between patients included in the study and patients excluded were evaluated using chi-square test, Fisher's exact test, and unpaired Student's *t*-test, as appropriate. To take into account the potential correlation between the multiple cross-sections and segments derived from the same patient, generalized estimation equation (GEE) with binary logistic regression was applied to obtain patient-clustered values, adjusted for distance from the ostium and type of vessel (RCA, LAD or LCX). Adjusted sensitivity, specificity, positive predictive value (PPV) and negative predictive value (NPV) of MDCT to detect plaque were calculated and the 95% confidence

Table 1
Patient characteristics.

	Included	Excluded	<i>p</i> -Value
Patients	<i>n</i> = 32	<i>n</i> = 14	
Age (mean ± SD), years	54 ± 10	53 ± 11	0.613
Male gender, <i>n</i> (%)	25 (78)	12 (86)	0.701
Risk factors			
Hypertension, <i>n</i> (%)	10 (31)	4 (29)	1.000
Hypercholesterolemia, <i>n</i> (%)	8 (25)	6 (43)	0.301
Diabetes mellitus, <i>n</i> (%)	2 (6)	1 (7)	1.000
Current smoking, <i>n</i> (%)	17 (53)	5 (36)	0.346
Family history of CAD, <i>n</i> (%)	17 (53)	5 (36)	0.346
Obesity, <i>n</i> (%)	5 (16)	3 (21)	0.684
Clinical condition at enrolment			
Unstable angina, <i>n</i> (%)	8 (25)	5 (36)	0.493
Acute myocardial infarction, <i>n</i> (%)	24 (75)	9 (64)	0.493

SD, standard deviation; CAD, coronary artery disease.

intervals were determined in addition to the crude (non-GEE based) analyses. Cohen's kappa was calculated to determine interobserver agreement. Receiver operating characteristics (ROC) curve analysis was performed in order to evaluate the ability of quantitative characteristics measured by MDCT to detect plaque, and the area under the curve (AUC) was calculated. Comparison between plaque volumes was performed using paired Student's *t*-test. Correlation and agreement between MDCT and IVUS measurements were evaluated by Pearson's correlation coefficient and Bland–Altman analysis respectively. The 95% limits of agreement were defined as the range of values between ±2 standard deviations from the mean difference. A two-tailed *p*-value <0.05 was considered statistically significant. The statistical package SPSS 17.0 was used for the analysis.

3. Results

Forty-seven vessels from 32 patients (mean age: 54 ± 10 years) with MDCT and IVUS of good image quality were successfully co-registered. From the total study population, 14 patients were not included in this analysis (4 did not have IVUS imaging, 2 had low quality IVUS imaging, 4 had low quality MDCT imaging and 4 could not be co-registered with the fusion technique due to technical problems, i.e. too few landmarks for matching). The mean time interval between IVUS and MDCT acquisitions was 4.8 ± 6.0 days. The baseline characteristics of all patients are presented in Table 1. Three vessels were excluded from further analysis because the ROI was occupied by long stents, thus 44 vessels were available for final head-to-head comparison [right coronary artery (RCA), *n* = 10; left anterior descending artery (LAD), *n* = 22; left circumflex artery (LCX), *n* = 12]. The mean length of the investigated ROIs was 31 ± 14 mm and comprised a total of 1364 registered 1-mm cross-sections and 255 segments of 5-mm length.

Table 2
Diagnostic accuracy of 64-slice MDCT to detect coronary plaque on cross-sectional and segmental level.

	Sensitivity	Specificity	PPV	NPV
Crude analysis				
Cross-sections (<i>n</i> = 1364)	86.2 (84.0–88.2)	70.6 (64.5–76.0)	92.7 (90.9–94.2)	54.1 (48.5–59.5)
5-mm segments (<i>n</i> = 255)	95.5 (91.7–97.7)	87.5 (70.1–96)	98.2 (95.0–99.4)	73.7 (56.6–86.0)
Adjusted analysis ^a				
Cross-sections (<i>n</i> = 1364)	86.3 (85.8–86.8)	70.6 (69.8–71.4)	92.7 (92.5–92.9)	54.2 (52.5–55.9)
5-mm segments (<i>n</i> = 255)	95.5 (94.8–96.3)	87.5 (84.5–90.5)	98.2 (97.6–98.7)	73.7 (67.3–80.1)

Values are presented as % (95% confidence interval). MDCT, multidetector computed tomography; PPV, positive predictive value; NPV, negative predictive value.

^a Patient-clustered and adjusted for distance from the ostium and vessel type.

3.1. Diagnostic performance on cross-sectional level

Presence of atherosclerotic plaque was confirmed by IVUS in 1109 out of the 1364 cross-sections (81.3%). Using the cut-off of >0.5 mm wall thickness, the 64-slice CT enabled a correct detection of any plaque in 957 of 1109 cross-sections, resulting in a sensitivity of 86%. Of these detected plaques, 755 were characterized as non-calcified (79%), 115 as mixed (12%) and 83 (1%) as calcified by MDCT. In 180 of 255 cross-sections, the presence of atherosclerotic lesions was correctly ruled out (specificity 71%). The 75 normal cross-sections misclassified by MDCT as diseased, were all incorrectly considered as containing non-calcified plaque. Both the crude and the adjusted analysis values for diagnostic performance are presented in Table 2. Coronary plaques that were missed on MDCT had smaller maximum plaque thickness (0.8 mm ± 0.2 vs. 1.1 mm ± 0.4, *p* < 0.001) and plaque area (5.1 mm² ± 1.9 vs. 7.0 mm² ± 2.6, *p* < 0.001) by IVUS, compared to the detected plaques (Table 3). The sensitivity of MDCT to detect plaque increased with plaque size (Fig. 2A), while it decreased with the distance from the coronary ostium (Fig. 2B), dropping below 80% for plaques located at 50 mm or more from the ostium. Logistic regression analysis confirmed that the distance from the ostium had a significant influence on sensitivity (odds ratio 1.38, 95% CI 1.09–1.76, for every 10 mm from the ostium). Moreover, the type of vessel had effect on the NPV (odds ratio 2.37, 95% CI 1.04–5.39). Cohen's kappa coefficient for the detection of atherosclerotic cross-sections using MDCT-derived wall thickness was 0.51, indicating moderate interobserver agreement.

3.2. Cut-off values of MDCT-derived quantitative parameters for plaque detection

ROC curve analysis for MDCT maximal wall thickness, plaque area and plaque burden is shown in Fig. 3. The MDCT maximal wall thickness presented non-significantly better discriminatory ability for plaque detection (AUC 0.876) than plaque area (AUC 0.847) and plaque burden (AUC 0.834). If MDCT plaque area and plaque burden were to be used as quantitative characteristics to detect plaque, the cut-off values of 3.8 mm² and 35% respectively would provide a sensitivity exceeding 80% with corresponding specificity values of 75% and 68%.

3.3. Diagnostic performance on segmental level

The analysis on a segmental basis revealed that MDCT correctly detected 213 of 220 segments with any atherosclerotic plaque (sensitivity 96%), whereas the presence of any plaque was correctly ruled out in 28 of 32 segments (specificity 88%). The majority of the segments with plaque detected by MDCT contained non-calcified plaque (154 out of 213, 72%). Mixed plaque was present in 44 segments (21%) and calcified plaque in 15 segments (7%). Four non-diseased segments were incorrectly characterized as containing non-calcified plaque. The crude and the adjusted analysis values for diagnostic performance are shown in Table 2. Mean plaque

Table 3
IVUS quantitative characteristics of MDCT detected vs. not detected coronary plaques.

	Detected (true positives)	Not detected (false negatives)	p-Value
Cross-sections 1 mm thickness			
n	957	152	
Maximum plaque thickness (mm)	1.1 ± 0.4	0.8 ± 0.2	<0.001
Plaque area (mm ²)	7.0 ± 2.6	5.1 ± 1.9	<0.001
% plaque burden	47 ± 12	40 ± 11	<0.001
Vessel area (mm ²)	15.1 ± 5.0	13.3 ± 5.2	<0.001
Distance from the ostium (mm)	36 ± 13	44 ± 13	<0.001
5-mm segments			
n	213	10	
Mean plaque area (mm ²)	6.7 ± 2.6	4.1 ± 1.5	0.002
Mean plaque volume (mm ³)	34 ± 13	21 ± 7	0.002
Mean % plaque burden	45 ± 12	37 ± 10	0.03

IVUS, intravascular ultrasound; MDCT, multidetector computed tomography. Quantitative parameters are presented as means ± standard deviation.

area measured by IVUS in the 10 segments with a false-negative MDCT result was $4.1 \pm 1.5 \text{ mm}^2$ versus $6.7 \pm 2.6 \text{ mm}^2$ ($p = 0.002$) for the 213 segments with a true-positive MDCT result (Table 3). The interobserver agreement for the detection of atherosclerotic segments using MDCT-derived wall thickness was excellent (Cohen's kappa = 1.0).

3.4. Plaque volume comparison between MDCT and IVUS

Pearson's correlation coefficient for regional plaque volumes measured by MDCT and IVUS was very good ($r = 0.91$,

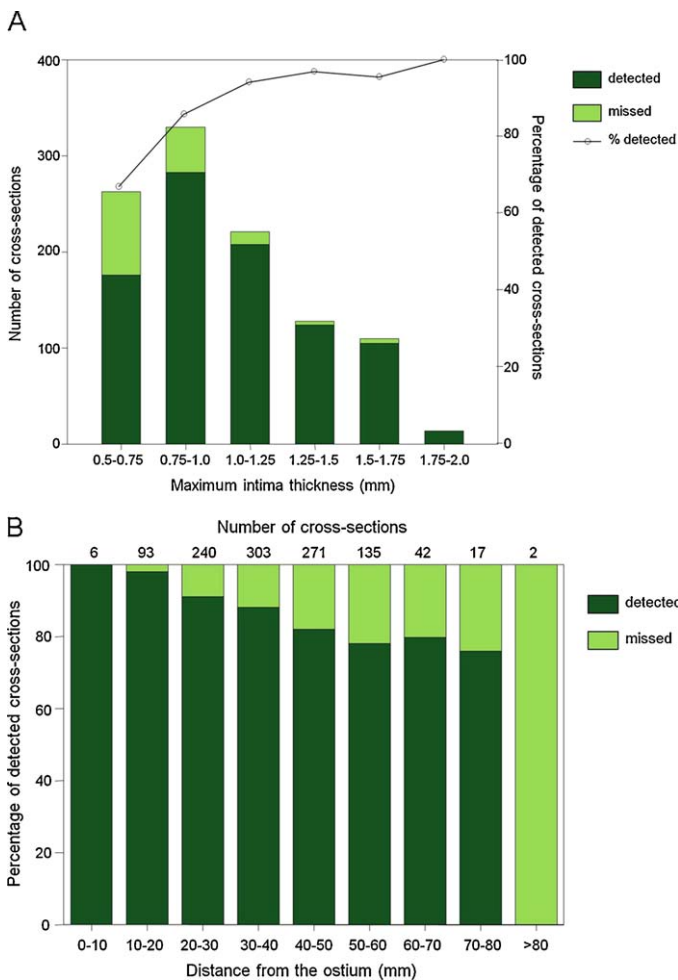


Fig. 2. Detection of plaque according to maximum intima thickness by IVUS (panel A) and according to distance from the coronary ostium (panel B).

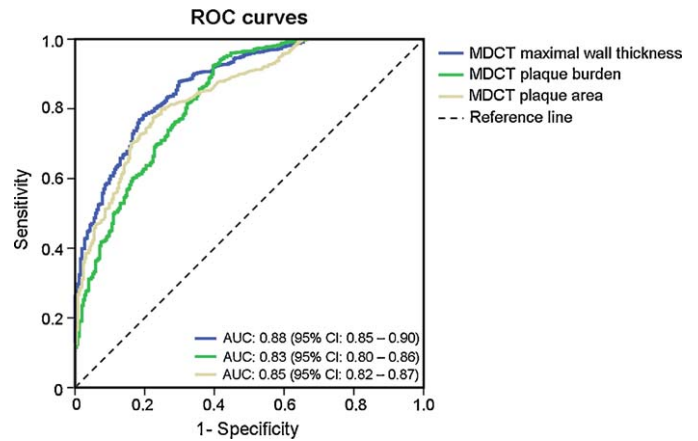


Fig. 3. Receiver operating characteristics (ROC) curve analysis of quantitative characteristics measured by 64-slice MDCT.

$p < 0.001$). Bland–Altman analysis showed a slight non-significant underestimation of plaque volume by MDCT ($177 \pm 101 \text{ mm}^3$ vs. $181 \pm 107 \text{ mm}^3$, $p = 0.5$; see Fig. 4), with a mean difference of -4.5 mm^3 and 95% limits of agreement between -92.7 and 83.7 mm^3 . A sub-analysis per ROI plaque type revealed that non-calcified plaque volumes ($n = 19$) were systematically but non-significantly underestimated ($129.3 \pm 88.2 \text{ mm}^3$ vs. $141.7 \pm 93.2 \text{ mm}^3$, $p = 0.22$). Plaque volume in the mixed/calcified ROIs ($n = 25$) was slightly overestimated ($213.2 \pm 96.5 \text{ mm}^3$ vs. $211.7 \pm 108.3 \text{ mm}^3$, $p = 0.87$).

4. Discussion

In the present study, we evaluated the ability of 64-slice MDCT to detect and quantify coronary atherosclerotic plaque, based on MDCT-derived parameters, using IVUS as a reference standard. The novel fusion technique we applied for the co-registration of IVUS and MDCT [8] provided cross-sectional images at identical positions for the whole length of the ROI and enabled a head-to-head comparison of the 2 imaging modalities.

The main findings of our study can be summarized as follows: plaque detection based on the threshold of $>0.5 \text{ mm}$ for MDCT-derived maximum wall thickness resulted in a reasonably good diagnostic accuracy on the cross-sectional level (sensitivity 86%, specificity 71%), and very good on the segmental level (sensitivity 96%, specificity 88%). Moreover, the accurate detection of atherosclerotic plaque depended on plaque and vessel size. Smaller plaques could not be reliably detected, which was in accordance with previous reports [11,12]. Plaque location was also playing an important role for the diagnostic accuracy; the sensitivity sig-

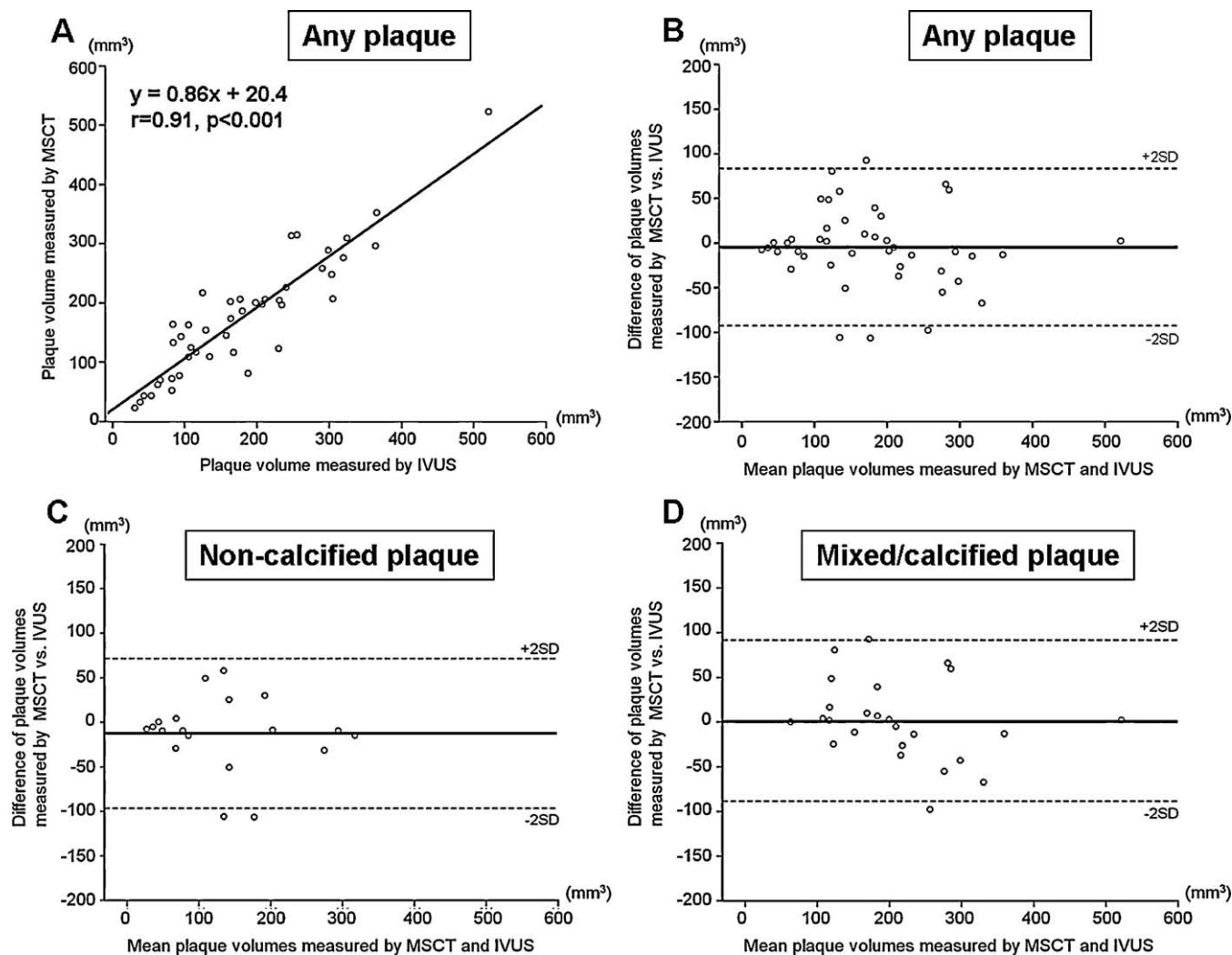


Fig. 4. Correlation plot (A) and Bland-Altman analyses (B-D) for plaque volumes per vessel determined by IVUS versus 64-slice MDCT.

nificantly decreased for plaques located more distally. Finally, quantification of plaque volumes showed a significantly strong correlation between MDCT and IVUS. The mean differences were small, with underestimation of non-calcified and overestimation for mixed/calcified plaque, however the limits of agreement were relatively wide.

MDCT angiography has the potential to become a non-invasive alternative to IVUS for plaque quantification and to be used for risk stratification of asymptomatic individuals or the assessment of atherosclerosis progression/regression. Previous studies [13–16] have focused on the comparison of MDCT- and IVUS-derived quantitative parameters, such as plaque area or plaque burden, showing moderate to good correlation, but the presence of atherosclerosis on MDCT was based on binary (yes/no) visual scoring. This is the first study, to our knowledge, that used a MDCT-derived quantitative parameter (wall thickness) to assess diagnostic accuracy on a slice-by-slice and segmental basis. Our data demonstrated that the detection of atherosclerotic plaque based on MDCT-derived quantitative parameters in a similar fashion to IVUS was feasible. Plaques located within the proximal 40 mm were detected with very high sensitivity (88–100%) and as invasive imaging studies have shown, the most clinically relevant lesions are highly clustered within the proximal sections of the coronaries [17–19]. Moreover, the very good diagnostic accuracy obtained at segmental level is promising for the potential development of prediction models based on plaque

presence on a per-segment basis. Nevertheless, it is important to keep in mind that the clinical use of MDCT for detection of early atherosclerosis is still limited by the current spatial and temporal resolution of the technique. Further technical improvements of the acquisition and reconstruction techniques will enable more reliable visualisation of the coronary arteries with better signal-to-noise ratio and decrease of partial voluming and motion artifacts.

Regarding the quantification of plaque volume by MDCT, our results add to the existing literature which only deals with stable angina patients. Several researchers compared plaque volumes derived from MDCT angiography with corresponding IVUS data and reported strong correlation and moderate agreement [20–25]. The differences between MDCT and IVUS volumetric measurements, which were also observed in our analysis, could be attributed to several technical and methodological factors. The spatial resolution of 64-slice CT may still be inadequate for accurate edge discrimination of MDCT images. The smaller coronary plaques, in particular non-calcified plaques, cannot be well defined and may occasionally not be detected, resulting in underestimation of plaque volume. Moreover, the real size of calcified plaque is overestimated by MDCT due to the blooming effects. Quantification of calcified plaque by IVUS can also be imprecise, because the acoustic shadowing in areas of calcification blocks the view of the outer vessel borders. In addition, on IVUS the outer boundaries were defined by the external elastic membrane (EEM), whereas on MDCT the outer vessel

border was annotated at the adventitia-fat boundary, which may also have accounted for the discrepancies in the measurements. Furthermore, the IVUS images are not strictly perpendicular to the centerline, depending on the catheter position and vessel tortuosity. The slice thickness is slightly different between the two techniques, but this was largely overcome by the co-registration technique we used.

5. Limitations

This study was performed on a selected patient population with acute coronary syndromes and the examined vessels were only the major epicardial arteries, for which IVUS data were available. This population presented with high prevalence of disease and diagnostic accuracy might be lower in populations with lower prevalence, i.e. asymptomatic patients. In addition, some patients were excluded, however their characteristics were not different from the study group, thus we assumed that exclusion of these patients did not have any major influence on our study. Furthermore, the ROIs selected for our analysis were free of image artifacts (for instance caused by coronary motion or noise), whereas in everyday clinical routine those artifacts occasionally do occur. However, contrary to other studies, we have to point out that we included extensively calcified plaques. In addition, manual plaque segmentation largely depended on the individual operator and was rather time consuming; more automated validated software would be required for MDCT plaque analysis in a routine clinical setting. Finally, the high radiation exposure during MDCT coronary angiography remains a matter of concern. For this study, the estimated radiation exposure for the contrast-enhanced scan without prospective X-ray tube modulation was 17 ± 1 mSv; nevertheless, this radiation dose reflected the CT technology available at that time. Significant reduction of radiation dose can currently be achieved by implementation of several dose-saving techniques [26], which does result in effective dose comparable or lower than invasive coronary angiography. By applying image reconstruction algorithms, such as iterative reconstruction [27], supplementary to other radiation dose-saving techniques, dose reduction can be achieved with comparable image noise at lower tube currents.

6. Conclusions

The present study demonstrated that 64-MDCT is able to detect and quantify atherosclerotic plaque using MDCT-derived parameters. Further improvement in CT resolution is required for more reliable assessment of very small and distal coronary plaques.

Conflict of interest

The authors declare no conflicts of interest.

Funding

This study was supported by a grant from the Fonds NutsOhra Organization.

Contributors

S-LP, LAN, MS, H-LL, EC, AGG, JCHS, FJHG, ASD, NRM, PJF were responsible for study design, analysis and interpretation of data; S-LP, LAN, PJF drafted the manuscript; S-LP, LAN, MS, JCHS, FJHG, ASD, KN, RJG, NRM, PJF contributed toward critical revision of the manuscript for important intellectual content; S-LP, LAN, MS, H-LL, EC, AGG, JCHS, FJHG, ASD, KN, RJG, NRM, PJF approved the final draft of the manuscript.

Acknowledgements

We are thankful to all the medical and technical staff of the interventional cardiology department for their valuable contribution.

References

- [1] Mintz GS, Nissen SE, Anderson WD, et al. A report of the American College of Cardiology Task Force on clinical expert consensus documents. *J Am Coll Cardiol* 2001;37:1478–92.
- [2] Meijboom WB, Meijjs MF, Schuijff JD, et al. Diagnostic accuracy of 64-slice computed tomography coronary angiography: a prospective, multicenter, multivendor study. *J Am Coll Cardiol* 2008;52:2135–44.
- [3] Miller JM, Rochitte CE, Dewey M, et al. Diagnostic performance of coronary angiography by 64-row CT. *N Engl J Med* 2008;359:2324–36.
- [4] Mollet NR, Cademartiri F, van Mieghem CA, et al. High-resolution spiral computed tomography coronary angiography in patients referred for diagnostic conventional coronary angiography. *Circulation* 2005;112:2318–23.
- [5] Raff GL, Gallagher MJ, O'Neill WW, Goldstein JA. Diagnostic accuracy of noninvasive coronary angiography using 64-slice spiral computed tomography. *J Am Coll Cardiol* 2005;46:552–7.
- [6] Schuijff JD, Pundziute G, Jukema JW, et al. Diagnostic accuracy of 64-slice multislice computed tomography in the noninvasive evaluation of significant coronary artery disease. *Am J Cardiol* 2006;98:145–8.
- [7] Weustink AC, Mollet NR, Neeffjes LA, et al. Diagnostic accuracy and clinical utility of noninvasive testing for coronary artery disease. *Ann Intern Med* 1888;152:630–9.
- [8] van der Giessen AG, Schaap M, Gijzen FJ, et al. 3D fusion of intravascular ultrasound and coronary computed tomography for in-vivo wall shear stress analysis: a feasibility study. *Int J Cardiovasc Imaging* 2010;26:781–96.
- [9] De Winter SA, Hamers R, Degertekin M, et al. Retrospective image-based gating of intracoronary ultrasound images for improved quantitative analysis: the intelligate method. *Catheter Cardiovasc Interv* 2004;61:84–94.
- [10] Mollet NR, Rengo M, Neeffjes LA, et al. Plaque quantification by CT coronary angiography: optimization of window level settings. In: *Radiological Society of North America, 94th Scientific Assembly and Annual Meeting*. 2008.
- [11] Leber AW, Knez A, Becker A, et al. Accuracy of multidetector spiral computed tomography in identifying and differentiating the composition of coronary atherosclerotic plaques: a comparative study with intracoronary ultrasound. *J Am Coll Cardiol* 2004;43:1241–7.
- [12] van der Giessen AG, Toepker MH, Donnelly PM, et al. Reproducibility, accuracy, and predictors of accuracy for the detection of coronary atherosclerotic plaque composition by computed tomography: an ex vivo comparison to intravascular ultrasound. *Invest Radiol* 2010;45:693–701.
- [13] Hur J, Kim YJ, Lee HJ, et al. Quantification and characterization of obstructive coronary plaques using 64-slice computed tomography: a comparison with intravascular ultrasound. *J Comput Assist Tomogr* 2009;33:186–92.
- [14] Petranovic M, Soni A, Bezzeria H, et al. Assessment of nonstenotic coronary lesions by 64-slice multidetector computed tomography in comparison to intravascular ultrasound: evaluation of nonculprit coronary lesions. *J Cardiovasc Comput Tomogr* 2009;3:24–31.
- [15] Sun J, Zhang Z, Lu B, et al. Identification and quantification of coronary atherosclerotic plaques: a comparison of 64-MDCT and intravascular ultrasound. *AJR Am J Roentgenol* 2008;190:748–54.
- [16] Voros S, Rinehart S, Qian Z, et al. Prospective validation of standardized, 3-dimensional, quantitative coronary computed tomographic plaque measurements using radiofrequency backscatter intravascular ultrasound as reference standard in intermediate coronary arterial lesions results from the ATLANTA (assessment of tissue characteristics, lesion morphology, and hemodynamics by angiography with fractional flow reserve, intravascular ultrasound and virtual histology, and noninvasive computed tomography in atherosclerotic plaques) I study. *JACC Cardiovasc Interv* 2011;4:198–208.
- [17] Hong MK, Mintz GS, Lee CW, et al. A three-vessel virtual histology intravascular ultrasound analysis of frequency and distribution of thin-cap fibroatheromas in patients with acute coronary syndrome or stable angina pectoris. *Am J Cardiol* 2008;101:568–72.
- [18] Rodriguez-Granillo GA, Garcia-Garcia HM, Mc Fadden EP, et al. In vivo intravascular ultrasound-derived thin-cap fibroatheroma detection using ultrasound radiofrequency data analysis. *J Am Coll Cardiol* 2005;46:2038–42.
- [19] Wang JC, Normand SL, Mauri L, Kuntz RE. Coronary artery spatial distribution of acute myocardial infarction occlusions. *Circulation* 2004;110:278–84.
- [20] Achenbach S, Moselewski F, Ropers D, et al. Detection of calcified and non-calcified coronary atherosclerotic plaque by contrast-enhanced, submillimeter multidetector spiral computed tomography: a segment-based comparison with intravascular ultrasound. *Circulation* 2004;109:14–7.
- [21] Leber AW, Becker A, Knez A, et al. Accuracy of 64-slice computed tomography to classify and quantify plaque volumes in the proximal coronary system: a comparative study using intravascular ultrasound. *J Am Coll Cardiol* 2006;47:672–7.
- [22] Otsuka M, Bruining N, Van Pelt NC, et al. Quantification of coronary plaque by 64-slice computed tomography: a comparison with quantitative intracoronary ultrasound. *Invest Radiol* 2008;43:314–21.

- [23] Schepis T, Marwan M, Pflederer T, et al. Quantification of non-calcified coronary atherosclerotic plaques with dual-source computed tomography: comparison with intravascular ultrasound. *Heart* 2010;96:610–5.
- [24] Ugolini P, Pressacco J, Lesperance J, et al. Evaluation of coronary atheroma by 64-slice multidetector computed tomography: comparison with intravascular ultrasound and angiography. *Can J Cardiol* 2009;25:641–7.
- [25] Dey D, Schepis T, Marwan M, Slomka PJ, Berman DS, Achenbach S. Automated three-dimensional quantification of noncalcified coronary plaque from coronary CT angiography: comparison with intravascular US. *Radiology* 1888;257:516–22.
- [26] Raff GL, Chinnaiyan KM, Share DA, et al. Radiation dose from cardiac computed tomography before and after implementation of radiation dose-reduction techniques. *JAMA* 2009;301:2340–8.
- [27] Leipsic J, Heilbron BG, Hague C. Iterative reconstruction for coronary CT angiography: finding its way. *Int J Cardiovasc Imaging* 2011.

Chapter 3

Reproducibility of computed tomography angiography data analysis using semiautomatic plaque quantification software: implications for the design of longitudinal studies.

International Journal of Cardiovascular Imaging. 2013 Jun;29(5):1095-104.

S.L. Papadopoulou, H.M. Garcia-Garcia, A. Rossi, C. Girasis , A.S. Dharampal, P.H. Kitslaar, G.P. Krestin, P.J. de Feyter

Reproducibility of computed tomography angiography data analysis using semiautomated plaque quantification software: implications for the design of longitudinal studies

Stella-Lida Papadopoulou · Hector M. Garcia-Garcia · Alexia Rossi · Chrysafios Girasis · Anoeshka S. Dharampal · Pieter H. Kitslaar · Gabriel P. Krestin · Pim J. de Feyter

Received: 27 July 2012 / Accepted: 29 November 2012 / Published online: 7 December 2012
© Springer Science+Business Media Dordrecht 2012

Abstract Reproducibility of the quantitative assessment of atherosclerosis by computed tomography coronary angiography (CTCA) is paramount for the design of longitudinal studies. The purpose of this study was to assess the inter- and intra-observer reproducibility using semiautomated CT plaque analysis software in symptomatic individuals. CTCA was performed in 10 symptomatic patients after percutaneous treatment of the culprit lesions and was repeated after 3 years. The plaque quantitative analysis was performed in untreated vessels with mild-to-moderate atherosclerosis and included geometrical and compositional characteristics using semiautomated CT plaque analysis software. A total of 945 matched cross-sections from 21 segments were analyzed independently by a second reviewer to assess inter-observer variability; the first observer repeated all the analyses after 3 months to assess intra-observer variability. The observer variability was also compared to the absolute plaque changes detected over time. Agreement was evaluated by Bland–Altman analysis and concordance correlation coefficient. Inter-

observer relative differences for lumen, vessel, plaque area and plaque burden were 1.2, 0.6, 2.2, 1.6 % respectively. Intra-observer relative differences for lumen, vessel, plaque area and plaque burden were 1.0, 0.4, 0.2, 0.4 % respectively. For the average plaque attenuation values the inter- and intra-observer variability was 5 and 2 % respectively. For the % low-attenuation-plaque the inter- and intra-observer variability was 16 and 6 % respectively. The absolute intra-observer variability for the plaque burden was 1.30 ± 1.09 %, while the temporal plaque burden difference was 3.55 ± 3.02 % ($p = 0.001$). The present study shows that the geometrical assessment of coronary atherosclerosis by CTCA is highly reproducible within and between observers using semiautomated quantification software and that serial plaque changes can be detected beyond observer variability. The compositional measurements are more variable between observers than geometrical measurements.

Keywords Agreement · Atherosclerosis · Computed tomography angiography · Plaque quantification · Reproducibility

S.-L. Papadopoulou (✉) · H. M. Garcia-Garcia · A. Rossi · C. Girasis · A. S. Dharampal · P. J. de Feyter
Department of Cardiology, Erasmus University Medical Center, Room Ca 207, PO Box 2040, 3000 CA Rotterdam, The Netherlands
e-mail: elpa98@gmail.com; s.papadopoulou@erasmusmc.nl

S.-L. Papadopoulou · A. Rossi · A. S. Dharampal · G. P. Krestin · P. J. de Feyter
Department of Radiology, Erasmus University Medical Center, PO Box 2040, 3000 CA Rotterdam, The Netherlands

P. H. Kitslaar
Division of Image Processing, Department of Radiology, Leiden University Medical Center, Leiden, The Netherlands

Introduction

Coronary atherosclerosis is a worldwide disease with a burden of 17 million deaths annually [1]. In the past, quantitative coronary angiography (QCA) [2] and intravascular ultrasound (IVUS) have been used to study the extent of the disease [3] and monitor the progression/regression of atherosclerosis. Nevertheless, both imaging techniques are invasive, expensive and not free of complications, thus unsuitable for routine serial assessment of atherosclerosis.

Computed tomography coronary angiography (CTCA) has been introduced as a noninvasive technique for atherosclerotic plaque quantification *in vivo*. To date, there are several CTCA studies describing the extent, severity, distribution, and morphology of coronary atherosclerosis, including several longitudinal studies assessing plaque progression/regression by CTCA [4–11].

Reproducibility of measurements is crucial for the internal validity of longitudinal studies using CTCA; as previous serial studies using IVUS and CTCA have shown, the temporal changes in atherosclerotic plaque are small [11, 12]. The use of semiautomated plaque analysis software which can produce accurate and reproducible quantitative measurements can facilitate the serial assessment of atherosclerosis by CTCA. However, only scarce data are available about the reproducibility of quantitative measurements for geometrical and compositional parameters of atherosclerotic plaque and a comparison with serial changes in plaque parameters is lacking.

Therefore, the aims of our study were the following: (1) to assess the inter-observer and intra-observer agreement of plaque geometrical measurements using semiautomated CTCA plaque analysis software; and as secondary objectives (2) to investigate the influence of the variability of the plaque contours position on the compositional measurements; and (3) to compare the observer variability with the serial changes in plaque burden and plaque area.

Methods

Patient population

In this exploratory study, the population comprised 10 randomly selected patients (21 segments and 945 cross-sections) from a prospective cohort of symptomatic patients; this main cohort included 32 patients with acute coronary syndromes who underwent CTCA after percutaneous treatment of the culprit lesions and follow-up CTCA after 3 years to assess plaque temporal changes in the untreated vessels, as part of the PROSPECT MSCT sub-study in our institution [11]. The institutional review board approved the study and all patients gave written informed consent.

CTCA acquisition

All patients received CT coronary angiography at baseline and 3 years follow-up which was performed using a 64-slice single source scanner (Sensation 64, Siemens Medical Solutions, Forchheim, Germany) and a 64-slice dual source CT scanner (Somatom Definition, Siemens Medical Solutions, Forchheim, Germany) respectively; the

scanning protocol has been previously described in detail [11]. The patients received nitrates and β -blockers prior to the scan provided there were no contraindications. The CT angiographic scan parameters were: (1) for the single source CT scanner a gantry rotation time of 330 ms; 32×2 slices per rotation; 0.6 mm detector collimation; spiral scan mode with a table feed of 3.8 mm per rotation; a tube voltage of 120 kV; and tube current of 900 effective mAs. A bolus of 100 mL of contrast material (400 mgI/mL; Iomeron, Bracco, Milan, Italy) was injected intravenously at 5 mL/s flow rate followed by a saline chaser. The initiation of the scan was synchronized to the arrival of contrast in the coronary arteries by a bolus-tracking technique; (2) for the dual source CT scanner $32 \times 2 \times 0.6$ mm collimation with z-flying focal spot for both detectors, gantry rotation time 330 ms, tube voltage 120 kV and tube current of 320–412 mAs per rotation. A bolus of iodinated contrast material (370 mgI/mL, Ultravist; Schering, Berlin, Germany), which varied between 60 and 100 mL, depending on the expected scan time, was injected intravenously (flow rate 5.5 mL/s) followed by a 40 mL saline chaser at the same injection rate. A bolus tracking technique was used to synchronize the arrival of contrast in the coronary arteries and the start of the acquisition. The mean effective radiation dose was 14.0 ± 0.8 mSv for the baseline and 10.4 ± 3.0 mSv for the follow-up scan, using the dose-length product and a conversion factor k (0.014 mSv/mGy/cm) [13]. For all datasets, axial images were reconstructed using retrospective ECG-gating, with a slice thickness of 0.75-mm, slice increment of 0.4-mm and a medium-to-smooth convolution kernel (filtered back projection method). Optimal datasets with the best image quality were reconstructed mainly in the mid- to end-diastolic phase.

CTCA image analysis

All datasets (baseline and follow-up) were transferred to an offline workstation for analysis using semi-automated plaque analysis software (QAngioCT Research Edition v1.3.61, Medis Medical Imaging Systems, Leiden, The Netherlands) [14]. An experienced observer (3 years CTCA experience) blinded to the sequence of imaging analyzed all the scans of the main study cohort; the complete results of this temporal analysis have been previously published [11]. To examine inter-observer variability of plaque analysis a second observer (1 year CTCA experience) performed blindly the analysis on 21 segments from 10 randomly selected patients at the follow-up time point, starting completely from the raw datasets; to examine the intra-observer variability, the first reader re-analyzed all the segments in a similar blinded fashion 3 months after his/her original analysis.

The major vessels (LAD, LCX, RCA) were considered for analysis using the modified 17-segment American Heart Association model for coronary segment classification [15]. The segments were carefully matched for all the comparisons using the bifurcations carina as landmarks. The segments of poor quality due to stack or movement artifacts, or severe calcification (with blooming artifacts preventing reliable assessment of the lumen) were excluded from analysis.

Definition of the inner lumen and outer vessel areas was performed semi-automatically following a stepwise approach. First, a centerline originating from the ostium was automatically extracted after an ostial proximal point and a distal point were placed by the observer; then straightened multi-planar reformatted images were generated and the lumen and vessel borders were detected longitudinally in 4 different longitudinal cutplanes by the software and then corrected by the observer. Based on these updated longitudinal contours, cross-sectional images at 0.5 mm intervals were calculated in order to create transversal lumen and vessel wall contours, which were examined and, if necessary, adjusted by the observer (Fig. 1). Gradient magnitude images, which are derived from the CTCA images and display the degree of CT density change, were used to verify the lumen and vessel wall borders.

The following quantitative parameters were derived per cross-section: the lumen area, the lumen diameter, the vessel area and the plaque burden [(plaque area/vessel area) * 100]. The plaque area was calculated by subtracting lumen area from vessel area. Geometrical parameters determined on a segmental level included the following: the mean lumen area, the mean vessel area, the mean plaque area, the plaque burden, the minimal lumen diameter (MLD) and the minimal lumen area (MLA). The mean areas were the averaged measurements of all cross-sections for each segment. Furthermore, the plaque composition was evaluated in each cross-section and in each coronary segment based on attenuation values in HU (Hounsfield Units); the mean HU and the % of voxels with attenuation values <30 HU (representing low attenuation plaque—%LAP) were calculated for each cross-section and each coronary segment.

Observer variability and detected plaque changes over time

In order to investigate whether the observer variability using semi-automated analysis software is acceptable for monitoring the longitudinal plaque changes over time, we compared the absolute plaque change with the absolute observer variability for each segment. In this way by comparing the absolute differences, we can investigate whether the magnitude of observer variability is smaller

than the magnitude of the plaque changes, while the direction of the change (positive/negative) is irrelevant to the comparison.

Statistical analysis

Continuous variables are presented as mean \pm SD or median (interquartile range—IQR) if not normally distributed. Discrete variables are presented as counts and/or percentages. The analyses were performed on both cross-sectional and segmental level. The inter-observer and intra-observer agreement were assessed using the Lin's concordance correlation coefficient [CCC with the 95 % confidence interval (CI)] [16]; Bland–Altman analysis [17] was performed by plotting the mean against the difference in measurements. Limits of agreement were determined by adding 1.96 standard deviations to the mean difference for the upper limit and by subtracting 1.96 standard deviations from the mean difference for the lower limit. The paired *t* test was used to compare the absolute plaque change with the absolute observer variability. A two-sided *p* value of less than 0.05 was used to indicate statistical significance. Statistical analyses were performed with SPSS 17.0 software (SPSS, Chicago IL).

Results

The baseline characteristics of the included patients (*n* = 10) are as follows: mean age was 56 ± 4 and 80 % were male. Regarding cardiac risk factors, 40, 10, and 50 % had hypertension, diabetes mellitus, and hyperlipidemia, respectively. The untreated vessels were examined (*n* = 19) and the ones with low image quality (due to motion or stack artifacts or extremely calcified coronary arteries) were excluded (*n* = 8). The analyzed vessels were the left anterior descending (*n* = 4, 36 %), the left circumflex (*n* = 4, 36 %) and the right coronary artery (*n* = 3, 27 %).

Inter-observer agreement

For the assessment of the inter-observer agreement, 945 matched cross-sections from 21 paired coronary segments were analyzed separately by 2 independent observers.

At the cross-sectional level, the mean differences for geometrical parameters were small (Table 1a), with narrow limits of agreement between observers (limits of agreement for lumen, vessel, plaque and plaque burden measurements of 2.39, -2.03 mm²; 2.81, -2.99 mm²; 2.86, -3.41 mm²; and 9.44, -11.10 %, respectively). The Bland–Altman analysis is shown in Fig. 2. The concordance correlation coefficients were high (Table 2a), except for the maximal plaque thickness (CCC: 0.65). For the compositional

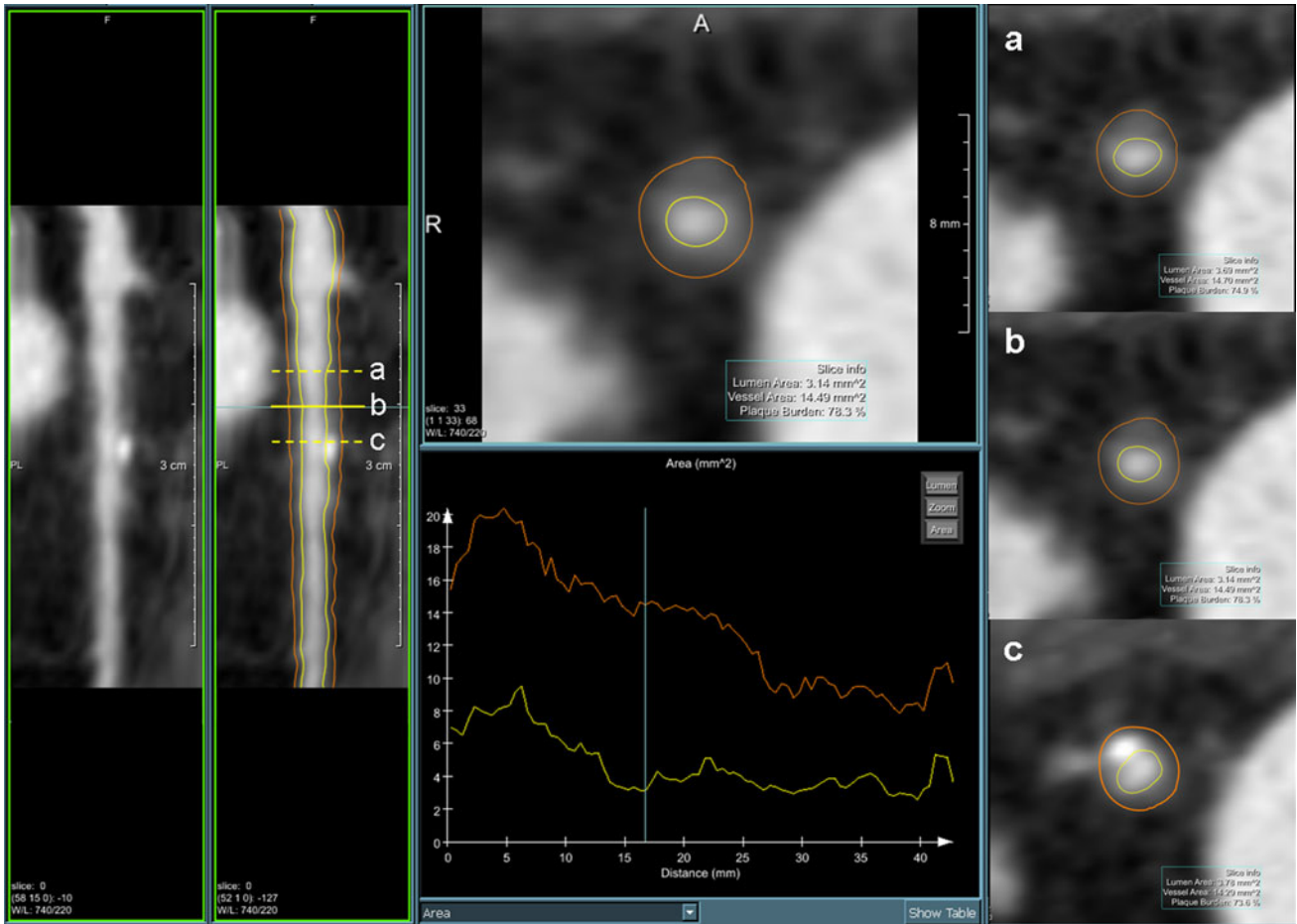


Fig. 1 Example of quantitative analysis of a left anterior descending artery. The analyzed cross-sections at 3 different levels are also shown (panels a–c)

analysis as expressed by the plaque attenuation values (Table 3a), the median (IQR) difference of the attenuation between observers was 6 (–4, 22) HU, which corresponds to a median of 5 % variability. The median (IQR) difference of the %LAP was –1.6 (–6.3, 2.1), which corresponds to a median of 16 % inter-observer variability.

At the segmental level, the mean differences for geometrical parameters were also small (Table 1b), with narrow limits of agreement between observers (limits of agreement for lumen, vessel, plaque and plaque burden measurements of 1.12, –0.76 mm²; 1.10, –1.26 mm²; 0.94, –1.46 mm²; and 3.64 %, –5.50 % respectively). The concordance correlation coefficients were high (Table 2b). For the compositional analysis as expressed by the plaque attenuation values (Table 3a), the median (IQR) difference of the attenuation between observers was 4 (–9, 9) HU, which corresponds to a median of 4 % variability. The median (IQR) difference of the %LAP was –1.7 (–3.9, 1.2), which corresponds to a median of 12 % inter-observer variability.

Intra-observer agreement

For the assessment of the intra-observer agreement, 945 matched cross-sections from 21 paired coronary segments were fully re-analyzed by the first observer after 3 months.

At the cross-sectional level, the mean differences for geometrical parameters were small (Table 4a), with narrow limits of agreement between the two rounds of analysis (limits of agreement for lumen, vessel, plaque and plaque burden measurements of 1.62, –1.77 mm²; 2.33, –2.54 mm²; 2.59, –2.66 mm²; and 7.49 %, –7.15 % respectively). The Bland–Altman analysis is shown in Fig. 3. The concordance correlation coefficients were high (Table 5a). For the compositional analysis as expressed by the plaque attenuation values (Table 3b), the median (IQR) difference of the attenuation between the two rounds of analysis was 2 (–5, 11) HU, which corresponds to a median of 2 % variability. The median (IQR) difference of the %LAP was –0.7 (–3.9, 2.2), which corresponds to a median of 6 % intra-observer variability.

Table 1 Inter-observer variability of geometrical measurements

Parameters	Observer 1	Observer 2	Mean absolute difference \pm SD	Mean relative difference (%)
<i>(a). Matched cross-sections (n = 945)</i>				
Lumen CSA (mm ²)	9.08 \pm 4.27	9.26 \pm 4.44	0.18 \pm 1.13	1.2
Lumen diameter (mm)	3.31 \pm 0.77	3.34 \pm 0.80	0.03 \pm 0.19	0.6
Vessel CSA (mm ²)	19.96 \pm 5.65	19.87 \pm 5.71	0.09 \pm 1.48	0.6
Plaque CSA (mm ²)	10.88 \pm 2.84	10.61 \pm 2.61	0.27 \pm 1.60	2.2
Plaque burden (%)	56.07 \pm 10.54	55.24 \pm 10.83	0.83 \pm 5.24	1.6
Plaque max. thickness (mm)	1.15 \pm 0.36	1.10 \pm 0.39	0.05 \pm 0.26	5.5
<i>(b). Matched segments (n = 21)</i>				
Average lumen CSA (mm ²)	8.92 \pm 3.90	9.09 \pm 4.10	0.18 \pm 0.48	1.3
Average vessel CSA (mm ²)	19.64 \pm 5.54	19.56 \pm 5.62	0.08 \pm 0.60	0.6
Average plaque CSA (mm ²)	10.73 \pm 2.29	10.47 \pm 2.20	0.26 \pm 0.61	2.4
Plaque burden (%)	56.15 \pm 7.97	55.22 \pm 8.61	0.93 \pm 2.33	1.9
Minimum lumen area (mm ²)	6.12 \pm 2.80	6.33 \pm 3.18	0.21 \pm 0.62	1.4
Minimum lumen diameter (mm)	2.72 \pm 0.64	2.76 \pm 0.71	0.03 \pm 0.12	0.7

CSA cross-sectional area, SD standard deviation

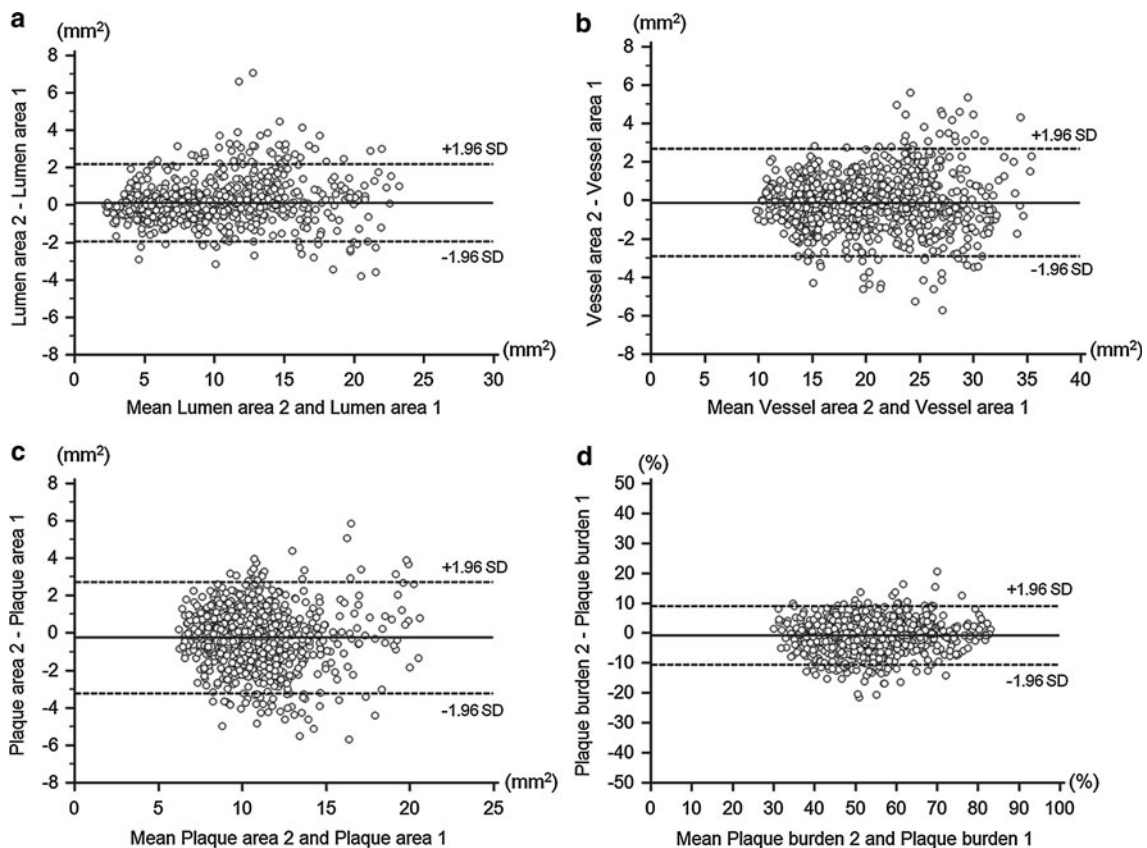


Fig. 2 Bland-Altman plots of inter-observer comparisons for lumen, vessel, plaque area and plaque burden

At the segmental level, the mean differences for geometrical parameters were small (Table 4b), with narrow limits of agreement between the two rounds of analysis (limits of agreement for lumen, vessel, plaque and plaque burden measurements of 0.83, -0.91 mm²; 0.67, -0.81 mm²; 0.83, -0.89 mm²; and 3.55 %, -3.15 % respectively). The concordance correlation coefficients

were very high (Table 5b). For the compositional analysis as expressed by the plaque attenuation values (Table 3b), the median (IQR) difference of the attenuation between the two rounds of analysis was 1 (-1 , 5) HU, which corresponds to a median of <1 % variability. The median (IQR) difference of the %LAP was -0.6 (-1.6 , 0.3), which corresponds to a median of 3 % intra-observer variability.

Table 2 Correlation between different observers for geometrical and compositional parameters

Geometrical and compositional parameters	CCC	95 % CI
<i>(a) Cross-sectional basis</i>		
Lumen area (mm ²)	0.97	0.966–0.974
Lumen diameter (mm)	0.97	0.969–0.976
Vessel area (mm ²)	0.97	0.964–0.972
Plaque area (mm ²)	0.83	0.810–0.849
Plaque burden (%)	0.89	0.872–0.899
Maximal plaque thickness (mm)	0.65	0.615–0.688
Mean plaque attenuation (HU)	0.85	0.837–0.869
% LAP	0.65	0.608–0.680
<i>(b) Segmental basis</i>		
Mean lumen area (mm ²)	0.99	0.988–0.998
Mean vessel area (mm ²)	0.99	0.986–0.998
Mean plaque area (mm ²)	0.96	0.902–0.983
Plaque burden (%)	0.96	0.913–0.983
Minimal lumen area (mm ²)	0.98	0.952–0.988
Minimal lumen diameter (mm)	0.98	0.968–0.992
Mean plaque attenuation (HU)	0.73	0.526–0.855
% LAP	0.73	0.490–0.865

CCC concordance correlation coefficient, CI confidence interval, LAP low attenuation plaque

Comparison of the observer variability with the plaque serial changes

For the 21 segments included in the reproducibility analysis, the absolute change (irrespective of progression or regression) in mean plaque area between the two time points was $1.65 \pm 1.42 \text{ mm}^2$ and the absolute change in % plaque burden was $3.55 \pm 3.02 \%$.

The absolute intra-observer variability for these parameters was significantly smaller than the serial plaque changes ($0.36 \pm 0.24 \text{ mm}^2$, $p < 0.001$ for mean plaque area and $1.30 \pm 1.09 \%$, $p = 0.001$ for plaque burden).

The absolute inter-observer variability for these parameters was also smaller than the serial plaque changes ($0.51 \pm 0.41 \text{ mm}^2$, $p < 0.001$ for mean plaque area and $1.99 \pm 1.49 \%$, $p = 0.044$ for plaque burden).

Discussion

The purpose of this study was to assess in detail the inter- and intra-observer reproducibility of plaque geometrical and compositional parameters using dedicated semiautomated CT plaque analysis software in vessels with mild-to-moderate atherosclerosis. To our knowledge this is the first

Table 3 Reproducibility of compositional measurements

	Observer 1	Observer 2	Mean absolute difference \pm SD	Median absolute difference (IQR)	Median relative difference (%)
<i>(a). Between different observers</i>					
Cross-sections (n = 945)					
Average attenuation (HU)	124 \pm 45	135 \pm 52	11 \pm 25	6 (–4, 22)	5.1
LAP (%)	12.7 \pm 8.2	10.5 \pm 8.7	2.2 \pm 6.9	–1.6 (–6.3, 2.1)	16.4
Segments (n = 21)					
Average attenuation (HU)	125 \pm 26	136 \pm 39	12 \pm 22	4 (–9, 9)	4.3
LAP (%)	13.1 \pm 5.6	10.6 \pm 7.3	2.6 \pm 4.2	–1.7 (–3.9, 1.2)	12.4
	Observer 1 (1st time)	Observer 1 (2nd time)	Mean absolute difference \pm SD	Median absolute difference (IQR)	Median relative difference (%)
<i>(b). Between the 2 rounds of the same observer</i>					
Cross-sections (n = 945)					
Average attenuation (HU)	124 \pm 45	126 \pm 46	4 \pm 22	2 (–5, 11)	1.6
LAP (%)	12.7 \pm 8.2	12.1 \pm 8.1	–1.0 \pm 5.4	–0.7 (–3.9, 2.2)	6.1
Segments (n = 21)					
Average attenuation (HU)	125 \pm 26	127 \pm 27	2 \pm 5	1 (–1, 5)	0.5
LAP (%)	13.1 \pm 5.5	12.4 \pm 5.6	–0.7 \pm 1.4	–0.6 (–1.6, 0.3)	2.5

IQR interquartile range, LAP low attenuation plaque, SD standard deviation

Table 4 Intra-observer variability of geometrical measurements

Parameters	Observer 1 (1st time)	Observer 1 (2nd time)	Mean absolute difference \pm SD	Mean relative difference (%)
<i>(a). Matched cross-sections (n = 945)</i>				
Lumen CSA (mm ²)	9.08 \pm 4.27	9.00 \pm 4.19	0.08 \pm 0.87	1.0
Lumen diameter (mm)	3.31 \pm 0.77	3.30 \pm 0.77	0.01 \pm 0.15	0.5
Vessel CSA (mm ²)	19.96 \pm 5.65	19.85 \pm 5.49	0.11 \pm 1.24	0.4
Plaque CSA (mm ²)	10.88 \pm 2.84	10.85 \pm 2.53	0.03 \pm 1.34	0.2
Plaque burden (%)	56.07 \pm 10.54	56.23 \pm 10.33	0.17 \pm 3.74	0.4
Plaque max. thickness (mm)	1.15 \pm 0.36	1.16 \pm 0.37	0.01 \pm 0.24	0.7
<i>(b). Matched segments (n = 21)</i>				
Average lumen CSA (mm ²)	8.92 \pm 3.90	8.87 \pm 3.85	0.04 \pm 0.44	0.8
Average vessel CSA (mm ²)	19.64 \pm 5.54	19.57 \pm 5.44	0.07 \pm 0.38	0.3
Average plaque CSA (mm ²)	10.73 \pm 2.29	10.70 \pm 2.12	0.03 \pm 0.44	0.1
Plaque burden (%)	56.15 \pm 7.97	56.35 \pm 8.16	0.20 \pm 1.71	0.4
Minimum lumen area (mm ²)	6.12 \pm 2.80	5.93 \pm 2.82	0.20 \pm 0.69	4.1
Minimum lumen diameter (mm)	2.72 \pm 0.64	2.63 \pm 0.67	0.09 \pm 0.24	3.7

CSA cross-sectional area, SD standard deviation

study in which the observer variability is compared with actual serial changes in atherosclerotic plaque size. The main findings of the present study were as follows: (1) the CTCA geometrical measurements were highly reproducible in both intra- and inter-observer comparisons; (2) the compositional measurements were indeed more variable

than geometrical measurements, and mostly influenced by the inter-observer variability; and (3) the intra- and inter-observer variability were lower than the detected changes in plaque burden and plaque area after 3 years.

Over the recent few years, CTCA has been more commonly used as a tool to non-invasively assess the temporal

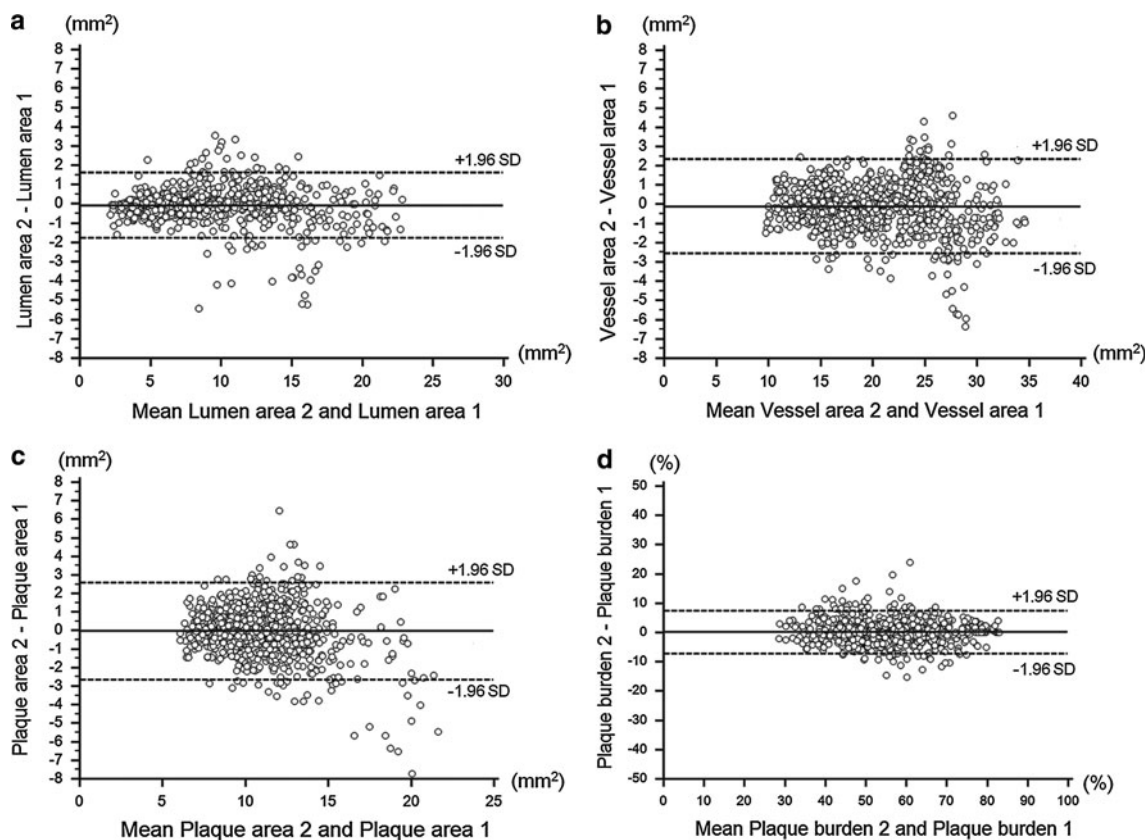


Fig. 3 Bland-Altman plots of intra-observer comparisons for lumen, vessel, plaque area and plaque burden

Table 5 Correlation between the 2 rounds of the same observer for geometrical and compositional parameters

Geometrical and compositional parameters	CCC	95 % CI
<i>(a). Cross-sectional basis</i>		
Lumen area (mm ²)	0.98	0.976–0.981
Lumen diameter (mm)	0.98	0.978–0.983
Vessel area (mm ²)	0.98	0.972–0.980
Plaque area (mm ²)	0.88	0.860–0.889
Plaque burden (%)	0.94	0.927–0.943
Maximal plaque thickness (mm)	0.79	0.762–0.810
Mean plaque attenuation (HU)	0.95	0.938–0.952
% LAP	0.82	0.798–0.840
<i>(b). Segmental basis</i>		
Mean lumen area (mm ²)	0.99	0.984–0.997
Mean vessel area (mm ²)	0.99	0.994–0.999
Mean plaque area (mm ²)	0.98	0.956–0.991
Plaque burden (%)	0.98	0.945–0.991
Minimal lumen area (mm ²)	0.97	0.923–0.987
Minimal lumen diameter (mm)	0.93	0.826–0.968
Mean plaque attenuation (HU)	0.98	0.945–0.990
% LAP	0.96	0.909–0.984

CCC concordance correlation coefficient, CI confidence interval, LAP low attenuation plaque

effect of medical therapies on coronary plaque size in longitudinal studies [4–11]. Moreover, this method has the potential to assess plaque composition and therefore to assess the effect of drug therapies on the phenotype of coronary atherosclerosis. As the impact of medical treatment on the atherosclerotic plaque size and composition over time is relatively small, highly reproducible CTCA quantitative measurements are pivotal.

Geometrical measurements

In the present study, the CTCA geometrical measurements were highly reproducible in both intra- and inter-observer comparisons. Furthermore, in comparison with IVUS studies, the CTCA reproducibility appears to be comparable or better (Table 6). This improved reproducibility could be partly attributed to the semi-automated manner of the contouring in CTCA analysis. Another important consideration is the methodology for the actual analysis, since in CTCA all frames were analyzed in a stepwise approach; first the lumen and vessel wall borders were delineated as continuous lines in the longitudinal view (L-view). These contour positions functioned as landmarks for the automated contour detection in the individual cross sections; a visual inspection was performed in every cross-section and a manual correction was applied if necessary. In contrast, in IVUS only the individual cross-sections are drawn

without the first step (i.e. longitudinal drawing). An additional issue is the fact that in CTCA all frames of the analyzed vessel are taken from the same cardiac cycle phase, whereas in IVUS this varies from cross-section to cross-section. In other words, in IVUS the frames are not only scrambled images (due to the longitudinal movement of the catheter inside the vessel), but also they are taken at fixed distances (i.e. 0.5–1.0 mm) irrespective of the cardiac cycle phase.

The moderate concordance correlation coefficient between observers for the maximal wall thickness can be mostly attributed to the fact that this parameter depends highly on the shape of the lumen and vessel contour; a small “bump” in one of the contours would not cause a large difference in the area measurement but could substantially influence the plaque thickness.

Compositional measurements

Regarding the plaque composition, overall the differences of the average plaque attenuation between observers were very small on the cross-sectional and segment level analyses. Despite this finding, the %LAP (<30 HU) showed a relatively high inter-observer variability of 12 %, which is of major significance since the temporal change of such component could potentially become an imaging endpoint of longitudinal studies. The LAP is probably the most clinically relevant component of coronary plaques as it has been shown to correlate closely with plaques of low echogenicity (presumably lipid rich) on IVUS [18] and to have prognostic value for the development of acute coronary syndromes [19]. On the other hand, the intra-observer variability for %LAP was low (median 3 % approximately), which underlines the fact that the position of the plaque contours can play a detrimental role in the distribution of attenuation values. Small differences in the lumen or vessel wall delineation would not dramatically influence the geometrical measurements, but they could result in much bigger differences in the compositional measurements due to partial volume, i.e. in case part of the lumen or the pericoronary fat is incorrectly included in the plaque area.

Implications for the design of longitudinal studies

In the present study, the observer variability was lower than the serial changes in plaque burden—the most common endpoint in IVUS progression/regression studies. This finding suggests that CTCA data analysis using semiautomated software can detect changes in atherosclerotic plaque size beyond the observer bias. Certainly, the best approach is that the same analyst analyzes in a blind fashion both the baseline and follow-up CTCA images,

Table 6 Observer variability for the assessment of plaque in IVUS studies

Author	Inter-observer variability (difference %)		Intra-observer variability (difference %)	
	Plaque area	Plaque burden	Plaque area	Plaque burden
Rodriguez-Granillo [20]	10.30	9.50	–	–
Hartmann [21]	0.89	0.20	0.35	0.04
Heo [22]	2.50	1.90	1.60	0.80
Present study	2.22	1.63	0.16	0.40

IVUS intravascular ultrasound

since the difference is much lower in the intra-observer comparison for both the cross-sectional and segment based analyses than in the inter-observer comparison; more importantly, for the compositional measurements only the intra-observer variability was below the generally acceptable threshold of 10 %.

It should be noted that the present study was conducted on a population with mild-to-moderately diseased arteries receiving contemporary medical therapy. This was driven by the intention to study the reproducibility of this quantitative method on patients that would be the most suitable candidates for serial assessment of atherosclerosis in the “real life”; since the severe lesions would have been treated with percutaneous coronary intervention, the efficacy of the statin therapy would be monitored mainly in the untreated, mild-to-moderately diseased atherosclerotic arteries.

Limitations

The studied population was small in terms of patients included; nevertheless the geometric and compositional analysis was performed on 945 matched cross-sections. Furthermore, our analysis was restricted to good quality images, which is a prerequisite for such precise CTCA quantitative analysis. We did not control for patients’ characteristics in the 3 year longitudinal study. Finally, the analyzed vessels belong to a cohort of patients with mild-to-moderately diseased arteries, thus our results may not apply to other patient populations with different extent of disease; however the patients used for this study would mostly benefit from the serial assessment of atherosclerosis.

Conclusions

Considering the small changes in atherosclerotic plaque over time, reproducibility of measurements is paramount for the validity of longitudinal studies. The present study

shows that the geometrical assessment of coronary atherosclerosis by CTCA is highly reproducible within and between observers using semiautomated quantification software. The compositional measurements were more variable than geometrical measurements, especially between different observers. The absolute observer variability was lower than the absolute detected serial changes in plaque burden and plaque area after 3 years.

Conflict of interest None.

References

1. Smith SC Jr, Jackson R, Pearson TA, Fuster V, Yusuf S, Fergeman O, Wood DA, Alderman M, Horgan J, Home P, Hunn M, Grundy SM (2004) Principles for national and regional guidelines on cardiovascular disease prevention: a scientific statement from the World Heart and Stroke Forum. *Circulation* 109(25):3112–3121. doi:10.1161/01.CIR.0000133427.35111.67
2. de Feyter PJ, Serruys PW, Davies MJ, Richardson P, Lubsen J, Oliver MF (1991) Quantitative coronary angiography to measure progression and regression of coronary atherosclerosis. Value, limitations, and implications for clinical trials. *Circulation* 84(1): 412–423
3. Mintz GS, Garcia-Garcia HM, Nicholls SJ, Weissman NJ, Bruining N, Crowe T, Tardif JC, Serruys PW (2011) Clinical expert consensus document on standards for acquisition, measurement and reporting of intravascular ultrasound regression/progression studies. *EuroIntervention* 6(9):1123–1130, 1129. doi:10.4244/EIJV6I9A195
4. Burgstahler C, Reimann A, Beck T, Kuettner A, Baumann D, Heuschmid M, Brodoefel H, Claussen CD, Kopp AF, Schroeder S (2007) Influence of a lipid-lowering therapy on calcified and noncalcified coronary plaques monitored by multislice detector computed tomography: results of the New Age II Pilot Study. *Invest Radiol* 42(3):189–195. doi:10.1097/01.ri.0000254408.96355.85
5. Uehara M, Funabashi N, Mikami Y, Shiina Y, Nakamura K, Komuro I (2008) Quantitative effect of atorvastatin on size and content of non-calcified plaques of coronary arteries 1 year after atorvastatin treatment by multislice computed tomography. *Int J Cardiol* 130(2):269–275. doi:10.1016/j.ijcard.2007.07.013
6. Schmid M, Achenbach S, Ropers D, Komatsu S, Ropers U, Daniel WG, Pflederer T (2008) Assessment of changes in non-calcified atherosclerotic plaque volume in the left main and left anterior descending coronary arteries over time by 64-slice computed tomography. *Am J Cardiol* 101(5):579–584. doi:10.1016/j.amjcard.2007.10.016
7. Lehman SJ, Schlett CL, Bamberg F, Lee H, Donnelly P, Shturman L, Krieger MF, Brady TJ, Hoffmann U (2009) Assessment of coronary plaque progression in coronary computed tomography angiography using a semiquantitative score. *JACC Cardiovasc Imaging* 2(11):1262–1270. doi:10.1016/j.jcmg.2009.07.007
8. Hoffmann H, Frieler K, Schlattmann P, Hamm B, Dewey M (2010) Influence of statin treatment on coronary atherosclerosis visualised using multidetector computed tomography. *Eur Radiol* 20(12):2824–2833. doi:10.1007/s00330-010-1880-x
9. Inoue K, Motoyama S, Sarai M, Sato T, Harigaya H, Hara T, Sanda Y, Anno H, Kondo T, Wong ND, Narula J, Ozaki Y (2010) Serial coronary CT angiography-verified changes in plaque characteristics as an end point: evaluation of effect of statin intervention. *JACC Cardiovasc Imaging* 3(7):691–698. doi:10.1016/j.jcmg.2010.04.011

10. Tardif JC, L'Allier PL, Ibrahim R, Gregoire JC, Nozza A, Cossette M, Kouz S, Lavoie MA, Paquin J, Brotz TM, Taub R, Pressacco J (2010) Treatment with 5-lipoxygenase inhibitor VIA-2291 (Atreleuton) in patients with recent acute coronary syndrome. *Circ Cardiovasc Imaging* 3(3):298–307. doi:[10.1161/CIRCIMAGING.110.937169](https://doi.org/10.1161/CIRCIMAGING.110.937169)
11. Papadopoulou SL, Neeffjes LA, Garcia-Garcia HM, Flu WJ, Rossi A, Dharampal AS, Kitslaar PH, Mollet NR, Veldhof S, Nieman K, Stone GW, Serruys PW, Krestin GP, de Feyter PJ (2012) Natural history of coronary atherosclerosis by multislice computed tomography. *JACC Cardiovasc Imaging* 5(3 Suppl):S28–S37. doi:[10.1016/j.jcmg.2012.01.009](https://doi.org/10.1016/j.jcmg.2012.01.009)
12. Nissen SE, Nicholls SJ, Sipahi I, Libby P, Raichlen JS, Ballantyne CM, Davignon J, Erbel R, Fruchart JC, Tardif JC, Schoenhagen P, Crowe T, Cain V, Wolski K, Goormastic M, Tuzcu EM (2006) Effect of very high-intensity statin therapy on regression of coronary atherosclerosis: the ASTEROID trial. *JAMA* 295(13):1556–1565. doi:[10.1001/jama.295.13.jpc60002](https://doi.org/10.1001/jama.295.13.jpc60002)
13. Bongartz G, Golding SJ, Jurik AG, Leonardi M, van Persijn van Meerten E, Rodríguez R, Schneider K, Calzado A, Geleijns J, Jessen KA, Panzer W, Shrimpton PC, Tosi G (2004) CT quality criteria—appendix C. European Guidelines for Multislice Computed Tomography, European Commission. Available at: http://www.msct.eu/CT_Quality_Criteria.htm
14. Boogers MJ, Broersen A, van Velzen JE, de Graaf FR, El-Naggar HM, Kitslaar PH, Dijkstra J, Delgado V, Boersma E, de Roos A, Schuijf JD, Schalij MJ, Reiber JH, Bax JJ, Jukema JW (2012) Automated quantification of coronary plaque with computed tomography: comparison with intravascular ultrasound using a dedicated registration algorithm for fusion-based quantification. *Eur Heart J* 33(8):1007–1016. doi:[10.1093/eurheartj/ehr465](https://doi.org/10.1093/eurheartj/ehr465)
15. Austen WG, Edwards JE, Frye RL, Gensini GG, Gott VL, Griffith LS, McGoon DC, Murphy ML, Roe BB (1975) A reporting system on patients evaluated for coronary artery disease. Report of the Ad Hoc Committee for Grading of Coronary Artery Disease, Council on Cardiovascular Surgery, American Heart Association. *Circulation* 51(4 Suppl):5–40
16. Lin LI (1989) A concordance correlation coefficient to evaluate reproducibility. *Biometrics* 45(1):255–268
17. Bland JM, Altman DG (1986) Statistical methods for assessing agreement between two methods of clinical measurement. *Lancet* 1(8476):307–310
18. Motoyama S, Kondo T, Anno H, Sugiura A, Ito Y, Mori K, Ishii J, Sato T, Inoue K, Sarai M, Hishida H, Narula J (2007) Atherosclerotic plaque characterization by 0.5-mm-slice multislice computed tomographic imaging. *Circ J* 71(3):363–366
19. Motoyama S, Sarai M, Harigaya H, Anno H, Inoue K, Hara T, Naruse H, Ishii J, Hishida H, Wong ND, Virmani R, Kondo T, Ozaki Y, Narula J (2009) Computed tomographic angiography characteristics of atherosclerotic plaques subsequently resulting in acute coronary syndrome. *J Am Coll Cardiol* 54(1):49–57. doi:[10.1016/j.jacc.2009.02.068](https://doi.org/10.1016/j.jacc.2009.02.068)
20. Rodriguez-Granillo GA, Vaina S, Garcia-Garcia HM, Valgimigli M, Duckers E, van Geuns RJ, Regar E, van der Giessen WJ, Bressers M, Goedhart D, Morel MA, de Feyter PJ, Serruys PW (2006) Reproducibility of intravascular ultrasound radiofrequency data analysis: implications for the design of longitudinal studies. *Int J Cardiovasc Imaging* 22(5):621–631. doi:[10.1007/s10554-006-9080-0](https://doi.org/10.1007/s10554-006-9080-0)
21. Hartmann M, Mattern ES, Huisman J, van Houwelingen GK, de Man FH, Stoel MG, Danse PW, Louwerenburg HW, von Birgelen C (2009) Reproducibility of volumetric intravascular ultrasound radiofrequency-based analysis of coronary plaque composition in vivo. *Int J Cardiovasc Imaging* 25(1):13–23. doi:[10.1007/s10554-008-9338-9](https://doi.org/10.1007/s10554-008-9338-9)
22. Heo JH, Brugaletta S, Garcia-Garcia HM, Gomez-Lara J, Ligthart JM, Witberg K, Magro M, Shin ES, Serruys PW (2011) Reproducibility of intravascular ultrasound iMAP for radiofrequency data analysis: implications for design of longitudinal studies. *Catheter Cardiovasc Interv*. doi:[10.1002/ccd.23335](https://doi.org/10.1002/ccd.23335)

Chapter 4

Natural History of Coronary Atherosclerosis by Multislice Computed Tomography: the PROSPECT study.

JACC Cardiovasc Imaging. 2012 Mar;5(3 Suppl):S28-37.

S.L. Papadopoulou, L.A. Neefjes, H.M. Garcia-Garcia, W-J Flu, A. Rossi, A.S. Dharampal, P.H. Kitslaar, N.R. Mollet, S. Veldhof, K. Nieman, G.W. Stone, P.W. Serruys, G.P. Krestin, P.J. de Feyter

Natural History of Coronary Atherosclerosis by Multislice Computed Tomography

Stella-Lida Papadopoulou, MD,*† Lisan A. Neefjes, MD,*† Hector M. Garcia-Garcia, MD, PhD,* Willem-Jan Flu, MD, PhD,‡ Alexia Rossi, MD,*† Anoeshka S. Dharampal, MD,*† Pieter H. Kitslaar, MSc,§ Nico R. Mollet, MD, PhD,† Susan Veldhof, RN,|| Koen Nieman, MD, PhD,*† Gregg W. Stone, MD,¶ Patrick W. Serruys, MD, PhD,* Gabriel P. Krestin, MD, PhD,† Pim J. de Feyter, MD, PhD*†

Rotterdam and Leiden, the Netherlands; Diegem, Belgium; and New York, New York

OBJECTIVES This study sought to analyze the natural history of coronary atherosclerosis by multislice computed tomography (MSCT) and assess the serial changes in coronary plaque burden, lumen dimensions, and arterial remodeling.

BACKGROUND MSCT can comprehensively assess coronary atherosclerosis by combining lumen and plaque size parameters.

METHODS Thirty-two patients with acute coronary syndromes underwent 64-slice computed tomography angiography after percutaneous coronary intervention at baseline and after a median of 39 months. All patients received contemporary medical treatment. All available coronary segments in every subject were analyzed. The progression of atherosclerosis per segment and per patient was assessed by means of change in percent atheroma volume (PAV), change in normalized total atheroma volume (TAVnorm), and percent change in TAV (% change in TAV). Serial coronary remodeling was also assessed. Measures of lumen stenosis included percent diameter stenosis (%DS), minimum lumen diameter (MLD), percent area stenosis (%AS), and minimum lumen area (MLA). For each patient, the mean of all matched segments was calculated at the 2 time points. Clinical events at follow-up were documented.

RESULTS The PAV did not change significantly ($-0.15 \pm 3.64\%$, $p = 0.72$). The mean change in TAVnorm was $47.36 \pm 143.24 \text{ mm}^3$ ($p = 0.071$), and the % change in TAV was 6.7% ($p = 0.029$). The MLD and MLA increased by 0.15 mm (-0.09 to 0.24, $p = 0.039$) and 0.52 mm^2 (-0.38 to 1.04, $p = 0.034$) respectively, which was accompanied by vessel enlargement, with 53% of the patients showing expansive positive remodeling. Patients with clinical events had a larger TAVnorm at baseline (969.72 mm^3 vs. 810.77 mm^3 , $p = 0.010$).

CONCLUSIONS MSCT can assess the progression of coronary atherosclerosis and may be used for noninvasive monitoring of pharmacological interventions in coronary artery disease. (PROSPECT: An Imaging Study in Patients With Unstable Atherosclerotic Lesions; NCT00180466) (J Am Coll Cardiol Img 2012;5:528–37) © 2012 by the American College of Cardiology Foundation

Coronary atherosclerosis is a worldwide pandemic disease and accounts for almost 17 million deaths annually (1). Although quantitative coronary angiography (QCA) has been used in the past to study the extent of the disease (2), this technique can only depict the contrast-enhanced lumen, whereas atherosclerotic disease of the arterial wall does not necessarily result in narrowing of the vessel lumen. Currently, the preferred method to study atherosclerosis is by intracoronary, cross-sectional imaging methods, such as intravascular ultrasound (IVUS) (3). There are numerous serial studies on atherosclerosis progression/regression by QCA and IVUS, including randomized medical trials using imaged plaque modification as surrogate endpoints. However, QCA and IVUS are invasive and costly and are not free of complications and thus are not used for routine serial assessment of atherosclerosis.

On the other hand, multislice computed tomography (MSCT) can assess coronary plaque in a noninvasive manner. MSCT coronary angiography has emerged as a noninvasive technique for the detection of coronary artery disease and has demonstrated good accuracy for the detection of coronary artery stenosis (4,5). Furthermore, studies in patients undergoing both IVUS and MSCT support the feasibility of MSCT to assess atherosclerotic plaque burden, remodeling, eccentricity, and calcified and noncalcified plaque in both stable and unstable patients (6–8).

Although a few serial studies with MSCT have been published (9–15), most prior analyses were confined to a small segment of the coronary tree or a specific subset of lesions (i.e., noncalcified). In the present study, our objective was to study the natural history of coronary atherosclerosis along the full length of the coronary tree by MSCT and to assess the serial changes in coronary plaque size, lumen dimensions, and arterial remodeling.

METHODS

Study population. We prospectively included patients who were enrolled at the Erasmus Medical Center in the PROSPECT (Providing Regional Observations to Study Predictors of Events in the Coronary Tree) study (16). PROSPECT was designed to identify nonobstructing lesions with an increased risk for future acute coronary events in patients presenting with acute coronary syndromes (ACS) using IVUS and serological markers of inflammation. ACS was defined as ST-segment

elevation myocardial infarction, non-ST-segment elevation myocardial infarction (troponin positive), or unstable angina with ECG changes (troponin negative). As a substudy of the multicenter study, we additionally performed contrast-enhanced computed tomography (CT) coronary angiography to noninvasively evaluate the extent of coronary atherosclerosis at baseline and at 3 years' follow-up. Patients were considered for inclusion in the MSCT substudy only if they had a heart rate lower than 70 beats/min during the MSCT acquisition and had no prior coronary bypass surgery. Exclusion criteria included impaired renal function (serum creatinine >120 mmol/l), contrast allergy, and irregular heart rhythms. Levels of fasting lipids were measured at baseline and follow-up. Medication use (including statins) after discharge was according to standard of care. The institutional review board of our hospital approved the study, and all patients provided written informed consent before study participation.

MSCT acquisition. At baseline, all patients underwent CT coronary angiography with a 64-slice scanner (Sensation 64, Siemens Medical Solutions, Forchheim, Germany). Because patients in the acute phase of ACS were already treated with intravenous nitrates and beta-blockers, additional medication before CT scan was not necessary. Scan parameters were as follows: a gantry rotation time of 330 ms, 32 × 2 slices per rotation, 0.6-mm detector collimation, spiral scan mode with a table feed of 3.8 mm per rotation, a tube voltage of 120 kV, and tube current of 900 effective mAs. Prospective ECG-triggered x-ray tube modulation was not applied. A bolus of 100 ml of contrast material (400 mg/ml; Iomeron, Bracco, Milan, Italy) was injected intravenously at 5 ml/s flow rate followed by a saline chaser. The initiation of the scan was synchronized to the arrival of contrast in the coronary arteries by a bolus-tracking technique. The mean effective radiation dose was 14.0 ± 0.8 mSv, using the dose-length product and a conversion factor k (0.014 mSv/mGy/cm) (17). Axial CT images were reconstructed with a slice thickness of 0.75-mm and 0.4-mm increments using a retrospective ECG gating algorithm to obtain optimal, motion-free image quality. Optimal datasets with the best image quality were reconstructed mainly in the mid- to end-diastolic phase, using a medium-smooth convolution kernel.

ABBREVIATIONS AND ACRONYMS

ACS	= acute coronary syndrome
AS	= area stenosis
CT	= computed tomography
DS	= diameter stenosis
ECG	= electrocardiogram
IQR	= interquartile range
IVUS	= intravascular ultrasound
LDL	= low-density lipoprotein
MLA	= minimum lumen area
MLD	= minimum lumen diameter
MSCT	= multislice computed tomography
PAV	= percent atheroma volume
QCA	= quantitative coronary angiography
TAV	= total atheroma volume

The follow-up scan was performed after 3 years, using a 64-slice dual-source CT scanner (Somatom Definition, Siemens Medical Solutions, Forchheim, Germany). Sublingual nitroglycerin was administered before the scan (0.4 mg/dose) provided that there were no contraindications, and pre-scan beta-blockers were given to patients with high heart rates >70 beats/min. The CT angiographic scan parameters were as follows: $32 \times 2 \times 0.6$ mm collimation with z-flying focal spot for both detectors, gantry rotation time of 330 ms, tube voltage of 120 kV, and tube current of 320 to 412 mAs per rotation. A bolus of iodinated contrast material (370 mg/ml; Ultravist, Schering, Berlin, Germany), which varied between 60 and 100 ml, depending on the expected scan time, was injected intravenously (flow rate 5.5 ml/s) followed by a 40-ml saline chaser at the same injection rate. A bolus tracking technique was used to synchronize the arrival of contrast in the coronary arteries and the start of the acquisition. A spiral scan protocol with prospective ECG-triggered x-ray tube modulation and variable table feed depending on the heart rate was applied. The estimated mean effective radiation dose was 10.0 ± 3.2 mSv. Axial images were reconstructed using retrospective ECG gating, with a slice thickness of 0.75-mm, slice increment of 0.4-mm, and medium-to-

smooth convolution kernel. Optimal datasets with the best image quality were reconstructed mainly in the mid- to end-diastolic phase.

MSCT analysis. All datasets were transferred to an offline workstation for analysis using a semiautomated plaque analysis software (QAngioCT Research Edition version 1.1.8, Medis Medical Imaging Systems, Leiden, the Netherlands) (18). An experienced observer blinded to the sequence of imaging evaluated the scans. Planimetry of the inner lumen and outer vessel areas was performed following a stepwise approach. First, a centerline originating from the ostium was automatically extracted; then straightened multiplanar reformatted images were generated, and the lumen and vessel borders were detected longitudinally on 4 different vessel views by the software. On the basis of these longitudinal contours, cross-sectional images at 0.5-mm intervals were calculated in order to create transversal lumen and vessel wall contours, which were examined and, if necessary, adjusted by an experienced observer (Fig. 1). The settings for window level and width were fixed at 740 HU and 220 HU, respectively. Gradient magnitude images, which are derived from the MSCT images and display the degree of CT density change, were used

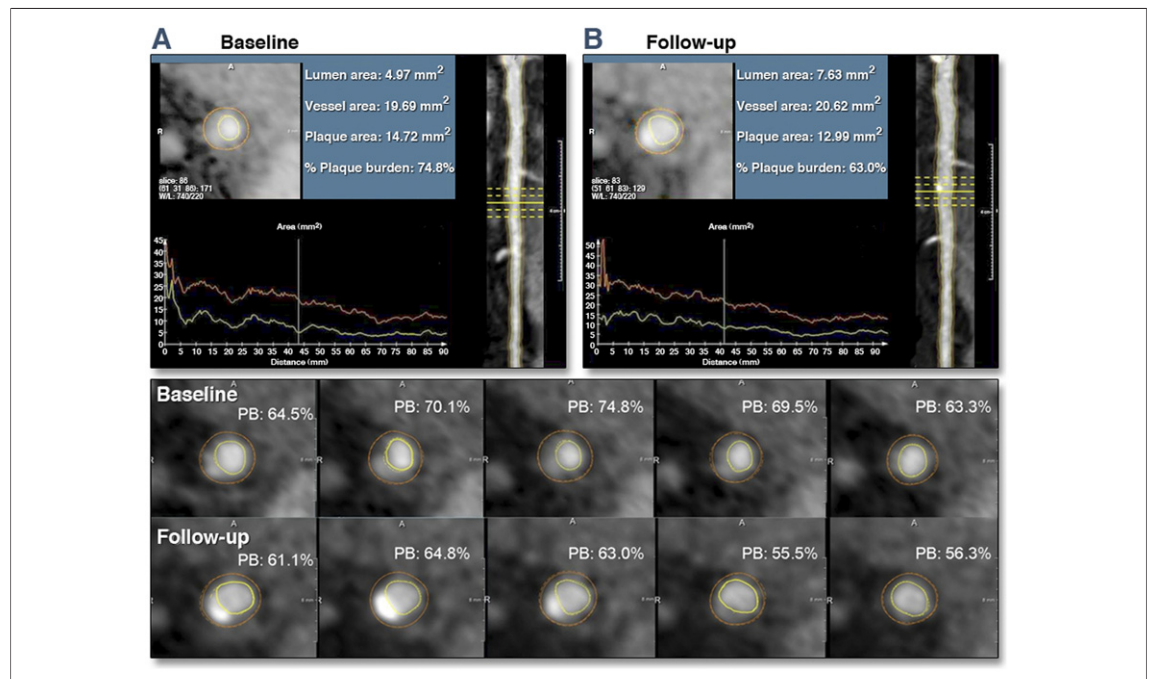


Figure 1. Multislice Computed Tomography Angiography Analysis

Example of vessel analyzed at baseline (A) and 3-year follow-up (B). In both panels, 5 lines indicate the location in the vessel of the cross-sections shown at the bottom of the figure (from proximal to distal). In this lesion, the plaque burden (PB, %) decreases consistently from baseline to follow-up in the 5 cross-sections analyzed.

to facilitate detection of lumen and vessel wall borders.

All 3 vessels were assessed in every patient using the modified 17-segment American Heart Association model for coronary segment classification (19). Only the major epicardial vessels were considered for analysis (segments 1, 2, 3, 6, 7, 8, 11, 13, and 15). All anatomically available segments without implanted stents were examined; the segments of poor quality due to stack or movement artifacts or extreme calcification were excluded from analysis, as well as the segments distal to stents.

The following parameters were derived per segment: the mean lumen area, the mean vessel area, the mean percent plaque burden, the minimum and maximum lumen diameter, and the minimum and maximum lumen area. The mean areas were the averaged measurements of all cross-sections for each segment. The mean plaque area was calculated by subtracting mean lumen area from mean vessel area, and the plaque volume was calculated for every segment by using the mean segment length from the 2 time points (3). Furthermore, the composition of each coronary segment was semiquantitatively evaluated: Each individual cross-section was binary labeled for the presence of calcium (yes/no), and the degree of calcification was assessed as a percent of the segment length (number of frames containing calcium/total number of frames in the segment). To examine inter- and intra-observer variability, a second reader re-analyzed 7 randomly selected segments, and the first reader re-analyzed 11 randomly selected segments 3 months after his/her original analysis.

Study imaging endpoints. The following parameters were calculated per segment and per patient.

QCA-LIKE PARAMETERS

Minimum lumen diameter (MLD): the narrowest lumen diameter within each segment

Percent diameter stenosis (%DS): $[(\text{reference diameter} - \text{MLD})/\text{reference diameter}] \times 100\%$. The reference diameter was the largest (maximal) lumen diameter within each segment.

For each patient, the average %DS of all segments at baseline and follow-up was calculated. From these values, the change from baseline was calculated for each patient. In addition, the per-patient average of MLD (mm) of all segments was calculated at baseline and at follow-up for the matching segments. The average change in MLD at baseline was calculated for each patient using these values. Clinically relevant regression or progression was defined as a nominal change (from

baseline to 3 years) of 10% for %DS and 0.2 mm for MLD (20).

IVUS-LIKE PARAMETERS

Percent atheroma volume (PAV): $[(\text{total vessel volume} - \text{total lumen volume})/\text{total vessel volume}] \times 100\%$

Total atheroma volume (TAV): total vessel volume – total lumen volume

Normalized TAV (TAV_{norm}): $[(\text{total vessel volume} - \text{total lumen volume})/\text{segment length}] \times \text{mean segment length in the population}$. Normalization for segment length provides equal weighting of each patient in the calculation of atheroma volume (3).

Percentage change in TAV (% change in TAV): $[(\text{TAV follow-up} - \text{TAV baseline})/\text{TAV baseline}] \times 100\%$

Minimum lumen area (MLA): the narrowest lumen area in each segment

Percent area stenosis (%AS): $[(\text{reference lumen area} - \text{MLA})/\text{reference lumen area}] \times 100$. The reference lumen area used was the largest (maximal) lumen area within each segment.

For each patient, the average %AS of all segments at baseline and follow-up was calculated. From these values, the change from baseline was calculated for each patient. Also, the per-patient average of MLA (mm²) of all segments was calculated at baseline and at follow-up for the corresponding segments. The average change in MLA from baseline was calculated for each patient using these values.

Clinically relevant regression or progression in PAV was defined as a change (from baseline to follow-up) of >1% for PAV, which was the threshold for significant regression previously detected under intensive lipid-lowering treatment (21).

Coronary remodeling. As recommended for serial studies (3), remodeling was assessed as vessel area at follow-up minus vessel area at baseline. An increase in vessel area was considered positive remodeling, no change in vessel area was considered absence of remodeling, and a decrease in vessel area was considered negative remodeling. Furthermore, segments with positive remodeling were subdivided as expansive (over-compensatory) when $\Delta\text{vessel area}/\Delta\text{atheroma} > 1$ or incomplete when $\Delta\text{vessel area}/\Delta\text{atheroma}$ was between 0 and 1.

Clinical endpoints. Clinical event data were collected throughout the duration of the study at regular follow-up intervals and registered in the hospital clinical database. Major adverse cardiovascular events were defined as the composite of cardiac

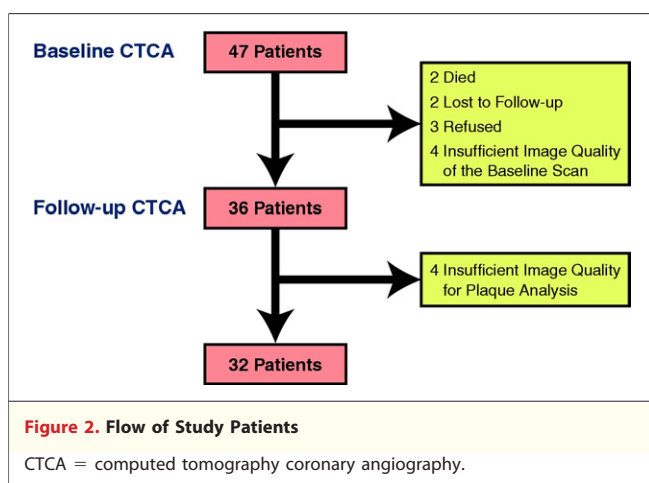
Table 1. Baseline Patient Characteristics (n = 32)

Age, yrs	53 ± 10
Male	26 (81)
Risk factors	
Hypertension	9 (28)
Hypercholesterolemia	11 (34)
Diabetes mellitus	3 (9)
Current smoking	18 (56)
Family history of coronary artery disease	19 (59)
Obesity	3 (9)
Clinical condition at enrollment	
Unstable angina	9 (28)
Acute myocardial infarction	23 (72)
Cholesterol	
Total, mg/dl	180 ± 41
Low-density lipoprotein, mg/dl	124 ± 42
High-density lipoprotein, mg/dl	43 ± 12
Triglycerides, mg/dl	139 ± 87

Values are mean ± SD or n (%).

death, cardiac arrest, myocardial infarction, and rehospitalization due to unstable or progressive angina (16).

Statistical analysis. Continuous variables are presented as mean ± SD and median (interquartile range [IQR]), as indicated. Categorical variables are presented as counts and percentages. Continuous variables between the 2 different time points were compared by the paired samples *t* test if the data were normally distributed or the Wilcoxon signed rank test for non-normal data (as tested by the Kolmogorov-Smirnov test). A *p* value <0.05 was considered significant. Statistical analyses were performed with use of SPSS version 17.0 software (SPSS, Chicago, Illinois).



RESULTS

Baseline clinical and angiographic characteristics.

From the original cohort of 47 patients undergoing baseline CTCA, 36 (77%) underwent a follow-up CTCA at 3 years. The follow-up scan was undertaken at a mean of 38 ± 3 months (median 39 months, IQR: 37 to 40 months) after the initial examination. The patients' baseline characteristics are shown in Table 1, and their disposition is shown in Figure 2. In total, 129 segments from 32 patients were analyzed. The mean length of analysis was 22.0 ± 9.5 mm per segment and 89.0 ± 40.5 mm per patient. The proportion of calcified frames per segment at baseline was 6 ± 12% versus 11 ± 17% at follow-up (*p* < 0.001).

All patients at discharge received standard-of-care medical therapy, including statins (29 patients received atorvastatin 40 mg/day, 2 patients received simvastatin 40 mg/day, and 1 patient received rosuvastatin 10 mg/day). One patient discontinued statin use due to an adverse effect. The mean total cholesterol was 180 ± 41 mg/dl at baseline and 150 ± 20 mg/dl at follow-up. The mean low-density lipoprotein (LDL) level was 124 ± 42 mg/dl at baseline and 85 ± 13 mg/dl at follow-up. The mean high-density lipoprotein level was 43 ± 12 mg/dl at baseline and 46 ± 15 mg/dl at follow-up. The mean triglycerides value was 139 ± 87 mg/dl at baseline and 114 ± 76 mg/dl at follow-up.

MSCT QCA-like analysis. MEASURES OF STENOSIS PER SEGMENT. From baseline to 3-year follow-up, there was an increase in lumen dimensions, resulting in a decrease in the relative lumen stenosis (Table 2). In particular, there was a significant increase in MLD by 0.11 mm (IQR: -0.15 to 0.27 mm; *p* = 0.010), and this was accompanied by a decrease in %DS of -1.05% (IQR -7.15% to 5.08%; *p* = 0.257).

There were no clinically relevant changes in MLD (>0.2mm) in 45.7% of the segments, whereas 32.6% segments showed regression (≥0.2-mm increase in MLD) and 21.7% showed progression (≥0.2mm decrease in MLD) (Online Appendix). There was no statistically significant difference in the prevalence of progressors and regressors.

There were also no clinically relevant changes in %DS (>10%) in most of the segments (70.5%), whereas 17.8% of the segments showed regression (≥10% decrease in %DS) and 11.6% showed progression (≥10% increase in %DS). There was no statistically significant difference in the prevalence of progressors and regressors.

Table 2. MSCT QCA-Like Analysis					
	Baseline	Follow-Up	Change	p Value	n (%) With Regression
Baseline and follow-up quantitative parameters analyzed per segment (n = 129)					
Minimum lumen diameter (mm)					82 (64)
Mean ± SD	2.49 ± 0.61	2.58 ± 0.72	0.09 ± 0.42		
Median (IQR)	2.36 (2.04–2.85)	2.41 (2.01–3.09)	0.11 (–0.15 to 0.27)	0.010*	
% Diameter stenosis					71 (55)
Mean ± SD	28.3 ± 10.0	27.6 ± 11.1	–0.68 ± 10.03		
Median (IQR)	27.6 (21.1–35.0)	26.0 (20.7–35.0)	–1.05 (–7.15 to 5.08)	0.257*	
Baseline and follow-up quantitative parameters analyzed per patient (n = 32)					
Minimum lumen diameter (mm)					23 (72)
Mean ± SD	2.51 ± 0.52	2.63 ± 0.62	0.11 ± 0.32		
Median (IQR)	2.42 (2.09–2.87)	2.47 (2.23–3.09)	0.15 (–0.09 to 0.24)	0.039*	
% Diameter stenosis					17 (53)
Mean ± SD	28.1 ± 6.6	27.0 ± 7.5	–1.13 ± 6.39	0.326†	
Median (IQR)	28.6 (23.8–32.2)	26.4 (20.4–32.2)	–0.83 (–6.30 to 3.16)		

*Wilcoxon signed rank test; †paired t test.

IQR = interquartile range; MSCT = multislice computed tomography; QCA = quantitative coronary angiography.

MEASURES OF STENOSIS PER PATIENT. Similar findings were found on a per-patient level (i.e., an increase in lumen diameter and relative decrease in stenosis). The MLD increased by 0.15 mm (IQR: –0.09 to 0.24 mm; $p = 0.039$) and the %DS decreased by 0.83% (IQR: –6.3 to 3.16; $p = 0.326$).

There were no clinically relevant changes in MLD (>0.2 mm) in 46.9% of the patients, whereas 37.5% of patients showed regression (≥ 0.2 mm increase in MLD) and 15.6% showed progression (≥ 0.2 mm decrease in MLD). There was no statistically significant difference in the prevalence of progressors and regressors.

There were also no clinically relevant changes in %DS ($>10\%$) in most of the patients (87.5%), whereas considerably fewer patients (9.4%) showed regression (≥ 10 decrease in %DS), and 3.1% showed progression ($\geq 10\%$ increase in %DS). There was no statistically significant difference in the prevalence of progressors and regressors.

MSCT IVUS-like analysis. PLAQUE VOLUMETRIC MEASURES PER SEGMENT. From baseline to 3-year follow-up, the PAV did not change significantly, whereas there was a significant relative percentage change in TAV by $5.8 \pm 18.0\%$ ($p < 0.001$) (Table 3). There were no clinically relevant changes in PAV ($>1\%$) in 24.0% of the segments, whereas 38.8% segments showed regression ($>1\%$ decrease in PAV) and 37.2% showed progression ($>1\%$ increase in PAV) (Online Appendix). There was no statistically significant difference in the prevalence of progressors and regressors.

PLAQUE VOLUMETRIC MEASURES PER PATIENT. At 3-year follow-up, there was no significant change in PAV (mean difference -0.15 ± 3.64 mm³; $p = 0.819$), whereas there was a trend toward increase in normalized TAV of 47.36 ± 143.24 mm³ ($p = 0.071$). Similarly, there was a significant percentage change in TAV by $6.7 \pm 16.6\%$ ($p = 0.029$).

There were no clinically relevant changes in PAV ($>1\%$) in 21.8% of the patients, whereas 34.4% patients showed regression ($>1\%$ decrease in PAV) and 43.8% showed progression ($>1\%$ increase in PAV). There was no statistically significant difference in the prevalence of progressors and regressors.

CORONARY REMODELING. Overall, the plaque increase occurred without compromising the lumen and was compensated for by an increase in vessel size (mostly expansive positive remodeling) (Table 4). Approximately one third of the patients/segments showed negative remodeling.

Clinical events. There were 8 clinical events in this cohort during the length of the study. Five events were related to the stented segment (3 patients with stent thrombosis, myocardial infarction, and repeat revascularization and 2 with repeat revascularization with angina), and the other 3 patients developed progressive angina. Of note, these patients presenting with clinical events had larger normalized TAV at baseline (969.72 vs. 810.77 mm³; $p = 0.010$). We found no difference between patients with and without events regarding plaque progression (i.e., change from baseline in PAV or TAV).

Table 3. MSCT IVUS-Like Analysis					
	Baseline	Follow-Up	Change	p Value	n (%) With Regression
Baseline and follow-up plaque quantitative parameters analyzed per segment (n = 129)					
Percent atheroma volume (%)					59 (46)
Mean ± SD	56.7 ± 7.3	56.7 ± 7.7	-0.07 ± 4.34		
Median (IQR)	58.0 (52.0–63.0)	58.0 (51.0–62.0)	0.0 (-3.0 to 3.0)	0.790*	
Total atheroma volume (mm ³)					49 (38)
Mean ± SD	217.2 ± 134.0	224.7 ± 136.9	7.52 ± 42.54		
Median (IQR)	183.4 (130.2–280.0)	194.2 (129.6–274.4)	7.08 (-14.38 to 29.01)	0.019*	
% Change in total atheroma volume					49 (38)
Mean ± SD			5.84 ± 17.98	<0.001‡	
Median (IQR)			4.55 (-4.27 to 20.96)		
Baseline and follow-up lumen quantitative parameters analyzed per segment (n = 129)					
Minimum lumen area (mm ²)					82 (64)
Mean ± SD	5.16 ± 2.68	5.65 ± 3.21	0.49 ± 1.84		
Median (IQR)	4.38 (3.27–6.34)	4.55 (3.17–7.49)	0.44 (-0.73 to 1.15)	0.009*	
% Area stenosis					70 (54)
Mean ± SD	47.6 ± 14.1	46.4 ± 15.2	-1.18 ± 13.86	0.336†	
Median (IQR)	47.8 (37.4–57.9)	44.8 (37.1–57.6)	-1.58 (-10.6 to 7.3)		
Baseline and follow-up plaque quantitative parameters analyzed per patient (n = 32)					
Percent atheroma volume (%)					15 (47)
Mean ± SD	56.0 ± 7.0	55.9 ± 7.3	-0.15 ± 3.64	0.819†	
Median (IQR)	56.6 (50.0–61.5)	57.9 (50.4–61.3)	0.72 (-2.75 to 2.41)		
Normalized total atheroma volume (mm ³)					11 (34)
Mean ± SD	850.5 ± 155.7	897.9 ± 175.4	7.36 ± 143.24	0.071†	
Median (IQR)	833.7 (753.4–930.1)	892.0 (736.0–993.1)	31.39 (-42.08 to 163.06)		
% Change in total atheroma volume					11 (34)
Mean ± SD			6.7 ± 16.55	0.029‡	
Median (IQR)			3.54 (-4.27 to 20.96)		
Baseline and follow-up lumen quantitative parameters analyzed per patient (n = 32)					
Minimum lumen area (mm ²)					22 (69)
Mean ± SD	5.26 ± 2.26	5.83 ± 2.78	0.57 ± 1.43		
Median (IQR)	4.66 (3.48–6.66)	4.84 (3.98–7.73)	0.52 (-0.38 to 1.04)	0.034*	
% Area stenosis					17 (53)
Mean ± SD	47.3 ± 9.4	45.5 ± 10.6	-1.72 ± 8.96	0.286†	
Median (IQR)	48.5 (41.8–43.5)	45.5 (36.5–52.8)	-0.68 (-9.31 to 3.92)		

*Wilcoxon signed rank test; †paired t test; ‡1-sample t test.
IVUS = intravascular ultrasound; other abbreviations as in Table 2.

Observer variability. For the 11 segments included in the intra-observer analysis, there were a total of 523 cross-sections analyzed. The mean differences were small for both lumen ($-0.16 \pm 0.93 \text{ mm}^2$) and vessel areas ($-0.11 \pm 1.17 \text{ mm}^2$). The correlations between the original and subsequent analysis were high ($r = 0.98$ for lumen areas, $r = 0.98$ for vessel areas). For the 7 segments included in the inter-observer analysis, there were a total of 335 cross-sections analyzed. The mean differences were also small for both lumen ($0.01 \pm 1.19 \text{ mm}^2$) and

vessel areas ($-0.08 \pm 1.31 \text{ mm}^2$). Close correlations between the original analysis and re-analysis were found ($r = 0.97$ for lumen, $r = 0.98$ for vessel areas). The repeatability results are very much in line with previous IVUS reports.

DISCUSSION

The purpose of this exploratory substudy was to assess the natural history of coronary atherosclerosis by MSCT in patients with an ACS who were

Table 4. Coronary Remodeling Endpoints	
Per segment (n = 129)	
Serial remodeling (mm ²)	0.82 ± 2.83*
Positive remodeling	
Expansive	61 (47)
Incomplete	23 (18)
Negative remodeling	45 (35)
Per patient (n = 32)	
Serial remodeling (mm ²)	1.10 ± 2.68†
Positive remodeling	
Expansive	17 (53)
Incomplete	6 (19)
Negative remodeling	9 (28)
Values are mean ± SD and n (%). *p = 0.001; †p = 0.027.	

treated with percutaneous coronary intervention and contemporary medical therapy.

The main findings of this report are as follows: despite standard-of-care treatment, the atheroma size in untreated non-culprit lesions increased over 3 years, compensated for by an increase in the vessel size (positive expansive remodeling) and without compromising the lumen. Our MSCT findings on atherosclerosis progression fit closely to the regres-

sion line of the relationship between mean LDL under treatment and median change in PAV from previous IVUS studies (Fig. 3).

Plaque burden and coronary events. IVUS studies (28) have demonstrated that there is a direct association between the burden of coronary atherosclerosis, its progression, and the presence of clinical events at follow-up. Similarly, in the main PROSPECT study, lesions with plaque burden >70% were shown to be strongly associated with future clinical events (16). Our data are in accordance with these findings, because the patients presenting with clinical events had greater amount of plaque at baseline. This observation could contribute to the potential development of prediction models based on atherosclerotic plaque burden.

Coronary remodeling. Motoyama et al. (29) and Hoffmann et al. (6) described that the plaques in patients with ACS have positive remodeling and are associated with events. Consistent with the original description by Glagov et al. (30), our MSCT data showed that arteries enlarge as atherosclerosis progresses. Previous serial IVUS reports have demonstrated that atheroma burden does not limit com-

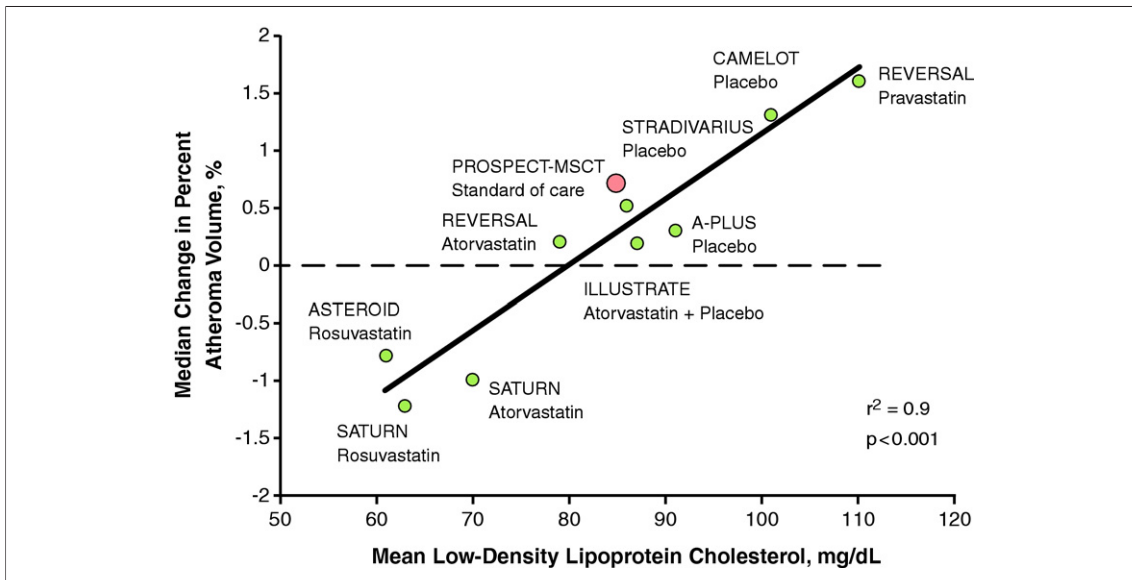


Figure 3. Association Between Mean Low-Density Lipoprotein Cholesterol Levels and Median Change in Percent Atheroma Volume for Several Intravascular Ultrasound Studies

A-Plus = Avasimibe and Progression of Lesions on Ultrasound (22); ASTEROID = A Study to Evaluate the Effect of Rosuvastatin on Intravascular Ultrasound-Derived Coronary Atheroma Burden (21); CAMELOT = Comparison of Amlodipine vs. Enalapril to Limit Occurrences of Thrombosis (23); ILLUSTRATE = Investigation of Lipid Level Management Using Coronary Ultrasound to Assess Reduction of Atherosclerosis by CETP Inhibition and HDL Elevation (24); REVERSAL = Reversal of Atherosclerosis With Aggressive Lipid-Lowering (25); SATURN = Study of Coronary Atheroma by Intravascular Ultrasound: Effect of Rosuvastatin versus Atorvastatin (26); STRADIVARIUS = Strategy to Reduce Atherosclerosis Development Involving Administration of Rimobant—The Intravascular Ultrasound Study (27); PROSPECT = Providing Regional Observations to Study Predictors of Events in the Coronary Tree (multislice computed tomography substudy). Modified from Nissen et al. (21).

pensatory remodeling (31), whereas there is a broad spectrum of serial remodeling responses in coronary atherosclerosis (32,33).

Importantly, arterial remodeling changes closely relate to changes in PAV, which is the most common primary IVUS endpoint. In the absence of actual change in plaque volume, positive remodeling could reduce PAV, whereas negative remodeling would increase PAV.

Progression/regression analysis using MSCT. MSCT can assess coronary atherosclerosis by combining the 2 “worlds” of QCA-like and IVUS-like parameters. To our knowledge, this comprehensive approach used in our study was not performed in previous MSCT studies. Furthermore, the follow-up time of our report (median 39 months) is the longest duration to date reported in progression/regression studies.

Previous papers have shown that MSCT is comparable to QCA angiography regarding lumen stenosis assessment (4,5); similarly, IVUS and MSCT comparative studies (6–8) have shown that the MSCT can reasonably evaluate atherosclerotic plaque size, remodeling, eccentricity, and composition, despite the acknowledged limitations of the technique. Voros et al. (8) suggested that quantitative MSCT angiography could be acceptably used in population-based approaches, given the small mean differences between MSCT and IVUS-virtual histology measurements.

Interestingly, our results closely fit the regression line in the classical graph depicting the relation between mean LDL levels and median change in PAV for several previous IVUS progression/regression studies.

Most prior IVUS studies have used PAV as the primary endpoint; however, the percentage change in TAV may be more suitable for MSCT studies, because not only 1 coronary segment can be imaged,

but the full coronary tree can be assessed. Conversely, considering the resolution and reproducibility of MSCT, the minute changes in PAV observed in IVUS studies may be more difficult to detect.

Study limitations. This is a single-center feasibility study that comprised a selected small population of patients presenting with ACS, and the findings may be different in stable patients. Due to the small sample size, multivariate analysis was not performed. Furthermore, the baseline CT scans were obtained with an earlier generation 64-slice CT scanner, which may have produced inferior image quality compared with dual-source CT equipment used during follow-up. Nevertheless, we were able to detect changes of coronary atherosclerosis during the follow-up period. Because this was not a drug efficacy study, the patients received contemporary medical therapy at the discretion of the treating physician; however, the vast majority of patients (91%) received 40 mg of atorvastatin, which made the statin use relatively uniform. Finally, radiation exposure during MSCT coronary angiography still remains a matter of concern. Nonetheless, significant reductions of radiation dose are currently being achieved by implementation of dose-saving techniques (34), which result in effective dose less than the ~5 mSv of the invasive coronary angiography.

CONCLUSIONS

MSCT provides insightful information on the natural history of coronary atherosclerosis and may be used for noninvasive monitoring of pharmacological interventions for coronary artery disease.

Reprint requests and correspondence: Dr. Hector M. Garcia-Garcia, Erasmus Medical Center, Thoraxcenter, Room z120, ‘s-Gravendijkwal 230, 3015 CE, Rotterdam, the Netherlands. *E-mail:* hect2701@gmail.com.

REFERENCES

1. Smith SC Jr., Jackson R, Pearson TA, et al. Principles for national and regional guidelines on cardiovascular disease prevention: a scientific statement from the World Heart and Stroke Forum. *Circulation* 2004;109:3112–21.
2. de Feyter PJ, Serruys PW, Davies MJ, Richardson P, Lubsen J, Oliver MF. Quantitative coronary angiography to measure progression and regression of coronary atherosclerosis. Value, limitations, and implications for clinical trials. *Circulation* 1991;84:412–23.
3. Mintz GS, Garcia-Garcia HM, Nicholls SJ, et al. Clinical expert consensus document on standards for acquisition, measurement and reporting of intravascular ultrasound regression/progression studies. *EuroIntervention* 2011;6:1123–30, 9.
4. Miller JM, Rochitte CE, Dewey M, et al. Diagnostic performance of coronary angiography by 64-row CT. *N Engl J Med* 2008;359:2324–36.
5. Weustink AC, Mollet NR, Neeffjes LA, et al. Diagnostic accuracy and clinical utility of noninvasive testing for coronary artery disease. *Ann Intern Med* 2010;152:630–9.
6. Hoffmann U, Moselewski F, Nieman K, et al. Noninvasive assessment of plaque morphology and composition in culprit and stable lesions in acute coronary syndrome and stable lesions in stable angina by multidetector computed tomography. *J Am Coll Cardiol* 2006;47:1655–62.
7. Papadopoulou SL, Neeffjes LA, Schaap M, et al. Detection and quantification of coronary atherosclerotic plaque by 64-slice multidetector CT: a systematic head-to-head comparison with intravascular ultrasound. *Atherosclerosis* 2011;219:163–70.

8. Voros S, Rinehart S, Qian Z, et al. Prospective validation of standardized, 3-dimensional, quantitative coronary computed tomographic plaque measurements using radiofrequency backscatter intravascular ultrasound as reference standard in intermediate coronary arterial lesions: results from the ATLANTA (Assessment of Tissue Characteristics, Lesion Morphology, and Hemodynamics by Angiography With Fractional Flow Reserve, Intravascular Ultrasound and Virtual Histology, and Noninvasive Computed Tomography in Atherosclerotic Plaques) I Study. *J Am Coll Cardiol Intv* 2011;4:198–208.
9. Burgstahler C, Reimann A, Beck T, et al. Influence of a lipid-lowering therapy on calcified and noncalcified coronary plaques monitored by multislice detector computed tomography: results of the New Age II Pilot Study. *Invest Radiol* 2007;42:189–95.
10. Hoffmann H, Frieler K, Schlattmann P, Hamm B, Dewey M. Influence of statin treatment on coronary atherosclerosis visualised using multidetector computed tomography. *Eur Radiol* 2010;20:2824–33.
11. Inoue K, Motoyama S, Sarai M, et al. Serial coronary CT angiography-verified changes in plaque characteristics as an end point: evaluation of effect of statin intervention. *J Am Coll Cardiol Img* 2010;3:691–8.
12. Lehman SJ, Schlett CL, Bamberg F, et al. Assessment of coronary plaque progression in coronary computed tomography angiography using a semi-quantitative score. *J Am Coll Cardiol Img* 2009;2:1262–70.
13. Schmid M, Achenbach S, Ropers D, et al. Assessment of changes in non-calcified atherosclerotic plaque volume in the left main and left anterior descending coronary arteries over time by 64-slice computed tomography. *Am J Cardiol* 2008;101:579–84.
14. Tardif JC, L'Allier PL, Ibrahim R, et al. Treatment with 5-lipoxygenase inhibitor VIA-2291 (Atreleuton) in patients with recent acute coronary syndrome. *Circ Cardiovasc Imaging* 2010;3:298–307.
15. Uehara M, Funabashi N, Mikami Y, Shiina Y, Nakamura K, Komuro I. Quantitative effect of atorvastatin on size and content of non-calcified plaques of coronary arteries 1 year after atorvastatin treatment by multislice computed tomography. *Int J Cardiol* 2008;130:269–75.
16. Stone GW, Machara A, Lansky AJ, et al. A prospective natural-history study of coronary atherosclerosis. *N Engl J Med* 2011;364:226–35.
17. Bongartz G, Golding SJ, Jurik AG, et al. 2004 CT Quality Criteria: Appendix C. European Guidelines for Multislice Computed Tomography, European Commission. Available at: http://www.msct.eu/CT_Quality_Criteria.htm. Accessed January 10, 2012.
18. Boogers MJ, Kroner ESJ, Broersen A, et al. Automated quantification of coronary plaque using a novel dedicated registration tool: a feasibility study with multi-detector row computed tomography and intravascular ultrasound. *Circulation* 2010;122:A17599.
19. Austen WG, Edwards JE, Frye RL, et al. A reporting system on patients evaluated for coronary artery disease. Report of the Ad Hoc Committee for Grading of Coronary Artery Disease, Council on Cardiovascular Surgery, American Heart Association. *Circulation* 1975;51:5–40.
20. Ballantyne CM, Raichlen JS, Nicholls SJ, et al. Effect of rosuvastatin therapy on coronary artery stenoses assessed by quantitative coronary angiography: a study to evaluate the effect of rosuvastatin on intravascular ultrasound-derived coronary atheroma burden. *Circulation* 2008;117:2458–66.
21. Nissen SE, Nicholls SJ, Sipahi I, et al. Effect of very high-intensity statin therapy on regression of coronary atherosclerosis: the ASTEROID trial. *JAMA* 2006;295:1556–65.
22. Tardif JC, Gregoire J, L'Allier PL, et al. Effects of the acyl coenzyme A:cholesterol acyltransferase inhibitor avasimibe on human atherosclerotic lesions. *Circulation* 2004;110:3372–7.
23. Nissen SE, Tuzcu EM, Libby P, et al. Effect of antihypertensive agents on cardiovascular events in patients with coronary disease and normal blood pressure: the CAMELOT study: a randomized controlled trial. *JAMA* 2004;292:2217–25.
24. Nissen SE, Tardif JC, Nicholls SJ, et al. Effect of torcetrapib on the progression of coronary atherosclerosis. *N Engl J Med* 2007;356:1304–16.
25. Nissen SE, Tuzcu EM, Schoenhagen P, et al. Effect of intensive compared with moderate lipid-lowering therapy on progression of coronary atherosclerosis: a randomized controlled trial. *JAMA* 2004;291:1071–80.
26. Nicholls SJ, Ballantyne CM, Barter PJ, et al. Effect of two intensive statin regimens on progression of coronary disease. *N Engl J Med* 2011;365:2078–87.
27. Nissen SE, Nicholls SJ, Wolski K, et al. Effect of rimonabant on progression of atherosclerosis in patients with abdominal obesity and coronary artery disease: the STRADIVARIUS randomized controlled trial. *JAMA* 2008;299:1547–60.
28. Nicholls SJ, Hsu A, Wolski K, et al. Intravascular ultrasound-derived measures of coronary atherosclerotic plaque burden and clinical outcome. *J Am Coll Cardiol* 2010;55:2399–407.
29. Motoyama S, Sarai M, Harigaya H, et al. Computed tomographic angiography characteristics of atherosclerotic plaques subsequently resulting in acute coronary syndrome. *J Am Coll Cardiol* 2009;54:49–57.
30. Glagov S, Weisenberg E, Zarins CK, Stankunavicius R, Kolettis GJ. Compensatory enlargement of human atherosclerotic coronary arteries. *N Engl J Med* 1987;316:1371–5.
31. Sipahi I, Tuzcu EM, Schoenhagen P, et al. Compensatory enlargement of human coronary arteries during progression of atherosclerosis is unrelated to atheroma burden: serial intravascular ultrasound observations from the REVERSAL trial. *Eur Heart J* 2006;27:1664–70.
32. Van Mieghem CA, Bruining N, Schaar JA, et al. Rationale and methods of the integrated biomarker and imaging study (IBIS): combining invasive and non-invasive imaging with biomarkers to detect subclinical atherosclerosis and assess coronary lesion biology. *Int J Cardiovasc Imaging* 2005;21:425–41.
33. Von Birgelen C, Hartmann M, Mintz GS, et al. Spectrum of remodeling behavior observed with serial long-term (>=12 months) follow-up intravascular ultrasound studies in left main coronary arteries. *Am J Cardiol* 2004;93:1107–13.
34. Raff GL, Chinnaiyan KM, Share DA, et al. Radiation dose from cardiac computed tomography before and after implementation of radiation dose-reduction techniques. *JAMA* 2009;301:2340–8.

Key Words: atherosclerosis ■ computed tomography coronary angiography ■ coronary plaque ■ disease progression.

► **APPENDIX**

For additional tables including supplemental data, please see the online version of this article.

Chapter 5

Quantitative CT coronary angiography: does it predict functionally significant coronary stenoses?

Circulation Cardiovascular Imaging 2014 Jan;7(1):43-51.

A. Rossi, **S.L. Papadopoulou**, F. Pugliese, B. Russo, A.S. Dharampal, A. Dedic, P.H. Kitslaar, A. Broersen, W.B. Meijboom, R.J. van Geuns, A. Wragg, J. Ligthart, C. Schultz, S.E. Petersen, K. Nieman, G.P. Krestin, P.J. de Feyter

Quantitative Computed Tomographic Coronary Angiography Does It Predict Functionally Significant Coronary Stenoses?

Alexia Rossi, MD, PhD; Stella-Lida Papadopoulou, MD; Francesca Pugliese, MD, PhD;
Brunella Russo, MD; Anoeshka S. Dharampal, MD; Admir Dedic, MD;
Pieter H. Kitslaar, MSc; Alexander Broersen, PhD; W. Bob Meijboom, MD, PhD;
Robert-Jan van Geuns, MD, PhD; Andrew Wragg, FRCP; Jurgen Ligthart, MSc;
Carl Schultz, MD; Steffen E. Petersen, MD, DPhil; Koen Nieman, MD, PhD;
Gabriel P. Krestin, MD, PhD; Pim J. de Feyter, MD, PhD

Background—Coronary lesions with a diameter narrowing $\geq 50\%$ on visual computed tomographic coronary angiography (CTCA) are generally considered for referral to invasive coronary angiography. However, similar to invasive coronary angiography, visual CTCA is often inaccurate in detecting functionally significant coronary lesions. We sought to compare the diagnostic performance of quantitative CTCA with visual CTCA for the detection of functionally significant coronary lesions using fractional flow reserve (FFR) as the reference standard.

Methods and Results—CTCA and FFR measurements were obtained in 99 symptomatic patients. In total, 144 coronary lesions detected on CTCA were visually graded for stenosis severity. Quantitative CTCA measurements included lesion length, minimal area diameter, % area stenosis, minimal lumen diameter, % diameter stenosis, and plaque burden [(vessel area–lumen area)/vessel area $\times 100$]. Optimal cutoff values of CTCA-derived parameters were determined, and their diagnostic accuracy for the detection of flow-limiting coronary lesions (FFR ≤ 0.80) was compared with visual CTCA. FFR was ≤ 0.80 in 54 of 144 (38%) coronary lesions. Optimal cutoff values to predict flow-limiting coronary lesion were 10 mm for lesion length, 1.8 mm² for minimal area diameter, 73% for % area stenosis, 1.5 mm for minimal lumen diameter, 48% for % diameter stenosis, and 76% for plaque burden. No significant difference in sensitivity was found between visual CTCA and quantitative CTCA parameters ($P > 0.05$). The specificity of visual CTCA (42%; 95% confidence interval [CI], 31%–54%) was lower than that of minimal area diameter (68%; 95% CI, 57%–77%; $P = 0.001$), % area stenosis (76%; 95% CI, 65%–84%; $P < 0.001$), minimal lumen diameter (67%; 95% CI, 55%–76%; $P = 0.001$), % diameter stenosis (72%; 95% CI, 62%–80%; $P < 0.001$), and plaque burden (63%; 95% CI, 52%–73%; $P = 0.004$). The specificity of lesion length was comparable with that of visual CTCA.

Conclusions—Quantitative CTCA improves the prediction of functionally significant coronary lesions compared with visual CTCA assessment but remains insufficient. Functional assessment is still required in lesions of moderate stenosis to accurately detect impaired FFR. (*Circ Cardiovasc Imaging*. 2014;7:43-51.)

Key Words: CT coronary angiography ■ coronary stenosis ■ fractional flow reserve

Computed tomographic coronary angiography (CTCA) is a reliable, noninvasive imaging modality to visualize coronary artery disease with a high diagnostic accuracy compared with invasive coronary angiography (ICA).¹⁻³ In addition, CTCA can provide quantitative information of a coronary stenosis, similar to intravascular ultrasound (IVUS), cross-sectional information, and plaque burden. In daily practice, lesions with a diameter stenosis $\geq 50\%$ on visual CTCA

are generally considered for referral to ICA. However, similar to ICA, CTCA is an anatomic imaging technique; thus, it may result in both under- and overestimation of a lesion's severity and is often inaccurate in identifying functionally significant coronary lesions that cause ischemia.^{4,5} Current guidelines suggest that treatment decisions based on the hemodynamic effect of a coronary lesion may improve clinical outcome.⁶⁻⁸ Therefore, it would be relevant if quantitative parameters derived from CTCA could be optimized to predict the functional significance of a coronary stenosis.

Clinical Perspective on p 51

Received October 11, 2012; accepted October 28, 2013.

From the Department of Radiology (A.R., S.-L.P., B.R., A.S.D., A.D., R.-J.v.G., K.N., P.J.d.F.) and Department of Cardiology (A.R., S.-L.P., A.S.D., A.D., W.B.M., R.-J.v.G., J.L., C.S., K.N., G.P.K., P.J.d.F.), Erasmus University Medical Center, Rotterdam, The Netherlands; Centre for Advanced Cardiovascular Imaging, NIHR Cardiovascular Biomedical Research Unit at Barts, Barts and The London School of Medicine & Barts Health NHS Trust, London, United Kingdom (F.P., A.W., S.E.P.); and Division of Image Processing, Department of Radiology, Leiden University Medical Center, Leiden, The Netherlands (P.H.K., A.B.).

Correspondence to Alexia Rossi, MD, Erasmus Medical Center, Rotterdam, Department of Radiology and Cardiology, Room Ca 207a, PO Box 2040, 3000 CA Rotterdam, The Netherlands. E-mail alexia.rossi03@gmail.com

© 2013 American Heart Association, Inc.

The aim of this study was to compare the diagnostic performance of CTCA-derived quantitative parameters with visual CTCA in the detection of functionally significant coronary lesions using fractional flow reserve (FFR) as the reference standard.

Methods

Study Population

We retrospectively included patients with stable angina who underwent both CTCA and ICA and a subsequent measurement of FFR in 2 teaching hospitals. The decision to measure FFR was based on the visual assessment of ICA and was made at the discretion of the interventional cardiologist. Because of the potential hemodynamic

interaction between ≥ 2 stenoses in series,^{9,10} we only included patients with a single coronary lesion per coronary vessel.

Exclusion criteria were impaired renal function (creatinine clearance < 60 mL/min), known allergy to iodine contrast material, calcium score per vessel > 400 , left main coronary lesions, and poor image quality. Poor image quality was defined as severe motion artifacts or poor contrast opacification.

All patients gave written informed consent to undergo CTCA as part of research protocols approved by the institutional review boards of the participating institutions. FFR was performed as part of routine clinical management.

CTCA Acquisition

All patients received nitroglycerin (0.4 mg/dose) sublingually just before the CT scan, provided there were no contraindications,

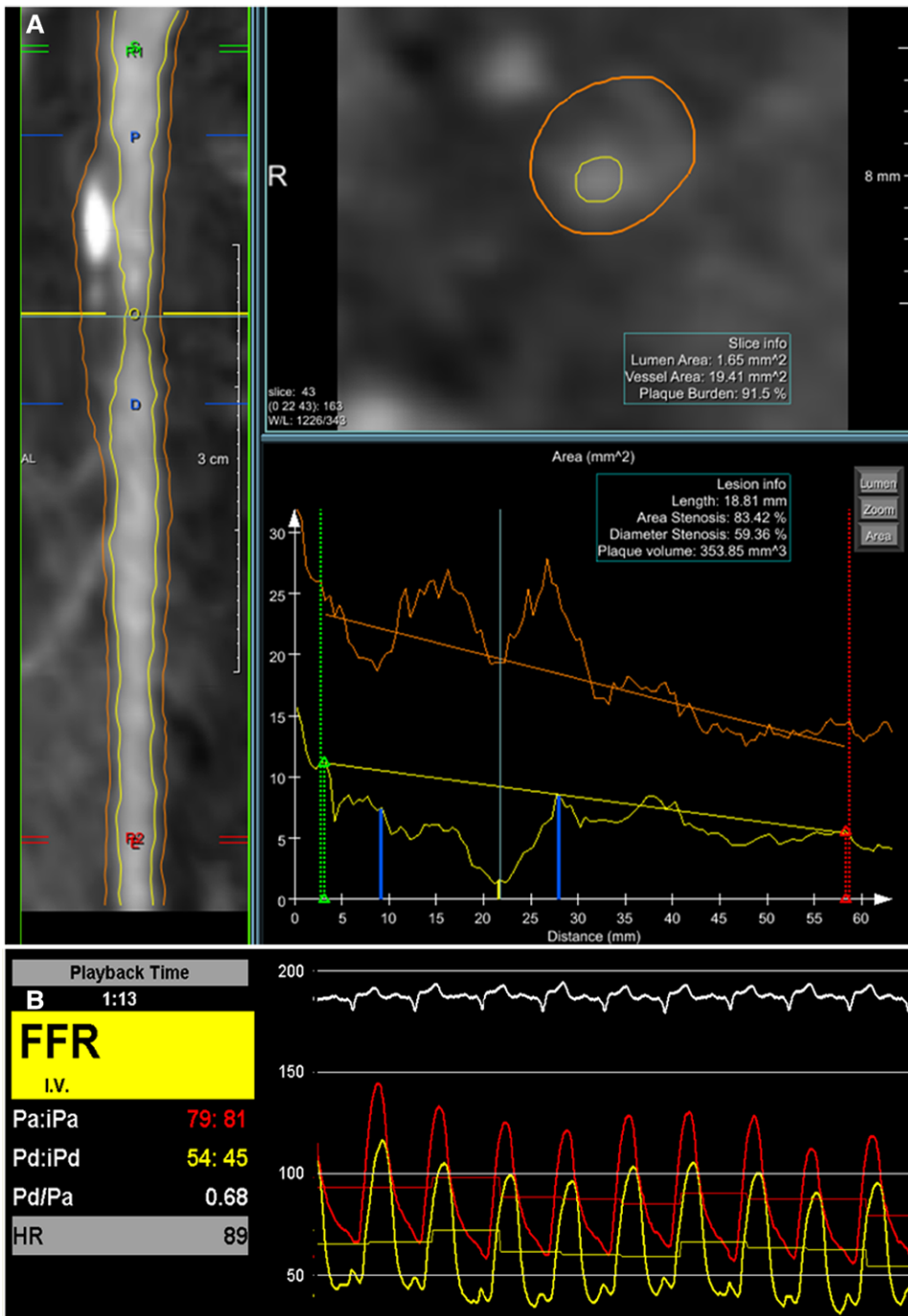


Figure 1. Quantitative computed tomographic coronary angiography (CTCA) and fractional flow reserve (FFR) measurement in a moderate coronary lesion. Example of a patient with a moderate (50%–70% lumen narrowing by visual CTCA) coronary lesion because of a partly calcified plaque in the left descending coronary artery. **A**, The screenshot of the quantitative CTCA analysis using dedicated software. The lesion was assessed as moderate by visual CTCA. Lumen (yellow) and wall (orange) contours were semiautomatically detected. At the level of the minimal lumen area (yellow line), lumen area, % area stenosis, and plaque burden were measured as 1.6 mm², 83%, and 91%, respectively. The FFR was 0.68 (**B**).

Table 1. Baseline Clinical Characteristics

	All (n=99)	FFR >0.80 (n=55)	FFR ≤0.80 (n=44)	P Value*
Men, n (%)	77 (78)	40 (73)	37 (84)	0.177
Age, y	61 ±11	60 ±12	62 ±10	0.222
Risk factors, n (%)				
Smoker	17 (17)	7 (13)	10 (23)	0.190
Hypertension†	63 (64)	36 (66)	27 (61)	0.674
Dyslipidemia‡	75 (76)	40 (73)	35 (79)	0.432
Diabetes mellitus§	22 (22)	16 (29)	6 (14)	0.066
Family history of CAD¶	51 (52)	29 (53)	22 (50)	0.787
Calcium score (Agatston)	284 (43–629)	197 (36–631)	355 (100–640)	0.428

Values are mean±standard deviation, median (interquartile range) or n (%). CAD indicates coronary artery disease; and FFR, fractional flow reserve.

*Comparison between FFR >0.80 vs FFR ≤0.80.

†Blood pressure ≥140/90 mm Hg or treatment for hypertension.

‡Total cholesterol >180 mg/dL or treatment for hypercholesterolemia.

§Treatment with oral antidiabetic medication or insulin.

¶Family history of coronary artery disease having first- or second-degree relatives with premature CAD (age <55 y).

and patients with a heart rate >65 bpm received preparation with β-blockers (50–100 mg metoprolol orally 1 hour before scanning or 1–30 mg metoprolol IV directly before scanning). The CT scan was performed using either a 64-slice dual-source scanner (Somatom Definition, Siemens Medical Solutions, Forchheim, Germany) or a 128-slice second-generation dual-source CT scanner (Somatom Definition Flash, Siemens Medical Solutions, Forchheim, Germany). First, all patients underwent an unenhanced scan for the calculation

Table 2. Cross-Sectional CT-Derived Parameters, Vessel Distribution, and FFR

	All (n=144)	FFR >0.80 (n=90)	FFR ≤0.80 (n=54)	P Value*
FFR	0.83 (0.75–0.90)	0.88 (0.84–0.93)	0.72 (0.68–0.77)	<0.001
Lesion length, mm	13 (9–19)	11 (8–17)	16 (11–25)	0.001
MLA, mm ²	1.8 (1.0–2.7)	2.3 (1.5–2.8)	1.0 (0.3–1.6)	<0.001
%AS	71 (62–82)	67 (56–73)	84 (74–91)	<0.001
MLD, mm	1.5 (1.1–1.8)	1.7 (1.4–1.9)	1.1 (0.6–1.4)	<0.001
%DS	47 (39–58)	44 (35–49)	60 (49–71)	<0.001
Plaque burden, %	76 (71–79)	73 (69–77)	79 (76–82)	<0.001
Vessel, n(%)				0.050
RCA	36 (25)	24 (27)	12 (22)	
LAD	76 (53)	41 (46)	35 (65)	
LCX	32 (22)	25 (28)	7 (13)	
Lesion location, n(%)				0.121
Proximal	76 (53)	43 (48)	33 (61)	
Mid	68 (47)	47 (52)	21 (39)	

Values are median (interquartile range) or n (%). %AS indicates % area stenosis; %DS, % diameter stenosis; CT, computed tomography; FFR, fractional flow reserve; LAD, left anterior descending coronary artery; LCX, left circumflex coronary artery; MLA, minimal lumen area; MLD, minimal lumen diameter; and RCA, right coronary artery.

*Comparison between FFR >0.80 and FFR ≤0.80.

of the calcium score with the Agatston method (32×1.2 mm collimation, 120-kV tube voltage, 75-mA tube current, and 3-mm slice thickness with increment 1.5 mm). The CT angiographic scan parameters were (1) for the 64-slice dual-source CT (DSCT) scanner, a gantry rotation time of 330 ms, 32×2×0.6 mm collimation with z-flying focal spot for both detectors, gantry rotation time of 330 ms, tube voltage of 120 kV, and tube current of 320 to 412 mA per rotation; and (2) for the 128-slice DSCT scanner, a gantry rotation time of 280 ms, 64×2×0.6 mm collimation with z-flying focal spot for both detectors, tube voltage of 100 or 120 kV, and tube current of 320 to 412 mA per rotation. A bolus of iodinated contrast agent (370 mgI/mL, Ultravist; Schering, Berlin, Germany, or 300 mgI/mL, Omnipaque, GE Healthcare, Milwaukee, MI), which varied between 60 and 100 mL depending on the expected scan time, was injected intravenously at an injection rate of either 5.5 or 7 mL/s (depending on the type of contrast used) followed by a 45-mL saline chaser at the same injection rate. The iodine deliver rates achieved with both injection protocols were similar (2.0–2.1 gI/s). A bolus tracking technique was used to synchronize the start of image acquisition with the arrival of the iodinated contrast agent in the coronary arteries. With the 64-slice DSCT scanner, an ECG-gated spiral scan mode with ECG pulsing was used for image acquisition. When scanning with the 128-slice DSCT, the prospectively ECG-triggered sequential scan mode (step-and-shoot) or the retrospective ECG-gated spiral scan mode with ECG pulsing or a high-pitch spiral scan mode was used, depending on the heart rate.

All CT images were reconstructed with a slice thickness of 0.75 mm and an increment of 0.4 mm. Images were analyzed using medium-to-smooth convolution kernels for noncalcified lesions and sharp convolution kernels for calcified lesions. More details about the CT protocol were previously described in detail.¹¹

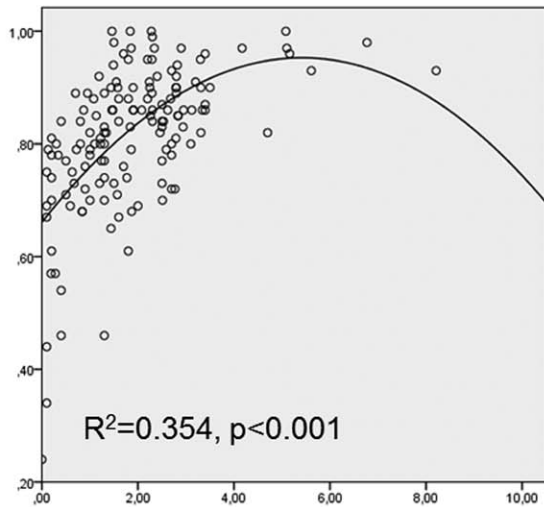
FFR Measurements

FFR was measured with a sensor-tipped 0.014-inch guidewire (Pressure Wire, Radi Medical Systems, Uppsala, Sweden). The pressure sensor was positioned just distal to the stenosis, and maximal myocardial hyperemia was induced by a continuous intravenous infusion of adenosine in a femoral vein (140 μg/kg per minute for a minimum of 2 minutes). FFR was calculated as the ratio of mean distal pressure measured by the pressure wire divided by the mean proximal pressure measured by the guiding catheter. A coronary stenosis with an FFR value ≤0.80 was considered functionally significant.¹²

CTCA Image Analysis

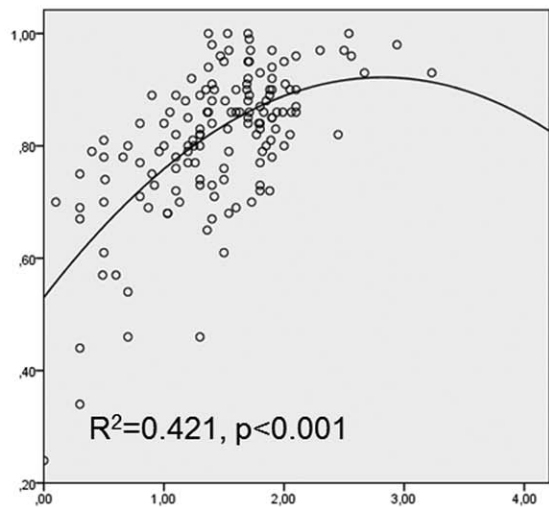
First, the CTCA data sets were evaluated visually, and the coronary lesion was graded as nonobstructive (<50% lumen narrowing), moderate (50%≤lumen narrowing<70%), and severe (≥70% lumen narrowing). Afterward, all data sets were transferred to an offline workstation for analysis using semiautomated plaque analysis software (QAngioCT Research Edition v1.3.61; Medis Medical Imaging Systems, Leiden, The Netherlands). The location and extent of the region of interest were manually defined using proximal and distal markers as the coronary vessel region where the lumen diameter was reduced ≥30% compared with the normal vessel. Planimetry of the inner lumen and outer vessel areas was performed following a stepwise approach as previously described.^{13–15} In summary, a centerline originating from the ostium was automatically extracted; then, straightened multiplanar reformatted images were generated, and the lumen and vessel borders were detected longitudinally on 4 different vessel views by the software; based on these longitudinal contours, cross-sectional images at 0.5 mm intervals were calculated to create transversal lumen and vessel wall contours, which were examined and, if necessary, adjusted by a single experienced observer. Based on the detected contours proximal and distal from the lesion region, a reference area function was derived modeling the tapering of a healthy vessel. From these data, the following cross-sectional CTCA-derived parameters were provided automatically by the software: lesion length, minimum lumen area (MLA), and % area stenosis (%AS) at the level of the MLA defined by [1-(MLA/corresponding reference lumen area)×100]. In addition, minimum lumen diameter (MLD) and

FFR



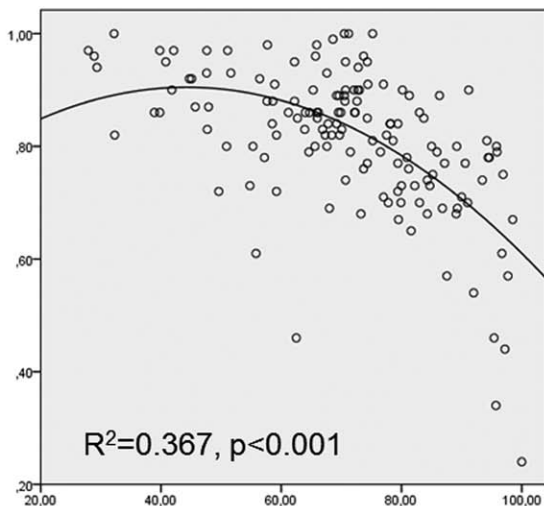
MLA (mm²)

FFR



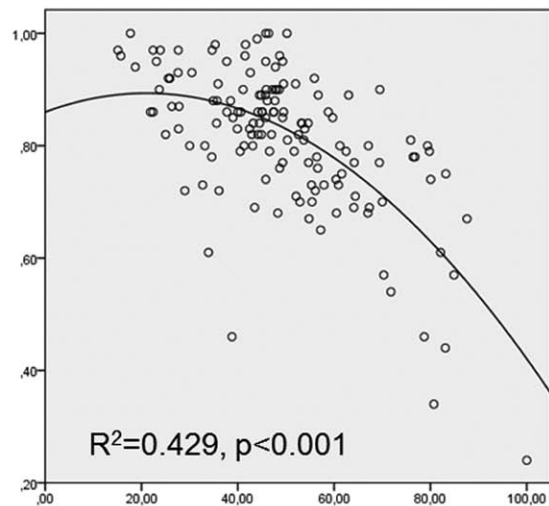
MLD (mm)

FFR



%AS

FFR



%DS

Figure 2. Curvilinear relationship between fractional flow reserve (FFR) and minimal lumen area (MLA), % area stenosis (%AS), minimal lumen diameter (MLD), and % diameter stenosis (%DS).

% diameter stenosis (%DS) were provided as derived mathematically from the contour and reference area functions. Plaque burden was calculated for the whole coronary lesion by the following equation: $(\text{vessel area} - \text{lumen area}) / \text{vessel area} \times 100$ (Figure 1).

Statistical Analysis

Statistical analysis was performed using commercially available software (IBM SPSS Statistic, version 20). Results are reported in accordance with the STARD criteria (Standards for Reporting of Diagnostic Accuracy).¹⁶ Continuous variables are presented as mean \pm SD or median with interquartile range when not normally distributed and compared using the unpaired *t* test or the Mann-Whitney test, respectively. Categorical variables are presented as frequencies and percentages and compared using the χ^2 test.

The correlation between quantitative CTCA-derived parameters and FFR was assessed using linear regression analysis with nonlinear predictors. Receiver operating characteristic curves were used

to assess the optimal cutoff values of quantitative CTCA-derived parameters to predict $\text{FFR} \leq 0.80$. In the choice of the cutoff value, we optimized the specificity, provided that sensitivity was $\geq 80\%$. Diagnostic performance of visual CTCA-derived and quantitative CTCA-derived parameters for the detection of functionally significant lesions was evaluated on a per-lesion level and expressed as sensitivity, specificity, positive and negative predictive values, and their corresponding 95% confidence intervals. A generalized estimating equation model was used to account for the clustering between lesions in the same subject. The McNemar test was used to compare the sensitivities and specificities of each quantitative CTCA-derived parameter versus visual CTCA.

Coronary lesions were divided into 3 groups based on visual assessment: nonobstructive ($<50\%$ lumen narrowing), moderate ($50\% \leq$ lumen narrowing $<70\%$), and severe ($\geq 70\%$ lumen narrowing). The cutoff values of quantitative CTCA-derived parameters derived from the receiver operating characteristic curves were used individually and in combination to investigate whether they could decrease

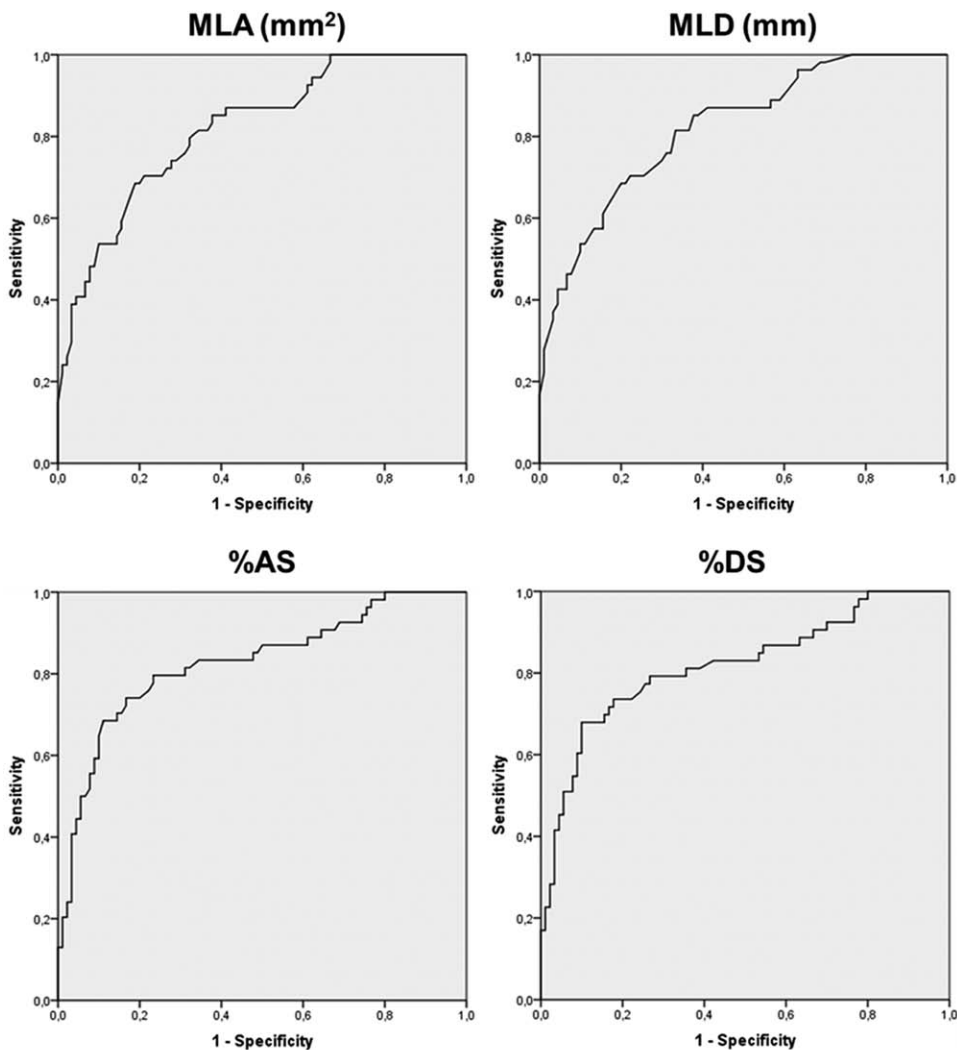


Figure 3. Receiver operating characteristic curves of minimal lumen area (MLA), % area stenosis (%AS), minimal lumen diameter (MLD), and % diameter stenosis (%DS).

the number of misclassified lesions in the 3 categories of lesion severity. When the combined approach was used, a positive outcome was adjudicated if both quantitative CTCA-derived parameters were positive as defined by the optimal cutoff value. A misclassified lesion was defined as a mismatch between CTCA results and FFR measurements. Statistical significance was defined as $P < 0.05$.

Results

Study Population

In total, 124 patients were considered for inclusion in the study. Twenty-five patients were excluded because of extreme calcifications (vessel calcium score > 400) in the target vessel ($n = 17$), left main coronary lesions ($n = 2$), and poor image quality ($n = 6$). Therefore, 144 coronary lesions in 99 patients were finally included in the analysis. Baseline clinical characteristics and quantitative CTCA-derived parameters are shown in Tables 1 and 2, respectively. The range of FFR values was between 0.24 and 1.00; 36% (36/99) of patients had multivessel FFR measurements. The FFR was ≤ 0.80 in 54 lesions (38%). Coronary lesions with FFR ≤ 0.80 were longer lesions with smaller lumen area and diameter, more severe stenosis, and higher plaque burden than those with FFR > 0.80 (Table 2).

FFR Versus Cross-Sectional CTCA-Derived Parameters

Nonlinear regression analysis between quantitative CTCA-derived parameters and FFR demonstrated a significant curvilinear relationship for %AS, %DS, MLA, and MLD (Figure 2). Significant curvilinear relationship was also found for plaque burden ($R^2 = 0.302$; $P < 0.001$) and lesion length ($R^2 = 0.148$; $P < 0.001$). Receiver operating characteristic analysis yielded an area under the curve of 0.66 (0.57–0.75) for length, 0.82 (0.75–0.89) for MLA, 0.82 (0.75–0.89) for MLD, 0.83 (0.75–0.90) for %AS, 0.82 (0.74–0.89) for %DS, and 0.80 (0.73–0.87) for plaque burden (Figure 3). Optimal cutoff values to predict the functional significance of coronary lesions were 10 mm for length, 1.8 mm² for MLA, 73% for %AS, 1.5 mm for MLD, 48% for %DS, and 76% for plaque burden.

Diagnostic Performance of Visual CTCA-Derived and Quantitative CTCA-Derived Parameters in Predicting Functionally Significant Coronary Lesions

The diagnostic performance of visual CTCA and quantitative CTCA for the assessment of functionally significant

Table 3. Diagnostic Accuracy of Visual CTCA and Optimal Cutoff Values of Lesion Length, MLA, %AS, MLD, %DS, and %DS Derived From Quantitative CTCA in the Detection of Flow-Limiting Coronary Lesions as Defined by an FFR ≤ 0.80

	TP	TN	FP	FN	Sensitivity, %	Specificity, %	PPV, %	NPV, %
Visual assessment	50	38	52	4	93 (82–97)	42 (31–54)	49 (38–60)	91 (77–96)
Length, mm	44	35	55	10	82 (69–90)	39 (28–51)	44 (34–56)	78 (63–88)
MLA, mm ²	43	61	29	11	80 (67–88)	68 (57–77)†	60 (46–72)	85 (75–91)
%AS	43	68	22	11	80 (65–89)	76 (65–84)†	66 (53–77)	86 (76–92)
MLD, mm	44	60	30	10	82 (69–90)	67 (55–76)†	60 (46–72)	86 (76–92)
%DS	43	65	25	11	80 (65–89)	72 (62–80)†	63 (50–74)	86 (75–92)
Plaque burden, %	43	57	33	11	80 (66–89)	63 (52–73)†	57 (43–69)	84 (72–91)

%AS indicates % area stenosis; %DS, % diameter stenosis; CTCA, computed tomographic coronary angiography; FFR, fractional flow reserve; FN, false negative; FP, false positive; MLA, minimal lumen area; MLD, minimal lumen diameter; NPV, negative predictive value; PPV, positive predictive value; TN, true negative; and TP, true positive.

† $P < 0.05$ derived from McNemar comparing the specificities of lesion length, MLA, %AS, MLD, %DS, and plaque burden with the specificity of visual assessment.

coronary lesions (FFR ≤ 0.80) is detailed in Table 3. No significant difference was found for sensitivity between visual CTCA and quantitative CTCA in terms of lesion length, MLA, %AS, MLD, %DS, and plaque burden ($P > 0.05$). The specificity of MLA, %AS, MLD, %DS, and plaque burden was significantly higher than the specificity of visual CTCA ($P = 0.001$, $P < 0.001$, $P = 0.001$, $P < 0.001$, and $P = 0.004$, respectively) for the detection of functionally significant coronary lesions. Specificity of lesion length was not significantly different than specificity of visual CTCA ($P = 0.749$).

Moderate Coronary Lesions

Visual CTCA showed 42 (29%) nonobstructive lesions, 85 (59%) moderate lesions, and 17 (12%) severe lesions. In the moderate lesion category, 46 lesions were misclassified by visual CTCA; the use of %AS and plaque burden in combination decreased the number of lesions incorrectly classified from 46 of 85 (54%) to 20 of 85 (24%), of which 15 lesions were incorrectly classified as nonfunctionally significant (Tables 4–9).

Discussion

In this exploratory study, we sought to investigate the ability of quantitative parameters derived by CTCA to predict the functional significance of coronary lesions using FFR as the reference standard.

The major findings of our study were the following: (1) the relationship between coronary lesion severity, as described by quantitative CTCA-derived parameters, and FFR is curvilinear; (2) the optimal cutoff values to predict the functional

significance of coronary lesions were 10 mm, 1.8 mm², 73%, 1.5 mm, 48%, and 76% for lesion length, MLA, %AS, MLD, %DS, and plaque burden, respectively; (3) in the moderate lesion category, the combined use of %AS and plaque burden decreased the number of lesions incorrectly classified from 46 of 85 (54%) to 20 of 85 (24%), of which 15 lesions were incorrectly classified as nonfunctionally significant.

Relationship Between Quantitative CTCA-Derived Parameters and FFR

As shown in previous IVUS studies,^{17,18} MLA is important in determining coronary blood flow based on the Bernoulli equation. However, other important factors can affect coronary flow: the degree of diameter stenosis, lesion length, plaque burden, vessel size, lesion morphology, plaque characteristics, blood viscosity, collateral circulation, and supplied myocardium.¹⁹ Several of these parameters can be measured using CTCA.¹⁴ In our study, similar to Kristensen et al,²⁰ a curvilinear significant relationship was found between quantitative CTCA-derived parameters and FFR for a wide range of coronary lesion severity.

Several IVUS studies have validated an MLA of 3.0 or 4.0 mm² as an anatomic predictor for physiological lesion significance.^{21,22} However, it has been shown that these cutoff values are not accurate; especially when applied in small vessels (diameter < 2.5 mm),¹⁷ a smaller cutoff value should be used. In our study, similar to the finding reported by Kristensen et al,²⁰ we found an MLA CT-derived cutoff value of 1.8

Table 4. Distribution of coronary lesion severity based on visual CTCA

	Visual Assessment		
	Nonobstructive Stenoses (n=42)	Moderate Stenoses (n=85)	Severe Stenoses (n=17)
FFR > 0.80	38	46*	6
FFR ≤ 0.80	4	39	11

Values are numbers. CTCA indicates computed tomographic coronary angiography; and FFR, fractional flow reserve.

*The number of misclassified coronary lesions in the moderate stenosis category.

Table 5. Diagnostic Performance of MLA to Predict Functionally Significant Lesions (FFR ≤ 0.80)

	MLA, mm ²					
	Nonobstructive Stenoses (n=42)		Moderate Stenoses (n=85)		Severe Stenoses (n=17)	
	> 1.8	≤ 1.8	> 1.8	≤ 1.8	> 1.8	≤ 1.8
FFR > 0.80	28	10	29	17*	4	2
FFR ≤ 0.80	1	3	10*	29	0	11

Values are numbers. Upper left cell=true negative, upper right cell=false positive, lower left cell=false negative, and lower right cell=true positive. FFR indicates fractional flow reserve; and MLA, minimal lumen area.

*The number of misclassified coronary lesions in the moderate stenosis category.

Table 6. Diagnostic Performance of %AS to Predict Functionally Significant Lesions (FFR≤0.80)

	%AS					
	Nonobstructive Stenoses (n=42)		Moderate Stenoses (n=85)		Severe Stenoses (n=17)	
	<73	≥73	<73	≥73	<73	≥73
FFR >0.80	33	5	31	15*	4	2
FFR ≤0.80	1	3	10*	29	0	11

Values are numbers. Upper left cell=true negative, upper right cell=false positive, lower left cell=false negative, and lower right cell=true positive. %AS indicates % area stenosis; and FFR, fractional flow reserve.

*The number of misclassified coronary lesions in the moderate stenosis category.

mm², which is smaller compared with the IVUS-derived one reported by Kang et al.¹⁷ This may be related to inherent differences between invasive and noninvasive imaging modalities. For instance, to avoid the induction of coronary spasm by the IVUS catheter, intracoronary nitrates are usually given before imaging at a dose of 100 to 200 µg, causing a status of coronary vasodilation greater than the one induced by nitrates administered orally before the CTCA acquisition. In addition, IVUS does not assess severe coronary lesions because of the large profile of the IVUS catheter, which is unable to pass through small coronary lumen.

CTCA-Derived Parameters in Predicting Flow-Limiting Coronary Lesions

Previous investigations have demonstrated that, similar to ICA, the anatomic assessment of a coronary stenosis by CTCA correlates poorly with the functional significance of the stenosis defined by FFR.^{4,5} As previously shown in a study by Tonino et al,²³ there was a high rate of nonfunctionally significant lesions in the range of angiographic severity of 50% to 70% diameter stenosis. Similarly, in our study, 54% of the coronary stenoses with an angiographic severity between 50% and 70% were not functionally significant. The use of quantitative CTCA decreased the number of misclassified lesions by half, mainly by reducing the number of lesions incorrectly classified as functionally significant from 46 to 20. However, 15 of these misclassified lesions were incorrectly classified as nonfunctionally significant, highlighting the fact that the increase in the specificity comes at the expense of a

Table 7. Diagnostic Performance of Plaque Burden to Predict Functionally Significant Lesions (FFR≤0.80)

	Plaque Burden, %					
	Nonobstructive Stenoses (n=42)		Moderate Stenoses (n=85)		Severe Stenoses (n=17)	
	<76	≥76	<76	≥76	<76	≥76
FFR >0.80	27	11	29	17*	1	5
FFR ≤0.80	1	3	10*	29	0	11

Values are numbers. Upper left cell=true negative, upper right cell=false positive, lower left cell=false negative, and lower right cell=true positive. FFR indicates fractional flow reserve.

*The number of misclassified coronary lesions in the moderate stenosis category.

Table 8. Diagnostic Performance of MLA + Plaque Burden to Predict Functionally Significant Lesions (FFR ≤0.80)

	MLA, mm ² and Plaque Burden, %					
	Nonobstructive Stenoses (n=42)		Moderate Stenoses (n=85)		Severe Stenoses (n=17)	
	MLA>1.8, PB<76	MLA≤1.8, PB≥76	MLA>1.8, PB<76	MLA≤1.8, PB≥76	MLA>1.8, PB<76	MLA≤1.8, PB≥76
FFR >0.80	35	3	36	10*	4	2
FFR ≤0.80	1	3	15*	24	0	11

Values are numbers. Upper left cell=true negative, upper right cell=false positive, lower left cell=false negative, and lower right cell=true positive. FFR indicates fractional flow reserve; MLA, minimal lumen area; and PB, plaque burden.

*The number of misclassified coronary lesions in the moderate stenosis category.

decrease in the sensitivity. Similarly, Godoy et al²⁴ and Gaemperli et al²⁵ found only a moderate diagnostic accuracy of quantitative CTCA for the detection of myocardial ischemia by single photon emission computed tomography. The modest association of anatomic assessment by quantitative CTCA with functional assessment may be explained by the complexity of factors leading to myocardial ischemia.²⁶ As proposed by Marzilli et al,²⁷ obstructive epicardial coronary stenosis is only 1 of the contributors to myocardial ischemia, and inflammation, endothelial dysfunction, microvascular dysfunction, platelet dysfunction, thrombosis, and vasomotor dysfunction should also be considered.

Limitations

First, our study was a retrospective study performed in a relatively small number of patients; the possibility of a type II error should be considered. Second, we included only patients referred for ICA with moderate-to-severe diseased coronary arteries. Future studies with a prospective design are required to evaluate the diagnostic accuracy of quantitative CTCA for the selection of patients who will benefit most from revascularization. In addition, the discriminatory power of CTCA cross-sectional quantitative parameters in the detection of functionally significant coronary lesions requires further investigation in the typical population, at low-to-intermediate pretest probability of coronary artery disease, referred for

Table 9. Diagnostic Performance of %AS + Plaque Burden to Predict Functionally Significant Lesions (FFR ≤0.80)

	%AS and Plaque Burden, %					
	Nonobstructive Stenoses (n=42)		Moderate Stenoses (n=85)		Severe Stenoses (n=17)	
	%AS<73, PB<76	%AS≥73, PB≥76	%AS<73, PB<76	%AS≥73, PB≥76	%AS<73, PB<76	%AS≥73, PB≥76
FFR >0.80	36	2	41	5*	4	2
FFR ≤0.80	1	3	15*	24	0	11

Values are numbers. Upper left cell=true negative, upper right cell=false positive, lower left cell=false negative, and lower right cell=true positive. %AS indicates percentage area stenosis; FFR, fractional flow reserve; and PB, plaque burden.

*The number of misclassified coronary lesions in the moderate stenosis category.

CTCA. Third, because of the relative small number of positive observations, we did not perform multivariate logistic regression to identify independent predictors of a positive FFR. Finally, we excluded vessels with poor image quality on CTCA; good image quality is a prerequisite for the reliable calculation of CT-derived cross-sectional parameters.

Clinical Implications and Future Directions

The interest in overcoming the mismatch between anatomy and function in cardiac imaging has initiated intense research to assess the feasibility of new noninvasive diagnostic techniques. In this study, we determined whether the analysis of quantitative cross-sectional CTCA parameters could improve the prediction of functionally significant lesions without further irradiation, contrast, or drug administration. In our study, stenosis quantification prolonged the postprocessing analysis time by 5 to 10 minutes, mainly depending on the amount of calcium per lesion, with a significant reduction in the number of moderate lesions incorrectly classified as functionally significant. Several automated software programs are now commercially available for stenosis quantification, and their use may be useful in clinical routine.

The possibility of a noninvasive FFR measurement has been shown with promising results.²⁸ In a multicenter study involving 252 patients with stable angina, noninvasive FFR in addition to CTCA improved the diagnostic accuracy and discrimination of CTCA alone for the diagnosis of functionally significant lesions.²⁹ Similar to our results, the diagnostic specificity and positive predictive value remained low, and further studies are warranted to determine the potential clinical implication of this more comprehensive coronary lesion assessment.

The safety and feasibility of stress myocardial CT perfusion imaging have also been demonstrated in few experimental and human studies.^{30–35} The addition of stress myocardial CT perfusion imaging to the standard CTCA can provide complementary anatomic and functional information in a single examination. However, CT perfusion imaging involves increased patient radiation exposure, increased contrast volume, and potential patient's discomfort related to the administration of a pharmacological stress agent.

Conclusions

CTCA quantitative parameters improve the prediction of flow-limiting lesions, compared with visual assessment, but remain insufficient. Functional assessment is still needed for lesions of moderate severity to accurately detect impaired FFR.

Sources of Funding

This work forms part of the research themes contributing to the translational research portfolio of the Cardiovascular Biomedical Research Unit at Barts, which is supported and funded by the National Institute for Health Research (F. Pugliese and S.E. Petersen).

Disclosures

P. Kitslaar is employed by Medis medical imaging systems bv and has a research appointment at the Leiden University Medical Center. G.P. Krestin has a consultancy relationship with GE Healthcare. The other authors report no conflicts.

References

1. Meijboom WB, Meijs MF, Schuijff JD, Cramer MJ, Mollet NR, van Mieghem CA, Nieman K, van Werkhoven JM, Pundziute G, Weustink AC, de Vos AM, Pugliese F, Rensing B, Jukema JW, Bax JJ, Prokop M, Doevendans PA, Hunink MG, Krestin GP, de Feyter PJ. Diagnostic accuracy of 64-slice computed tomography coronary angiography: a prospective, multicenter, multivendor study. *J Am Coll Cardiol*. 2008;52:2135–2144.
2. Miller JM, Dewey M, Vavere AL, Rochitte CE, Niinuma H, Arbab-Zadeh A, Paul N, Hoe J, de Roos A, Yoshioka K, Lemos PA, Bush DE, Lardo AC, Texter J, Brinker J, Cox C, Clouse ME, Lima JA. Coronary CT angiography using 64 detector rows: methods and design of the multi-centre trial CORE-64. *Eur Radiol*. 2009;19:816–828.
3. Budoff MJ, Dowe D, Jollis JG, Gitter M, Sutherland J, Halamert E, Scherer M, Bellinger R, Martin A, Benton R, Delago A, Min JK. Diagnostic performance of 64-multidetector row coronary computed tomographic angiography for evaluation of coronary artery stenosis in individuals without known coronary artery disease: results from the prospective multicenter ACCURACY (Assessment by Coronary Computed Tomographic Angiography of Individuals Undergoing Invasive Coronary Angiography) trial. *J Am Coll Cardiol*. 2008;52:1724–1732.
4. Sarno G, Decraemer I, Vanhoenacker PK, De Bruyne B, Hamilos M, Cuisset T, Wyffels E, Bartunek J, Heyndrickx GR, Wijns W. On the inappropriateness of noninvasive multidetector computed tomography coronary angiography to trigger coronary revascularization: a comparison with invasive angiography. *JACC Cardiovasc Interv*. 2009;2:550–557.
5. Meijboom WB, Van Mieghem CA, van Pelt N, Weustink A, Pugliese F, Mollet NR, Boersma E, Regar E, van Geuns RJ, de Jaegere PJ, Serruys PW, Krestin GP, de Feyter PJ. Comprehensive assessment of coronary artery stenoses: computed tomography coronary angiography versus conventional coronary angiography and correlation with fractional flow reserve in patients with stable angina. *J Am Coll Cardiol*. 2008;52:636–643.
6. Hachamovitch R, Hayes SW, Friedman JD, Cohen I, Berman DS. Comparison of the short-term survival benefit associated with revascularization compared with medical therapy in patients with no prior coronary artery disease undergoing stress myocardial perfusion single photon emission computed tomography. *Circulation*. 2003;107:2900–2907.
7. Kolh P, Wijns W, Danchin N, Di Mario C, Falk V, Folliguet T, Garg S, Huber K, James S, Knuuti J, Lopez-Sendon J, Marco J, Menicanti L, Ostojic M, Piepoli MF, Pirllet C, Pomar JL, Reifart N, Ribichini FL, Schalij MJ, Sergeant P, Serruys PW, Silber S, Sousa Uva M, Taggart D. Guidelines on myocardial revascularization. *Eur J Cardiothorac Surg* 2010;38(suppl):S1–S52.
8. Wijns W, Kolh P, Danchin N, Di Mario C, Falk V, Folliguet T, Garg S, Huber K, James S, Knuuti J, Lopez-Sendon J, Marco J, Menicanti L, Ostojic M, Piepoli MF, Pirllet C, Pomar JL, Reifart N, Ribichini FL, Schalij MJ, Sergeant P, Serruys PW, Silber S, Sousa Uva M, Taggart D. Guidelines on myocardial revascularization. *Eur Heart J*. 2010;31:2501–2555.
9. Pijls NH, De Bruyne B, Bech GJ, Liestro F, Heyndrickx GR, Bonnier HJ, Koolen JJ. Coronary pressure measurement to assess the hemodynamic significance of serial stenoses within one coronary artery: validation in humans. *Circulation*. 2000;102:2371–2377.
10. De Bruyne B, Pijls NH, Heyndrickx GR, Hodeige D, Kirkeeide R, Gould KL. Pressure-derived fractional flow reserve to assess serial epicardial stenoses: theoretical basis and animal validation. *Circulation*. 2000;101:1840–1847.
11. Neeffjes LA, Dharampal AS, Rossi A, Nieman K, Weustink AC, Dijkshoorn ML, Ten Kate GJ, Dedic A, Papadopoulou SL, van Straten M, Cademartiri F, Krestin GP, de Feyter PJ, Mollet NR. Image quality and radiation exposure using different low-dose scan protocols in dual-source CT coronary angiography: randomized study. *Radiology*. 2011;261:779–786.
12. Tonino PA, De Bruyne B, Pijls NH, Siebert U, Ikeno F, van't Veer M, Klauss V, Manoharan G, Engström T, Oldroyd KG, Ver Lee PN, McCarthy PA, Fearon WF; FAME Study Investigators. Fractional flow reserve versus angiography for guiding percutaneous coronary intervention. *N Engl J Med*. 2009;360:213–224.
13. Boogers MJ, Schuijff JD, Kitslaar PH, van Werkhoven JM, de Graaf FR, Boersma E, van Velzen JE, Dijkstra J, Adame IM, Kroft LJ, de Roos A, Schreur JH, Heijnenbroek MW, Jukema JW, Reiber JH, Bax JJ. Automated quantification of stenosis severity on 64-slice CT: a comparison with quantitative coronary angiography. *JACC Cardiovasc Imaging*. 2010;3:699–709.
14. Papadopoulou SL, Neeffjes LA, Garcia-Garcia HM, Flu WJ, Rossi A, Dharampal AS, Kitslaar PH, Mollet NR, Veldhof S, Nieman K, Stone GW, Serruys PW, Krestin GP, de Feyter PJ. Natural history of coronary atherosclerosis by multislice computed tomography. *JACC Cardiovasc Imaging*. 2012;5(3 suppl):S28–S37.
15. Boogers MJ, Broersen A, van Velzen JE, de Graaf FR, El-Naggar HM, Kitslaar PH, Dijkstra J, Delgado V, Boersma E, de Roos A, Schuijff JD,

- Schalij MJ, Reiber JH, Bax JJ, Jukema JW. Automated quantification of coronary plaque with computed tomography: comparison with intravascular ultrasound using a dedicated registration algorithm for fusion-based quantification. *Eur Heart J*. 2012;33:1007–1016.
16. Bossuyt PM, Reitsma JB, Bruns DE, Gatsonis CA, Glasziou PP, Irwig LM, Moher D, Rennie D, de Vet HC, Lijmer JG; Standards for Reporting of Diagnostic Accuracy. The STARD statement for reporting studies of diagnostic accuracy: explanation and elaboration. *Ann Intern Med*. 2003;138:W1–W12.
 17. Kang SJ, Lee JY, Ahn JM, Mintz GS, Kim WJ, Park DW, Yun SC, Lee SW, Kim YH, Lee CW, Park SW, Park SJ. Validation of intravascular ultrasound-derived parameters with fractional flow reserve for assessment of coronary stenosis severity. *Circ Cardiovasc Interv*. 2011;4:65–71.
 18. Koo BK, Yang HM, Doh JH, Choe H, Lee SY, Yoon CH, Cho YK, Nam CW, Hur SH, Lim HS, Yoon MH, Park KW, Na SH, Youn TJ, Chung WY, Ma S, Park SK, Kim HS, Tahk SJ. Optimal intravascular ultrasound criteria and their accuracy for defining the functional significance of intermediate coronary stenoses of different locations. *JACC Cardiovasc Interv*. 2011;4:803–811.
 19. Park SJ, Ahn JM, Kang SJ. Paradigm shift to functional angioplasty: new insights for fractional flow reserve- and intravascular ultrasound-guided percutaneous coronary intervention. *Circulation*. 2011;124:951–957.
 20. Kristensen TS, Engstrøm T, Kelbæk H, von der Recke P, Nielsen MB, Kofoed KF. Correlation between coronary computed tomographic angiography and fractional flow reserve. *Int J Cardiol*. 2010;144:200–205.
 21. Takagi A, Tsurumi Y, Ishii Y, Suzuki K, Kawana M, Kasanuki H. Clinical potential of intravascular ultrasound for physiological assessment of coronary stenosis: relationship between quantitative ultrasound tomography and pressure-derived fractional flow reserve. *Circulation*. 1999;100:250–255.
 22. Nishioka T, Amanullah AM, Luo H, Berglund H, Kim CJ, Nagai T, Hakamata N, Katsushika S, Uehata A, Takase B, Isojima K, Berman DS, Siegel RJ. Clinical validation of intravascular ultrasound imaging for assessment of coronary stenosis severity: comparison with stress myocardial perfusion imaging. *J Am Coll Cardiol*. 1999;33:1870–1878.
 23. Tonino PA, Fearon WF, De Bruyne B, Oldroyd KG, Leesar MA, Ver Lee PN, Maccarthy PA, Van't Veer M, Pijls NH. Angiographic versus functional severity of coronary artery stenoses in the FAME study fractional flow reserve versus angiography in multivessel evaluation. *J Am Coll Cardiol*. 2010;55:2816–2821.
 24. Godoy GK, Vavere A, Miller JM, Chahal H, Niinuma H, Lemos P, Hoe J, Paul N, Clouse ME, Ramos CD, Lima JA, Arbab-Zadeh A. Quantitative coronary arterial stenosis assessment by multidetector CT and invasive coronary angiography for identifying patients with myocardial perfusion abnormalities. *J Nucl Cardiol*. 2012;19:922–930.
 25. Gaemperli O, Schepis T, Valenta I, Koepfli P, Husmann L, Scheffel H, Leschka S, Eberli FR, Lüscher TF, Alkadhi H, Kaufmann PA. Functionally relevant coronary artery disease: comparison of 64-section CT angiography with myocardial perfusion SPECT. *Radiology*. 2008;248:414–423.
 26. Gould KL. Does coronary flow trump coronary anatomy? *JACC Cardiovasc Imaging*. 2009;2:1009–1023.
 27. Marzilli M, Merz CN, Boden WE, Bonow RO, Capozza PG, Chilian WM, DeMaria AN, Guarini G, Huqi A, Morrone D, Patel MR, Weintraub WS. Obstructive coronary atherosclerosis and ischemic heart disease: an elusive link! *J Am Coll Cardiol*. 2012;60:951–956.
 28. Koo BK, Erglis A, Doh JH, Daniels DV, Jegere S, Kim HS, Dunning A, DeFrance T, Lansky A, Leipsic J, Min JK. Diagnosis of ischemia-causing coronary stenoses by noninvasive fractional flow reserve computed from coronary computed tomographic angiograms: results from the prospective multicenter DISCOVER-FLOW (Diagnosis of Ischemia-Causing Stenoses Obtained Via Noninvasive Fractional Flow Reserve) study. *J Am Coll Cardiol*. 2011;58:1989–1997.
 29. Min JK, Leipsic J, Pencina MJ, Berman DS, Koo BK, van Mieghem C, Erglis A, Lin FY, Dunning AM, Apruzzese P, Budoff MJ, Cole JH, Jaffer FA, Leon MB, Malpeso J, Mancini GB, Park SJ, Schwartz RS, Shaw LJ, Mauri L. Diagnostic accuracy of fractional flow reserve from anatomic CT angiography. *JAMA*. 2012;308:1237–1245.
 30. Bamberg F, Becker A, Schwarz F, Marcus RP, Greif M, von Ziegler F, Blankstein R, Hoffmann U, Sommer WH, Hoffmann VS, Johnson TR, Becker HC, Wintersperger BJ, Reiser MF, Nikolaou K. Detection of hemodynamically significant coronary artery stenosis: incremental diagnostic value of dynamic CT-based myocardial perfusion imaging. *Radiology*. 2011;260:689–698.
 31. Ho KT, Chua KC, Klotz E, Panknin C. Stress and rest dynamic myocardial perfusion imaging by evaluation of complete time-attenuation curves with dual-source CT. *JACC Cardiovasc Imaging*. 2010;3:811–820.
 32. Ko BS, Cameron JD, Meredith IT, Leung M, Antonis PR, Nasir A, Crossett M, Hope SA, Lehman SJ, Troupis J, DeFrance T, Seneviratne SK. Computed tomography stress myocardial perfusion imaging in patients considered for revascularization: a comparison with fractional flow reserve. *Eur Heart J*. 2012;33:67–77.
 33. Bamberg F, Hinkel R, Schwarz F, Sandner TA, Baloch E, Marcus R, Becker A, Kupatt C, Wintersperger BJ, Johnson TR, Theisen D, Klotz E, Reiser MF, Nikolaou K. Accuracy of dynamic computed tomography adenosine stress myocardial perfusion imaging in estimating myocardial blood flow at various degrees of coronary artery stenosis using a porcine animal model. *Invest Radiol*. 2012;47:71–77.
 34. Rossi A, Uitterdijk A, Dijkshoorn M, Klotz E, Dharampal A, van Straten M, van der Giessen WJ, Mollet N, van Geuns RJ, Krestin GP, Duncker DJ, de Feyter PJ, Merkus D. Quantification of myocardial blood flow by adenosine-stress CT perfusion imaging in pigs during various degrees of stenosis correlates well with coronary artery blood flow and fractional flow reserve. *Eur Heart J Cardiovasc Imaging*. 2013;14:331–338.
 35. Rossi A, Dharampal A, Wragg A, Davies LC, van Geuns RJ, Anagnostopoulos C, Klotz E, Kitslaar P, Broersen A, Mathur A, Nieman K, Hunink MG, de Feyter PJ, Petersen SE, Pugliese F. Diagnostic performance of hyperaemic myocardial blood flow index obtained by dynamic computed tomography: does it predict functionally significant coronary lesions? *Eur Heart J Cardiovasc Imaging*. Epub 2013 Aug 9.

CLINICAL PERSPECTIVE

Computed tomographic coronary angiography (CTCA) is a reliable, noninvasive imaging modality to visualize coronary artery disease with a high diagnostic accuracy compared with invasive coronary angiography. In daily practice, lesions with a diameter stenosis $\geq 50\%$, interpreted visually, are generally considered for referral to invasive coronary angiography. However, similar to invasive coronary angiography, CTCA is an anatomic imaging technique; thus, it may result in both under and overestimation of a lesion's severity and is often inaccurate in identifying functionally significant coronary lesions that cause ischemia. Current guidelines suggest that treatment decisions based on the hemodynamic effect of a coronary lesion may improve clinical outcome. Studies using intravascular ultrasound have demonstrated that cross-sectional measurements of coronary artery stenosis correlated well with fractional flow reserve. Similar to intravascular ultrasound, quantitative CTCA, using automated border lumen detection algorithms, allows assessment of parameters such as minimum lumen area, % area stenosis, minimum lumen diameter, % diameter stenosis, and plaque burden. A more comprehensive coronary lesion assessment using quantitative CTCA-derived parameters, without further patient irradiation or administration of contrast material, may improve the overall diagnostic accuracy of visual CTCA in the detection of functional significant coronary lesions as defined by a fractional flow reserve ≤ 0.80 . The results of our study show that the additional use of quantitative CTCA-derived parameters improves the prediction of flow-limiting lesions, compared with visual assessment, but remain insufficient. Functional assessment is still needed for lesions of moderate severity to detect impaired fractional flow reserve accurately.

PART III

CT coronary angiography
for the assessment of
coronary bifurcations

Chapter 6

Assessment of Atherosclerotic Plaques at Coronary Bifurcations with Multidetector Computed Tomography Angiography and Intravascular Ultrasound – Virtual Histology

European Heart Journal – Cardiovascular Imaging. 2012 Aug;13(8):635-42.

S.L. Papadopoulou, S. Brugaletta, H.M. Garcia-Garcia, A. Rossi, C. Girasis, A. S. Dharampal, L. A. Neefjes, J. Ligthart, K. Nieman, G.P. Krestin, P.W. Serruys, P. J. de Feyter

Assessment of atherosclerotic plaques at coronary bifurcations with multidetector computed tomography angiography and intravascular ultrasound-virtual histology

Stella-Lida Papadopoulou^{1,2*}, Salvatore Brugaletta¹, Hector M. Garcia-Garcia¹, Alexia Rossi^{1,2}, Chrysaifios Girasis¹, Anoeshka S. Dharampal^{1,2}, Lisan A. Neefjes^{1,2}, Jurgen Ligthart¹, Koehn Nieman^{1,2}, Gabriel P. Krestin², Patrick W. Serruys¹, and Pim J. de Feyter^{1,2}

¹Department of Cardiology, Thoraxcenter, Erasmus University Medical Center, PO Box 2040, Rotterdam, 3000 CA, The Netherlands; and ²Department of Radiology, Erasmus University Medical Center, PO Box 2040, Rotterdam, 3000 CA, The Netherlands

Received 5 January 2012; accepted after revision 29 March 2012

Aims

We evaluated the distribution and composition of atherosclerotic plaques at bifurcations with intravascular ultrasound-virtual histology (IVUS-VH) and multidetector computed tomography (MDCT) in relation to the bifurcation angle (BA).

Methods and results

In 33 patients (age 63 ± 11 years, 79% male) imaged with IVUS-VH and MDCT, 33 bifurcations were matched and studied. The analysed main vessel was divided into a 5 mm proximal segment, the in-bifurcation segment, and a 5 mm distal segment. Plaque contours were manually traced on MDCT and IVUS-VH. Plaques with $>10\%$ confluent necrotic core and $<10\%$ dense calcium on IVUS-VH were considered high risk, whereas plaque composition by MDCT was graded as non-calcified, calcified, or mixed. The maximum BA between the main vessel and the side branch was measured on diastolic MDCT data sets. Overall the mean plaque area decreased from the proximal to the distal segment [8.5 ± 2.8 vs. 6.0 ± 3.0 mm² ($P < 0.001$) by IVUS-VH and 9.0 ± 2.6 vs. 6.5 ± 2.5 mm² ($P < 0.001$) by MDCT]. Similarly, the necrotic core area was higher in the proximal compared with the distal segment (1.12 ± 0.7 vs. 0.71 ± 0.7 mm², $P = 0.001$). The proximal segment had the higher percentage of high-risk plaques (13/25, 52%), followed by the in-bifurcation (6/25, 24%), and the distal segment (6/25, 24%); these plaques were characterized by MDCT as non-calcified (72%) or mixed (28%). The presence of high-risk and non-calcified plaques in the proximal segment was associated with higher BA values ($71 \pm 19^\circ$ vs. $55 \pm 19^\circ$, $P = 0.028$ and $74 \pm 20^\circ$ vs. $50 \pm 14^\circ$, $P = 0.001$, respectively).

Conclusion

The proximal segment of bifurcations is more likely to contain high-risk plaques, especially when the branching angle is wide.

Keywords

Bifurcation • High-risk coronary plaques • Computed tomography coronary angiography • IVUS virtual histology

Introduction

In patients with an atherogenic profile, plaque does not develop evenly across the entire coronary tree, but shows a predilection

for sites where the laminar blood flow gets disturbed.¹ The low-oscillatory endothelial shear stress has been shown to facilitate atherosclerosis and promote the development of plaques with high-risk features;^{2,3} these phenomena may explain the increased

incidence of high-risk (i.e. lipid rich) plaques in the vicinity of coronary artery bifurcations.^{4,5}

Percutaneous treatment of coronary bifurcation lesions remains a challenging task and has been associated with higher restenosis and stent thrombosis rates.^{6–8} Better understanding of the underlying pathology, such as the tissue distribution and composition, may allow for safer and more efficient treatment strategies. Intravascular ultrasound–virtual histology (IVUS-VH) is an imaging method that uses the spectral analysis of radiofrequency data to encode four different plaque components, allowing for quantification and characterization of atherosclerotic plaque.^{9,10}

The complex three-dimensional (3D) geometry of coronary artery bifurcations can affect the local haemodynamic conditions and thereby the plaque distribution and composition. This plausible effect mediated by the bifurcation angle (BA) can only be studied *in vivo* by means of imaging modalities that provide a 3D reconstruction of the bifurcation, such as multidetector computed tomography (MDCT). MDCT coronary angiography has emerged as a means of non-invasive evaluation of coronary atherosclerotic plaques; its ability to assess the plaque burden, remodelling, eccentricity, and composition has been based on extensive cross-sectional correlation with IVUS data in both stable and unstable patients.^{11–13}

The objective of the current study is two-fold: (i) to assess *in vivo* the distribution, composition, and morphology of plaques at bifurcation sites using MDCT and IVUS-VH, and (ii) to explore any possible association of the BA with plaque distribution and composition.

Methods

Study population

All patients admitted to our hospital between March 2008 and March 2010 who underwent both IVUS-VH and MDCT within a 2-month interval were retrospectively screened for bifurcations adequately visualized by both imaging techniques. The indication for the IVUS-VH was the assessment of angiographically intermediate lesions and/or the result of stent implantation; MDCT was performed for either clinical or research purposes. All patients gave informed consent. Only bifurcations visualized with high quality by both imaging techniques and located at a distance >10 mm from adjacent stents were considered for inclusion.

Bifurcation selection and matching

Bifurcation sites involving a side branch (SB) with an ostial diameter ≥ 1.5 mm on MDCT were only considered for inclusion; left main coronary artery bifurcations were not part of this analysis, because of their entirely different morphology.¹⁴ To avoid multiple observations, only a single bifurcation site per patient, the one with the largest SB diameter, was analysed. To ensure proper matching between IVUS-VH and MDCT, the identical bifurcations were identified using the coronary ostia and other bifurcations as landmarks. We chose to analyse only the main branch; the region of interest (ROI) comprised: (i) the proximal segment, extending 5 mm upstream from the proximal take-off of the SB; (ii) the in-bifurcation segment; and (iii) the distal segment, extending 5 mm downstream from the distal take-off of the SB (Figure 1).

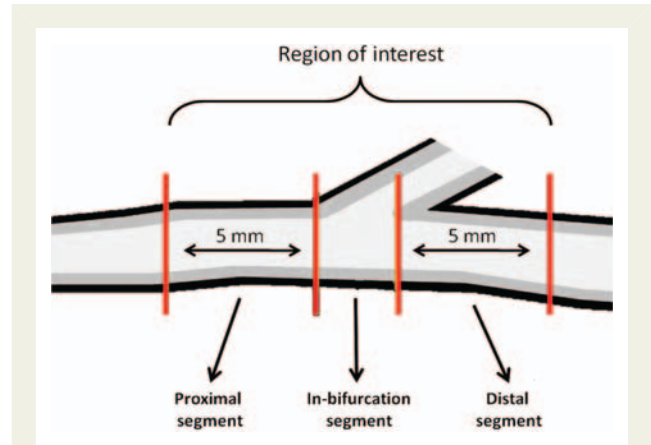


Figure 1 Bifurcation selection and region of interest. Bifurcations that could be identified on both modalities were included. Only the main branch was analysed. The region of interest consisted of: (i) the proximal 5 mm segment; (ii) the in-bifurcation segment; and (iii) the distal 5 mm segment.

IVUS-VH acquisition and analysis

The IVUS-VH imaging was performed using the Eagle Eye 20 MHz catheter (Volcano Corp., Rancho Cordova, CA, USA) with an automatic continuous pullback at a rate of 0.5 mm/s. Grayscale images and radiofrequency data required for VH analysis were acquired during the same pullback. The VH data processing was performed offline by an experienced cardiologist with the VIAS software (Volcano Corp., Rancho Cordova, CA, USA) that allows semi-automated contour detection and provides the compositional analysis. Quantitative IVUS measurements included the vessel area, lumen area, plaque area (vessel area minus lumen area), and plaque burden % [(plaque area/vessel area)*100]. For the radiofrequency-IVUS analyses, four colour-coded tissue components [necrotic core (NC)—red; dense calcium (DC)—white; fibrous (FT)—dark green; and fibrofatty (FF)—light green] were identified with autoregressive classification systems. For every frame, each individual tissue component was quantified as cross-sectional area and percentage (NC + DC + FT + FF = 100%).^{9,15} Volumetric and compositional parameters obtained per cross-section were averaged for each bifurcation segment.

MDCT acquisition

The patients were scanned with a first generation dual-source CT scanner (Somatom Definition, Siemens Healthcare, Forchheim, Germany) or a second generation dual-source CT scanner (Somatom Definition Flash, Siemens Healthcare, Forchheim, Germany) which was available after May 2009. Sublingual nitroglycerin was administered prior to the scan (0.4 mg/dose), provided there were no contraindications; no pre-scan beta-blockers were given. An initial non-enhanced ECG-gated scan (120-kV tube voltage, 75-mAs tube current, and 3-mm slice thickness) was performed to calculate calcium-related scores (Agatston, volume, and equivalent mass),^{16–18} and was followed by a contrast enhanced CT angiography. The CT angiographic parameters were (i) for the first generation dual-source scanner: $32 \times 2 \times 0.6$ mm collimation with the z-flying focal spot for both detectors, gantry rotation time 330 ms, tube voltage 120 kV, current of 320 to 412 mAs, and (ii) for the second generation dual-source scanner: $64 \times 2 \times 0.6$ mm collimation with the z-flying focal spot for both detectors, gantry rotation time 280 ms, tube voltage

of 100–120 kV, current of 320–370 mAs. A bolus of iodinated contrast material (370 mgI/mL, Ultravist; Schering, Berlin, Germany), which varied between 60 and 100 mL depending on the expected scan time, was injected intravenously (flow rate, 5.5 mL/s) followed by a 40 mL saline chaser at the same injection rate. A bolus tracking technique was used to synchronize the arrival of contrast in the coronary arteries and the start of the MDCT acquisition. For acquisitions with the first generation dual-source CT scanner, retrospective ECG-gated technique with ECG-pulsing was used; when scanning with the second generation dual-source CT either the prospectively ECG-triggered axial scan mode ('step-and-shoot') or the retrospective ECG-gated spiral scan mode with ECG-pulsing was used, depending on the heart rate. The pitch for the retrospective scan was set automatically by the scanner software, prior to scanning. The mean effective radiation dose was 9.0 ± 3.9 mSv, using the dose-length product and a conversion factor k of 0.014 mSv/mGy/cm.¹⁹ All MDCT coronary angiograms were reconstructed with a slice thickness 0.75 mm, an increment 0.4 mm, and a medium-to-smooth (B26f) convolution kernel. Optimal data sets with the best image quality were reconstructed mainly in the mid- to end-diastolic phase.

MDCT image analysis

All data sets from the MDCT angiography scans were transferred to a dedicated workstation (Leonardo; Siemens Medical Systems, Erlangen,

Germany) for further analysis by an experienced observer, blinded to the results of the IVUS-VH analysis. After the identification of the bifurcation ROI in the original cross-sectional images, serial multiplanar reformatted images (1.0-mm slice thickness, interval 0.5-mm) orthogonal to the longitudinal axis of the main vessel were rendered to obtain cross-sectional images of the respective vessel segment (Figure 2A). The settings for the window level and width were previously optimized by an independent investigator and fixed at 740 and 220 HU, respectively²⁰ (Rengo M. *et al.*, submitted). Subsequently, the lumen and vessel areas were manually traced in each image, and the plaque areas were calculated as the difference between the vessel and lumen areas (Figure 2D). The plaque areas measured on each cross-section were averaged for each segment and reported as the mean areas.

Plaque type classification

For each one of the three bifurcation segments, the existing plaque phenotype was examined by both modalities. Based on IVUS-VH, lesions were considered present when the percentage plaque area was $\geq 40\%$ on three consecutive frames. Plaques with $> 10\%$ confluent NC and $< 10\%$ dense calcium on three consecutive frames were classified as high-risk (i.e. NC rich) and represented thick-capped fibroatheromas (VH-ThCFAs) or thin-capped fibroatheromas

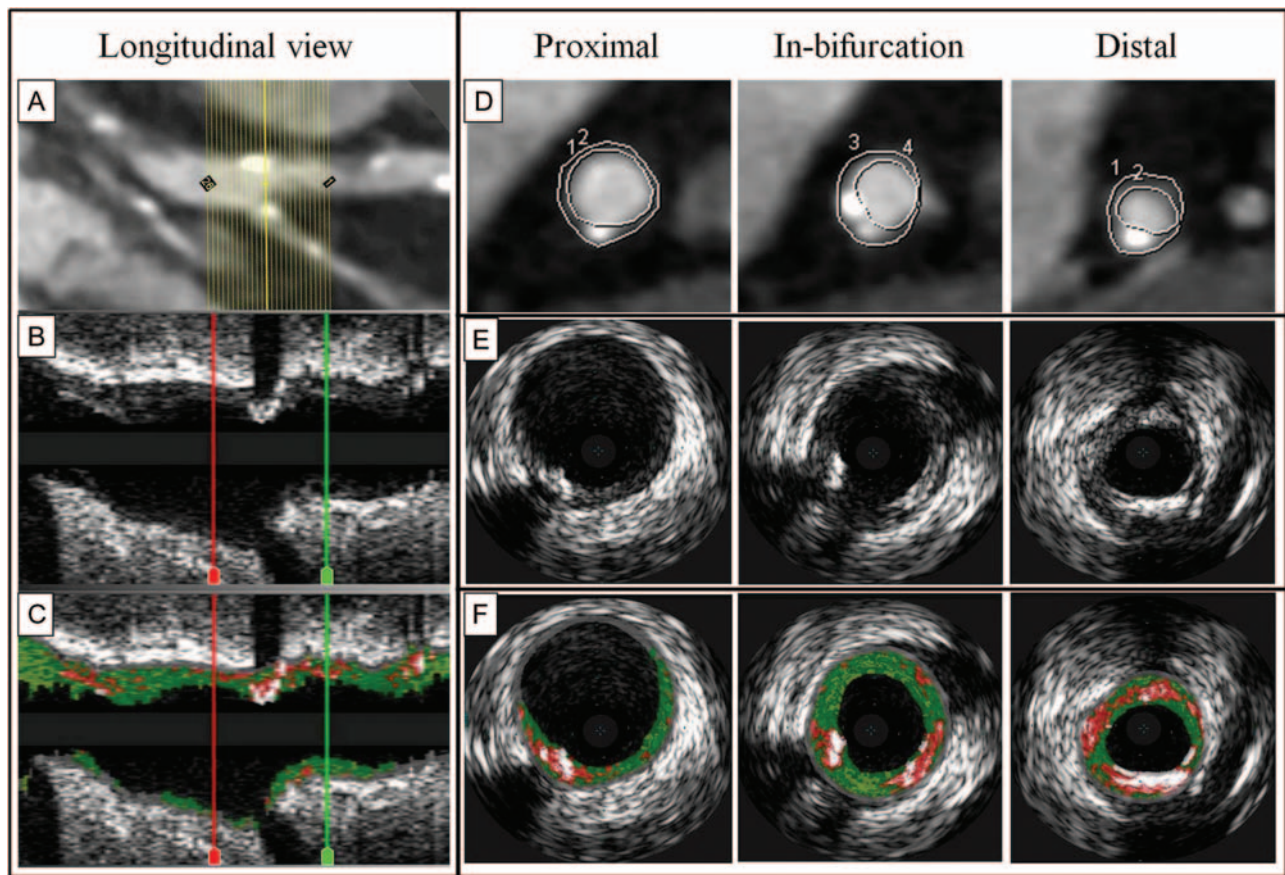


Figure 2 Bifurcation matching and analysis by MDCT and IVUS-VH. To ensure correct matching of the bifurcations with the two techniques, anatomic landmarks, and characteristic calcifications were used. Longitudinal vessel view by MDCT (A), grayscale IVUS (B), and virtual histology (C). Examples of corresponding analysed cross-sections (D–F) in the proximal, in-bifurcation, and distal segment. IVUS-VH, intravascular ultrasound-virtual histology; MDCT, multidetector computed tomography.

(VH-TCFAs), which are considered high-risk plaques according to the American Heart Association and Virmani classifications.^{21,22}

Based on MDCT, plaques were classified into three types: calcified plaques ($\geq 50\%$ of the plaque area occupied by calcified tissue), mixed plaques ($< 50\%$ of the plaque area occupied by calcified tissue), and non-calcified plaques which did not contain any calcium at all.¹¹

Measurement of bifurcation angles with MDCT

Multipolar reconstructions (MPRs) were rendered exactly in the plane defined by the main vessel and SB at the bifurcation site, as previously described.²³ The MPR view where the angulation between the main vessel and SB was maximal was used to determine the BA values. The angle was delineated by two centreline vectors drawn along the initial 5-mm course of the distal main vessel and SB, respectively (Figure 3); only diastolic data sets were used for BA measurements.

Statistical analysis

Continuous variables were presented as means \pm 1 SD, unless otherwise indicated, and categorical variables were reported as counts and/or percentages. The distribution of data was examined with the Shapiro-Wilk test of normality. Continuous variables were compared between different bifurcation segments and between the two modalities with the paired samples *t*-test or the Wilcoxon signed ranks

test for two-dependent samples as appropriate. The BA values were compared between groups using the unpaired *t*-test. A two-sided *P*-value < 0.05 was considered statistically significant. Statistical analyses were performed using SPSS 17.0 for Windows (SPSS, Inc., Chicago, IL, USA).

Results

Clinical and procedural characteristics

Out of 64 consecutive patients with IVUS-VH and MDCT imaging who were screened, 38 were eligible for inclusion. Reasons for exclusion were poor MDCT or IVUS-VH image quality ($n = 6$), presence of stents within the ROI ($n = 9$), and lack of true bifurcations (diameter of the SB ostium < 1.5 mm) ($n = 11$). Moreover, in five patients matching of bifurcations between the two imaging modalities was not possible, because more than one bifurcation were located in proximity to each other and could not be reliably identified for the analysis. A total of 33 bifurcation sites from 33 patients were analysed; the mean age was 63 ± 11 years, and 79% of the patients were male. The patients' characteristics are summarized in Table 1. Regarding the bifurcation location, 14 left anterior descending coronary artery/diagonal (42%), 8 left circumflex coronary artery/marginal (24%), 8 right coronary artery/right

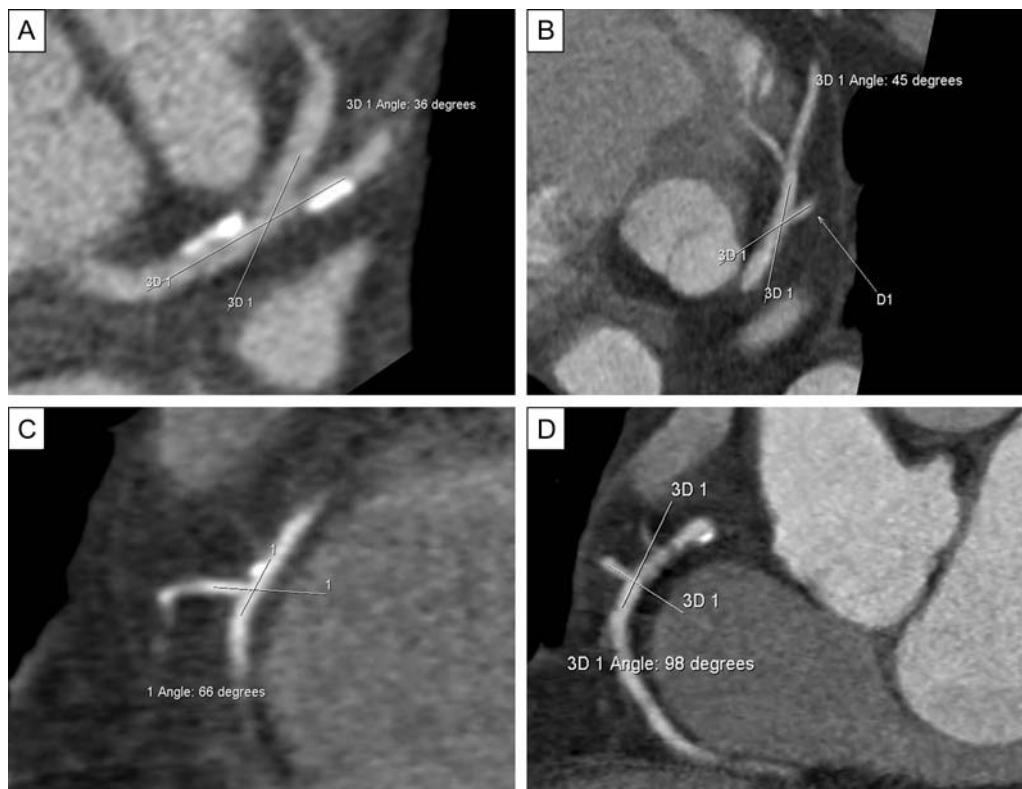


Figure 3 Coronary bifurcation angle measurements with MDCT. Multipolar reconstructions were rendered exactly in the plane described by the main vessel and side branch at the bifurcation site. Examples of the bifurcation angles between LAD and D1 (A, 36° and B, 45°) and between RCA and RVB (C, 66° and D, 98°). D1, first diagonal branch; LAD, left anterior descending coronary artery; MDCT, multidetector computed tomography; RCA, right coronary artery; RVB, right ventricular branch.

Table 1 Baseline patients' characteristics, *n* = 33

Age (mean ± SD), years	63 ± 11
Male gender, <i>n</i> (%)	26 (79)
Risk factors	
Hypertension, <i>n</i> (%)	24 (73)
Hypercholesterolaemia, <i>n</i> (%)	27 (82)
Diabetes mellitus, <i>n</i> (%)	6 (18)
Current smoking, <i>n</i> (%)	7 (21)
Family history of CAD, <i>n</i> (%)	15 (45)
Previous ACS, <i>n</i> (%)	10 (30)
Previous PCI, <i>n</i> (%)	8 (24)
Clinical presentation	
Stable angina, <i>n</i> (%)	24 (73)
Unstable angina, <i>n</i> (%)	6 (18)
Acute myocardial infarction, <i>n</i> (%)	3 (9)
Studied vessel	
Left anterior descending, <i>n</i> (%)	14 (42)
Left circumflex, <i>n</i> (%)	8 (24)
Right coronary artery, <i>n</i> (%)	11 (34)
Vessel disease, <i>n</i> (%)	
One vessel disease	16 (50)
Two vessel disease	13 (41)
Three vessel disease	3 (9)
Calcium-related scores ^a	
Agatston score	313 (147–842)
Equivalent mass, mg	59 (29–152)
Volume, mm ³	259 (150–701)

^aValues are median (inter-quartile range). ACS, acute coronary syndrome; CAD, coronary artery disease; PCI, percutaneous coronary intervention; SD, standard deviation.

ventricular branch (24%), and 3 right coronary artery/acute marginal branch (9%) were studied.

Plaque volumetric and compositional characteristics

Overall, the mean plaque area was increased in the proximal compared with the distal segment (IVUS-VH: 8.5 ± 2.8 vs. 6.0 ± 3.0 mm², $P < 0.001$ and MDCT: 9.0 ± 2.6 vs. 6.5 ± 2.5 mm², $P < 0.001$, respectively). The mean plaque burden % was higher in the proximal compared with the distal segment (IVUS-VH: 52 ± 13 vs. $44\% \pm 15\%$, $P = 0.002$ and MDCT 51 ± 11 vs. $46\% \pm 11\%$, $P = 0.029$, respectively). The volumetric data (Table 2) did not differ significantly between the two modalities. Finally, the mean NC area and the mean percentage of NC were increased in the proximal compared with the distal segment (Figure 4).

Frequency of plaque type

Based on IVUS-VH, 2 bifurcations (6%) had no atherosclerotic plaques at all, whereas in 14 bifurcations (42%) the plaque was contiguous from the proximal to the distal segment. In total there were 69 bifurcation segments with plaques, where of 25

Table 2 Volumetric data in each segment of the bifurcation by MDCT and IVUS-VH

Parameter	Mean values		
	MDCT (mean ± SD)	IVUS-VH (mean ± SD)	P-value (t-test)
Mean plaque area (mm ²)			
Proximal	9.0 ± 2.6	8.5 ± 2.8	0.09
In-bifurcation	7.2 ± 2.4	7.4 ± 3.0	0.94
Distal	6.5 ± 2.5	6.0 ± 3.0	0.09
Mean plaque burden (%)			
Proximal	51 ± 11	52 ± 13	0.69
In-bifurcation	46 ± 11	45 ± 13	0.20
Distal	46 ± 11	44 ± 15	0.15

IVUS-VH, intravascular ultrasound-virtual histology; MDCT, multidetector computed tomography; SD, standard deviation.

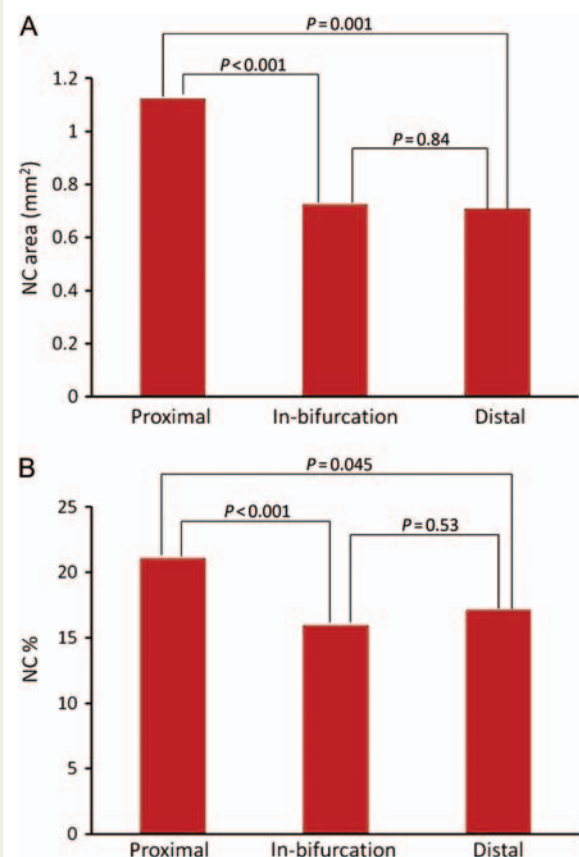


Figure 4 Necrotic core (NC) distribution. NC area (A) and NC percentage (B) distribution in the proximal, in-bifurcation, and distal segments.

were high-risk plaques. The proximal segment had the higher percentage of high-risk plaques (13 of 25, 52%), followed by the in-bifurcation segment (6 of 25, 24%) and the distal segment

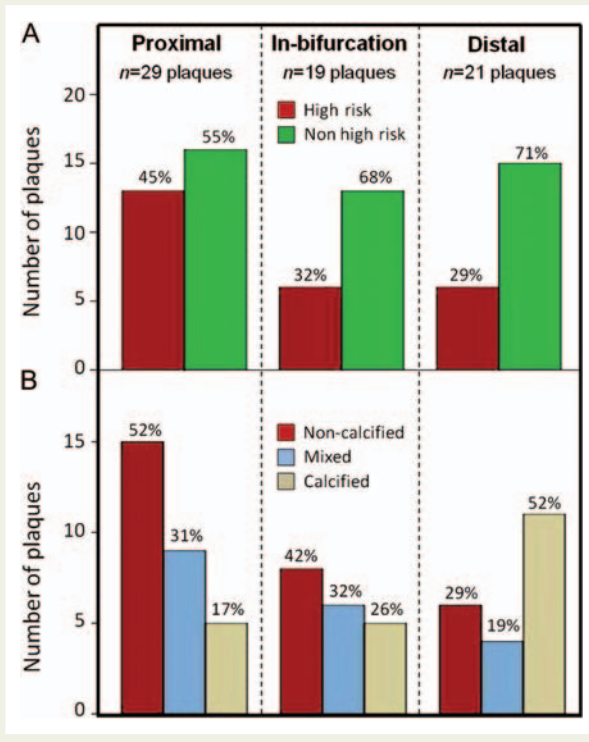


Figure 5 Distribution of the different plaque types in each segment. (A) virtual histology, (B) multidetector computed tomography. The percentages indicate the frequencies of the different plaque types within each segment.

(6 of 25, 24%); the distribution of the different plaque types within each segment is shown in Figure 5A. On MDCT, non-calcified plaques presented more frequently in the proximal segment, whereas the calcified plaques were more frequent in the distal segment (Figure 5B). The majority of high-risk plaques as determined by IVUS-VH were characterized by MDCT as non-calcified ones (72%); the remaining 28% were classified as mixed. The plaque type distribution per segment is shown in Figure 6.

Plaque distribution and composition in relation to the bifurcation angle

Bifurcations containing plaques in their proximal segments had significantly larger BA values compared with those without ($P = 0.002$), Table 3. Moreover, the presence of high-risk and non-calcified plaques in the proximal segment was associated with higher BA values (71 ± 19 vs. $55 \pm 19^\circ$, $P = 0.028$ and 74 ± 20 vs. $50 \pm 14^\circ$, $P = 0.001$, respectively). The BA was not related significantly with either plaque distribution or composition in the other segments.

Discussion

In this exploratory study, we evaluated the distribution and composition of atherosclerotic plaques at coronary bifurcations using invasive and non-invasive imaging. To our knowledge, this is the

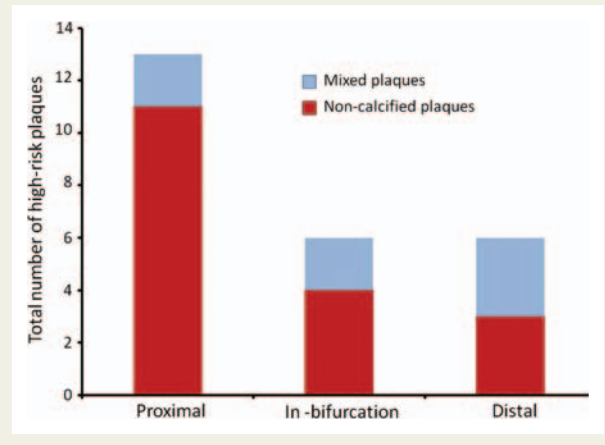


Figure 6 Classification of the high-risk plaques by MDCT. The IVUS-VH high-risk plaques were characterized by MDCT as non-calcified and mixed. The distribution per segment is presented. IVUS-VH, intravascular ultrasound-virtual histology; MDCT, multidetector computed tomography.

Table 3 Bifurcation angle in relation to plaque distribution and composition

Segment	Bifurcation angle		P-value
	Any plaque	No plaque	
Proximal	62 ± 20	46 ± 5	0.002
In-bifurcation	56 ± 18	66 ± 22	0.139
Distal	57 ± 20	66 ± 20	0.186
	High-risk plaques	Non-high-risk plaques	
Proximal	71 ± 19	55 ± 19	0.028
In-bifurcation	49 ± 8	58 ± 20	0.155
Distal	60 ± 25	55 ± 17	0.654
	Non-calcified plaques ^a	Mixed/calcified plaques ^a	
Proximal	74 ± 20	50 ± 14	0.001
In-bifurcation	61 ± 20	52 ± 16	0.286
Distal	74 ± 22	50 ± 14	0.047

^aAs characterized by multidetector computed tomography.

first *in vivo* study to examine the volumetric and compositional plaque characteristics in combination with the 3D geometry of coronary bifurcations (as expressed by the BA).

Our main findings can be summarized as follows: (i) the proximal segment has a more extensive plaque burden with more NC; (ii) the plaques with high-risk features on IVUS-VH and the non-calcified plaques on MDCT both show a differential distribution along the bifurcation being more frequent in the proximal segment; (iii) the distribution and composition of plaques in the proximal segment is associated with the BA values.

The current study corroborates earlier findings on plaque volumetric and compositional characteristics at bifurcation sites. In a previous IVUS study, Badak *et al.*²⁴ suggested that significantly more atheroma was located proximal to the bifurcation than distally. Han *et al.*¹⁴ expanded on these findings using IVUS-VH to report on tissue characterization; that study showed that the plaque burden and the percentage of the NC were significantly larger in the proximal segment of the non-left main bifurcations. These data appear to be largely concordant with a prior report by Gonzalo *et al.*,⁵ using IVUS-VH and Optical Coherence Tomography (OCT); they suggested that the percentage of the NC was higher at the proximal 'rim' of the bifurcation. It has been shown that the distribution of inflammatory cells in atherosclerotic plaques is associated with the direction of the arterial flow, with higher content of macrophages in the upstream (proximal) part.²⁵ The differential distribution of the NC and the high-risk plaques along the coronary tree could be attributed to the influence of local haemodynamic factors altered at bifurcation sites.

Our data demonstrated that predominantly non-calcified plaque type by MDCT corresponded to the IVUS-VH high-risk phenotype. This finding is in agreement with histopathology studies²² and with previous greyscale IVUS studies showing that plaques with low echogenicity (presumably lipid rich) are mainly soft (non-calcified) by MDCT.^{11,26,27} Conversely, other studies suggested that mixed plaques on MDCT are associated more frequently with high-risk features on IVUS-VH.^{28,29} A recent more systematic evaluation³⁰ demonstrated that only the non-calcified plaques with small (<1 mm) spotty calcifications on MDCT were associated with plaque characteristics deemed more high risk on IVUS-VH; however, these plaques did not have significantly more VH-TCFAs compared with non-calcified plaques. In our analysis, the ROI included only plaques located within 5-mm long segments proximal and distal to the SB; since atherosclerotic plaque can be diffuse, in case a spotty calcification was located outside this ROI, it would have not been included in our analysis.

The present study extended the assessment of bifurcation lesions beyond volumetric and compositional analysis by integrating the MDCT-based BA measurements, which emphasizes the added value of this 3D imaging modality. Our *in vivo* data showed that the presence and phenotype of atherosclerotic plaque in the proximal bifurcation segment is related to the BA size. This finding could be supported by computational fluid dynamics^{31–33} and histopathology³⁴ studies demonstrating that the haemodynamic phenomena important in atherogenesis are more pronounced in widely angulated bifurcations. Moreover, the BA size has been described as a determinant of treatment strategy in bifurcation lesions.³⁵ In numerous bench and clinical studies,^{36–40} a wide BA has been associated with a greater risk for suboptimal post-procedural result and long-term adverse clinical events. Additionally, our data demonstrated that a wide BA is associated with a greater plaque burden and a high-risk phenotype of bifurcation lesions, which make us speculate that NC-rich plaques could be related to the higher restenosis and thrombosis rates.^{41–43} Eventually, a comprehensive assessment of bifurcation lesions including plaque characterization and BA measurements could lead to optimized interventional strategies and improved long-term clinical outcomes.

Limitations

Although this is the first study combining invasive and non-invasive imaging of bifurcations, it was retrospectively performed in a selected patient population undergoing invasive and non-invasive imaging, thus generalization of our results should be done with caution. Given the inclusion of a limited number of patients, the possibility of a type II error should be considered and multivariate analysis for risk factors was not performed. Furthermore, the limited axial resolution of the IVUS (~200 µm) does not permit an accurate evaluation of the thin fibrous cap (<65 µm). A proposed method of combined use of IVUS-VH and OCT^{5,44} could facilitate more accurate identification of VH-TCFAs, but was not available for this study. Finally, the radiation exposure during MDCT coronary angiography remains a matter of concern; significant reduction in radiation dose can currently be achieved by implementation of dose-saving techniques.⁴⁵

Conclusions

This study extended the evaluation of bifurcation lesions beyond volumetric and compositional analysis by integrating information on the geometry of coronary bifurcations. A larger plaque burden and increased NC content were found in the proximal bifurcation segments. The high-risk plaques on IVUS-VH and the non-calcified plaques on MDCT tend to accumulate in the proximal bifurcation segments, especially in the presence of a wide BA.

Conflict of interest: None declared.

References

1. Malek AM, Alper SL, Izumo S. Hemodynamic shear stress and its role in atherosclerosis. *JAMA* 1999;**282**:2035–42.
2. Chatzizisis YS, Jonas M, Coskun AU, Beigel R, Stone BV, Maynard C *et al.* Prediction of the localization of high-risk coronary atherosclerotic plaques on the basis of low endothelial shear stress: an intravascular ultrasound and histopathology natural history study. *Circulation* 2008;**117**:993–1002.
3. Slager CJ, Wentzel JJ, Gijzen FJ, Schuurbiens JC, van der Wal AC, van der Steen AF *et al.* The role of shear stress in the generation of rupture-prone vulnerable plaques. *Nat Clin Pract Cardiovasc Med* 2005;**2**:401–7.
4. Garcia-Garcia HM, Gomez-Lara J, Gonzalo N, Garg S, Shin ES, Goedhart D *et al.* A comparison of the distribution of necrotic core in bifurcation and non-bifurcation coronary lesions: an *in vivo* assessment using intravascular ultrasound radiofrequency data analysis. *EuroIntervention* 2010;**6**:321–7.
5. Gonzalo N, Garcia-Garcia HM, Regar E, Barlis P, Wentzel J, Onuma Y *et al.* *In vivo* assessment of high-risk coronary plaques at bifurcations with combined intravascular ultrasound and optical coherence tomography. *JACC Cardiovasc Imaging* 2009;**2**:473–82.
6. Colombo A, Moses JW, Morice MC, Ludwig J, Holmes DR Jr, Spanos V *et al.* Randomized study to evaluate sirolimus-eluting stents implanted at coronary bifurcation lesions. *Circulation* 2004;**109**:1244–9.
7. Ge L, Airoldi F, Iakovou I, Cosgrave J, Michev I, Sangiorgi GM *et al.* Clinical and angiographic outcome after implantation of drug-eluting stents in bifurcation lesions with the crush stent technique: importance of final kissing balloon post-dilation. *J Am Coll Cardiol* 2005;**46**:613–20.
8. Routledge HC, Lefevre T, Colombo A, Oldroyd KG, Hamm CW, Guagliumi G *et al.* Three-year clinical outcome of percutaneous treatment of bifurcation lesions in multivessel coronary artery disease with the sirolimus-eluting stent: insights from the Arterial Revascularisation Therapies Study, part II (ARTS II). *EuroIntervention* 2009;**5**:190–6.
9. Nair A, Kuban BD, Tuzcu EM, Schoenhagen P, Nissen SE, Vince DG. Coronary plaque classification with intravascular ultrasound radiofrequency data analysis. *Circulation* 2002;**106**:2200–6.
10. Nasu K, Tsuchikane E, Katoh O, Vince DG, Virmani R, Surmely JF *et al.* Accuracy of *in vivo* coronary plaque morphology assessment: a validation study of *in vivo*

- virtual histology compared with *in vitro* histopathology. *J Am Coll Cardiol* 2006;**47**:2405–12.
11. Leber AW, Becker A, Knez A, von Ziegler F, Sirol M, Nikolaou K *et al*. Accuracy of 64-slice computed tomography to classify and quantify plaque volumes in the proximal coronary system: a comparative study using intravascular ultrasound. *J Am Coll Cardiol* 2006;**47**:672–7.
 12. Papadopoulou SL, Neeffes LA, Schaap M, Li HL, Capuano E, van der Giessen AG *et al*. Detection and quantification of coronary atherosclerotic plaque by 64-slice multidetector CT: A systematic head-to-head comparison with intravascular ultrasound. *Atherosclerosis* 2011;**219**:163–70.
 13. Voros S, Rinehart S, Qian Z, Vazquez G, Anderson H, Murrieta L *et al*. Prospective validation of standardized, 3-dimensional, quantitative coronary computed tomographic plaque measurements using radiofrequency backscatter intravascular ultrasound as reference standard in intermediate coronary arterial lesions: results from the ATLANTA (assessment of tissue characteristics, lesion morphology, and hemodynamics by angiography with fractional flow reserve, intravascular ultrasound and virtual histology, and noninvasive computed tomography in atherosclerotic plaques) I study. *JACC Cardiovasc Interv* 2011;**4**:198–208.
 14. Han SH, Puma J, Garcia-Garcia HM, Nasu K, Margolis P, Leon MB *et al*. Tissue characterisation of atherosclerotic plaque in coronary artery bifurcations: an intravascular ultrasound radiofrequency data analysis in humans. *EuroIntervention* 2010;**6**:313–20.
 15. Garcia-Garcia HM, Mintz GS, Lerman A, Vince DG, Margolis MP, van Es GA *et al*. Tissue characterisation using intravascular radiofrequency data analysis: recommendations for acquisition, analysis, interpretation and reporting. *EuroIntervention* 2009;**5**:177–189.
 16. Agatston AS, Janowitz WR, Hildner FJ, Zusmer NR, Viamonte M Jr, Detrano R. Quantification of coronary artery calcium using ultrafast computed tomography. *J Am Coll Cardiol* 1990;**15**:827–32.
 17. Callister TQ, Cooil B, Raya SP, Lippolis NJ, Russo DJ, Raggi P. Coronary artery disease: improved reproducibility of calcium scoring with an electron-beam CT volumetric method. *Radiology* 1998;**208**:807–14.
 18. Hoffmann U, Siebert U, Bull-Stewart A, Achenbach S, Ferencik M, Moselewski F *et al*. Evidence for lower variability of coronary artery calcium mineral mass measurements by multi-detector computed tomography in a community-based cohort—consequences for progression studies. *Eur J Radiol* 2006;**57**:396–402.
 19. Bongartz G, Golding SJ, Jurik AG, Leonardi M, van Persijn van Meerten E, Rodríguez R *et al*. 2004 CT Quality Criteria—Appendix C. European Guidelines for Multislice Computed Tomography, European Commission. Available at: http://www.msct.eu/CT_Quality_Criteria.htm.
 20. Mollet NR, Rengo M, Neeffes LA, van der Giessen AG, Weustink AC, Pugliese F *et al*. Plaque Quantification by CT Coronary Angiography: Optimization of Window Level Settings. *Radiological Society of North America, 94th Scientific Assembly and Annual Meeting*. Chicago, IL, USA, 2008.
 21. Stary HC, Chandler AB, Dinsmore RE, Fuster V, Glagov S, Inwall W Jr *et al*. A definition of advanced types of atherosclerotic lesions and a histological classification of atherosclerosis. A report from the Committee on Vascular Lesions of the Council on Arteriosclerosis, American Heart Association. *Arterioscler Thromb Vasc Biol* 1995;**15**:1512–31.
 22. Virmani R, Kolodgie FD, Burke AP, Farb A, Schwartz SM. Lessons from sudden coronary death: a comprehensive morphological classification scheme for atherosclerotic lesions. *Arterioscler Thromb Vasc Biol* 2000;**20**:1262–75.
 23. Pflederer T, Ludwig J, Ropers D, Daniel WG, Achenbach S. Measurement of coronary artery bifurcation angles by multidetector computed tomography. *Invest Radiol* 2006;**41**:793–8.
 24. Badak O, Schoenhagen P, Tsunoda T, Magyar WA, Coughlin J, Kapadia S *et al*. Characteristics of atherosclerotic plaque distribution in coronary artery bifurcations: an intravascular ultrasound analysis. *Coron Artery Dis* 2003;**14**:309–16.
 25. Dirksen MT, van der Wal AC, van den Berg FM, van der Loos CM, Becker AE. Distribution of inflammatory cells in atherosclerotic plaques relates to the direction of flow. *Circulation* 1998;**98**:2000–3.
 26. Leber AW, Knez A, Becker A, Becker C, von Ziegler F, Nikolaou K *et al*. Accuracy of multidetector spiral computed tomography in identifying and differentiating the composition of coronary atherosclerotic plaques: a comparative study with intracoronary ultrasound. *J Am Coll Cardiol* 2004;**43**:1241–7.
 27. Schroeder S, Kopp AF, Baumbach A, Meisner C, Kuettner A, Georg C *et al*. Non-invasive detection and evaluation of atherosclerotic coronary plaques with multislice computed tomography. *J Am Coll Cardiol* 2001;**37**:1430–5.
 28. Pundziute G, Schuijff JD, Jukema JW, Decramer I, Sarno G, Vanhoenacker PK *et al*. Head-to-head comparison of coronary plaque evaluation between multislice computed tomography and intravascular ultrasound radiofrequency data analysis. *JACC Cardiovasc Interv* 2008;**1**:176–82.
 29. Sarno G, Vanhoenacker P, Decramer I, Schuijff JD, Pundziute G, Margolis P *et al*. Characterisation of the 'vulnerable' coronary plaque by multi-detector computed tomography: a correlative study with intravascular ultrasound-derived radiofrequency analysis of plaque composition. *EuroIntervention* 2008;**4**:318–23.
 30. van Velzen JE, de Graaf FR, de Graaf MA, Schuijff JD, Kroft LJ, de Roos A *et al*. Comprehensive assessment of spotty calcifications on computed tomography angiography: comparison to plaque characteristics on intravascular ultrasound with radiofrequency backscatter analysis. *J Nucl Cardiol* 2011;**18**:893–903.
 31. Perktold K, Resch M, Florian H. Pulsatile non-Newtonian flow characteristics in a three-dimensional human carotid bifurcation model. *J Biomech Eng* 1991;**113**:464–75.
 32. Markl M, Wegent F, Zech T, Bauer S, Strecker C, Schumacher M *et al*. *In vivo* wall shear stress distribution in the carotid artery: effect of bifurcation geometry, intimal carotid artery stenosis, and recanalization therapy. *Circ Cardiovasc Imaging* 2010;**3**:647–55.
 33. Moore JE Jr, Timmins LH, Ladisa JF Jr. Coronary artery bifurcation biomechanics and implications for interventional strategies. *Catheter Cardiovasc Interv* 2010;**76**:836–43.
 34. Friedman MH, Ding Z. Relation between the structural asymmetry of coronary branch vessels and the angle at their origin. *J Biomech* 1998;**31**:273–8.
 35. Hildick-Smith D, Lassen JF, Albiero R, Lefevre T, Darremont O, Pan M *et al*. Consensus from the 5th European Bifurcation Club meeting. *EuroIntervention* 2010;**6**:34–8.
 36. Ormiston JA, Currie E, Webster MW, Kay P, Ruygrok PN, Stewart JT *et al*. Drug-eluting stents for coronary bifurcations: insights into the crush technique. *Catheter Cardiovasc Interv* 2004;**63**:332–6.
 37. Murasato Y. Impact of three-dimensional characteristics of the left main coronary artery bifurcation on outcome of crush stenting. *Catheter Cardiovasc Interv* 2007;**69**:248–56.
 38. Dzavik V, Kharbanda R, Ivanov J, Ing DJ, Bui S, Mackie K *et al*. Predictors of long-term outcome after crush stenting of coronary bifurcation lesions: importance of the bifurcation angle. *Am Heart J* 2006;**152**:762–9.
 39. Adriaenssens T, Byrne RA, Dibra A, Iijima R, Mehili J, Bruskin O *et al*. Culotte stenting technique in coronary bifurcation disease: angiographic follow-up using dedicated quantitative coronary angiographic analysis and 12-month clinical outcomes. *Eur Heart J* 2008;**29**:2868–76.
 40. Collins N, Seidelin PH, Daly P, Ivanov J, Barolet A, Mackie K *et al*. Long-term outcomes after percutaneous coronary intervention of bifurcation narrowings. *Am J Cardiol* 2008;**102**:404–10.
 41. Joner M, Finn AV, Farb A, Mont EK, Kolodgie FD, Ladich E *et al*. Pathology of drug-eluting stents in humans: delayed healing and late thrombotic risk. *J Am Coll Cardiol* 2006;**48**:193–202.
 42. Kawaguchi R, Oshima S, Jingu M, Tsurugaya H, Toyama T, Hoshizaki H *et al*. Usefulness of virtual histology intravascular ultrasound to predict distal embolization for ST-segment elevation myocardial infarction. *J Am Coll Cardiol* 2007;**50**:1641–6.
 43. Nakazawa G, Yazdani SK, Finn AV, Vorpahl M, Kolodgie FD, Virmani R. Pathological findings at bifurcation lesions: the impact of flow distribution on atherosclerosis and arterial healing after stent implantation. *J Am Coll Cardiol* 2010;**55**:1679–87.
 44. Sawada T, Shite J, Garcia-Garcia HM, Shinke T, Watanabe S, Otake H *et al*. Feasibility of combined use of intravascular ultrasound radiofrequency data analysis and optical coherence tomography for detecting thin-cap fibroatheroma. *Eur Heart J* 2008;**29**:1136–46.
 45. Raff GL, Chinnaiyan KM, Share DA, Goraya TY, Kazerooni EA, Moscucci M *et al*. Radiation dose from cardiac computed tomography before and after implementation of radiation dose-reduction techniques. *JAMA* 2009;**301**:2340–8.

Chapter 7

A CT-based Medina classification in coronary bifurcations: does the lumen assessment provide sufficient information?

Catheterization and Cardiovascular Interventions. 2014 Sep 1;84(3):445-52

S.L. Papadopoulou, C. Girasis, F.J. Gijsen, A. Rossi, J. Ottama, A. van der Giessen, J.C. Schuurbijs, H.M. Garcia-Garcia, P.J. de Feyter, J.J. Wentzel

A CT-based Medina Classification in Coronary Bifurcations: Does the Lumen Assessment Provide Sufficient Information?

Stella-Lida Papadopoulou,^{1,2} MD, Chrysafios Girasis,¹ MD, Frank J. Gijsen,³ PhD, Alexia Rossi,^{1,2} MD, Jade Ottema,³ MD, Alina van der Giessen,³ PhD, Johan C. Schuurbijs,³ BSc, Hector M. Garcia-Garcia,¹ MD, PhD, Pim J. de Feyter,^{1,2} MD, PhD, and Jolanda J. Wentzel,^{3*} PhD

Aims: To evaluate the distribution of atherosclerosis at bifurcations with computed tomography coronary angiography (CTCA) and propose a novel CT-Medina classification for bifurcation lesions. **Methods:** In 26 patients (age 55 ± 10 years, 81% male) imaged with CTCA, 39 bifurcations were studied. The bifurcations analysis included the proximal main vessel, the distal main vessel and the side branch (SB). Plaque contours were manually traced on CTCA; the lumen, vessel and plaque area were measured, as well as plaque burden (%). The carina cross-sections were divided into four equal parts according to the expected wall shear stress (WSS) to assess circumferential plaque distribution. All the bifurcation lesions were classified using the Medina classification and a novel CT-Medina classification combining lumen narrowing and plaque burden $\geq 70\%$. **Results:** Presence of severe plaque (plaque burden $\geq 70\%$) by CTCA was demonstrated in 12.8% (5/39) of the proximal segments, 15.4% (6/39) of the distal segments and 7.7% (3/39) of the SB segments. The thickest plaque was located more often in low WSS parts of the carina cross-sections, whereas the flow divider was rarely affected. Although in the majority of bifurcations plaque was present, based on the Medina classification 92% of the assessed bifurcations were identified as 0,0,0. Characterization of bifurcation lesions using the new CT-Medina classification provided additional information in seven cases (18%) compared to the Medina classification. **Conclusion:** Atherosclerotic plaque is widely present in all bifurcation segments, even in the absence of coronary lumen stenosis. A CT-Medina classification combining lumen and plaque parameters is more informative than angiographic classification of bifurcation lesions and could potentially facilitate the decision-making on the treatment of these lesions. © 2014 Wiley Periodicals, Inc.

Key words: bifurcation; computed tomography coronary angiography; atherosclerosis; medina classification

¹Department of Cardiology, Thoraxcenter, Erasmus MC, 3000 CA, Rotterdam, The Netherlands

²Department of Radiology, Erasmus MC, 3000 CA, Rotterdam, The Netherlands

³Department of Biomedical Engineering, Thoraxcenter, Erasmus MC, 3000 CA, Rotterdam, The Netherlands

*Correspondence to: Dr. Jolanda Wentzel, Erasmus MC, Thoraxcenter, Department of Biomedical Engineering, Room EE2322, PO Box 2040, 3000 CA Rotterdam, The Netherlands.
E-mail: j.wentzel@erasmusmc.nl

Received 15 October 2013; Revision accepted 12 March 2014

INTRODUCTION

In patients with risk factors for atherosclerosis, the development of plaque is not uniform across the entire coronary tree, but shows a predilection for sites where the laminar blood flow gets disturbed [1,2]. The low-oscillatory endothelial shear stress has been shown to facilitate atherogenesis and promotes the development of rupture-prone plaques in the vicinity of coronary artery bifurcations [3–5].

Percutaneous treatment of coronary bifurcation lesions remains a challenging procedure and has been associated with higher restenosis and stent thrombosis rates [6–8]. More precise and detailed assessment of the plaque distribution may allow for safer and more efficient treatment strategies. Invasive coronary angiography (ICA) is regarded as the common diagnostic tool for the detection of significant ($\geq 50\%$ lumen diameter stenosis) bifurcation lesions and the planning of percutaneous coronary intervention (PCI) in the coronary bifurcations. The Medina classification [9] based on ICA has been widely accepted as a simplified method to characterize bifurcation lesions and facilitate the decision-making on the treatment of these lesions.

Computed tomography coronary angiography (CTCA) has emerged as a noninvasive method to visualize coronary atherosclerosis, based on extensive cross-sectional correlation with IVUS data [10–12]. Similarly to IVUS, CTCA goes beyond lumenography and enables the assessment of atherosclerotic plaque. Moreover, the complex three-dimensional (3D) geometry of coronary artery bifurcations can be better visualized by means of this imaging modality which can provide a 3D reconstruction of the bifurcation, without the limitations of vessel foreshortening and overlap that exist in conventional angiography; CTCA has been previously shown to allow accurate assessment of complex bifurcation lesions [13].

The objective of the current study is twofold: (1) to assess the distribution of atherosclerosis at bifurcation sites using CTCA; and (2) to propose a novel CT-based Medina classification scheme for bifurcation lesions, combining lumen stenosis and plaque severity.

METHODS

Patients

We retrospectively analyzed a cohort of patients who were treated in our institution for acute coronary syndromes between May 2005 and January 2006. Acute coronary syndrome (ACS) was defined as ST-segment elevation myocardial infarction, non-ST-segment elevation myocardial infarction (troponin positive) or unstable angina (troponin negative). Imme-

diately after initial management of the culprit lesions, these patients were asked to participate in the CTCA study. They were considered for inclusion only if they had a heart rate lower than 70 bpm during the CTCA acquisition and had no prior coronary bypass surgery. Exclusion criteria included renal dysfunction (serum creatinine >120 mmol L⁻¹), contrast allergy and irregular heart rhythm. The institutional review board of our hospital approved the study, and all patients provided written informed consent before study participation.

CTCA Acquisition

All patients underwent CTCA with a 64-slice scanner (Sensation 64, Siemens Medical Solutions, Forchheim, Germany). As the ACS patients were already treated with intravenous nitrates and β -blockers, additional medication prior to CT scan was not necessary. The CT angiographic scan parameters were: gantry rotation time of 330 ms; 32×2 slices per rotation; 0.6 mm detector collimation; spiral scan mode with a table feed of 3.8 mm per rotation; a tube voltage of 120 kV; and tube current of 900 effective mAs. Prospective ECG-triggered X-ray tube modulation was not applied. A bolus of 100 mL of contrast material (400 mgI mL⁻¹; Iomeron, Bracco, Milan, Italy) was injected intravenously at 5 mL sec⁻¹ flow rate followed by a saline chaser. The initiation of the scan was synchronized to the arrival of contrast in the coronary arteries by a bolus-tracking technique. The mean effective radiation dose was 14.0 ± 0.8 mSv, using the dose-length product and a conversion factor k (0.014 mSv/mGy/cm) [14]. Axial CT images were reconstructed with a slice thickness of 0.75 and 0.4 mm increments using a retrospectively ECG gating algorithm to obtain optimal, motion-free image quality. Optimal data sets with the best image quality were reconstructed mainly in the mid- to end-diastolic phase, using a medium-smooth convolution kernel.

Bifurcation Selection

All untreated vessels with diameter ≥ 1.5 mm were retrospectively screened for bifurcations visualized with high quality; only major bifurcations [side branch (SB) with an ostial diameter ≥ 1.5 mm] which were located at a distance >10 mm from adjacent branches were considered for inclusion. The region of interest (ROI) selected for analysis comprised the three segments of the bifurcations: proximal main vessel (MV), distal MV and SB, up to a distance of 5-mm away from the bifurcation carina (-5 mm to 5 mm from carina) (Fig. 1).

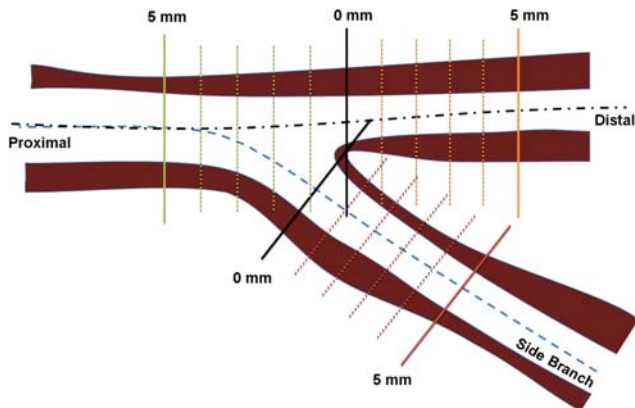


Fig. 1. The region of interest selected for analysis comprised the three segments of the bifurcations (proximal main vessel, distal main vessel and side branch), up to a distance of 5 mm away from the bifurcation carina.

CTCA Image Analysis

Datasets were transferred to an offline workstation for further analysis using an in-house developed tool, based on MeVisLab software (MeVisLab, Mevis, Bremen, Germany, <http://www.mevislab.de>). The methodology used for this analysis has been previously investigated and described in detail [11], showing a correlation of $r=0.91$ between CTCA and IVUS for plaque volume quantification. In brief, both the inner lumen and the outer vessel boundaries were annotated following a step-wise approach. Multiplanar reformatted images were generated and the lumen and vessel borders were traced longitudinally on at least three different vessel views; the intersections between these longitudinal contours and cross-sectional images at 1-mm intervals were calculated in order to create cross-sectional contours, which were inspected and, if necessary, adjusted by an experienced observer (Fig. 2). The settings for window level and width were fixed at 740 and 220 HU, respectively. The annotation of lumen and vessel wall borders was also facilitated by gradient magnitude images, which are derived from the CTCA images (Fig. 2B) and represent the amount of local change in image intensity.

Plaque quantitative parameters for each 1-mm cross-section included lumen, vessel, and plaque area and they were averaged over the 5-mm length of each one of the three bifurcation segments. The % plaque burden [(plaque area/vessel area) \times 100] was also calculated and two different thresholds were used to classify plaque presence and distribution within the coronary bifurcation segments: $\geq 40\%$ for any plaque, similarly to previous IVUS studies [15]; and $\geq 70\%$ for severe plaque, which has been also shown to be an independent predictor of events in the PROSPECT study [16]. Finally, for the cross-sections at the level of the bifurcation carina (MV carina cross-section and SB carina cross-section),

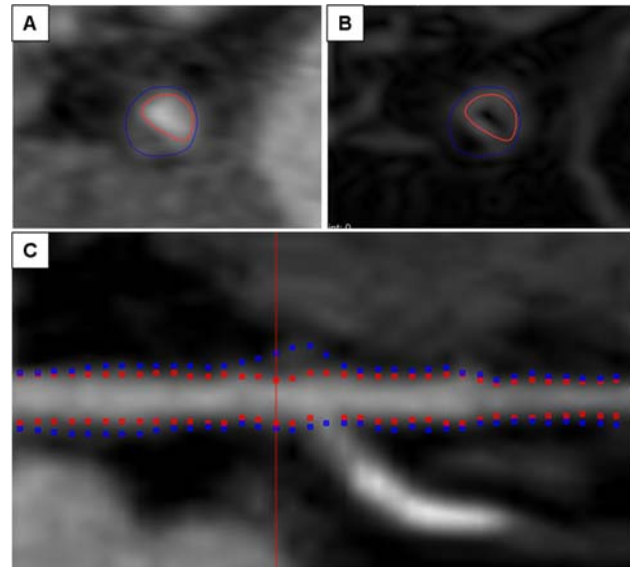


Fig. 2. Example of bifurcation quantitative analysis. Panel A: in the normal MDCT image, the vessel lumen is brightly enhanced, and a non-calcified, eccentric plaque is visible. Panel B: in the gradient MDCT image, the greater change in image intensity is depicted brighter, which facilitates the discrimination of borders between tissues with different intensity. Panel C: longitudinal main vessel view.

the maximum wall thickness was measured; the carina cross-section was the frame immediately distal to the take-off of the SB in which both ostia of the MV and SB could be visualized as a figure-of-eight shape (0 mm in MV Fig. 1). To investigate the plaque location in relation to the carina, we divided each carina cross-section into four parts from the center of the lumen and the part with the thickest plaque was documented. The cross-section was divided in such way that the flow divider was in the middle of one of the parts. We labelled the part opposite to the flow divider, I; the part facing the myocardial side of the heart, II; the part facing the pericardium, III; and the part containing the flow divider, IV (Fig. 3). In this way, the numbering of the parts is according to the expected wall shear stress (WSS): in part I the lowest and in part IV the highest WSS [17].

The Medina Classification and the CT-medina Classification for Bifurcation Lesions

All coronary bifurcation segments were visually scored for the presence of significant lesions (diameter reduction of $\geq 50\%$) by carefully axial scrolling and using multiplanar reconstructions, as previously described [13]. The bifurcation lesions with significant lumen narrowing were categorized using a widely used classification scheme, known as the Medina [9] bifurcation classification. The Medina classification is a simple binary system whereby significant lumen

narrowing is classified as present (1) or absent (0) in the proximal main vessel, distal main vessel and SB segments. The Medina classification was further modified into a new CT-based Medina classification to incorporate information about severe ($\geq 70\%$) plaque presence by adding an asterisk (*) as a superscript to the existing segments' score (example shown in Fig. 4).

Statistical Analysis

Continuous variables were presented as means ± 1 standard deviation, unless otherwise indicated, and cat-

egorical variables were reported as counts and/or percentages. Continuous variables were compared between the different bifurcation segments using paired *t* test. A two-sided *P* value < 0.05 was considered statistically significant with Bonferroni correction for multiple comparisons when necessary. Statistical analyses were performed using SPSS 17.0 for Windows (SPSS, Chicago, IL).

RESULTS

Forty-four patients of the main cohort were screened, and 66 major bifurcations (SB ostium ≥ 1.5 mm) were inspected for inclusion. Reasons for exclusion of bifurcations were poor image quality due to coronary motion or stack artifacts ($n=9$), extreme calcification ($n=2$), and presence of trifurcations ($n=9$). Moreover, in seven cases more than one bifurcation were located in proximity to each other and could not be isolated for analysis. Finally, a total of 39 bifurcation sites from 26 patients were analyzed; mean age was 55 ± 10 years, whereas 81% of the patients were male. The patients' characteristics are summarized in Table I. Regarding the bifurcation location, the bifurcations studied were 13 left main (LM), 15 left anterior descending artery (LAD)/diagonal, 3 left circumflex artery (LCX)/marginal, 3 right coronary artery (RCA)/

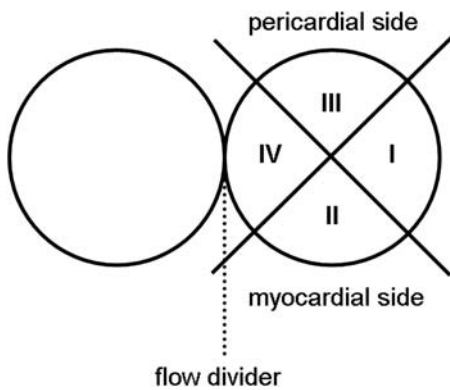


Fig. 3. The drawing illustrates the division of the carina cross-section into parts and the corresponding numbering according to the expected shear stress levels.

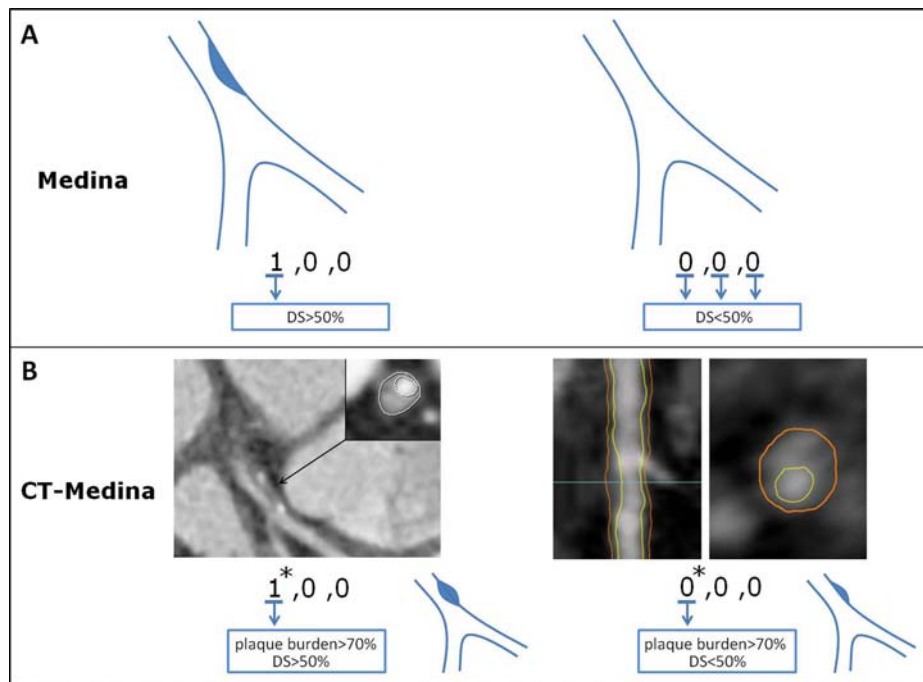


Fig. 4. The Medina classification was further modified into a new CT-based Medina classification to incorporate information about severe ($\geq 70\%$) plaque presence by adding an asterisk (*) as a superscript to the existing segments' score. DS: diameter stenosis.

right ventricular branch, 2 RCA/acute marginal branch and 3 RCA/posterolateral branch.

Plaque Quantitative Geometrical Characteristics

Non-LM bifurcations. The analysis for the geometrical characteristics of the 26 bifurcations is presented in Table II. Overall, as expected, the mean lumen, vessel and plaque area were larger in the proximal compared to the distal main vessel (7.7 ± 3.4 vs.

6.7 ± 3.2 mm², $P < 0.001$; 14.1 ± 5.1 vs. 11.9 ± 5.0 mm², $P < 0.001$; and 6.4 ± 2.7 vs. 5.3 ± 2.7 mm², $P = 0.004$, respectively). The plaque burden was not significantly different between all three bifurcation segments.

LM bifurcations. The quantitative geometrical characteristics are presented in Table III. Overall, the mean plaque area was significantly lower in the LCX compared to the LM (5.7 ± 1.7 vs. 10.1 ± 5.3 mm², $P = 0.004$) and to the LAD (5.7 ± 1.7 vs. 8.3 ± 3.3 mm², $P = 0.003$). The plaque burden was highest in the LAD, but not significantly different from the LM and the LCX.

TABLE I. Patient Characteristics

Patients	<i>n</i> = 26
Age (mean ± SD), yrs	55 ± 10
Male gender, <i>n</i> (%)	21 (81%)
Clinical status at enrolment	
AMI, <i>n</i> (%)	19 (73%)
Unstable angina, <i>n</i> (%)	7 (27%)
Risk factors	
Obesity, <i>n</i> (%)	4 (15%)
Current smoking, <i>n</i> (%)	16 (61%)
Hypertension, <i>n</i> (%)	7 (27%)
Hyperlipidaemia, <i>n</i> (%)	7 (27%)
Diabetes mellitus, <i>n</i> (%)	1 (4%)
Family history of CAD, <i>n</i> (%)	15 (58%)

Plaque Location in Relation to the Flow Divider

In general, the MV carina cross-section and the SB carina cross-section demonstrated a plaque burden of $47\% \pm 14\%$ and $43\% \pm 16\%$, respectively ($P = 0.124$). For the LM-bifurcations, the LAD carina cross-section demonstrated a significantly higher plaque burden compared to the LCX carina cross-section ($54\% \pm 15\%$ vs. $37\% \pm 12\%$ respectively, $P = 0.001$) and a significantly

TABLE II. Geometrical Characteristics in Non-LM Bifurcation Sites (*n* = 26)

Variables	Proximal main vessel	Distal main vessel	Side branch	P/D	P/SB	D/SB
Volume						
Average lumen CSA (mm ³ mm ⁻¹)	7.7 ± 3.4	6.7 ± 3.2	6.3 ± 2.7	<0.001	NS	NS
Average vessel CSA (mm ³ mm ⁻¹)	14.1 ± 5.1	11.9 ± 5.0	11.5 ± 4.3	<0.001	NS	NS
Average plaque CSA (mm ³ mm ⁻¹)	6.4 ± 2.7	5.3 ± 2.7	5.2 ± 2.7	0.004	NS	NS
Plaque burden (%)	45 ± 12	44 ± 12	45 ± 13	NS	NS	NS
Minimum lumen area (mm ²)	6.6 ± 3.3	5.8 ± 3.2	5.4 ± 2.5	0.005	NS	NS
Carina cross-section						
Lumen CSA (mm ²)	–	6.7 ± 3.4	6.8 ± 3.1	–	–	NS
Vessel CSA (mm ²)	–	12.4 ± 5.0	12.1 ± 4.6	–	–	NS
Plaque CSA (mm ²)	–	5.7 ± 2.7	5.3 ± 3.2	–	–	NS
Plaque burden (%)	–	47 ± 14	43 ± 16	–	–	NS
Maximum wall thickness	–	1.15 ± 0.46	1.06 ± 0.40	–	–	NS

CSA: cross-sectional area; D: distal main vessel; LM: left main; P: proximal main vessel; SB: side branch.

TABLE III. Geometrical Characteristics in LM Bifurcation Sites (*n* = 13)

Variables	LM	LAD	LCX	LM/LAD	LM/LCX	LAD/LCX
Volume						
Average lumen CSA (mm ³ mm ⁻¹)	11.0 ± 3.5	8.3 ± 2.7	8.5 ± 4.5	0.004	NS	NS
Average vessel CSA (mm ³ mm ⁻¹)	21.1 ± 7.0	16.6 ± 4.6	14.2 ± 5.0	0.002	0.005	NS
Average plaque CSA (mm ³ mm ⁻¹)	10.1 ± 5.3	8.3 ± 3.3	5.7 ± 1.7	NS	0.004	0.003
Plaque burden (%)	46 ± 15	49 ± 13	42 ± 12	NS	NS	NS
Minimum lumen area (mm ²)	8.9 ± 3.7	6.9 ± 2.3	7.5 ± 4.1	0.014	NS	NS
Carina cross-section						
Lumen CSA (mm ²)	–	8.5 ± 3.4	9.7 ± 4.2	–	–	NS
Vessel CSA (mm ²)	–	18.9 ± 6.5	15.4 ± 5.4	–	–	NS
Plaque CSA (mm ²)	–	10.5 ± 5.2	5.7 ± 2.3	–	–	0.002
Plaque burden (%)	–	54 ± 15	37 ± 12	–	–	0.001
Maximum wall thickness	–	1.66 ± 0.39	1.01 ± 0.36	–	–	0.001

CSA: cross-sectional area; LAD: left anterior descending artery; LCX: left circumflex artery; LM: left main.

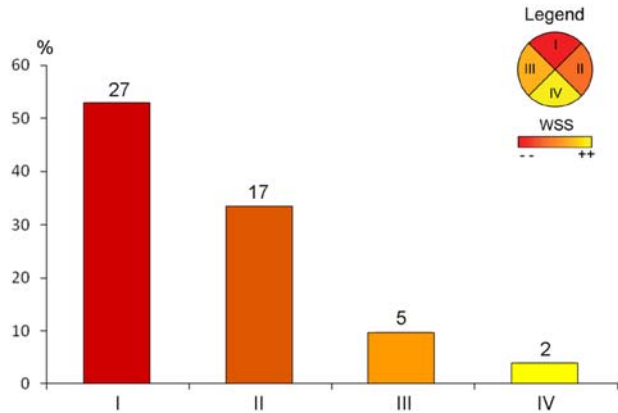


Fig. 5. Circumferential plaque distribution in the carina cross-sections. The figure gives the percentage (and absolute number) of cross-sections with occurrence of maximal plaque in each part.

higher maximum wall thickness (1.66 ± 0.39 mm vs. 1.01 ± 0.36 mm, respectively, $P = 0.001$).

The thickest plaque was located in presumably low WSS parts I and II in 53% (27/51) and 33% (17/51) of the carina cross-sections respectively. The high WSS parts III and IV were less often affected than parts I and II, only in 10% (5/51) and 4% (2/51) of the cross-sections (Fig. 5). The two cross-sections with the thickest plaque located on the carina (part IV) were non-LM bifurcations and the plaque was expanding to other parts.

Medina Classification and CT-based Medina Classification of Plaque Distribution

Overall, in this study three bifurcations (8%) had a stenosis $\geq 50\%$ in at least one of the three segments of the bifurcation, resulting in 92% having a Medina classification of 0,0,0 (Table IV). However, CTCA demonstrated plaque burden $\geq 40\%$ in 84.6% (33/39) of the proximal segments, 82.1% (32/39) of the distal segments and 82.1% (32/39) of the SB segments. Presence of severe plaque (plaque burden $\geq 70\%$) by CTCA was demonstrated in 12.8% (5/39) of the proximal segments, 15.4% (6/39) of the distal segments and 7.7% (3/39) of the SB segments.

The distribution of bifurcation lesions using both the Medina classification and the CT-based Medina classification combining lumen narrowing and plaque severity is shown in Table IV. Characterization of the bifurcation lesions using the new CT-based Medina classification provided additional information in seven cases (18%) compared to the original Medina classification.

DISCUSSION

In this exploratory study we sought to investigate the distribution of atherosclerosis at bifurcation sites

TABLE IV. Distribution of Bifurcation Lesions Using Medina Classification and CT-Medina Classification Schemes

Medina classification	CT-Medina classification ($\geq 50\%$ lumen diameter reduction and plaque burden $\geq 70\%$)
0,0,0 ($n = 36$)	→ 0,0,0 ($n = 32$) → 0,0*,0 ($n = 1$) → 0,0,0* ($n = 1$) → 0*,0*,0 ($n = 2$)
1,0,0 ($n = 1$)	→ 1*,0*,0* ($n = 1$)
1,1,0 ($n = 2$)	→ 1*,1*,0 ($n = 1$) → 1*,1*,0* ($n = 1$)

CT: computed tomography.

using CTCA and to propose a novel CT-based Medina classification scheme for bifurcation lesions, combining lumen and plaque information. The main findings of this report are as follows: (1) the plaque is widely present in all bifurcation segments, even in the absence of coronary lumen stenosis; (2) the plaque is more often located opposite to the flow divider, whereas the carina is rarely affected with plaque; and (3) a CT-Medina classification scheme combining lumen and plaque severity could be more informative than angiographic classification for the description of atherosclerosis at bifurcation sites.

In the present study, we found that atherosclerotic plaque is widely present in all bifurcation segments. Regarding the quantitative analysis, in the non-LM bifurcations, the proximal segment had a greater plaque burden than the distal, whereas in the LM bifurcations greater plaque burden was found in the distal segment (LAD). This observation is in line with earlier reports on plaque geometrical characteristics at bifurcation sites [18–20], which demonstrated the heterogeneous nature of coronary atherosclerosis at coronary bifurcations according to their segments and anatomical locations (LM vs. non-LM bifurcations).

As shown in previous reports, atherosclerosis has a predilection for the outer wall of bifurcations, where shear stress is low and blood flow is oscillatory; the flow divider is minimally diseased or spared [15,17,21–23]. Our analysis with CTCA corroborates this pattern; the thickest plaque was primarily located in low WSS parts I and II, while the high WSS parts III and IV were less often affected.

Currently, angiographic classification of bifurcations is widely accepted in clinical practice; nevertheless conventional angiography is an imperfect tool, which considerably underestimates the extent of atherosclerotic lesions when compensatory positive remodeling is present [24–26]. In addition, the angiographic assessment of coronary bifurcations is limited by vessel foreshortening and overlap. In a previous IVUS study,

Oviedo et al. [15] reported the distribution of plaque at the LM bifurcation, and proposed an IVUS classification of plaque morphology which was compared with the commonly used Medina system. The authors concluded that there was no relation between the Medina angiographic classification and IVUS plaque distribution. Similarly to IVUS, imaging by CTCA goes beyond lumenography and enables the assessment of atherosclerotic lesions that are angiographically “silent.” In our investigation, we propose a simple modification of the Medina classification to incorporate plaque severity, by using a threshold of $\geq 70\%$ plaque burden which was shown as independent predictor of events in the PROSPECT study [16]. In addition, the severity of pre-procedural plaque burden at the MV was shown to correlate with functional SB compromise after stent implantation [27].

Clinical Implications

As CTCA is becoming widely available and its value in detecting significant lumen narrowing has been robustly established, many patients are being brought into the cathlab based on the CTCA findings. Percutaneous treatment of coronary bifurcation lesions has been associated with worse acute and late outcomes due to higher restenosis and stent thrombosis rates [6–8]. Comprehensive pre-interventional assessment of both lumen stenosis and plaque severity of a diseased coronary bifurcation may be important to better plan a percutaneous strategy. Although carina shift is suggested to be the predominant mechanism of SB lumen loss after MV stent implantation, plaque shift from the MV also contributes to the aggravation of an SB ostial lesion and was more frequently observed in hemodynamically significant SB lesions [27,28]. Therefore, we envision that a CT-based Medina classification of bifurcation lesions may assist the preparation for the bifurcation stent implantation, regarding for example the location of the stent or even the need for a second stent, whereas the prevailing technique is the provisional stenting. Especially the presence of 0* at the side branch ostium in a case of 1, 0, 0* classification, could herald acute SB occlusion after provisional stenting, which could necessitate a two-stent strategy from the beginning or the use of dedicated bifurcation stent. Although novel, this classification was based on an analysis of a small number of patients, thus it must be considered work in progress. Larger studies with procedural and clinical outcomes are warranted to examine the value of the newly introduced CT-Medina classification.

Limitations

We acknowledge that our investigation has several limitations. This exploratory study was retrospectively

performed and is relatively small in terms of number of patients included, thus the possibility of a type II error should be considered. The analysis was performed on a cohort of consecutive ACS patients treated in our hospital, thus our population may not be representative of all the patients reaching the cath lab (for example stable angina patients who tend to be older). In this population, the majority of bifurcations did not have significant lumen narrowing; however our intention was to investigate the plaque presence and distribution at bifurcations irrespective of lumen stenosis. It is not clear from this study how the clinical and procedural outcome for the re-classified bifurcations would be altered, thus larger prospective studies to obtain prognostic information are warranted. Finally, the radiation exposure during MSCT coronary angiography remains a matter of concern; nevertheless, the implementation of dose-saving techniques results in effective dose less than the ~ 5 mSv of the invasive coronary angiography and plaque assessment using newer scanning technology and protocols has been shown feasible [20].

CONCLUSION

Atherosclerotic plaque is widely present in all bifurcation segments, even in the absence of coronary lumen stenosis. The plaque is more often located opposite to the flow divider, whereas the carina is rarely affected. A CT-Medina classification scheme combining lumen stenosis and plaque severity is more informative than angiographic classification of bifurcation lesions and could potentially facilitate the decision-making on the treatment of these lesions.

REFERENCES

1. Malek AM, Alper SL, Izumo S. Hemodynamic shear stress and its role in atherosclerosis. *JAMA* 1999;282:2035–2042.
2. Wentzel JJ, Chatzizisis YS, Gijzen FJ, Giannoglou GD, Feldman CL, Stone PH. Endothelial shear stress in the evolution of coronary atherosclerotic plaque and vascular remodelling: Current understanding and remaining questions. *Cardiovasc Res* 96:234–243.
3. Rodriguez-Granillo GA, Garcia-Garcia HM, Wentzel J, Valgimigli M, Tsuchida K, van der Giessen W, de Jaegere P, Regar E, de Feyter PJ, Serruys PW. Plaque composition and its relationship with acknowledged shear stress patterns in coronary arteries. *J Am Coll Cardiol* 2006;47:884–885.
4. Chatzizisis YS, Jonas M, Coskun AU, Beigel R, Stone BV, Maynard C, Gerrity RG, Daley W, Rogers C, Edelman ER, Feldman CL, Stone PH. Prediction of the localization of high-risk coronary atherosclerotic plaques on the basis of low endothelial shear stress: An intravascular ultrasound and histopathology natural history study. *Circulation* 2008;117:993–1002.
5. Slager CJ, Wentzel JJ, Gijzen FJ, Schuurbijs JC, van der Wal AC, van der Steen AF, Serruys PW. The role of shear stress in

- the generation of rupture-prone vulnerable plaques. *Nat Clin Pract Cardiovasc Med* 2005;2:401–407.
6. Colombo A, Moses JW, Morice MC, Ludwig J, Holmes DR Jr, Spanos V, Louvard Y, Desmedt B, Di Mario C, Leon MB. Randomized study to evaluate sirolimus-eluting stents implanted at coronary bifurcation lesions. *Circulation* 2004;109:1244–1249.
 7. Ge L, Airolidi F, Iakovou I, Cosgrave J, Michev I, Sangiorgi GM, Montorfano M, Chieffo A, Carlino M, Corvaja N, Colombo A. Clinical and angiographic outcome after implantation of drug-eluting stents in bifurcation lesions with the crush stent technique: Importance of final kissing balloon post-dilatation. *J Am Coll Cardiol* 2005;46:613–620.
 8. Routledge HC, Lefevre T, Colombo A, Oldroyd KG, Hamm CW, Guagliumi G, von Scheidt W, Guetta V, Ruzyllo W, Wittebols K, Goedhart DM, Serruys PW. Three-year clinical outcome of percutaneous treatment of bifurcation lesions in multivessel coronary artery disease with the sirolimus-eluting stent: Insights from the arterial revascularisation therapies study, part II (ARTS II). *EuroIntervention* 2009;5:190–196.
 9. Medina A, Suarez de Lezo J, Pan M. A new classification of coronary bifurcation lesions (Una clasificacion simple de las lesiones coronarias en bifurcacion). *Rev Esp Cardiol* 2006;59:183.
 10. Leber AW, Becker A, Knez A, von Ziegler F, Sirol M, Nikolaou K, Ohnesorge B, Fayad ZA, Becker CR, Reiser M, Steinbeck G, Boekstegers P. Accuracy of 64-slice computed tomography to classify and quantify plaque volumes in the proximal coronary system: A comparative study using intravascular ultrasound. *J Am Coll Cardiol* 2006;47:672–677.
 11. Papadopoulou SL, Neefjes LA, Schaap M, Li HL, Capuano E, van der Giessen AG, Schuurbiers JC, Gijsen FJ, Dharampal AS, Nieman K, van Geuns RJ, Mollet NR, de Feyter PJ. Detection and quantification of coronary atherosclerotic plaque by 64-slice multidetector CT: A systematic head-to-head comparison with intravascular ultrasound. *Atherosclerosis* 2011;219:163–170.
 12. Voros S, Rinehart S, Qian Z, Vazquez G, Anderson H, Murrieta L, Wilmer C, Carlson H, Taylor K, Ballard W, Karpaliotis D, Kalynych A, Brown C III. Prospective validation of standardized, 3-dimensional, quantitative coronary computed tomographic plaque measurements using radiofrequency backscatter intravascular ultrasound as reference standard in intermediate coronary arterial lesions: Results from the ATLANTA (assessment of tissue characteristics, lesion morphology, and hemodynamics by angiography with fractional flow reserve, intravascular ultrasound and virtual histology, and noninvasive computed tomography in atherosclerotic plaques) I study. *JACC Cardiovasc Interv* 2011;4:198–208.
 13. Van Mieghem CA, Thury A, Meijboom WB, Cademartiri F, Mollet NR, Weustink AC, Sianos G, de Jaegere PP, Serruys PW, de Feyter P. Detection and characterization of coronary bifurcation lesions with 64-slice computed tomography coronary angiography. *Eur Heart J* 2007;28:1968–1976.
 14. Bongartz G, Golding SJ, Jurik AG, Leonardi M, van Persijn van Meerten E, Rodriguez R, Schneider K, Calzado A, Geleijns J, Jessen KA, Panzer W, Shrimpton PC, Tosi G. 2004 CT Quality Criteria—Appendix C. European Guidelines for Multislice Computed Tomography, European Commission. Available at: http://www.msct.eu/CT_Quality_Criteria.htm.
 15. Oviedo C, Maehara A, Mintz GS, Araki H, Choi SY, Tsujita K, Kubo T, Doi H, Templin B, Lansky AJ, Dangas G, Leon MB, Mehran R, Tahk SJ, Stone GW, Ochiai M, Moses JW. Intravascular ultrasound classification of plaque distribution in left main coronary artery bifurcations: where is the plaque really located? *Circ Cardiovasc Interv* 2010;3:105–112.
 16. Stone GW, Maehara A, Lansky AJ, de Bruyne B, Cristea E, Mintz GS, Mehran R, McPherson J, Farhat N, Marso SP, Parise H, Templin B, White R, Zhang Z, Serruys PW, Investigators P. A prospective natural-history study of coronary atherosclerosis. *N Engl J Med* 2011;364:226–235.
 17. van der Giessen AG, Wentzel JJ, Meijboom WB, Mollet NR, van der Steen AF, van de Vosse FN, de Feyter PJ, Gijsen FJ. Plaque and shear stress distribution in human coronary bifurcations: A multislice computed tomography study. *EuroIntervention* 2009;4:654–661.
 18. Rodriguez-Granillo GA, Rosales MA, Degrossi E, Durbano I, Rodriguez AE. Multislice CT coronary angiography for the detection of burden, morphology and distribution of atherosclerotic plaques in the left main bifurcation. *Int J Cardiovasc Imaging* 2007;23:389–392.
 19. Han SH, Puma J, Garcia-Garcia HM, Nasu K, Margolis P, Leon MB, Lerman A. Tissue characterisation of atherosclerotic plaque in coronary artery bifurcations: An intravascular ultrasound radiofrequency data analysis in humans. *EuroIntervention* 2010;6:313–320.
 20. Papadopoulou SL, Brugaletta S, Garcia-Garcia HM, Rossi A, Girasis C, Dharampal AS, Neefjes LA, Ligthart J, Nieman K, Krestin GP, Serruys PW, de Feyter PJ. Assessment of atherosclerotic plaques at coronary bifurcations with multidetector computed tomography angiography and intravascular ultrasound-virtual histology. *Eur Heart J Cardiovasc Imaging* 2012;13:635–642.
 21. Asakura T, Karino T. Flow patterns and spatial distribution of atherosclerotic lesions in human coronary arteries. *Circ Res* 1990;66:1045–1066.
 22. Kimura BJ, Russo RJ, Bhargava V, McDaniel MB, Peterson KL, DeMaria AN. Atheroma morphology and distribution in proximal left anterior descending coronary artery: In vivo observations. *J Am Coll Cardiol* 1996;27:825–831.
 23. Badak O, Schoenhagen P, Tsunoda T, Magyar WA, Coughlin J, Kapadia S, Nissen SE, Tuzcu EM. Characteristics of atherosclerotic plaque distribution in coronary artery bifurcations: An intravascular ultrasound analysis. *Coron Artery Dis* 2003;14:309–316.
 24. Alfonso F, Macaya C, Goicolea J, Iniguez A, Hernandez R, Zamorano J, Perez-Vizcayne MJ, Zarco P. Intravascular ultrasound imaging of angiographically normal coronary segments in patients with coronary artery disease. *Am Heart J* 1994;127:536–544.
 25. Mintz GS, Painter JA, Pichard AD, Kent KM, Satler LF, Popma JJ, Chuang YC, Bucher TA, Sokolowicz LE, Leon MB. Atherosclerosis in angiographically “normal” coronary artery reference segments: An intravascular ultrasound study with clinical correlations. *J Am Coll Cardiol* 1995;25:1479–1485.
 26. Nakamura Y, Takemori H, Shiraishi K, Inoki I, Sakagami M, Shimakura A, Usuda K, Kubota K, Takata S, Kobayashi K. Compensatory enlargement of angiographically normal coronary segments in patients with coronary artery disease. In vivo documentation using intravascular ultrasound. *Angiology* 1996;47:775–781.
 27. Kang SJ, Kim WJ, Lee JY, Park DW, Lee SW, Kim YH, Lee CW, Mintz GS, Park SW, Park SJ. Hemodynamic impact of changes in bifurcation geometry after single-stent cross-over technique assessed by intravascular ultrasound and fractional flow reserve. *Catheter Cardiovasc Interv* 2013.
 28. Koo BK, Waseda K, Kang HJ, Kim HS, Nam CW, Hur SH, Kim JS, Choi D, Jang Y, Hahn JY, Gwon HC, Yoon MH, Tahk SJ, Chung WY, Cho YS, Choi DJ, Hasegawa T, Kataoka T, Oh SJ, Honda Y, Fitzgerald PJ, Fearon WF. Anatomic and functional evaluation of bifurcation lesions undergoing percutaneous coronary intervention. *Circ Cardiovasc Interv* 2010;3:113–119.

PART IV

CT coronary angiography
for risk stratification of
coronary atherosclerotic
disease

Chapter 8

The Multislice Computed Tomography (MSCT) SYNTAX Score: a feasibility and reproducibility study

Based on: JACC Cardiovasc Imaging. 2013 Mar;6(3):413-5.

S.L. Papadopoulou, C. Girasis, A.S. Dharampal, V. Farooq, Y. Onuma, A. Rossi, M-A Morel, G.P. Krestin, P.W. Serruys, P.J. de Feyter, H.M. Garcia-Garcia

Abstract

Objectives: To investigate the feasibility and reproducibility of the multislice computed tomography SYNTAX score (MSCT SXscore).

Background: The invasive coronary angiography SYNTAX score (ICA SXscore) is an important prognostic tool in risk stratifying patients undergoing revascularisation, as well as an independent predictor of adverse cardiac events.

Methods: The ICA SXscore definitions were reviewed and adapted for MSCT. The SXscore of 80 symptomatic patients who underwent ICA and MSCT was retrospectively calculated for both modalities by 2 independent teams of experienced reviewers. Corresponding scores were compared between modalities with the Spearman correlation coefficient and Bland-Altman analysis. The MSCT SXscore was re-calculated after two months in 40 random patients to assess intra-observer variability with kappa statistics. The Agatston calcium score was also calculated, reflecting the overall burden of disease.

Results: There was good correlation between the ICA SXscore and the MSCT SXscore ($r_s=0.76$, $p<0.001$), whereas the median MSCT SXscore was higher compared to the median ICA SXscore [13.0 (IQR 7-24) vs. 10.5 (IQR 5-20.75) respectively, $p=0.004$]. Kappa statistics indicated a substantial intra-observer agreement for MSCT SXscore tertiles ($\kappa=0.80$; 95%CI [0.67,0.94], $p<0.001$), and the correlation between the two rounds of analyses was high ($r=0.95$, $p<0.001$). The median calcium score across the MSCT SXscore tertiles was 145.8, 312.0 and 743.6 respectively ($p<0.001$); across the ICA SXscore tertiles, it was 145.8, 188.7 and 932.0 respectively ($p<0.001$).

Conclusion: In this exploratory study the calculation of the MSCT SXscore in symptomatic patients appeared feasible and reproducible. The long-term prognostic role of this scoring methodology should be further investigated.

Abbreviations list:

Ca score: calcium score

CAD: coronary artery disease

ECG: electrocardiogram

ICA: invasive coronary angiography

MSCT: multislice computed tomography

SXscore: SYNTAX score

Introduction

The SYNTAX Score (SXscore) (1) is an important tool to grade angiographic complexity and to risk stratify patients being considered for revascularisation (2-4); in addition, it has been shown to be an independent predictor of major adverse cardiac events in 'all-comers' type populations with a varying extent of coronary artery disease (5-9). The SXscore has been integrated in both the European and U.S. revascularisation guidelines for the risk stratification of patients with complex coronary artery disease, facilitating the choice of the most appropriate revascularisation modality (10-12).

The potential of multislice computed tomography (MSCT) to obtain information noninvasively comparable to that provided by invasive coronary angiography has been the most important factor behind the broad adoption and dissemination of cardiac CT imaging. It is envisioned that MSCT coronary angiography may have the ability to provide information not currently available from invasive angiography (i.e. plaque burden and calcium score) and may change the way patients with atherosclerotic cardiovascular disease are stratified and managed (13).

A number of comparative reports have examined the diagnostic performance of MSCT angiography against conventional invasive coronary angiography (ICA), reporting a very high sensitivity and specificity (14). Therefore in this study we explore for the first time the feasibility of a MSCT-derived SXscore in a population of symptomatic patients with suspected coronary artery disease (CAD); in addition, we investigate the reproducibility of the newly developed MSCT SXscore.

Methods

Study population

The study comprised all consecutive symptomatic patients suspected of having CAD who were referred for invasive coronary angiography and were invited to undergo a MSCT angiography examination between May 2009 and October 2010. Exclusion criteria were prior revascularization, iodine allergy or impaired renal function. All patients gave informed consent and were entered in our single center cardiac database.

MSCT acquisition

The patients were scanned with a second generation dual-source CT scanner (Somatom Definition Flash, Siemens Healthcare, Forchheim, Germany). All patients received nitroglycerin (0.4 mg/dose) sublingually just prior to the CT scan, provided there were no contraindications and patients with a heart rate above 65 bpm received beta-blockers. An initial non-enhanced ECG gated scan (120-kV tube voltage, 75 mAs tube current and 3-mm slice thickness) was performed to calculate the Agatston calcium score (15), and was followed by a contrast enhanced CT angiography. The CT angiographic parameters were: 64 x 2 x 0.6 mm collimation with z-flying focal spot for both detectors, gantry rotation time 280 ms, tube voltage of 100 to 120 kV, current of 320 to 370 mAs. A bolus of iodinated contrast material (370 mgI/mL, Ultravist; Schering, Berlin, Germany), which varied between 60 and 100 mL depending on the expected scan time, was injected intravenously (flow rate, 5.5 mL/sec) followed by a 45 mL saline chaser at the same injection rate. A bolus tracking technique was used to synchronize the arrival of contrast in the coronary arteries and the start of the MSCT acquisition. The prospectively ECG-triggered axial scan mode ("step-and-shoot") or the low pitch ECG-gated spiral scan mode with ECG-pulsing was used, depending on the heart rate; the high pitch spiral scan protocol was used in selected patients (16). Overall, the mean effective radiation dose was 5.4 ± 3.5 mSv, using the dose-length product and a conversion factor k of 0.014 mSv/mGy/cm (17): 4.8 ± 3.2 mSv for the contrast-enhanced scan and 0.6 ± 0.5 mSv for the non-enhanced scan. All MSCT coronary angiograms were reconstructed with a slice thickness 0.75 mm and an increment 0.4 mm. Datasets were reconstructed retrospectively for the low pitch scan and "step-and-shoot" sequential scans in systolic and diastolic phases of the RR-interval for

high (≥ 80 bpm) and low heart rates (≤ 65 bpm) respectively, to obtain motion-free images; both systolic and diastolic phases of the RR-interval were used in medium heart rates. Datasets for the high pitch spiral scans could only be reconstructed at one diastolic phase. Images were analyzed using medium-to-smooth convolution kernels for non-calcified lesions and sharp convolution kernels for calcified lesions.

ICA SYNTAX Score and angiographic analysis

The SYNTAX score algorithm, which is described in full elsewhere and is available on the SYNTAX score website (<http://www.syntaxscore.com>), was used to score all coronary lesions deemed to have a percentage diameter stenosis $\geq 50\%$, in vessels ≥ 1.5 mm. The conventional coronary angiograms were analysed side by side by a panel of 2 interventional cardiologists; in case of disagreement, the opinion of a third analyst was obtained and the final decision was reached by consensus. The final score was calculated on a patient basis from the individual lesion scores, which were saved in a dedicated database.

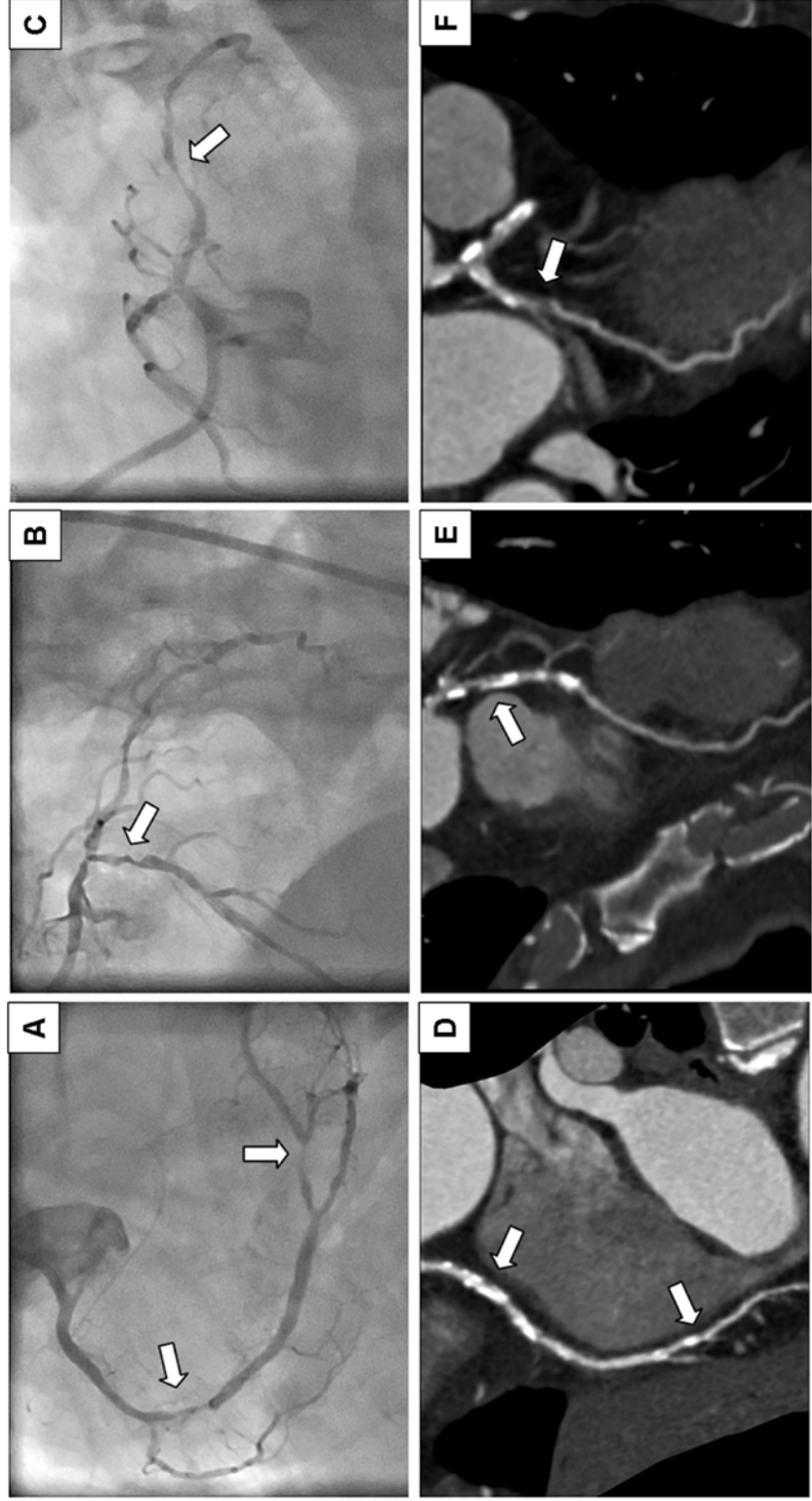
MSCT SYNTAX Score and MSCT analysis

All datasets were transferred for analyses to an offline multi-modality workstation (MMWP workstation, Leonardo, Siemens, Erlangen, Germany). All definitions of the ICA SXscore components were reviewed and adapted for the MSCT capabilities (**Table 1**); the online SXscore algorithm (<http://www.syntaxscore.com>) was used to calculate the MSCT SXscore. Similarly to the conventional angiography, the MSCT scans were analysed side by side by a panel of 2 experienced reviewers to identify the lesions with percentage diameter stenosis $\geq 50\%$ and then calculate the MSCT SXscore (example shown in **Figure 1**). Before the study, 20 cases were reviewed as training cohort for the MSCT SXscore calculation and then discarded from the final analysis. To assess intra-observer variability, the MSCT SXscore calculation was repeated in 40 randomly selected cases at a 2-month interval with the reviewers blinded to the original MSCT SXscores. The time required for the MSCT SXscore calculation was also measured, on top of the MSCT assessment for the detection of significant lesions.

Table 1. Definitions of the ICA SXscore features as reviewed and adapted for the MSCT SXscore	
Conventional definition [Sianos et al.(1), Serruys et al. (3)]	MSCT definition
<p>Dominance Right dominance: the posterior descending coronary artery is a branch of the right coronary artery (segment 4) Left dominance: the posterior descending artery is a branch of the left coronary artery (segment 15). Co-dominance does not exist as an option in the SYNTAX score.</p>	<p>Dominance (=) Right dominance: the posterior descending coronary artery is a branch of the right coronary artery (segment 4) Left dominance: the posterior descending artery is a branch of the left coronary artery (segment 15). Co-dominance does not exist as an option in the SYNTAX score.</p>
<p>Total occlusion No intra-luminal antegrade flow (TIMI 0) beyond the point of occlusion. However, antegrade flow beyond the total occlusion might be maintained by bridging collaterals (Small channels running in parallel to the vessel and connecting proximal vessel to distal and being responsible for the ipsilateral collateralization) and/or ipsi collaterals.</p>	<p>Total occlusion (~) No intra-luminal antegrade flow (TIMI 0) beyond the point of occlusion; it is visualized as the non-contrast enhanced segment of the vessel. Bridging collaterals and/or ipsi collaterals can only be measured by conventional angiography. (25)</p>
<p>Stump Defined as the entry site of the occlusion that has either a tapered- (central or eccentric) or a blunt appearance.</p>	<p>Stump (=) Defined as the entry site of the occlusion that has either a tapered- (central or eccentric) or a blunt appearance. (25)</p>
<p>Segment numbers beyond the total occlusion Specify the first that is visualized by antegrade or retrograde contrast.</p>	<p>Segment numbers beyond the total occlusion (=) Specify the first that is visualized by antegrade or retrograde contrast.</p>
<p>Sidebranch at the origin of the occlusion Specify whether this is smaller or at least 1.5 mm diameter.</p>	<p>Sidebranch at the origin of the occlusion (=) Specify whether this is smaller or at least 1.5 mm diameter</p>
<p>Trifurcation A trifurcation is a division of a mainbranch into three branches of at least 1.5mm. Trifurcations are only scored for the following segment junctions: 3/4/16/16a, 5/6/11/12, 11/12a/12b/13, 6/7/9/9a and 7/8/10/10a.</p>	<p>Trifurcation (=) A trifurcation is a division of a mainbranch into three branches of at least 1.5mm. Trifurcations are only scored for the following segment junctions: 3/4/16/16a, 5/6/11/12, 11/12a/12b/13, 6/7/9/9a and 7/8/10/10a.</p>
<p>Bifurcation A bifurcation is a division of a main, parent, branch into two daughter branches of at least 1.5mm. Bifurcation lesions may involve the proximal main vessel, the distal main vessel and the side branch according to the Medina classification. The smaller of the two daughter branches should be designated as the 'side branch'. In case of the main stem either the LCX or the LAD can be designated as the side branch depending on their respective calibres. Bifurcations are only scored for the following segment junctions: 5/6/11, 6/7/9, 7/8/10, 11/13/12a, 13/14/14a, 3/4/16 and 13/14/15.</p>	<p>Bifurcation (=) A bifurcation is a division of a main, parent, branch into two daughter branches of at least 1.5mm. Bifurcation lesions may involve the proximal main vessel, the distal main vessel and the side branch according to the Medina classification. The smaller of the two daughter branches should be designated as the 'side branch'. In case of the main stem either the LCX or the LAD can be designated as the side branch depending on their respective calibres. Bifurcations are only scored for the following segment junctions: 5/6/11, 6/7/9, 7/8/10, 11/13/12a, 13/14/14a, 3/4/16 and 13/14/15.</p>

Table 1. (Cont'd)	
<p>Aorto ostial A lesion is classified as aorto-ostial when it is located immediately at the origin of the coronary vessels from the aorta (applies only to segments 1 and 5, or to 6 and 11 in case of double ostium of the LCA).</p>	<p>Aorto ostial (=) A lesion is classified as aorto-ostial when it is located immediately at the origin of the coronary vessels from the aorta (applies only to segments 1 and 5, or to 6 and 11 in case of double ostium of the LCA).</p>
<p>Severe tortuosity One or more bends of 90° or more, or three or more bends of 45° to 90° proximal of the diseased segment.</p>	<p>Severe tortuosity (=) One or more bends of 90° or more, or three or more bends of 45° to 90° proximal of the diseased segment.</p>
<p>Length >20mm Estimation of the length of that portion of the stenosis that has ≥50% reduction in luminal diameter in the projection where the lesion appears to be the longest. (In case of a bifurcation lesion at least one of the branches has a lesion length of >20mm).</p>	<p>Length >20mm (=) Estimation of the length of that portion of the stenosis that has ≥50% reduction in luminal diameter in the projection where the lesion appears to be the longest. (In case of a bifurcation lesion at least one of the branches has a lesion length of >20mm).</p>
<p>Heavy calcification Multiple persisting opacifications of the coronary wall visible in more than one projection surrounding the complete lumen of the coronary artery at the site of the lesion.</p>	<p>Heavy calcification (≠) Severe calcification was defined as the presence of calcium that occupies more than 50% of the vessel cross-sectional area at any location within the lesion (25)</p>
<p>Thrombus Spheric, ovoid or irregular intraluminal filling defect or lucency surrounded on three sides by contrast medium seen just distal or within the coronary stenosis in multiple projections or a visible embolization of intraluminal material downstream.</p>	<p>Thrombus (≠) It is difficult for MSCT to distinguish thrombus from plaque; therefore this feature was not scored.</p>
<p>Diffuse disease Present when at least 75% of the length of any segment(s) proximal to the lesion, at the site of the lesion or distal to the lesion has a vessel diameter of <2mm.</p>	<p>Diffuse disease (=) Present when at least 75% of the length of any segment(s) proximal to the lesion, at the site of the lesion or distal to the lesion has a vessel diameter of <2mm.</p>
<p>Coding of the symbols used: = definition remains the same; ~ definition slightly different; ≠ definition totally different</p> <p>ICA: invasive coronary angiography; MSCT: multislice computed tomography; SXscore: SYNTAX score</p>	

Figure 1. Example of the calculation of the conventional ICA SXscore and the MSCT SXscore in a patient with three-vessel disease (right coronary artery in panels A and D; left anterior descending in panels B and E; left circumflex artery in panels C and F). The ICA SXscore was 34 (upper images); the MSCT SXscore was 41 (lower images). ICA: invasive coronary angiography; MSCT: multislice computed tomography.



Coronary calcium

The unenhanced CT-scan was used to calculate the total calcium score (Ca score) using the Agatston method (15). The coronary calcium reflects the overall burden of disease per patient; furthermore it has been shown to have incremental prognostic value in asymptomatic individuals (18), as well as in symptomatic patients (19-22). Under this perspective, we examined the further categorization of the SXscore tertiles into 2 other categories, one with low Ca score (≤ 400) and the other with high Ca score (>400), referred to as “extended MSCT SXscore”. More importantly, coronary calcium often prevents the reliable assessment of the coronary lumen and constitutes one of the main limitations of MSCT imaging; thus it is relevant to our study to investigate whether higher amounts of calcium tamper with the calculation of SXscore by MSCT compared to ICA.

Statistical Analysis

Continuous variables were expressed as means \pm standard deviation or medians with interquartile range (IQR) when not normally distributed; categorical variables were presented as counts and/or percentages. Spearman’s rank correlation coefficient (r_s) was used to measure the strength of the association of MSCT SXscore with ICA SXscore and Bland-Altman analysis was performed. The continuous variables not normally distributed were compared with the non-parametric Kruskal-Wallis test and the Wilcoxon signed ranks test. Intra-observer variability was determined with weighted kappa statistics that reflect the agreement between two or more observations using weight to quantify the relative difference between categories (23). It is usual to characterize strength of agreement with kappa values as follows: <0 none, 0-0.20 slight, 0.21-0.40 fair, 0.41-0.60 moderate, 0.61-0.80 substantial, 0.81-1.00 almost perfect (24).

To complete our analysis, a stratified comparison of the Ca score was also performed across the ICA and MSCT SXscore tertiles. In addition, any potential association between the coronary calcium and the bias in MSCT SXscore calculation compared to ICA SXscore was evaluated with a scatter plot of the Ca score and the MSCT – ICA SXscore differences. A 2-sided p-value <0.05 was considered significant for all tests. Analyses were performed with SPSS 17.0 (SPSS Inc., Chicago IL, USA).

Results

In total 93 eligible patients were retrospectively screened for inclusion in the study; in 6 cases the conventional angiography recordings were not complete or available and in 7 cases the MSCT scan quality was low due to stack and motion artifacts. In total 80 patients were analyzed for the purpose of the MSCT SYNTAX score study. The mean age was 62 ± 11 years, and 73% were male. Regarding cardiac risk factors, 74.4%, 20.5%, and 70.5% had hypertension, diabetes mellitus, and hyperlipidemia, respectively, and 16.7% were smokers. There were 12.5% of the patients without significant lesions, whereas 42.5% had one-vessel disease, 28.8% had two-vessel disease and 16.3% had three-vessel disease. The duration of the MSCT SXscore calculation was on average 5:30 ($\pm 4:23$) min.

Comparison of the ICA and the MSCT SYNTAX Scores

There was a good correlation between the ICA and the MSCT SXscores ($r_s = 0.76$, $p < 0.001$), **Figure 2**. The overall median values of ICA and MSCT SXscores were 10.5 (IQR 5 - 20.75) and 13.0 (IQR 7 - 24) respectively, $p = 0.004$ (**Table 2**). The mean difference was 2.7 with a standard deviation of 7.9; Bland-Altman analysis is shown in **Figure 3**. The tertiles by ICA were defined as $SXscore_{LOW} \leq 7$, $7 < SXscore_{MID} \leq 16.5$ and $SXscore_{HIGH} > 16.5$, whereas the tertiles by MSCT were defined as $SXscore_{LOW} \leq 9$, $9 < SXscore_{MID} \leq 22$ and $SXscore_{HIGH} > 22$. Taking ICA SXscore tertiles as reference, in the $SXscore_{LOW}$ exact agreement was found in 64.5% cases, whereas in the remaining ones (35.5%) MSCT SXscore was overestimated. Within $SXscore_{MID}$, exact agreement was found in 52.2%, whereas MSCT SXscore was underestimated in 30.4% and overestimated in 17.4% of the cases respectively; finally, within $SXscore_{HIGH}$ the rates of exact agreement were 80.8% whereas MSCT SXscore was underestimated in 19.2% of the cases.

Reproducibility Analyses

There was a high correlation between the first and second rounds of analyses of the raw MSCT SXscores, $r = 0.95$ ($p < 0.001$), **Figure 4**. The intra-observer variability for the MSCT SXscore tertiles showed substantial agreement [$\kappa = 0.80$; 95% CI (0.67, 0.94)], **Table 3**. The weighted kappa value for the number of lesions, total occlusions and

Figure 2. Correlation plot of the MSCT SXscore and ICA SXscore measurements. The SXscoreLOW, SXscoreMID and SXscoreHIGH tertiles for each modality are represented with blue, green and red colour respectively. ICA: invasive coronary angiography; MSCT: multislice computed tomography.

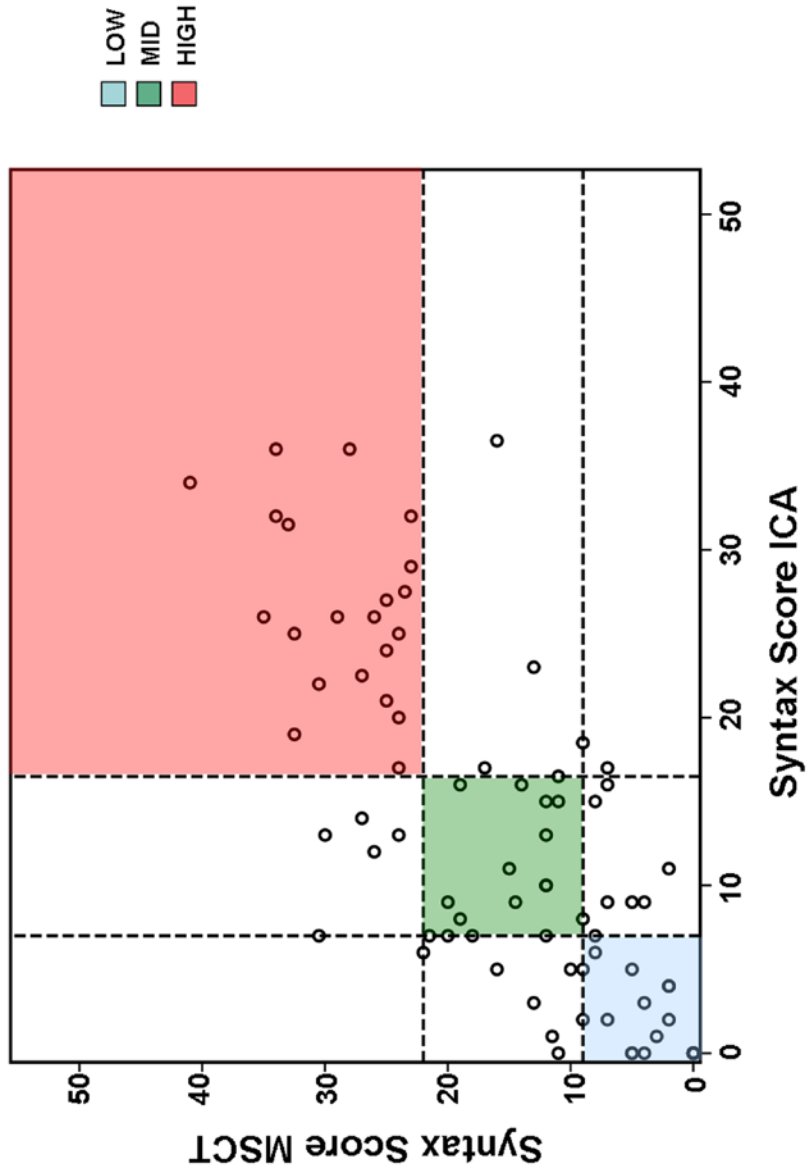


Table 2. Distribution of SYNTAX Score by ICA and MSCT

	ICA		MSCT	
	No. of lesions ICA	SYNTAX Score ICA	No. of lesions MSCT	SYNTAX Score MSCT
Median (IQR)	2 (1 – 4)	10.5 (5 – 20.25)	2 (1 – 3)	13.5 (7 – 25)
Range	0 - 9	0 - 36.5	0 - 6	0 - 41
1 st tertile	-	SxScoreLOW ≤7	-	SxScoreLOW ≤9
2 nd tertile	-	7 < SxScoreMID ≤16.5	-	9 < SxScoreMID ≤22
3 rd tertile	-	SxScoreHIGH >16.5	-	SxScoreHIGH >22

ICA: invasive coronary angiography; MSCT: multislice computed tomography

Table 3. MSCT SYNTAX Score According to Tertiles Recorded During Both Rounds of the Study

	Round one				MSCT SYNTAX
	Score				
		≤9	>9-≤22	>22	Total
Round two MSCT SYNTAX Score	≤9	14	3	0	17
	>9-≤22	1	9	1	11
	>22	0	2	10	12
	Total	15	14	11	40

MSCT: multislice computed tomography

Figure 3. Bland-Altman analysis for the agreement between MSCT SXscore and ICA SXscore. ICA: invasive coronary angiography; MSCT: multislice computed tomography.

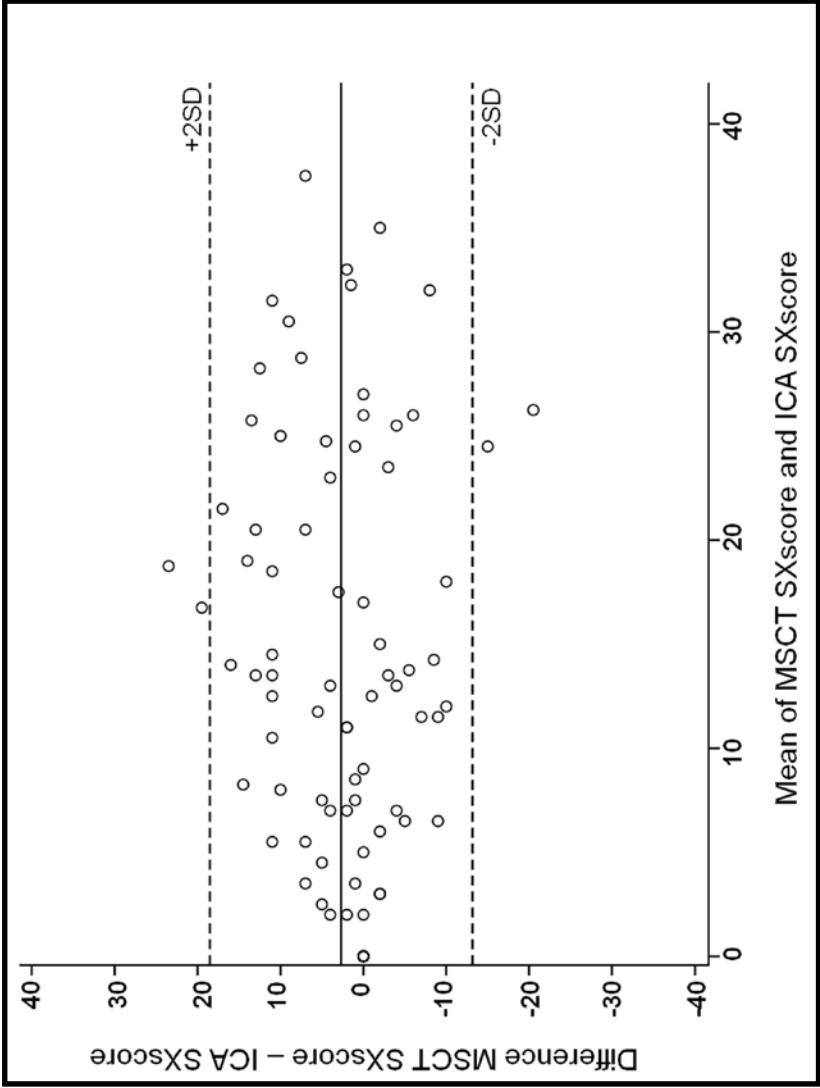
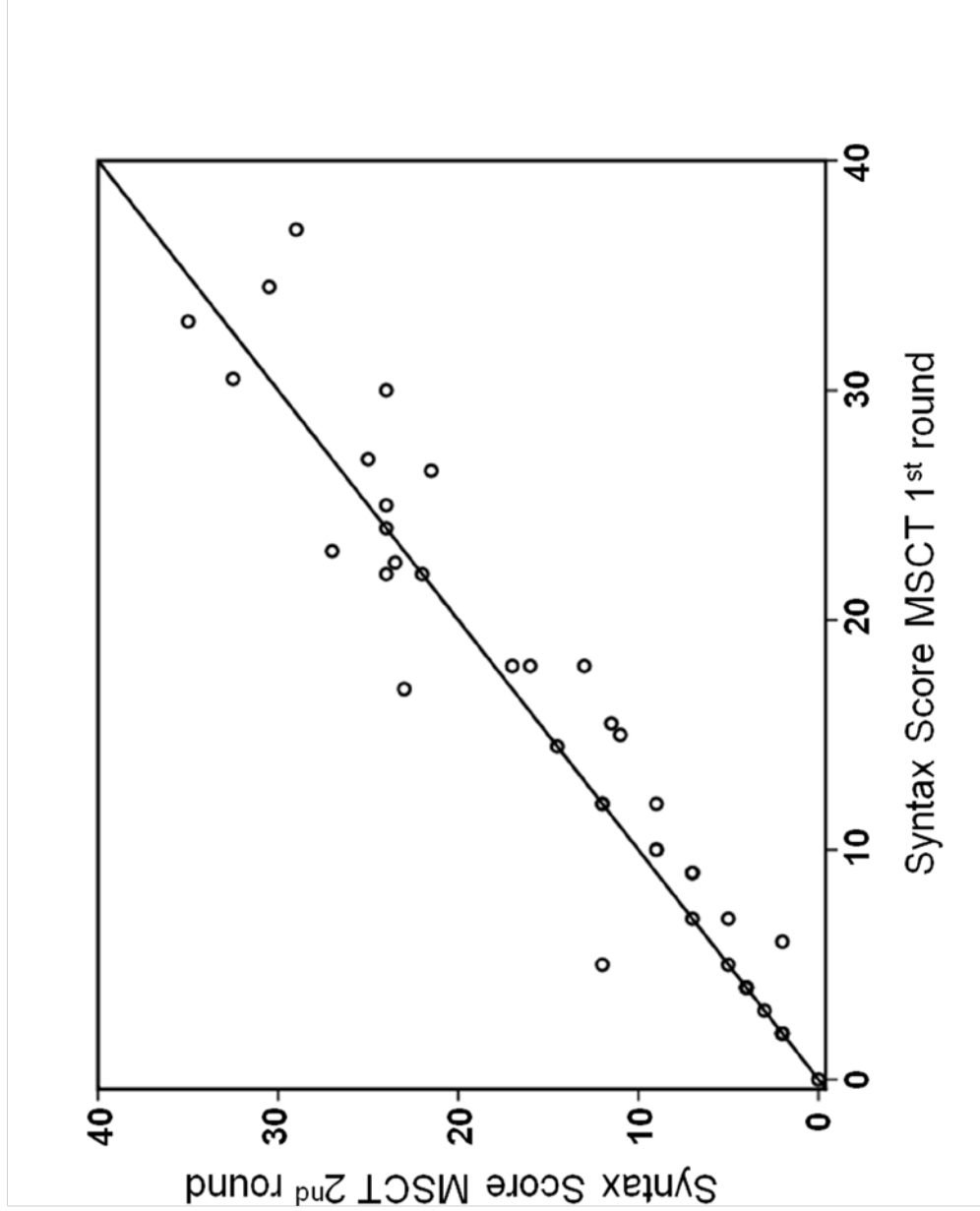


Figure 4. Scatter plot comparing MSCT SXscore values from first and second rounds of analyses. The majority of the values lie close to the line of concordance. MSCT: multislice computed tomography.



bifurcation/trifurcation lesions was 0.87, 0.88 and 0.70, respectively. The variable with the lowest agreement was the number of long lesions [$\kappa=0.49$; 95% CI (0.25, 0.73)].

Calcium score and the MSCT SXscore

The overall median Ca score was 313 (IQR 81 - 688). There was a moderate but significant correlation between the Ca score and both the ICA and the MSCT SXscores ($r_s=0.53$ and $r_s=0.54$ respectively, $p<0.001$). There was no correlation between the amount of calcium and the differences between MSCT and ICA SXscores (**Figure 5**).

Across the ICA SXscore tertiles, the median Ca Score was 145.8, 188.7 and 932.0 in SXscoreLOW, SXscoreMID and SXscoreHIGH respectively ($P<0.001$); across the MSCT SXscore tertiles, the median Ca Score was 145.8, 312.0 and 743.6 in the SXscoreLOW, SXscoreMID and SXscoreHIGH respectively ($P<0.001$), **Figure 6**. The extended MSCT SXscore (categorization of the tertiles into 2 other categories, one with Ca score \leq 400 and the other with Ca score $>$ 400) is presented in **Figure 7**. In the Ca score \leq 400 patients, there were 50%, 40.5% and 9.5% patients across the ICA SXscoreLOW, SXscoreMID and SXscoreHIGH tertiles respectively, while there were 52.4%, 35.7% and 11.9% across the MSCT SXscoreLOW, SXscoreMID and SXscoreHIGH tertiles respectively. In the Ca score $>$ 400 patients, there were 27.3%, 18.2% and 54.5% patients with ICA SXscoreLOW, SXscoreMID and SXscoreHIGH respectively, while in MSCT SXscore, there were 18.2%, 30.3% and 51.5% with MSCT SXscoreLOW, SXscoreMID and SXscoreHIGH respectively.

Figure 5. Scatter plot with line of best fit for the MSCT – ICA SXscore differences and the calcium score per patient. ICA: invasive coronary angiography; MSCT: multislice computed tomography.

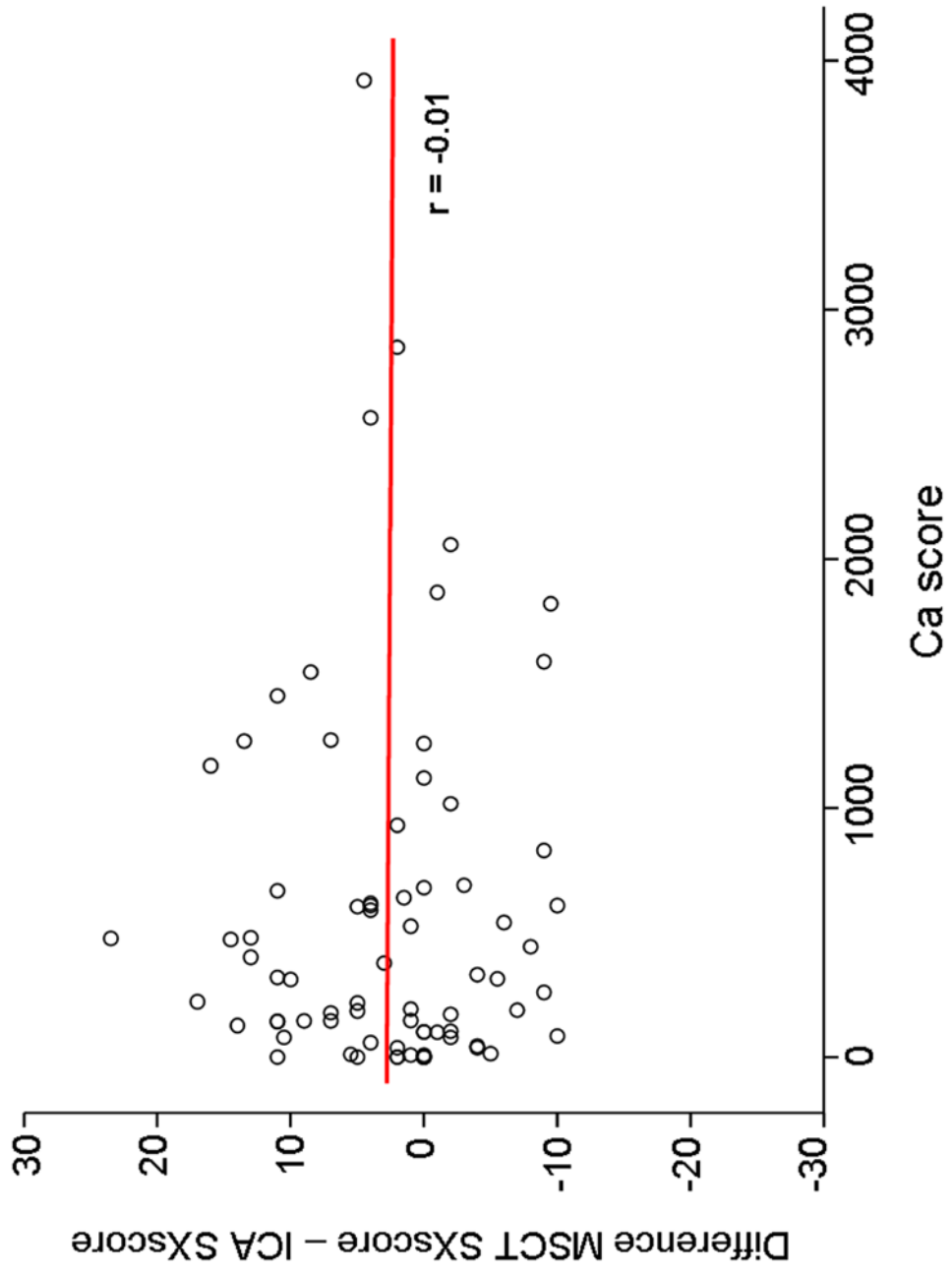


Figure 6. Stratification of the Ca score across the ICA Sxscore and MSCT Sxscore tertiles. ICA: invasive coronary angiography; MSCT: multislice computed tomography.

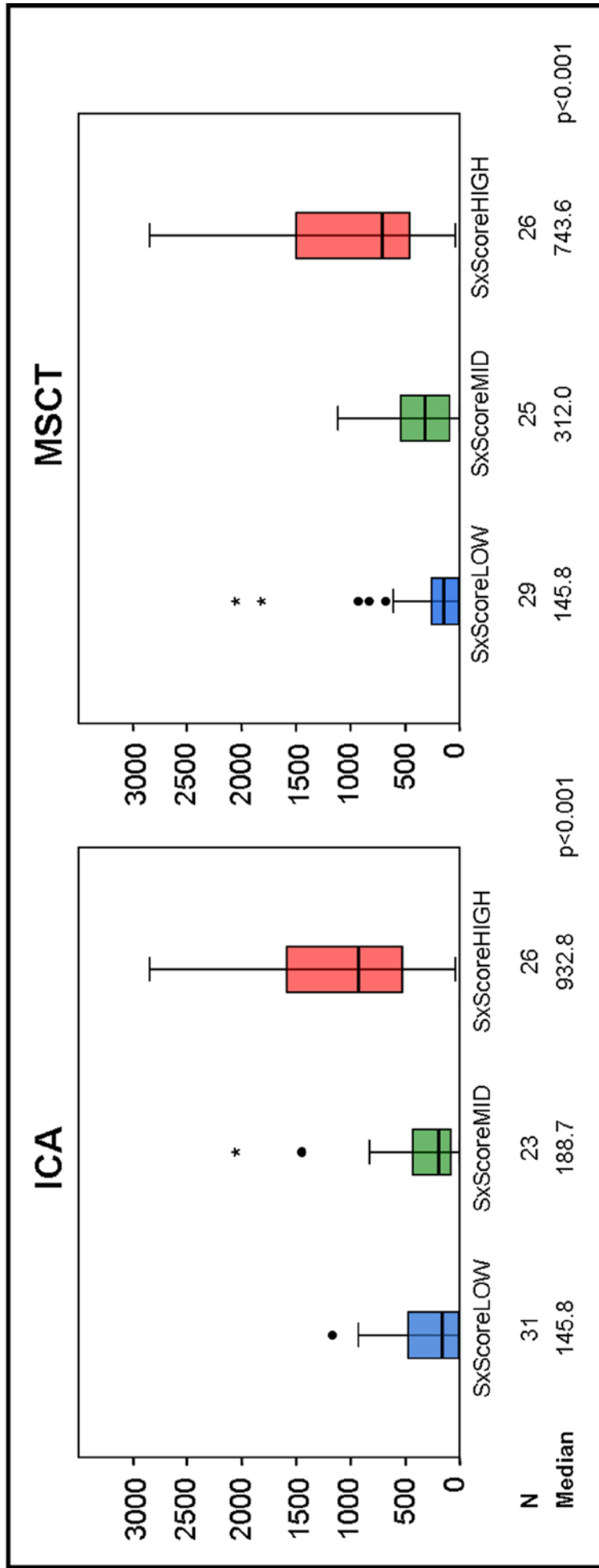
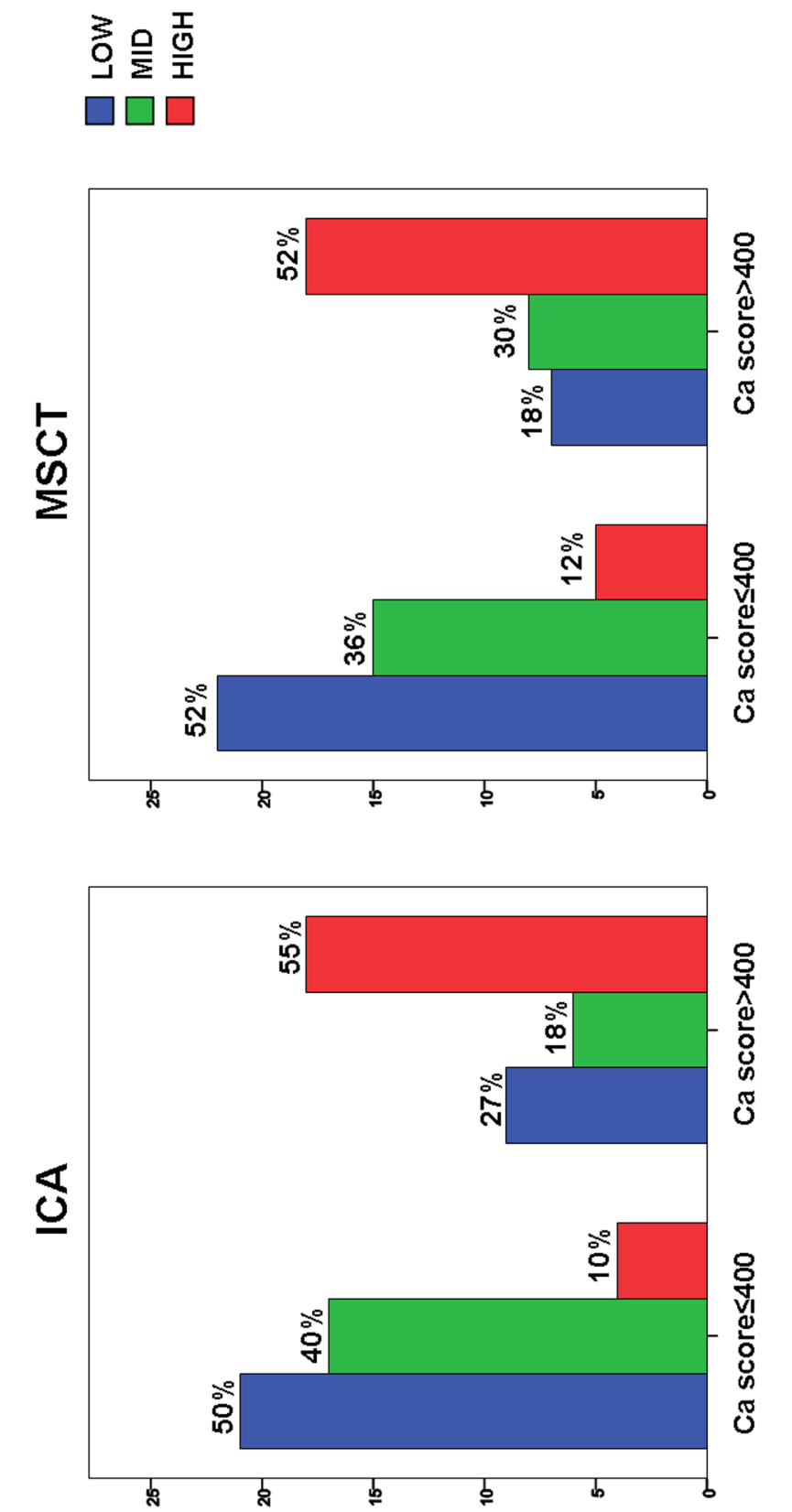


Figure 7. Frequency of the ICA and MSCT Sxscore tertiles within patient groups with low (≤ 400) and high (>400) Ca score. ICA: invasive coronary angiography; MSCT: multislice computed tomography.



Discussion

The main findings of this exploratory study are: 1) The application of the newly developed MSCT SXscore is feasible and is comparable to ICA SXscore; 2) the MSCT SXscore appears to be highly reproducible considering historical conventional SXscore data.

ICA SXscore vs. MSCT SXscore

This report investigates for the first time the feasibility of the MSCT SXscore and shows that it is comparable to the conventional ICA SXscore. For the purpose of this study, we reviewed all the definitions from the ICA SXscore and adapted them to the MSCT capabilities. One example is the scoring of heavy calcification by ICA; this was defined as multiple persisting opacifications of the coronary wall visible in more than one projection surrounding the complete lumen of the coronary artery at the site of the lesion (1), however this is known to correlate weakly with the Ca score (25). In contrast, for the MSCT SXscore we have used the following modified definition: severe calcification was defined as the presence of calcium that occupies more than 50% of the vessel cross-sectional area at any location within the lesion (25). This definition was deemed more suitable for MSCT, since it has been reported as an independent predictor of procedural failure for percutaneous revascularization (25).

Of note, in our study the absolute difference between MSCT and ICA SXscores per patient did not correlate with the Ca Score, as presented in **Figure 5**. Although it can be hypothesized that extreme calcification, which is making the assessment of the coronary lumen more difficult, is responsible for the overestimation of SXscore by MSCT, it appears that the presence of high amount of calcium does not account for the difference between the SXscore calculation with the 2 modalities. Not unexpectedly, the median Ca score in each MSCT SXscore tertile increased gradually and proportionally with the increase of the MSCT SXscore value; conversely, this was not the case with the ICA SXscore, as in the two lower tertiles, the median Ca score was similar. This finding suggests that the stratification based on the MSCT SXscore tertiles reflects better the overall burden of the disease.

Furthermore, the inability of MSCT to evaluate the presence of bridging collaterals and thrombus did not appear to have a detrimental effect on the comparability with the conventional ICA SXscore.

Reproducibility of the MSCT SXscore

A diagnostic tool should be easy to perform and to analyze, accessible and reproducible. Generally speaking, both SXscores share the first qualities, but the MSCT SXscore as investigated by our group appears to have better reproducibility considering historical data (3,26-29). The general correlation of MSCT SXscore values between the first and second rounds of analysis was high, and so was the intra-observer agreement of the MSCT SXscore tertiles (weighted kappa 0.80). The latter has been reported to be lower in all previous studies using conventional angiography (3,26-28), except for a study by Genereux et al. (29) reporting a kappa value of 0.88 for one of the reviewers. One important consideration is the fact that these reports have mean ICA SXcores ranging from 16.2 to 34.1 while our overall ICA SXscore was much lower (median 10.5, mean 13.05). We acknowledge that the extent and complexity of the disease may affect the reproducibility. Nevertheless, the ICA SXscores of the cases included in our study are in the same range of values reported in the SIRTAX (SIRolimus-eluting stent compared with pacliTAXel-eluting stent for coronary revascularization) (8) and the LEADERS (Limus Eluted from A Durable versus ERodable Stent coating) (5) all-comers trials; to put our results in perspective, we envision that the MSCT SXscore could be used in the future in such populations since it has a better precision.

Finally, it could be assumed that the MSCT SXscore is in part more reproducible than the ICA SXscore because the coronary bifurcations can be better visualized by MSCT, without the limitations of the vessel foreshortening and overlap that exist in conventional angiography. Indeed the reproducibility of the number of bifurcation/trifurcation lesions in MSCT SXscore is much better than the one reported in the studies using conventional angiography (3,26-29).

Coronary calcium and the MSCT SXscore

Coronary calcium and lumen stenoses are both different manifestations of atherosclerosis. The ICA SXscore is a lesion-based angiographic scoring system which cannot only quantify coronary anatomy, but has an additional role in the short- and long-term risk stratification

of patients having percutaneous revascularisation, as previous studies have demonstrated (5-9). Furthermore, the Ca score has been identified as an independent predictor of events in asymptomatic individuals (18), as well as in symptomatic patients (19-22).

We propose that the MSCT SXscore could be extended by adding the Ca score as a variable; thereafter, a categorization could be made within each tertile according to the Ca score and might improve the risk stratification of the patients. Using 400 as a cut-off for high Ca score in our study, we have observed that among patients with Ca score \leq 400, there was 12% in the MSCT SXscoreHIGH tertile, which may have a different prognosis from their counterparts with Ca score $>$ 400; conversely, 18% of patients in the Ca score $>$ 400 group were in the MSCT SXscoreLOW tertile, and may also have different outcome than their counterparts with Ca score \leq 400.

Study Limitations

We acknowledge that our investigation has several limitations. This study is relatively small in terms of number of patients included (total number of readings 120 MSCTs and 80 ICAs) and the inclusion was not prospectively done. It has never been our intention to correlate the findings with clinical outcomes since our study might have been underpowered; therefore it should be seen only as an exploratory and feasibility study, without formal statistical hypotheses. Similarly to conventional angiography, the reliability of the MSCT SXscore depends considerably on the experience of the MSCT readers and on the quality of the scans. Finally, the radiation exposure during MSCT coronary angiography remains a matter of concern; nonetheless, the implementation of dose-saving techniques results in effective dose less than the \sim 5 mSv of the invasive coronary angiography.

Future directions

The development of an online algorithm customized for the MSCT SXscore calculation (i.e. incorporating the Ca score values), as is currently available for the conventional SXscore, could be of great interest.

Furthermore, the “functional SYNTAX score” – a fractional flow reserve guided SYNTAX score – has been shown to improve the diagnostic accuracy of the SXscore (30). Recently, the feasibility of non-invasive fractional flow measurements has been demonstrated, by applying computational fluid dynamics to MSCT angiography (31); thus the application of this promising technology to the MSCT SXscore may improve its diagnostic accuracy and reproducibility.

In addition, the angiographic SYNTAX score is lacking the information related to clinical factors which are known to have prognostic value, such as a patients’ age, left ventricular ejection fraction and renal function (32). Integrating the aforementioned variables to the SYNTAX score resulted in the development of the Clinical SYNTAX score, which has shown improved predictive value for adverse clinical events after revascularization (8,33,34). Under this perspective, the ability of MSCT to comprehensively assess the heart can have great potential. Apart from the evaluation of the coronary vessels, MSCT can be used for the evaluation of the left ventricular ejection fraction, the valves and the ischemic myocardium; adding the information from all these parameters may serve to add incremental value to the prognostic utility of the MSCT SXscore.

Conclusion

The calculation of the MSCT SXscore in symptomatic patients appeared feasible and reproducible. The long-term prognostic role of this scoring methodology remains to be further investigated.

References

1. Sianos G, Morel MA, Kappetein AP, et al. The SYNTAX Score: an angiographic tool grading the complexity of coronary artery disease. *EuroIntervention* 2005;1:219-27.
2. Valgimigli M, Serruys PW, Tsuchida K, et al. Cyphering the complexity of coronary artery disease using the syntax score to predict clinical outcome in patients with three-vessel lumen obstruction undergoing percutaneous coronary intervention. *Am J Cardiol* 2007;99:1072-81.
3. Serruys PW, Onuma Y, Garg S, et al. Assessment of the SYNTAX score in the Syntax study. *EuroIntervention* 2009;5:50-6.
4. Park DW, Kim YH, Yun SC, et al. Complexity of atherosclerotic coronary artery disease and long-term outcomes in patients with unprotected left main disease treated with drug-eluting stents or coronary artery bypass grafting. *J Am Coll Cardiol* 2011;57:2152-9.
5. Wykrzykowska JJ, Garg S, Girasis C, et al. Value of the SYNTAX score for risk assessment in the all-comers population of the randomized multicenter LEADERS (Limus Eluted from A Durable versus ERodable Stent coating) trial. *J Am Coll Cardiol* 2010;56:272-7.
6. Garg S, Sarno G, Girasis C, et al. A patient-level pooled analysis assessing the impact of the SYNTAX (synergy between percutaneous coronary intervention with taxus and cardiac surgery) score on 1-year clinical outcomes in 6,508 patients enrolled in contemporary coronary stent trials. *JACC Cardiovasc Interv* 2011;4:645-53.
7. Garg S, Serruys PW, Silber S, et al. The prognostic utility of the SYNTAX score on 1-year outcomes after revascularization with zotarolimus- and everolimus-eluting stents: a substudy of the RESOLUTE All Comers Trial. *JACC Cardiovasc Interv* 2011;4:432-41.
8. Girasis C, Garg S, Raber L, et al. SYNTAX score and Clinical SYNTAX score as predictors of very long-term clinical outcomes in patients undergoing percutaneous coronary interventions: a substudy of SIRolimus-eluting stent compared with pacliTAXel-eluting stent for coronary revascularization (SIRTAX) trial. *Eur Heart J* 2011;32:3115-27.

9. Palmerini T, Genereux P, Caixeta A, et al. Prognostic value of the SYNTAX score in patients with acute coronary syndromes undergoing percutaneous coronary intervention: analysis from the ACUITY (Acute Catheterization and Urgent Intervention Triage Strategy) trial. *J Am Coll Cardiol* 2011;57:2389-97.
10. Wijns W, Kolh P, Danchin N, et al. Task Force on Myocardial Revascularization of the European Society of Cardiology the European Association for Cardio-Thoracic, Surgery European Association for Percutaneous Cardiovascular, Interventions: Guidelines on myocardial revascularization. *Eur Heart J* 2010;31:2501-55.
11. Hillis LD, Smith PK, Anderson JL, et al. 2011 ACCF/AHA Guideline for Coronary Artery Bypass Graft Surgery. A report of the American College of Cardiology Foundation/American Heart Association Task Force on Practice Guidelines. Developed in collaboration with the American Association for Thoracic Surgery, Society of Cardiovascular Anesthesiologists, and Society of Thoracic Surgeons. *J Am Coll Cardiol* 2011;58:e123-210.
12. Levine GN, Bates ER, Blankenship JC, et al. 2011 ACCF/AHA/SCAI Guideline for Percutaneous Coronary Intervention. A report of the American College of Cardiology Foundation/American Heart Association Task Force on Practice Guidelines and the Society for Cardiovascular Angiography and Interventions. *J Am Coll Cardiol* 2011;58:e44-122.
13. Mark DB, Berman DS, Budoff MJ, et al. ACCF/ACR/AHA/NASCI/SAIP/SCAI/SCCT 2010 expert consensus document on coronary computed tomographic angiography: a report of the American College of Cardiology Foundation Task Force on Expert Consensus Documents. *J Am Coll Cardiol* 2010;55:2663-99.
14. Stein PD, Yaekoub AY, Matta F, Sostman HD. 64-slice CT for diagnosis of coronary artery disease: a systematic review. *Am J Med* 2008;121:715-25.
15. Agatston AS, Janowitz WR, Hildner FJ, Zusmer NR, Viamonte M, Jr., Detrano R. Quantification of coronary artery calcium using ultrafast computed tomography. *J Am Coll Cardiol* 1990;15:827-32.
16. Neefjes LA, Dharampala AS, Rossi A, et al. Image quality and radiation exposure using different low-dose scan protocols in dual-source CT coronary angiography: randomized study. *Radiology* 2011;261:779-86.
17. Bongartz G, Golding SJ, Jurik AG, et al. 2004 CT Quality Criteria - Appendix C. European Guidelines for Multislice Computed Tomography, European Commission. Available at: http://www.msct.eu/CT_Quality_Criteria.htm.

18. Budoff MJ, Shaw LJ, Liu ST, et al. Long-term prognosis associated with coronary calcification: observations from a registry of 25,253 patients. *J Am Coll Cardiol* 2007;49:1860-70.
19. Detrano R, Hsiai T, Wang S, et al. Prognostic value of coronary calcification and angiographic stenoses in patients undergoing coronary angiography. *J Am Coll Cardiol* 1996;27:285-90.
20. Georgiou D, Budoff MJ, Kaufer E, Kennedy JM, Lu B, Brundage BH. Screening patients with chest pain in the emergency department using electron beam tomography: a follow-up study. *J Am Coll Cardiol* 2001;38:105-10.
21. Keelan PC, Bielak LF, Ashai K, et al. Long-term prognostic value of coronary calcification detected by electron-beam computed tomography in patients undergoing coronary angiography. *Circulation* 2001;104:412-7.
22. Mohlenkamp S, Lehmann N, Schmermund A, et al. Prognostic value of extensive coronary calcium quantities in symptomatic males--a 5-year follow-up study. *Eur Heart J* 2003;24:845-54.
23. Cohen J. Weighted kappa: nominal scale agreement with provision for scaled disagreement or partial credit. *Psychol Bull* 1968;70:213-20.
24. Landis JR, Koch GG. The measurement of observer agreement for categorical data. *Biometrics* 1977;33:159-74.
25. Garcia-Garcia HM, van Mieghem CA, Gonzalo N, et al. Computed tomography in total coronary occlusions (CTTO registry): radiation exposure and predictors of successful percutaneous intervention. *EuroIntervention* 2009;4:607-16.
26. Garg S, Girasis C, Sarno G, et al. The SYNTAX score revisited: a reassessment of the SYNTAX score reproducibility. *Catheter Cardiovasc Interv* 2010;75:946-52.
27. Shiomi H, Tamura T, Niki S, et al. Inter- and intra-observer variability for assessment of the synergy between percutaneous coronary intervention with TAXUS and cardiac surgery (SYNTAX) score and association of the SYNTAX score with clinical outcome in patients undergoing unprotected left main stenting in the real world. *Circ J* 2011;75:1130-7.
28. Tanboga IH, Ekinci M, Isik T, Kurt M, Kaya A, Sevimli S. Reproducibility of syntax score: from core lab to real world. *J Interv Cardiol* 2011;24:302-6.
29. Genereux P, Palmerini T, Caixeta A, et al. SYNTAX score reproducibility and variability between interventional cardiologists, core laboratory technicians, and quantitative coronary measurements. *Circ Cardiovasc Interv* 2011;4:553-61.

30. Nam CW, Mangiacapra F, Entjes R, et al. Functional SYNTAX score for risk assessment in multivessel coronary artery disease. *J Am Coll Cardiol* 2011;58:1211-8.
31. Koo BK, Erglis A, Doh JH, et al. Diagnosis of ischemia-causing coronary stenoses by noninvasive fractional flow reserve computed from coronary computed tomographic angiograms. Results from the prospective multicenter DISCOVER-FLOW (Diagnosis of Ischemia-Causing Stenoses Obtained Via Noninvasive Fractional Flow Reserve) study. *J Am Coll Cardiol* 2011;58:1989-97.
32. Ranucci M, Castelvechio S, Menicanti L, Frigiola A, Pelissero G. Risk of assessing mortality risk in elective cardiac operations: age, creatinine, ejection fraction, and the law of parsimony. *Circulation* 2009;119:3053-61.
33. Garg S, Sarno G, Garcia-Garcia HM, et al. A new tool for the risk stratification of patients with complex coronary artery disease: the Clinical SYNTAX Score. *Circ Cardiovasc Interv* 2010;3:317-26.
34. Capodanno D, Caggegi A, Miano M, et al. Global risk classification and clinical SYNTAX (synergy between percutaneous coronary intervention with TAXUS and cardiac surgery) score in patients undergoing percutaneous or surgical left main revascularization. *JACC Cardiovasc Interv* 2011;4:287-97.

Chapter 9

Diagnostic Performance of
Computed Tomography
Coronary Angiography to
detect and exclude left main
and/or three-vessel coronary
artery disease.

European Radiology. 2013 Nov;23(11):2934-43.

A.S. Dharampal, **S.L. Papadopoulou**, A. Rossi, W.B. Meijboom, A.C.
Weustink, M. Dijkshoorn, K. Nieman, E.H. Boersma, P.J. de Feijter, G.P.
Krestin

Diagnostic performance of computed tomography coronary angiography to detect and exclude left main and/or three-vessel coronary artery disease

Anoeshka S. Dharampal · Stella L. Papadopoulou · Alexia Rossi ·
W. Bob Meijboom · Annick Weustink · Marcel Dijkshoorn · Koen Nieman ·
Eric H. Boersma · Pim J. de Feijter · Gabriel P. Krestin

Received: 9 May 2013 / Accepted: 16 May 2013 / Published online: 28 June 2013
© European Society of Radiology 2013

Abstract

Objectives To determine the diagnostic performance of CT coronary angiography (CTCA) in detecting and excluding left main (LM) and/or three-vessel CAD (“high-risk” CAD) in symptomatic patients and to compare its discriminatory value with the Duke risk score and calcium score.

Materials and methods Between 2004 and 2011, a total of 1,159 symptomatic patients (61±11 years, 31 % women) with stable angina, without prior revascularisation underwent both invasive coronary angiography (ICA) and CTCA. All patients gave written informed consent for the additional CTCA. High-risk CAD was defined as LM and/or three-vessel obstructive CAD (≥50 % diameter stenosis).

Results A total of 197 (17 %) patients had high-risk CAD as determined by ICA. The sensitivity, specificity, positive predictive value, negative predictive value, positive and negative likelihood ratios of CTCA were 95 % (95 % CI 91–97 %), 83 % (80–85 %), 53 % (48–58 %), 99 % (98–99 %), 5.47 and 0.06, respectively. CTCA provided incremental value (AUC 0.90, $P<0.001$) in the discrimination of high-risk CAD compared with the Duke risk score and calcium score.

Conclusions CTCA accurately excludes high-risk CAD in symptomatic patients. The detection of high-risk CAD is suboptimal owing to the high percentage (47 %) of overestimation of high-risk CAD. CTCA provides incremental value in the discrimination of high-risk CAD compared with the Duke risk score and calcium score.

Key Points

- Computed tomography coronary angiography (CTCA) accurately excludes high-risk coronary artery disease.
- CTCA overestimates high-risk coronary artery disease in 47%.
- CTCA discriminates high-risk CAD better than clinical evaluation and coronary calcification.

Keywords Computed tomography coronary angiography · Diagnostic performance · Left main and/or three-vessel CAD · “High-risk” CAD · Calcium score, coronary calcification · Duke risk score, clinical evaluation

Abbreviations

1VD	One-vessel CAD
2VD	Two-vessel CAD
3VD	Three-vessel CAD
AUC	Area under the receiver operating characteristic curve
CAD	Coronary artery disease
CTCA	Computed tomography coronary angiography
CX	Circumflex
DSCT	Dual-source CT
ECG	Electrocardiogram
HR	Heart rate
ICA	Invasive coronary angiography
LAD	Left anterior descending artery
LM	Left main

A. S. Dharampal (✉) · S. L. Papadopoulou · A. Rossi ·
W. B. Meijboom · A. Weustink · M. Dijkshoorn · K. Nieman ·
P. J. de Feijter · G. P. Krestin
Department of Radiology, Erasmus MC, Room Ca207a,
s-Gravendijkwal 230, PO Box 2040, 3015 CE Rotterdam,
The Netherlands
e-mail: a.dharampal@erasmusmc.nl

A. S. Dharampal · S. L. Papadopoulou · A. Rossi ·
W. B. Meijboom · A. Weustink · K. Nieman · E. H. Boersma ·
P. J. de Feijter
Department of Cardiology, Erasmus MC, Rotterdam,
The Netherlands

NS	Not significant
PPV	Positive predictive value
NPV	Negative predictive value
RCA	Right coronary artery
SN	Sensitivity
SP	Specificity
SSCT	Single-source CT
QCA	Quantitative coronary angiography

Introduction

Cardiovascular disease is the leading cause of death in women and men in the western world [1–3]. Identification of symptomatic patients with obstructive coronary artery disease (CAD), in particular those patients with left main (LM) and/or three-vessel CAD (3VD), defined herein as “high-risk” CAD, is important because optimal medical treatment combined with revascularisation not only relieves symptoms but also improves prognosis in this patient group [4–6].

Exercise testing (ET), myocardial perfusion imaging (MPI) or stress echocardiography (SE) are performed for risk stratification of obstructive CAD and high-risk CAD [7–10]. The sensitivity for the diagnosis of LM and/or 3VD by ET is comparable (88 % vs. 92 %) to that of MPI, while the specificity is slightly higher (46 % vs. 34 %) [8]. The sensitivity of SE in detecting high-risk CAD is reported to be approximately 94 % with a specificity of 40 % [10].

Computed tomography coronary angiography (CTCA) has been shown to be an alternative imaging technique for the evaluation of CAD. CTCA excludes obstructive CAD with high accuracy, but has the tendency to overestimate stenosis severity compared with invasive coronary angiography (ICA) [11]. CTCA may be used to detect or exclude high-risk CAD; however, the diagnostic performance of CTCA in detecting or excluding patients with high-risk CAD has not been fully explored. The goal of this study was to determine the diagnostic performance of CTCA in detecting and excluding high-risk CAD in symptomatic patients suspected of having CAD and to compare its discriminatory value, for detecting and excluding high-risk CAD, with clinical risk factors (Duke risk score) and calcium score.

Materials and methods

Study population

Between July 2004 and August 2011 patients referred for ICA on the basis of chest pain symptoms, risk factors, with or without stress testing were invited to undergo a CTCA examination. Exclusion criteria were previous revascularisation,

iodine allergy or impaired renal function. Consenting patients were entered into our single-centre cardiac database. The final study population comprised 1,159 patients with stable chest pain complaints who were suspected of having CAD. The pre-test probability of obstructive CAD was determined using the Duke risk score [12] which uses clinical factors such as type of complaints, gender, age, smoking, hypercholesterolaemia, diabetes mellitus, history of myocardial infarction and ECG abnormalities [13]. Parts of this single-centre cardiac database have been used in previous studies [14–18]. The study was approved by the institutional review board of our medical hospital.

Computed tomography imaging protocol and image reconstruction

During the inclusion period three consecutive CT systems were used (Table 1). All patients initially underwent unenhanced CT. Subsequently a bolus tracking technique was used to synchronise the start of image acquisition with the arrival of the iodinated contrast agent [Iomeron, iomeprol (400 mg I/mL), Bracco, Milan, Italy; Ultravist, iopromide (370 mg I/mL), Schering Berlin, Germany] in the coronary arteries followed by a saline chaser. CTCA was performed using a conventional ECG-synchronised low-pitch helical CT protocol between 2004 and 2006. Since 2006 CT protocols have been adjusted to reduce the effective radiation dose, to a low-pitch helical protocol with ECG-triggered tube current modulation (2006–2009) [19], to the “step-and-shoot” sequential CT protocol and in selected patients a high-pitch helical protocol in subsequent years [20]. Data sets were reconstructed retrospectively for the low-pitch and step-and-shoot sequential CT protocols in systolic (31–47 %) and diastolic phases (60–76 %) of the RR interval for high (≥ 80 beats/min) and low heart rates (≤ 65 beats/min), respectively, to obtain motion-free images; both systolic and diastolic phases (30–77 %) of the RR interval were used in medium heart rates (66–79 beats/min). CT data sets for the high-pitch helical protocol could only be reconstructed at one diastolic phase. Images were analysed using medium-to-smooth convolution kernels for non-calcified lesions and sharp convolution kernels for calcified lesions.

Computed tomography image evaluation

All data sets were transferred for analyses to an offline workstation (MMWP workstation, Siemens, Erlangen, Germany). The unenhanced CT was used to calculate the total calcium score employing the Agatston method [21] (CaScoring[®], MMWP workstation, Siemens, Erlangen, Germany). Two experienced observers with more than 2 years of experience in cardiac CT, who were blinded to the ICA results, independently evaluated all CTCA for the presence of CAD, using

Table 1 CT device generations and respective imaging protocols

	64-slice SSCT ^a	64-slice DSCT 1st generation ^b	128-slice DSCT 2nd generation ^c
β -blocker ^d	Yes	No	Yes
Nitroglycerin ^e	No	Yes	Yes
X-ray tube	1	2	2
Z-FFS	Yes	Yes	
Collimation	32×0.6	32×0.6	64×0.6
Gantry rotation time (ms)	330	330	285
Temporal resolution (ms)	165	83	75
Spatial resolution (mm)	0.4×0.4×0.4	0.4×0.4×0.4	0.4×0.4×0.4
Pitch	0.2	0.2–0.5	0.2–3.4
Unenhanced acquisition			
Tube voltage (kV)	120	120	120
Tube current	200–150 effective mAs	75 mAs/rotation	75 mAs/rotation
ECG-triggered tube current modulation	Yes	Yes	Yes
Imaging protocol			
Low-pitch helical imaging	Yes	Yes	No
High-pitch helical imaging ^f	No	No	Yes
Step and shoot sequential imaging	No	No	Yes
Contrast-enhanced imaging			
Tube voltage (kV)	120	120	80–120
Tube current	850–960 effective mAs	320–412 mAs/rotation	320–412 mAs/rotation
ECG-triggered tube current modulation	No	Yes	Yes
Imaging protocol			
Low-pitch helical imaging	Yes	Yes	Yes
High-pitch helical imaging ^f	No	No	Yes
Step-and-shoot sequential imaging	No	No	Yes
Effective radiation dose (mSv)	13.43	12.26	3.93

SSCT single-source CT, DSCT dual-source CT, Z-FFS Z-flying focal spot, ECG electrocardiogram, mAs/rotation total mA×rotation time; mSv (millisievert) dose–length product×0.014 [50]

^a Somatom Sensation, Siemens Healthcare, Forchheim, Germany

^b Somatom Definition, Siemens Healthcare, Forchheim, Germany

^c Somatom Definition Flash, Siemens Healthcare, Forchheim, Germany

^d Metoprolol (Seloken, Astra Zeneca, Zoetermeer, Netherlands) administration before imaging when no contraindication was present to achieve better quality images

^e Nitrolingual (Nitroglycerin Pumpspray, G.Pohl-boskamp, Itohenlockstedt, Germany) was administered before imaging in the absence of contraindications for better visualisation of the small coronary arteries

^f Imaging protocol in patients with regular stable heart rate below 65 beats/min

axial source images, multiplanar, curved reformatted reconstructions, and thin-slab maximum intensity projections (Circulation[®], MMWP workstation, Siemens, Erlangen, Germany). Inter-observer disagreements were resolved by a joint consensus reading.

The modified 17-segment American Heart Association model was used to classify each segment. Each segment was visually scored as obstructive in the presence of at least 50 % lumen diameter stenosis and non-obstructive when the lumen diameter stenosis was less than 50 % in comparison with the proximal and distal lumen. All anatomically available segments with a diameter of at least 1.5 mm, irrespective

of image quality or calcification, were included and scored with the intention to diagnose. Non-evaluable segments of poor quality owing to calcification, stack and motion artefacts or low contrast enhancement were classified as obstructive. Coronary segments distal to a total occlusion were excluded from the analyses.

Invasive coronary angiogram image evaluation

One experienced cardiologist, blinded to the CT results, visually assessed each coronary segment (American Heart Association model) for the presence of luminal stenosis in two orthogonal

planes. Segments scored as more than 20 % stenosis on visual assessment were quantified using a validated quantitative coronary angiography (QCA) algorithm [CAASII (Cardiovascular Angiography Analysis System II); Pie Medical Imaging Maastricht, the Netherlands]. Quantitative at least 50 % lumen diameter stenosis was considered significantly obstructive. Patients were classified as having one- (1VD), two- (2VD) or three-vessel CAD (3VD) (at least 50 % diameter stenosis in one, two or three vessels, respectively) or LM CAD (at least 50 % diameter stenosis). High-risk CAD was defined as LM and/or three-vessel CAD.

Statistical analyses

The statistical analysis was performed using dedicated statistical software programs (IBM SPSS statistics 20.0.0.1 and STATA/SE 12.0). Categorical variables were expressed as percentages and continuous variables were expressed as means±standard deviation. Continuous variables with a skewed distribution were expressed as median with interquartile range. The inter-observer agreement was tested between the two CT readers on a vessel level using the κ statistic. CTCA results were compared with ICA as the reference standard on a patient level to calculate the κ statistic, sensitivity (SN), specificity (SP), positive predictive value (PPV) and negative predictive value (NPV) for the detection of at least one obstructive lesion, LM CAD, 3VD and high-risk CAD (LM and/or 3VD). The Wilson score [22] was used to calculate the confidence intervals for small groups. We calculated the positive likelihood ratio (LR+) of CTCA, which is equal to the ratio of the odds of high-risk CAD given a positive CTCA result and the odds of high-risk CAD regardless of the CTCA result (i.e. the pre-test odds of high-risk CAD). Thus, LR+ represents the performance of CTCA in detecting high-risk CAD. We also determined the negative likelihood ratio (LR-) of CTCA, which is equal to the odds of absent high-risk CAD given a negative CTCA result and the odds of absent high-risk CAD regardless of the CTCA result (i.e. the pre-test odds of absent high-risk CAD). Thus, LR- represents the performance of CTCA in excluding high-risk CAD. The area under the receiver operating characteristic curve (AUC) was calculated as the ability of a diagnostic test to discriminate patients with and without high-risk CAD. The AUC takes into account the influence of referral bias that may influence the diagnostic performance in our population [23, 24]. The AUC as a value of high-risk CAD discrimination was calculated for univariate and multivariate models that predicted high-risk CAD. Binary logistic regression analysis was used to create these predicting models (see Table 5) using the following variables separate and combined: Duke risk score, calcium score, and CTCA model (LM CAD and 3VD detected by CTCA). The method of Delong et al. [25] was applied to compare the AUC.

Next we also tested whether other variables such as heart rate, calcium score, body mass index and CT generation had

an influence on the diagnostic performance of CTCA in ruling in/out high-risk CAD using multivariate logistic regression. A *P* value of less than 0.05 was considered statistically significant. This study was performed according to the criteria set forth in the Standard for Reporting of Diagnostic Accuracy Initiative [26].

Results

A total of 1,159 patients were included in the study; the mean age was 61±11 years and 31 % (*n*=360) were women. The patients' clinical and angiographic demographics are detailed in Table 2. High-risk CAD was present in 17 % of the patients (197/1,159; Table 2). The LM coronary artery was absent in 1 patient. ICA identified LM CAD in 48 patients (4 %). In 4 patients with LM CAD there was no additional obstructive CAD (8 %). In 35 % of patients with LM CAD (17/48) there was additional 1VD, in 29 % (14/48) 2VD and in 27 % (13/48) 3VD. 3VD without LM CAD was identified in 149 patients (13 %). The inter-observer agreement for per-vessel detection of obstructive stenosis by the two CT readers showed a good agreement (κ =0.94 [95 % CI 0.93–0.95]).

Diagnostic performance of CTCA

The diagnostic performance of CTCA in detecting CAD is detailed in Table 3. CTCA excluded high-risk CAD in 805 patients out of the 1,159, which was correct in 99 % (795/805) but underestimated the severity of CAD in 10 patients (1 %; Table 3). More specifically, CTCA underestimated 3VD in 13 patients and scored them all as 2VD (Table 4) and correctly detected LM CAD in 3 of these 13 patients (Table 3).

CTCA detected high-risk CAD in 354 patients out of the 1,159, which was correct in 53 % (187/354), but overestimated high-risk CAD in 167 patients (47 %; Table 3). More specifically, CTCA overestimated 3VD in 148 patients, LM CAD in 9 patients, and both LM and 3VD in another 10 patients. These patients with overestimated high-risk CAD by CTCA showed 2VD in 69 % (115/167), 1VD in 27 % (45/167) and obstructive CAD was absent in 4 % (7/167) by ICA (Table 4).

Discrimination of high-risk CAD

All models, univariate and multivariate, significantly contributed to the prediction and discrimination of high-risk CAD (Table 5, Fig. 1). The CTCA outperformed the Duke risk score ($P<0.0001$) as well as the calcium score ($P<0.0001$) for the discrimination of high-risk CAD. Calcium score ($P=0.23$) did not contribute to the prediction and discrimination of high-risk CAD (Table 5) when it was combined with the Duke risk score and CTCA.

Table 2 Patient characteristics

	Mean	Standard deviation
Number patients	1,159	
Women	31 % (360)	
Age (years)	61	[10.8]
Chest pain complaints ^a		
Typical	46 % (538)	[0.50]
Atypical	30 % (353)	[0.46]
Non-anginal	23 % (263)	[0.41]
Current smoker	28 % (319)	[0.45]
Diabetes mellitus ^b	17 % (196)	[0.38]
CAD in family ^c	47 % (546)	[0.50]
Hypercholesterolaemia ^d	57 % (664)	[0.50]
Hypertension ^e	51 % (595)	[0.51]
Body mass index (kg/m ²)	27	[4.3]
ECG pathological Q	15 % (173)	[0.36]
ECG repolarisation disturbances	36 % (423)	[0.48]
Pre-test probability ^f	67 %	[0.30]
Calcium score ^g	250	[42–679]
Prevalence of CAD ^h	74 % (849)	[0.44]
One-vessel CAD	33 % (385)	[0.47]
Two-vessel CAD	27 % (308)	[0.44]
Three-vessel CAD	14 % (162)	[0.35]
Left main CAD	4 % (48)	[0.20]
Left main and/or three-vessel CAD	17 % (197)	[0.38]
Heart rate during CTCA (beats per minute)	65	[12.1]
Effective radiation dose CTCA (mSv) ⁱ	11	[4.6]

Data are presented as means with the number of patients in parentheses. Data in brackets are the standard deviations and for the calcium score this is the 25th and 75th percentiles

^a We defined typical angina as substernal discomfort that was precipitated by physical exertion or emotion and relieved by rest or nitroglycerin within 10 min. We classified chest pain with only 1 or 2 of these 3 symptom characteristics as atypical angina pectoris; if none of the characteristics was present, we classified it as non-anginal chest pain [51]

^b Treatment with oral antidiabetic medication or insulin

^c Patient had first- or second-degree relatives with premature coronary artery disease

^d Total cholesterol >180 mg/dL or treatment for hypercholesterolaemia

^e Blood pressure >120/90 mmHg or treatment for hypertension

^f Pre-test probability of obstructive CAD using the Duke risk score [13]

^g Calcium score (Agatston) with median and interquartile range in brackets

^h Prevalence of having at least one obstructive lesion on a patient level determined by invasive coronary angiography

ⁱ mSv (millisievert): conversion factor 0.014 [mSv/mGy/cm] × dose-length product

Influence of variables on the diagnostic performance of CTCA

Heart rate during CTCA, calcium score, gender, body mass index, CT imaging protocol, and CT device generation did

not have an influence on the sensitivity of CTCA in detecting high-risk CAD (Table 6). The specificity of CTCA in detecting high-risk CAD was influenced by the imaging protocol and calcium score used. When the CTCA was performed using a high-pitch helical imaging protocol or when CTCA was performed in a patient with a calcium score above 400 the specificity decreased significantly. The NPV also significantly decreased with increasing calcium score. The PPV was influenced by the heart rate during the CTCA, but a threshold of 60 beats/min did not result in a significant difference in PPV. The CT device generation showed a significant influence on the PPV. The inter-generation comparison showed no significant differences (Table 6).

Discussion

Numerous studies using ICA in the past [27–30] and more recently using non-invasive CTCA have indicated that higher extent and severity of CAD (LM/3VD) carry a worse prognosis [31–33], which can be improved by revascularisation [4]. In this study we demonstrated the performance of CTCA in detecting and excluding out LM and/or 3VD, defined as high-risk CAD.

The main results of this study are:

1. CTCA accurately excludes high-risk CAD. LM CAD was never missed and 3VD was rarely missed (2 %).
2. CTCA accurately detects high-risk CAD. The high accuracy of CTCA in detecting high-risk CAD was at the expense of the overestimation of high-risk CAD.
3. CTCA provided independent incremental value in the discrimination of high-risk CAD compared with the Duke risk score or calcium score.

Current guidelines indicate that the diagnostic work-up of patients with stable angina and intermediate pre-test probability of CAD requires initial assessment with stress testing with or without imaging [6]. In the presence of ischaemia, stress testing is often followed by anatomical assessment with ICA to assess the appropriateness of percutaneous coronary intervention (PCI) or coronary artery bypass graft (CABG) in addition to optimal medical treatment [6].

However, stress tests such as ET, MPI and SE are limited in detecting and excluding the presence of high-risk CAD anatomy. ET is often used for risk stratification of symptomatic patients as a first-line diagnostic test, because it is widely available, does not use radiation and is inexpensive [8, 34, 35]. In ET the presence of high-risk CAD may be suspected with severe ST segment depression, short exercise duration or blood pressure drop during exercise [7, 35–38] but these parameters are not very sensitive. ET diagnostic performance studies have shown sensitivities ranging from 74 % to 91 % for the detection of LM CAD [8, 36] and from 63 %

Table 3 Diagnostic performance of CT coronary angiography

	Prevalence	TP	TN	FP	FN	κ	SN %	SP %	PPV %	NPV %	LR+	LR-
CAD ^a	74 %	850	227	73	9	0.80*	99 [98–99]	76 [71–80]	92 [90–94]	96 [93–98]	4.07	0.01
LM CAD	4 %	48	1,081	29	0	0.76*	100 [93–100]	97 [96–98]	62 [51–72]	100 [100–100]	38.28	0.000
3VD	14 %	149	827	170	13	0.53*	92 [87–95]	83 [80–85]	47 [41–52]	98 [97–99]	5.39	0.10
LM and/or 3VD	17 %	187	795	167	10	0.59*	95 [91–97]	83 [80–85]	53 [48–58]	99 [98–99]	5.47	0.06

TP true positive, TN true negative, FP false positive, FN false negative, κ kappa statistic for the agreement analyses between invasive coronary angiography and CT coronary angiography, SN sensitivity, SP specificity, PPV positive predictive value, NPV negative predictive value, LR+ positive likelihood ratio, LR- negative likelihood ratio, CAD coronary artery disease, LM left main, 3VD three-vessel CAD





^aDiagnosis of at least one significant stenosis per patient by ICA

*P<0.001

Table 4 The performance of CT coronary angiography in detecting and excluding high-risk CAD compared with invasive coronary angiography

				CTCA							
				LM CAD -				LM CAD +			
				3VD -		3VD +		3VD -		3VD +	
ICA	LM CAD -	3VD	-	795		148		9		10	
			+	10		129		0		10	
	LM CAD +	3VD	-	0		0		23		12	
			+	0		0		3		10	

				CTCA							
				LM CAD -				LM CAD +			
				Extent vessel CAD				Extent vessel CAD			
				0VD	1VD	2VD	3VD	0VD	1VD	2VD	3VD
ICA	LM CAD -	Extent vessel CAD	0VD	224	56	13	4	1	0	1	1
			1VD	7	212 ^a	104	39	0	2	1	3
			2VD	2	13	164	105	0	0	4	6
			3VD	0	0	10	129	0	0	0	10
	LM CAD +	Extent vessel CAD	0VD	0	0	0	0	2	1	1	0
			1VD	0	0	0	0	0	8	6	3
			2VD	0	0	0	0	0	1	4	9
			3VD	0	0	0	0	0	0	3	10

 Correct exclusion of high-risk CAD
 Correct detection of high-risk CAD
 Overestimation of high-risk CAD
 Underestimation of high-risk CAD

CAD coronary artery disease, CTCA computed tomography coronary angiography, ICA invasive coronary angiography, 0VD no obstructive CAD, 1VD 1-vessel CAD, 2VD two-vessel CAD, 3VD three-vessel CAD

^aOne patient with 1VD with absent LM

Table 5 Discrimination of high-risk CAD by univariate and multivariate models

Model ^a	AUC [95 % CI]	se AUC	P	High-risk CAD discrimination comparison ^b		
				Duke	CaSc	CTCA
Duke	0.68 [0.65–0.72]	0.02	<0.001			
CaSc	0.72 [0.69–0.76]	0.02	<0.001	0.10		
CTCA ^c	0.90 [0.88–0.93]	0.01	<0.001	<0.001	<0.001	
Duke+CaSc+CTCA ^c	0.93 [0.91–0.94]	0.01	<0.001 ^d	<0.001	<0.001	<0.001

Duke Duke risk score, *CaSc* Calcium score, *CTCA* CT coronary angiography, *LM CAD* left main coronary artery disease, *3VD* three-vessel CAD, *AUC* area under the receiver operating characteristic curve, *se* standard error

^a Logistic regression (univariate and multivariate) analyses were used to calculate the probability of high-risk CAD

^b Comparison of discrimination of high-risk CAD using the different models with the DeLong method

^c CTCA model: LM CAD and 3VD were inserted as separate variables into the logistic regression model

^d CaSc did not contribute ($P=0.23$) to the prediction of high-risk CAD

to 67 % for the detection of 3VD [7, 36]. The specificity of ET for the diagnosis of LM and/or 3VD is around 46 % and for LM CAD this is only 38 % [8].

MPI has a sensitivity of 92 % in detecting high-risk CAD [8]. The specificity of MPI is slightly lower compared with ET (34 % vs. 46 %, $P<0.01$). The under-diagnosis of high-risk CAD by MPI is believed to be a result of a balanced reduction of perfusion [10, 39–41]. The combination with other indirect findings, such as LV function and stress-induced wall motion

abnormality (transient ischaemic dilatation), has been shown to improve the prediction of high-risk CAD by MPI [37–40].

SE has a sensitivity and specificity of 94 % and 40 %, respectively, in detecting high-risk CAD [10]. In a meta-analysis by Mahajan et al., MPI (15 studies with 2,310 patients in total) was compared with SE (14 studies with 1,403 patients in total) for the detection of high-risk CAD; the investigators found a significantly higher sensitivity by SE compared with MPI (94 % vs. 75 %, $P<0.001$), with a similar specificity (40 % vs. 48 %, $P=0.16$) [10]. Although SE discriminates high-risk CAD better than MPI [summary receiver operating characteristic curve (ROC) AUC 0.82 vs. 0.73, $P=0.01$] [10] this technique has its own inherent limitations [42]. Factors such as suboptimal acoustic window can be partly improved by the use of echo-contrast media, but still requires sufficient training and experience for proper evaluation [43].

In our study we used CTCA as an alternative first-line non-invasive diagnostic tool to detect high-risk CAD. CTCA demonstrated a sensitivity of 95 %, which is at least comparable to the conventional non-invasive diagnostic techniques (ET, MPI and SE). Importantly, the specificity of CTCA in excluding LM and/or 3VD appears to be higher (CTCA, 83 %; ET, 46 % [8]; MPI, 48 % [10]; SE, 40 % [10]) with a better negative likelihood ratio of 0.06 compared with SE (0.21) and MPI (0.47) [10]; and CTCA discriminates high-risk CAD better than SE and MPI (AUC CTCA, 0.90; SE, 0.82; MPI, 0.73 [8]). We also assessed the discrimination of high-risk CAD using the Duke risk score and calcium score in addition to CTCA. CTCA was superior to the Duke risk score and calcium score, and showed that the calcium score did not contribute to the prediction of high-risk CAD when the Duke risk score and CTCA were used in symptomatic patients.

The diagnostic performance of CTCA is limited because it overestimates the extent and severity of CAD. Patients in whom CTCA overestimated high-risk CAD (47 %) predominantly had 2VD (69 %) and only 4 % had no obstructive CAD (Table 4). The tendency to overestimate the stenosis

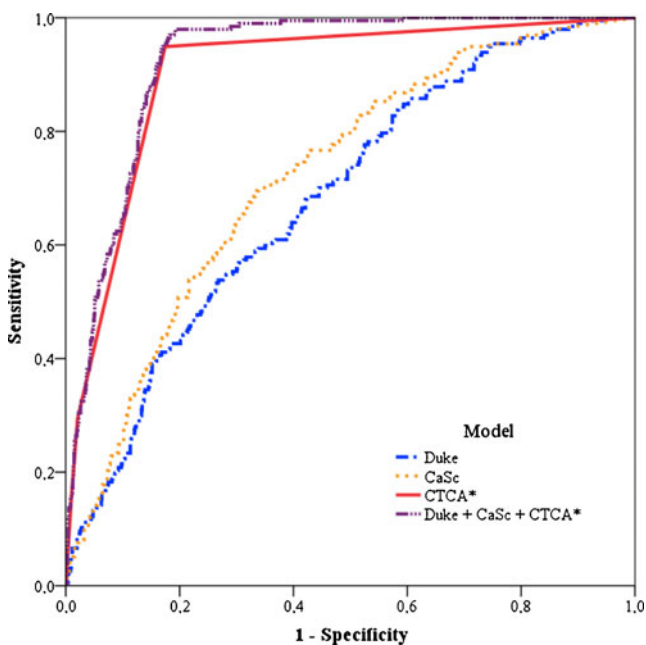


Fig. 1 Receiver operating characteristic curves in the discrimination of high-risk CAD using different models. Logistic regression (univariate and multivariate) analyses were used to calculate the probability of high-risk CAD. *Duke* Duke risk score, *CaSc* calcium score, *CTCA* CT coronary angiography, *LM CAD* left main coronary artery disease, *3VD* three-vessel CAD, *AUC* area under the receiver operating characteristic curve. *CTCA model: LM CAD and 3VD were inserted as separate variables into the logistic regression model

Table 6 Influence of the variables on the diagnostic performance of CTCA in the detection and exclusion of high-risk CAD

	SN % <i>P</i> =NS	SP % <i>P</i> =NS	PPV % <i>P</i> =0.007	NPV % <i>P</i> =NS
Heart rate				
<60 beats/min	97 [91–99]	85 [80–88]	60 [52–68]	99 [97–100]
≥60 beats/min	93 [87–96]	82 [79–85]	49 [43–56]	98 [97–99]
Calcium score	<i>P</i> =NS	<i>P</i> <0.001	<i>P</i> =NS	<i>P</i> <0.001
<400	95 [90–97]	90 [87–92]	48 [39–56]	99 [99–100]
≥400	95 [89–97]	68 [63–73]	56 [49–62]	97 [94–98]
Gender	<i>P</i> =NS	<i>P</i> =NS	<i>P</i> =NS	<i>P</i> =NS
Women	98 [88–100]	86 [82–90]	48 [38–59]	100 [98–100]
Men	94 [89–97]	81 [78–84]	54 [48–60]	98 [97–99]
BMI	<i>P</i> =NS	<i>P</i> =NS	<i>P</i> =NS	<i>P</i> =NS
<30	96 [91–98]	83 [80–85]	52 [46–58]	99 [98–100]
≥30	92 [81–97]	81 [75–86]	54 [44–65]	98 [94–99]
CT imaging protocol ^a	<i>P</i> =NS	<i>P</i> <0.01 ^b	<i>P</i> =NS	<i>P</i> =NS
Low-pitch helical	96 [92–98]	84 [81–86]	54 [48–60]	99 [98–100]
Sequential imaging	88 [64–97]	82 [73–89]	48 [31–66]	97 [90–99]
High pitch helical	100 [72–100]	64 [47–78]	45 [27–65]	100 [85–100]
CT device generation ^c	<i>P</i> =NS	<i>P</i> =NS	<i>P</i> <0.001 ^d	<i>P</i> =NS
SSCT	95 [83–99]	83 [78–86]	38 [28–47]	99 [97–100]
DSCT 1st generation	96 [90–98]	85 [81–88]	65 [57–71]	99 [97–99]
DSCT 2nd generation	93 [81–97]	78 [72–83]	46 [35–56]	98 [95–99]

P values were determined for heart rate, calcium score and BMI as continuous variables and for gender, CT imaging protocol and CT device generation as categorical variables in the multivariate logistic regression. The diagnostic performance of CTCA is shown at arbitrary thresholds of heart rate, calcium score and BMI

SN sensitivity, SP specificity, PPV positive predictive value, NPV negative predictive value, NS not significant ($P \geq 0.05$), BMI body mass index, SSCT single-source CT, DSCT dual-source CT

^a CT-imaging protocol was inserted as a dummy variable into the multivariate logistic regression. Low-pitch helical imaging protocol was taken as a reference and was compared with a sequential imaging protocol and a high-pitch helical imaging protocol

^b Sequential imaging protocol ($P=0.007$) and high-pitch helical imaging protocol ($P=0.005$) were significantly different from the low-pitch helical imaging protocol

^c CT generation was inserted as a dummy variable into the multivariate logistic regression. SSCT was taken as the reference and was compared with 1st and 2nd generation DSCT

^d 1st generation DSCT ($P=0.56$) and 2nd generation DSCT ($P=0.17$) were not significantly different from the SSCT

severity of a given obstruction is because the CT reader is careful not to “miss” an obstructive stenosis (in the case of breathing, motion or artefacts due to the calcifications), thus to avoid “under-diagnosis” and delay of appropriate treatment, which could negatively affect the prognosis. We found false-positive observations to be associated with a higher heart rate (Table 6). The substantial rate of CAD overestimation and the inability of CTCA to assess the functional significance of lesions [14, 44] require referral of these symptomatic patients with CT-determined high-risk CAD for ICA combined with measurement of the fractional flow reserve (FFR). The FAME study ($n=1,005$) demonstrated that FFR-guided revascularisation of multi-vessel CAD by ICA was associated with lower adverse event rates, use of fewer stents and lower healthcare costs [45].

To overcome the high rates of referral to ICA, the integration of anatomical and functional testing is required. Currently this

can be achieved by combining PET or SPECT with CT, but more recently by the fusion of CTCA anatomy and CT-derived FFR using computational fluid dynamics during simulated maximal hyperaemia [46]. Another CT-derived method is to compare myocardial enhancement at rest and during adenosine-induced stress CT perfusion to assess the impedance of coronary stenosis on myocardial blood flow [47, 48]. However, these novel approaches are only in their infancy, and further investigation is needed to confirm their applicability in the clinical setting.

The study had a number of limitations. Referral bias was present, because the patients in our population were referred by their treating physician to undergo ICA on the basis of their chest-pain presentation with or without an outcome of stress testing. To account for this referral bias on the diagnostic accuracy of CTCA in detecting high-risk CAD we assessed the ROC AUC [23] for CTCA (0.90) which is comparable to that of stress echocardiography (0.82) [10].

Our study population only consisted of symptomatic patients with stable angina, and our results may not apply to the wider spectrum of patients with suspected CAD, who have unstable symptoms or did not undergo ICA. Of concern was the rather high radiation exposure of CTCA (11 mSv) owing to the most frequently used low-pitch helical imaging protocol, which was standard in the first-generation CT systems [19, 49]. Currently with the newer generation systems and optimal imaging protocols radiation exposure can be kept within much lower levels (<3 mSv) in patients with low heart rates (<65 beats/min) [20].

In conclusion, CTCA accurately excludes high-risk CAD in patients with suggestive symptoms. However, the performance of CTCA in detecting high-risk CAD is suboptimal, owing to the high number of false-positive observations made by overestimating the severity of stenosis. CTCA provides incremental value in the discrimination of high-risk CAD compared with the Duke risk score and the calcium score.

Acknowledgements Parts of this single-centre cardiac database have been used in previous studies [14–18].

References

- Mosca L, Benjamin EJ, Berra K et al (2011) Effectiveness-based guidelines for the prevention of cardiovascular disease in women—2011 update: a guideline from the American Heart Association. *J Am Coll Cardiol* 57:1404–1423
- Thom T, Haase N, Rosamond W et al (2006) Heart disease and stroke statistics—2006 update: a report from the American Heart Association Statistics Committee and Stroke Statistics Subcommittee. *Circulation* 113:e85–e151
- Roger VL, Go AS, Lloyd-Jones DM et al (2012) Heart disease and stroke statistics—2012 update: a report from the American Heart Association. *Circulation* 125:e2–e220
- Yusuf S, Zucker D, Peduzzi P et al (1994) Effect of coronary artery bypass graft surgery on survival: overview of 10-year results from randomised trials by the Coronary Artery Bypass Graft Surgery Trialists Collaboration. *Lancet* 344:563–570
- Jeremias A, Kaul S, Rosengart TK, Gruberg L, Brown DL (2009) The impact of revascularization on mortality in patients with nonacute coronary artery disease. *Am J Med* 122:152–161
- Wijns W, Kolh P, Danchin N et al (2010) Guidelines on myocardial revascularization. *Eur Heart J* 31:2501–2555
- Weiner DA, Ryan TJ, McCabe CH et al (1987) Value of exercise testing in determining the risk classification and the response to coronary artery bypass grafting in three-vessel coronary artery disease: a report from the Coronary Artery Surgery Study (CASS) registry. *Am J Cardiol* 60:262–266
- Campos CT, Chu HW, D'Agostino HJ Jr, Jones RH (1983) Comparison of rest and exercise radionuclide angiography and exercise treadmill testing for diagnosis of anatomically extensive coronary artery disease. *Circulation* 67:1204–1210
- Fox K, Garcia MA, Ardissino D et al (2006) Guidelines on the management of stable angina pectoris: executive summary: The Task Force on the Management of Stable Angina Pectoris of the European Society of Cardiology. *Eur Heart J* 27:1341–1381
- Mahajan N, Polavaram L, Vankayala H et al (2010) Diagnostic accuracy of myocardial perfusion imaging and stress echocardiography for the diagnosis of left main and triple vessel coronary artery disease: a comparative meta-analysis. *Heart* 96:956–966
- Budoff MJ, Dowe D, Jollis JG et al (2008) Diagnostic performance of 64-multidetector row coronary computed tomographic angiography for evaluation of coronary artery stenosis in individuals without known coronary artery disease: results from the prospective multicenter ACCURACY (Assessment by Coronary Computed Tomographic Angiography of Individuals Undergoing Invasive Coronary Angiography) trial. *J Am Coll Cardiol* 52:1724–1732
- Taylor AJ, Cerqueira M, Hodgson JM et al (2010) ACCF/SCCT/ACR/AHA/ASE/ASNC/NASCI/SCAI/SCMR 2010 appropriate use criteria for cardiac computed tomography. A report of the American College of Cardiology Foundation Appropriate Use Criteria Task Force, the Society of Cardiovascular Computed Tomography, the American College of Radiology, the American Heart Association, the American Society of Echocardiography, the American Society of Nuclear Cardiology, the North American Society for Cardiovascular Imaging, the Society for Cardiovascular Angiography and Interventions, and the Society for Cardiovascular Magnetic Resonance. *J Am Coll Cardiol* 56:1864–1894
- Pryor DB, Shaw L, McCants CB et al (1993) Value of the history and physical in identifying patients at increased risk for coronary artery disease. *Ann Intern Med* 118:81–90
- Meijboom WB, Van Mieghem CA, van Pelt N et al (2008) Comprehensive assessment of coronary artery stenoses: computed tomography coronary angiography versus conventional coronary angiography and correlation with fractional flow reserve in patients with stable angina. *J Am Coll Cardiol* 52:636–643
- Weustink AC, Mollet NR, Neeffjes LA et al (2009) Preserved diagnostic performance of dual-source CT coronary angiography with reduced radiation exposure and cancer risk. *Radiology* 252:53–60
- Weustink AC, Mollet NR, Neeffjes LA et al (2010) Diagnostic accuracy and clinical utility of noninvasive testing for coronary artery disease. *Ann Intern Med* 152:630–639
- Dharampal AS, Rossi A, Papadopoulou SL et al (2011) Is there a difference in the diagnostic accuracy of computed tomography coronary angiography between women and men? *Coron Artery Dis* 22:421–427
- Dharampal AS, Papadopoulou SL, Rossi A et al (2012) Computed tomography coronary angiography accuracy in women and men at low to intermediate risk of coronary artery disease. *Eur Radiol* 22:2415–2423
- Weustink AC, Mollet NR, Pugliese F et al (2008) Optimal electrocardiographic pulsing windows and heart rate: effect on image quality and radiation exposure at dual-source coronary CT angiography. *Radiology* 248:792–798
- Neeffjes LA, Dharampal AS, Rossi A et al (2011) Image quality and radiation exposure using different low-dose scan protocols in dual-source ct coronary angiography: randomized study. *Radiology* 261:779–786
- Agatston AS, Janowitz WR, Hildner FJ, Zusmer NR, Viamonte M Jr, Detrano R (1990) Quantification of coronary artery calcium using ultrafast computed tomography. *J Am Coll Cardiol* 15:827–832
- Wilson EB (1927) Probable inference, law of succession, and statistical inference. *J Am Stat Assoc* 22:209–212
- Diamond GA (1991) Affirmative actions: can the discriminant accuracy of a test be determined in the face of selection bias? *Med Decis Making* 11:48–56
- Fischer JE, Bachmann LM, Jaeschke R (2003) A readers' guide to the interpretation of diagnostic test properties: clinical example of sepsis. *Intensive Care Med* 29:1043–1051
- DeLong ER, DeLong DM, Clarke-Pearson DL (1988) Comparing the areas under two or more correlated receiver operating characteristic curves: a nonparametric approach. *Biometrics* 44:837–845

26. Bossuyt PM, Reitsma JB, Bruns DE et al (2003) Towards complete and accurate reporting of studies of diagnostic accuracy: the STARD initiative. *Clin Radiol* 58:575–580
27. Bruschke AV, Proudfit WL, Sones FM Jr (1973) Progress study of 590 consecutive nonsurgical cases of coronary disease followed 5–9 years. I. Arteriographic correlations. *Circulation* 47:1147–1153
28. Platia EV, Grunwald L, Mellits ED, Humphries JO, Griffith LS (1980) Clinical and arteriographic variables predictive of survival in coronary artery disease. *Am J Cardiol* 46:543–552
29. Chaitman BR, Davis K, Fisher LD et al (1983) A life table and Cox regression analysis of patients with combined proximal left anterior descending and proximal left circumflex coronary artery disease: non-left main equivalent lesions (CASS). *Circulation* 68:1163–1170
30. Proudfit WJ, Bruschke AV, MacMillan JP, Williams GW, Sones FM Jr (1983) Fifteen year survival study of patients with obstructive coronary artery disease. *Circulation* 68:986–997
31. Ostrom MP, Gopal A, Ahmadi N et al (2008) Mortality incidence and the severity of coronary atherosclerosis assessed by computed tomography angiography. *J Am Coll Cardiol* 52:1335–1343
32. Min JK, Shaw LJ, Devereux RB et al (2007) Prognostic value of multidetector coronary computed tomographic angiography for prediction of all-cause mortality. *J Am Coll Cardiol* 50:1161–1170
33. Min JK, Dunning A, Lin FY et al (2011) Age- and sex-related differences in all-cause mortality risk based on coronary computed tomography angiography findings results from the International Multicenter CONFIRM (Coronary CT Angiography Evaluation for Clinical Outcomes: An International Multicenter Registry) of 23,854 patients without known coronary artery disease. *J Am Coll Cardiol* 58:849–860
34. Shaw LJ, Mieres JH, Hendel RH et al (2011) Comparative effectiveness of exercise electrocardiography with or without myocardial perfusion single photon emission computed tomography in women with suspected coronary artery disease: results from the What Is the Optimal Method for Ischemia Evaluation in Women (WOMEN) trial. *Circulation* 124:1239–1249
35. Christian TF, Miller TD, Bailey KR, Gibbons RJ (1994) Exercise tomographic thallium-201 imaging in patients with severe coronary artery disease and normal electrocardiograms. *Ann Intern Med* 121:825–832
36. McNeer JF, Margolis JR, Lee KL et al (1978) The role of the exercise test in the evaluation of patients for ischemic heart disease. *Circulation* 57:64–70
37. Uthamalingam S, Zheng H, Leavitt M et al (2011) Exercise-induced ST-segment elevation in ECG lead aVR is a useful indicator of significant left main or ostial LAD coronary artery stenosis. *JACC Cardiovasc Imaging* 4:176–186
38. Daou D, Delahaye N, Vilain D, Lebtahi R, Faraggi M, Le Guludec D (2002) Identification of extensive coronary artery disease: incremental value of exercise TI-201 SPECT to clinical and stress test variables. *J Nucl Cardiol* 9:161–168
39. Lima RS, Watson DD, Goode AR et al (2003) Incremental value of combined perfusion and function over perfusion alone by gated SPECT myocardial perfusion imaging for detection of severe three-vessel coronary artery disease. *J Am Coll Cardiol* 42:64–70
40. Berman DS, Kang X, Slomka PJ et al (2007) Underestimation of extent of ischemia by gated SPECT myocardial perfusion imaging in patients with left main coronary artery disease. *J Nucl Cardiol* 14:521–528
41. Ragosta M, Bishop AH, Lipson LC et al (2007) Comparison between angiography and fractional flow reserve versus single-photon emission computed tomographic myocardial perfusion imaging for determining lesion significance in patients with multivessel coronary disease. *Am J Cardiol* 99:896–902
42. Pellikka PA, Nagueh SF, Elhendy AA, Kuehl CA, Sawada SG (2007) American Society of Echocardiography recommendations for performance, interpretation, and application of stress echocardiography. *J Am Soc Echocardiogr* 20:1021–1041
43. Hoffmann R, Lethen H, Marwick T et al (1996) Analysis of interinstitutional observer agreement in interpretation of dobutamine stress echocardiograms. *J Am Coll Cardiol* 27:330–336
44. Sarno G, Decraemer I, Vanhoenacker PK et al (2009) On the inappropriateness of noninvasive multidetector computed tomography coronary angiography to trigger coronary revascularization: a comparison with invasive angiography. *JACC Cardiovasc Interv* 2:550–557
45. Tonino PA, De Bruyne B, Pijls NH et al (2009) Fractional flow reserve versus angiography for guiding percutaneous coronary intervention. *N Engl J Med* 360:213–224
46. Koo BK, Erglis A, Doh JH et al (2011) Diagnosis of ischemia-causing coronary stenoses by noninvasive fractional flow reserve computed from coronary computed tomographic angiograms. Results from the prospective multicenter DISCOVER-FLOW (Diagnosis of Ischemia-Causing Stenoses Obtained Via Noninvasive Fractional Flow Reserve) study. *J Am Coll Cardiol* 58:1989–1997
47. Bastarika G, Ramos-Duran L, Rosenblum MA, Kang DK, Rowe GW, Schoepf UJ (2010) Adenosine-stress dynamic myocardial CT perfusion imaging: initial clinical experience. *Invest Radiol* 45:306–313
48. Bamberg F, Becker A, Schwarz F et al (2011) Detection of hemodynamically significant coronary artery stenosis: incremental diagnostic value of dynamic CT-based myocardial perfusion imaging. *Radiology* 260:689–698
49. Meijboom WB, Meijjs MF, Schuijf JD et al (2008) Diagnostic accuracy of 64-slice computed tomography coronary angiography: a prospective, multicenter, multivendor study. *J Am Coll Cardiol* 52:2135–2144
50. Halliburton SS, Abbara S, Chen MY et al (2011) SCCT guidelines on radiation dose and dose-optimization strategies in cardiovascular CT. *J Cardiovasc Comput Tomogr* 5:198–224
51. Diamond GA (1983) A clinically relevant classification of chest discomfort. *J Am Coll Cardiol* 1:574–575

Chapter 10

CT Coronary Angiography Accuracy in Women and Men at Low to Intermediate Risk of Coronary Artery Disease

European Radiology. 2012 Nov;22(11):2415-23.

A.S. Dharampal, **S.L. Papadopoulou**, A. Rossi, A.C. Weustink, N.R.A. Mollet,
W.B. Meijboom, L.A. Neefjes, K. Nieman, E. Boersma, P.J de Feijter, G.P.
Krestin

Computed tomography coronary angiography accuracy in women and men at low to intermediate risk of coronary artery disease

Anoeshka S. Dharampal · Stella L. Papadopoulou · Alexia Rossi · Annick C. Weustink · Nico R. A. Mollet · W. Bob Meijboom · Lisan A. Neeffjes · Koen Nieman · Eric Boersma · Pim J. de Feijter · Gabriel P. Krestin

Received: 6 January 2012 / Revised: 23 March 2012 / Accepted: 12 April 2012
© The Author(s) 2012. This article is published with open access at Springerlink.com

Abstract

Objectives To investigate the diagnostic accuracy of CT coronary angiography (CTCA) in women at low to intermediate pre-test probability of coronary artery disease (CAD) compared with men.

Methods In this retrospective study we included symptomatic patients with low to intermediate risk who underwent both invasive coronary angiography and CTCA. Exclusion criteria were previous revascularisation or myocardial infarction. The pre-test probability of CAD was estimated using the Duke risk score. Thresholds of less than 30 % and 30–90 % were used for determining low and intermediate risk, respectively. The diagnostic accuracy of CTCA in detecting obstructive CAD (≥ 50 % lumen diameter narrowing) was calculated on patient level. $P < 0.05$ was considered significant.

Results A total of 570 patients (46 % women [262/570]) were included and stratified as low (women 73 % [80/109]) and intermediate risk (women 39 % [182/461]). Sensitivity, specificity, PPV and NPV were not significantly different in and between women and men at low and intermediate risk. For women vs. men at low risk they were 97 % vs. 100 %,

79 % vs. 90 %, 80 % vs. 80 % and 97 % vs. 100 %, respectively. For intermediate risk they were 99 % vs. 99 %, 72 % vs. 83 %, 88 % vs. 93 % and 98 % vs. 99 %, respectively.

Conclusion CTCA has similar diagnostic accuracy in women and men at low and intermediate risk.

Key Points

- Coronary artery disease (CAD) is increasingly investigated by computed tomography angiography (CTCA).
- CAD detection or exclusion by CTCA is not different between sexes.
- CTCA diagnostic accuracy was similar between low and intermediate risk sex-specific-groups.
- CTCA rarely misses obstructive CAD in low–intermediate risk women and men.
- CAD yield by invasive coronary angiography after positive CTCA is similar between sex-risk-specific groups.

Keywords Diagnostic accuracy · CT coronary angiography · Multidetector computed tomography · Coronary artery disease · Duke pre-test probability · Sex, women and men

A. S. Dharampal (✉) · S. L. Papadopoulou · A. Rossi · A. C. Weustink · N. R. A. Mollet · W. B. Meijboom · L. A. Neeffjes · K. Nieman · P. J. de Feijter · G. P. Krestin
Department of Radiology, Erasmus MC,
Room Ca207a, 's-Gravendijkwal 230, P.O. Box 2040, 3015 CE,
Rotterdam, The Netherlands
e-mail: a.dharampal@erasmusmc.nl

A. S. Dharampal · S. L. Papadopoulou · A. Rossi · A. C. Weustink · N. R. A. Mollet · W. B. Meijboom · L. A. Neeffjes · K. Nieman · E. Boersma · P. J. de Feijter
Department of Cardiology, Erasmus MC,
Rotterdam, The Netherlands

Abbreviations

AUC	area under receiver-operating characteristic curve
CAD	coronary artery disease
CTCA	computed tomography coronary angiography
ECG	electrocardiography
HR	heart rate
ICA	invasive coronary angiography
NPV	negative predictive value
PPV	positive predictive value
PTP	pre-test probability
SN	sensitivity

SP	specificity
SPECT	single photon emission computed tomography
QCA	quantitative coronary angiography

Introduction

Cardiovascular disease is the leading cause of death in the western world [1]. For several years awareness has been growing that cardiovascular disease is also the primary cause of death in women not only in the western world but also in economic developing countries [2]. Part of this high mortality is related to under-recognition, underdiagnosis and undertreatment of coronary artery disease (CAD) in women [3–7].

The interpretation of chest pain in women caused by CAD is often difficult because of the “less typical” symptoms in women compared with the classical “typical” symptoms in men [3, 4, 8]. This may cause a delay or lead to incorrect diagnosis [3, 4]. Additionally first-line non-invasive diagnostic tests such as exercise electrocardiography and single photon emission computed tomography (SPECT) imaging in women are less sensitive and specific [5, 6].

Paradoxically, because of the diagnostic uncertainty there appears to be an overuse of invasive coronary angiography (ICA) in women, with a rather low diagnostic yield of obstructive CAD [9, 10]. This prompted a “red alert call” for the promotion of advanced non-invasive imaging techniques in women including CT coronary angiography (CTCA) [11]. CTCA has evolved as a reliable gatekeeper of ICA because negative CT findings virtually rule out the presence of obstructive CAD [12–14]. Whether this also applies to women remains unresolved because women have been under-represented in studies assessing the diagnostic accuracy of CTCA [12–17]. The pre-test probability (PTP) of obstructive CAD plays a significant role in the assessment of the clinical utility of CTCA. This PTP of obstructive CAD can be derived from reported clinical prediction rules [18] and may influence the post-CTCA probability of obstructive CAD and thus the need for further testing and management.

The purpose of our study was to assess the diagnostic accuracy and clinical utility of CTCA to detect or exclude obstructive CAD in women with low to intermediate PTP of obstructive CAD in comparison to men.

Methods and materials

Study population

Patients referred by their treating physician for ICA between July 2004 and June 2009 on the basis of chest pain

presentation (typical, atypical and non-anginal complaints) with or without outcome of stress testing were invited to undergo CTCA within 2 weeks of ICA. The CTCA outcome did not affect referral to ICA. We excluded patients with known iodine allergy, impaired renal function and patients with previous revascularisation. A total of 907 patients gave consent for CT accuracy studies and were entered in our single-centre registry. Out of these 907 patients we excluded patients with previous myocardial infarct ($n=54$) as well as patients with a high PTP ($>90\%$) of having obstructive CAD ($n=283$). The final study sample comprised a total of 570 symptomatic patients. The study was approved by the institutional review board of our medical hospital.

Computed tomography imaging protocol and image reconstruction

Patients underwent single-source CT (Somatom Sensation, Siemens Healthcare, Forchheim, Germany) between 2004 and 2006 and subsequently underwent dual-source CT (Somatom Definition, Siemens Healthcare). The imaging settings are described in Table 1. Heart-rate-lowering medication (Metoprolol, Seloken, Astra Zeneca, Zoetermeer, Netherlands) was administered when the heart rate was above 65 beats per minute before the single-source CT in the absence of contraindications to achieve better quality images. To achieve better visualisation of the small coronary arteries the vasodilating agent Nitrolingual (Nitroglycerin Pumpspray, G.Pohl-boskamp, Itohenlockstedt, Germany) was administered before imaging in the absence of contraindications.

All patients initially underwent unenhanced CT to calculate the calcium score using the Agatston method [19]. Subsequently a bolus tracking technique was used to synchronise the start of image acquisition with the arrival of the iodinated contrast agent [Iomeprol, iomeron (400 milligram iodine per millilitre), Bracco, Milan, Italy; Ultravist, iopromide (370 milligram iodine per millilitre), Schering Berlin, Germany] in the coronary arteries followed by a saline chaser.

Between 2004 and 2006 a full-dose ECG-synchronised spiral imaging technique was used. After the introduction of ECG-triggered tube current modulation, the spiral imaging technique with ECG pulsing was used in the subsequent years to reduce the effective radiation dose. Data sets were reconstructed retrospectively according to the heart rate to obtain motion-free images. For heart rates of at least 80 beats per minute the data sets were reconstructed in 31–47% of the R–R interval (systolic phases). For heart rates of no greater than 65 beats per minute this value was 60–76% of the R–R interval (diastolic phases). For heart rates between 66 and 79 beats per minute reconstructions were needed in both systolic and diastolic phases, 30–77% of the R–R interval. Images were analysed using medium-to-

Table 1 Imaging protocol

	SSCT ^b	DSCT ^c
β-blocker ^a	Yes	No
Nitroglycerin ^a	No	Yes
X-ray tube	1	2
Collimation	32×0.6 (Z-FFS)	32×0.6 (Z-FFS)
Gantry rotation time (ms)	330	330
Temporal resolution (ms)	165	83
Spatial resolution (mm)	0.4×0.4×0.4	0.4×0.4×0.4
Pitch	0.2	0.2–0.53
Rotation time (ms)	330	330
Unenhanced imaging		
Tube voltage (kV)	120	120
Tube current	200–150 effective mAs	75 mAs/rotation
ECG-triggered tube current modulation	Yes	Yes
Contrast-enhanced imaging		
Tube voltage (kV)	120	120
Tube current	850–960 effective mAs	320–412 mAs/rotation
ECG-triggered tube current modulation	No	Yes

SSCT single-source CT, DSCT dual-source CT, Z-FFS Z-flying focal spot, ECG electrocardiogram, mAs/rotation total mA × rotation time

^a Administration before imaging when no contraindication was present

^b Somatom Sensation, Siemens Healthcare, Forchheim, Germany

^c Somatom Definition, Siemens Healthcare, Forchheim, Germany

smooth convolution kernels for non-calcified lesions and sharp convolution kernels for calcified lesions.

Computed tomography image evaluation

All data sets were transferred for analyses to an offline proprietary workstation (Leonardo, Siemens, Erlangen, Germany); the total calcium score was calculated using dedicated proprietary software (CaScoring). Two experienced observers with more than 2 years of experience in cardiac CT, blinded to the ICA results, independently evaluated all CTCAs for the presence of CAD, using axial source images, multiplanar, curved reformatted reconstructions, and thin-slab maximum intensity projections using “Circulation” software on the proprietary workstation. Interobserver disagreements were resolved by a joint consensus reading.

The modified 17-segment American Heart Association model was used to classify each segment [20]. Each segment was visually scored as obstructive in the presence of at least 50 % lumen diameter narrowing and non-obstructive when the lumen diameter narrowing was less than 50 % in comparison with the proximal and distal lumen. All anatomically available coronary segments with a diameter of at

least 1.5 mm, irrespective of image quality or calcification, were included and scored with the intention to diagnose. Un-evaluable segments of poor quality due to calcification, stack, motion artefacts, or low contrast enhancement were scored as obstructive. Coronary segments distal to a total occlusion could not be optimally visualised by ICA and thus were excluded from the analyses. The image quality was scored on a segment level as diagnostic and non-diagnostic. The average of this score per patient was compared between women and men.

Invasive coronary angiogram image evaluation

One experienced cardiologist, blinded to the CT results, visually assessed each coronary segment (American Heart Association model) for the presence of luminal narrowing in two orthogonal planes. Stenoses scored as having more than 20 % narrowing on visual assessment were quantified using the validated quantitative coronary angiography (QCA) algorithm (CAASII [Cardiovascular Angiography Analysis System II]; Pie Medical Imaging Maastricht, the Netherlands). The segments were considered obstructive when the quantified lumen diameter narrowing in one of the two planes was at least 50 %. Obstructive lesions on a segment level were used to determine obstructive CAD on a patient level as having one or more obstructive stenoses (≥50 % lumen diameter stenosis) irrespective of the segment in which they were located.

PTP of obstructive CAD

We used the Duke risk score [18] to estimate the PTP of obstructive CAD due to the presence of multiple risk factors such as age, gender, symptoms, history of myocardial infarction, ECG, smoking, hypercholesterolaemia and diabetes mellitus. We used less than 30 %, 30–90 %, and greater than 90 % as thresholds for the low, intermediate and high risk group, respectively. As patients with a high risk are directly referred for ICA we did not include these patients in our analyses [21, 22].

The observed PTP of obstructive CAD is the prevalence of obstructive CAD defined as having at least one lesion with at least 50 % lumen diameter stenosis per patient detected by ICA.

Statistical analyses

The statistical analysis was performed using a dedicated statistical software program (SPSS, version 16.0, IMB, Chicago, IL, USA). Categorical variables were expressed as percentages and continuous variables were expressed as means ± standard deviation. Continuous variables with a

skewed distribution were expressed as median with interquartile range.

The estimated PTP was compared in women, men and in the different risk groups with the observed PTP (observed prevalence) using the paired *t* test.

The patients' characteristics were compared between women and men and between different risk groups using the independent *t* test; otherwise the Mann-Whitney *U* test was used (skewed distribution of continuous data). The interobserver variability was tested between the two CT readers on segment and patient level using the κ statistic.

The CTCA results were compared with the reference standard ICA on a patient level to calculate the sensitivity (SN), specificity (SP), positive predictive value (PPV) and negative predictive value (NPV) [23]. The Wilson score [24] was used to calculate the confidence intervals for small groups. The diagnostic accuracy and utility were compared across the different risk groups, between women and men using the chi-squared test or the Fisher's exact test in the presence of less than five observations in a cell of the 2×2 table. A *P* value of less than 0.05 was considered statistically significant.

The receiver-operating characteristic (ROC) curve was used for visual analyses of the trade-offs between the sensitivity and the specificity of CTCA. The area under the ROC curve (AUC) was calculated to account for the influence of referral bias and prevalence of disease on the diagnostic accuracy of CTCA in our population [25, 26].

The clinical utility of CTCA was a measure of diagnostic certainty or remaining uncertainty of absence or presence of CAD that is derived from the post-test probability of CAD. In case of diagnostic certainty no further testing is required, whereas remaining uncertainty requires further diagnostic testing. It was assumed that a post-test probability of obstructive CAD of less than 5% indicated high certainty with no further requirement for diagnostic testing; probabilities between 5 and 90 % represented uncertainty and indicated a requirement for further diagnostic testing; and probabilities of greater than 90 % indicated high certainty with direct referral to ICA, as proposed by previous studies [27].

This study was performed according to the criteria set forth in the Standard for Reporting of Diagnostic Accuracy Initiative [28].

Results

In total, 570 patients at low to intermediate risk were included of which 46 % were women ($n=262$). The patients' characteristics are provided according to sex and risk group in Table 2. Women overall had a significantly higher heart rate (HR) than men ($P=0.03$). The HR was similar in the different risk groups (Table 2). The prevalence of CAD (at least one obstructive lesion) in women was 61 % and in men

this was 64 % ($P=0.42$). The PTP of obstructive CAD determined by the Duke risk score (estimated PTP) was significantly lower than the observed prevalence of obstructive CAD determined by ICA in women in the overall group (45 % vs. 61 %, $P<0.01$) as well as in the low (17 % vs. 48 %, $P<0.01$) and intermediate risk groups (60 % vs. 66 %, $P=0.02$) separately. In men there was no difference between the estimated PTP and observed prevalence (overall 65 % vs. 64 %, $P=0.56$; low 21 % vs. 28 %, $P=0.43$; intermediate risk group (70 % vs. 68 %, $P=0.38$).

In this population the prevalence of obstructive CAD and extent of CAD in terms of multi-vessel disease and calcium score were similar between women and men (Table 2).

The interobserver variability for detection of obstructive stenosis showed a good agreement on segment ($\kappa=0.94$ [95 % CI 0.93–0.95]) and patient levels ($\kappa=0.91$ [95 % CI 0.87–0.95]). The diagnostic image quality was not significantly different between women and men (0.96 vs. 0.97, $P=0.06$).

Diagnostic accuracy of CTCA

The patient-based diagnostic accuracy of CTCA for detecting or ruling out obstructive CAD according to ICA revealed an AUC of 0.895 (95 % CI: 0.862 - 0.928) which was similar between women and men (0.867 [95 % CI: 0.815 - 0.920] vs. 0.921 [95 % CI: 0.880 - 0.961], $P=0.06$), with similar sensitivity and specificity for women and men when grouped in the low and intermediate risk groups and across the low and intermediate risk groups in both women and men (Table 3).

Because different CT systems were used over the years we also assessed the diagnostic performance for detecting CAD between these two machines. No significant differences were found between the single-source and dual-source CT systems for sensitivity (99 % vs. 99 %, $P=0.93$), specificity (84 % vs. 75 %, $P=0.10$), positive predictive value (85 % vs. 91 %, $P=0.06$) and negative predictive value (99 % vs. 97 %, $P=0.39$).

Clinical utility of CTCA

Certainty defined as probabilities for obstructive CAD of no greater than 5 % after negative CTCA was achieved in both women (NPV 97 % and 98 % for low and intermediate risk, respectively) and men (NPV 100 % and 99 % for low and intermediate risk, respectively) at low to intermediate risk. No certainty of obstructive CAD after positive CTCA could be achieved (probability <90 %) in women at low (PPV 80 %) and intermediate risk (PPV 88 %), and men at low risk (PPV 80 %) (Table 3).

Yield of obstructive CAD by ICA after CTCA

A negative CTCA would prevent 31 % (174/570) of the low to intermediate risk patients proceeding to ICA (30 % (79/262)

Table 2 Patients' characteristics

	All				Low				Intermediate			
	Women		Men		Women		Men		Women		Men	
	Mean	[SD]	Mean	[SD]	Mean	[SD]	Mean	[SD]	Mean	[SD]	Mean	[SD]
Number patients	262		308		80		29		182		279	
Age (years)	62*	[10.96]	55*	[9.52]	54*	[8.58]	40*	[8.15]	66*	[9.57]	57*	[8.18]
Chest pain complaints ^a												
Typical	30 %* (78)	[0.46]	20 %* (63)	[0.40]	1 %* (1)	[0.11]	0 %* (0)	[0.00]	42 %* (77)	[0.50]	23 %* (63)	[0.42]
Atypical	38 %* (100)	[0.49]	50 %* (155)	[0.50]	49 %* (39)	[0.50]	41 %* (12)	[0.50]	34 %* (61)	[0.47]	51 %* (143)	[0.50]
Non-anginal	32 % (84)	[0.47]	29 % (90)	[0.46]	50 % (40)	[0.50]	59 % (17)	[0.50]	24 % (44)	[0.43]	26 % (73)	[0.44]
Current smoker	23 % (59)	[0.42]	28 % (86)	[0.45]	14 % (11)	[0.34]	10 % (3)	[0.31]	26 % (48)	[0.44]	29 % (83)	[0.46]
Diabetes mellitus ^b	16 % (43)	[0.37]	12 % (36)	[0.33]	4 % (3)	[0.19]	0 % (0)	[0.00]	22 %* (40)	[0.42]	13 %* (36)	[0.34]
CAD in family ^c	55 %* (143)	[0.50]	44 %* (137)	[0.50]	59 % (47)	[0.50]	41 % (12)	[0.50]	53 % (96)	[0.50]	45 % (125)	[0.50]
Hypercholesterolaemia ^d	56 %* (147)	[0.50]	44 %* (135)	[0.50]	41 %* (35)	[0.50]	10 %* (3)	[0.31]	62 %* (112)	[0.49]	47 %* (132)	[0.50]
Hypertension ^e	52 %* (138)	[0.50]	40 %* (122)	[0.49]	48 %* (38)	[0.50]	10 %* (3)	[0.31]	54 %* (100)	[0.50]	42 %* (119)	[0.50]
Body mass index (kg/m ²)	27		27		27		26		27		27	
Calcium score ^f	139*	[5–446]	349*	[9–401]	20	[0–194]	2	[0–65]	211	[36–613]	155	[14–444]
Prevalence CAD segments/patient ^g	9 %	[0.11]	10 %	[0.12]	7 %*	[0.09]	3 %*	[0.06]	10 %	[0.11]	11 %	[0.13]
One vessel disease	35 % (92)	[0.48]	32 % (98)	[0.47]	33 % (26)	[0.47]	21 % (6)	[0.41]	36 % (66)	[0.48]	33 % (92)	[0.47]
Multi-vessel disease ^h	25 % (65)	[0.43]	32 % (99)	[0.47]	14 % (11)	[0.35]	7 % (2)	[0.26]	30 % (54)	[0.46]	35 % (97)	[0.48]
Estimated PTP ⁱ	45 %*	[0.25]	65 %*	[0.21]	17 %*	[0.07]	21 %*	[0.08]	60 %*	[0.18]	70 %*	[0.17]
Observed PTP ^j	61 % (159)	[0.49]	64 % (197)	[0.48]	48 % (38)	[0.50]	28 % (8)	[0.45]	66 % (121)	[0.47]	68 % (189)	[0.47]
HR (beats per minute)	67*	[11.94]	65*	[12.64]	67	[11.91]	65	[13.78]	67	[11.98]	65	[12.54]
Radiation exposure (mSv) ^k	12	[3.78]	12	[4.05]	12	[3.24]	13	[3.56]	12	[3.92]	12	[4.09]

Data in parentheses are number of patients. Data in brackets are the standard deviations and for the calcium score the 25th and 75th percentiles
*Bold values represent significant values ($P < 0.05$) in the comparison between women and men using Student's t test or Mann–Whitney U test (italics)

^a We defined typical angina as substernal discomfort that was precipitated by physical exertion or emotion and relieved by rest or nitroglycerin within 10 min. We classified chest pain with only 1 or 2 of these 3 symptom characteristics as atypical angina pectoris; if none of the characteristics was present, we classified it as non-anginal chest pain

^b Treatment with oral antidiabetic medication or insulin

^c Patient had first- or second-degree relatives with premature CAD

^d Total cholesterol >180 mg/dl or treatment for hypercholesterolaemia

^e Blood pressure $>120/90$ mmHg or treatment for hypertension

^f Agatston score with median and [interquartile range]

^g [(Number diseased segments \times 100%)/(total of number segments)] per patient

^h >1 vessel with obstructive CAD detected by ICA

ⁱ Estimated pre-test probability of obstructive CAD [18]: low, <30 % (estimated PTP); intermediate, 30–90 % (estimated PTP)

^j Prevalence of obstructive CAD on a patient level: observed probability of obstructive CAD determined by ICA

^k mSv (millisievert): dose length product \times 0.017

women; 31 % (95/308) men, $P=0.86$; Fig. 1). This prevention of ICA would be more pronounced in patients at low risk (low 49 % (53/109) vs. intermediate 26 % (121/461), $P < 0.001$) compared to patients at intermediate risk. Obstructive CAD would be missed in less than 1 % after a negative CTCA with no significant differences between women and men (1 % (2/262) women vs. 0 % (1/308) men, $P=0.48$), or between the low and intermediate risk groups (1 % (1/109) low vs. 0 % (2/461) intermediate risk group, $P=0.52$). A positive CTCA would result in 89 % (353/396) yield of obstructive CAD by

ICA with no significant differences between women and men (86 % (157/183) women vs. 92 % (196/213) men, $P=0.0502$) or between the low and intermediate risk groups (80 % (45/56) low vs. 91 % (308/340) intermediate risk group, $P=0.06$).

Discussion

In our clinical evaluation of CTCA in low to intermediate risk women and men with suspected CAD who were

Table 3 Diagnostic accuracy and clinical utility of CTCA between women and men across different risk groups

Risk groups	Women		Women				Men				P value (W-M)	
	n	n	SN	SP	PPV	NPV	SN	SP	PPV	NPV		
All	TP	157	196	SN	99 [96–100]				99 [97–100]		0.59*	
	TN	77	94	SP	77 [66–82]				85 [77–90]		0.07	
	FP	26	17	PPV	86 [80–90]				92 [88–95]		0.047	
	FN	2	1	NPV	97 [91–99]				99 [94–100]		0.59*	
Low	TP	37	8	SN	97 [87–100]				100 [68–100]		1.00*	
	TN	33	19	SP	79 [64–88]				90 [71–97]		0.31*	
	FP	9	2	PPV	80 [67–89]				80 [49–94]		1.00*	
	FN	1	0	NPV	97 [85–99]				100 [83–100]		1.00*	
Intermediate	TP	120	188	SN	99 [95–100]				99 [97–100]		1.00*	
	TN	44	75	SP	72 [60–82]				83 [74–90]		0.10	
	FP	17	15	PPV	88 [81–92]				93 [88–96]		0.12	
	FN	1	1	NP	98 [88–100]				99 [93–100]		1.00*	
P value (L-I)				0.42*	0.46	0.23	1.00*	1.00*	0.52*	0.19*	1.00*	

The diagnostic accuracy (SN, SP) and clinical utility (PPV, NPV) values are expressed as percentages with [95 % confidence interval]. Estimated PTP [18] <30 % was defined as low and 30–90 % as belonging to the intermediate risk group. P value L-I (low vs. intermediate risk group) and W-M (women vs. men) estimated using chi-squared test and (*) Fisher’s exact test

TP true positive, TN true negative, FP false positive, FN false negative, SN sensitivity, SP specificity, PPV positive predictive value, NPV negative predictive value

referred for ICA but underwent additional CTCA we found that:

- The Duke risk score underestimated the prevalence of angiographically obstructive CAD in women, especially in those at low risk;
- The sensitivity and specificity of CTCA were similar across low and intermediate risk groups in and between women and men;
- The clinical utility of a positive CTCA was moderate, with remaining diagnostic uncertainty in low to intermediate risk women and low risk men requiring additional functional testing;

- The yield of obstructive CAD by ICA was similar in women and men with low and intermediate risk;
- CTCA was highly accurate in excluding the presence of obstructive CAD in women and men at low and intermediate risk.

In our study the overall predicted probability of having obstructive CAD using the Duke risk score was underestimated in women (45 % vs. 61 %, $P < 0.01$) compared with the actual presence of CAD assessed by ICA. This finding probably reflects the difficulties of evaluating women with symptoms suspected of CAD and has been described in previous studies [3, 8]. Physicians may misclassify the

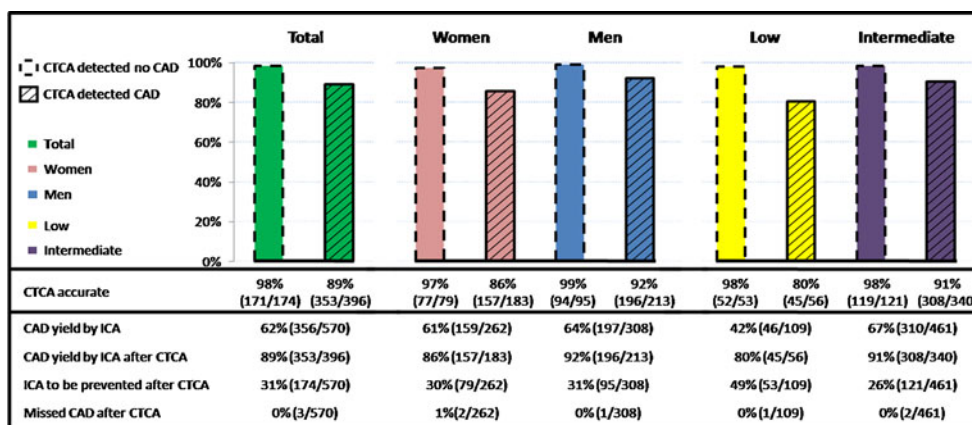


Fig. 1 CAD detection by CTCA and its influence on the yield of CAD by ICA

symptoms as non-anginal or atypical angina in women, which consequently affects the Duke risk score where symptom presentation plays a significant role in the calculation of the PTP. Underestimation of the Duke risk score may also be related to the referral bias of our study population, in particular in women who were referred by their treating physicians for ICA.

It is noteworthy that the diagnostic accuracy of CTCA in detecting obstructive CAD was similar in women and men (Table 3; sensitivity 99 % vs. 99 %; specificity 77 % vs. 85 % for women and men, respectively). Similar findings were shown by Meijboom et al. in a multicentre study (sensitivity 100 % vs. 99 %; specificity 63 % vs. 66 %) [14] and by Pundziute et al. in a single-centre study (sensitivity 95 % vs. 100 %; specificity 93 % vs. 89 % for women and men, respectively) [29]. This is in contrast to the reported technical limitations and diminished accuracy in women of other non-invasive ischaemia tests [6, 30] and underscores the gender neutrality (equality) of the diagnostic accuracy of CTCA.

The clinical utility of CTCA, i.e. reflecting the remaining diagnostic certainty of the presence or absence of significant CAD, is an important criterion in the overall clinical assessment of CTCA. The clinical utility is derived from the post-test probability of CAD and even with the same diagnostic accuracy of a test (sensitivity/specificity) it is different in patients with low or intermediate PTP of CAD. We arbitrarily assumed that in patients with a post-test probability of less than 5 % or greater than 90 % sufficient diagnostic certainty was achieved and no further diagnostic testing was required. In patients with a post-test probability between 5 % and 90 % diagnostic certainty was not sufficient and in these patients further diagnostic testing was deemed necessary. In our population we found that the clinical utility of a positive CTCA was high (>90 %) in men at intermediate PTP of CAD and further diagnostic testing was not necessary. These patients may then be referred to ICA. The clinical utility of a positive CTCA was moderate in women at low to intermediate PTP and in men of low PTP of CAD. In these patients diagnostic certainty was insufficient and further diagnostic testing may be needed. Higher certainty may be then achieved by functional testing for ischaemia e.g. by SPECT or by stress echocardiography [31, 32].

The clinical utility of a negative CTCA was high in women and men at low or intermediate PTP of CAD providing high certainty (<5 %) of absence of obstructive CAD, and no further testing would be necessary. It has been shown in numerous studies that the absence of CAD detected by CTCA is associated with an excellent prognosis [33, 34], which further lends support that these patients may be safely discharged. It should be noted that in patients with persistent chest complaints due to microvascular dysfunction, normal CT findings with no obstructive epicardial CAD may be seen [35]. In these patients, who are often women, further

diagnostic testing for ischaemia to detect microvascular dysfunction will be needed to adjust clinical management and survival [36].

Recent studies reported that the yield of elective ICA to demonstrate the presence of obstructive CAD in women and men is 27–49 % and 47–67 %, respectively, in patients referred for ICA [9, 10], whereas by performing CTCA before diagnostic ICA the yield may improve to 86 % for women and 92 % for men (Fig. 1) and may decrease the number of unnecessary ICA in women and men by 30 % and 31 %, respectively, as suggested by our study.

Our study has limitations. Referral bias was present, because the patients in our population were referred by their treating physicians to undergo invasive coronary imaging on the basis of their chest pain presentation with or without outcome of stress testing. This may explain the relatively high prevalence of obstructive CAD, in particular in women. To account for the influence of referral bias on the diagnostic accuracy [25, 26] of CTCA we also reported the AUC which was not different between women and men (0.87 vs. 0.92, $P=0.056$). Our study population only consisted of stable patients and our results may not apply to the wider spectrum of patients with suspected CAD who did not undergo ICA or who have unstable symptoms. Of concern was the rather high radiation exposure of CTCA (12 mSv) due to the use of a retrospective imaging protocol, which was standard in first-generation CT [14, 37]. Currently with the newer-generation systems and optimal imaging protocols much lower levels of radiation exposure (<3 mSv) can be achieved in patients with low heart rates (<65 beats per minute) [38].

In conclusion, computed tomography coronary angiography has similar diagnostic accuracy in women and men with low and intermediate risk, and may function as an efficient gatekeeper for ICA in women as well as in men.

Acknowledgement All authors contributed substantially to this manuscript and they have read and approved submission of the manuscript.

Funding sources None.

Disclosures None.

Open Access This article is distributed under the terms of the Creative Commons Attribution License which permits any use, distribution, and reproduction in any medium, provided the original author(s) and the source are credited.

References

1. Thom T, Haase N, Rosamond W et al (2006) Heart disease and stroke statistics—2006 update: a report from the American Heart Association Statistics Committee and Stroke Statistics Subcommittee. *Circulation* 113:e85–151

2. Gholizadeh L, Davidson P (2008) More similarities than differences: an international comparison of CVD mortality and risk factors in women. *Health Care Women Int* 29:3–22
3. Canto JG, Goldberg RJ, Hand MM et al (2007) Symptom presentation of women with acute coronary syndromes: myth vs reality. *Arch Intern Med* 167:2405–2413
4. Shaw LJ, Bairey Merz CN, Pepine CJ et al (2006) Insights from the NHLBI-Sponsored Women's Ischemia Syndrome Evaluation (WISE) Study: Part I: gender differences in traditional and novel risk factors, symptom evaluation, and gender-optimized diagnostic strategies. *J Am Coll Cardiol* 47:S4–S20
5. Detry JM, Kapita BM, Cosyns J, Sottiaux B, Brasseur LA, Rousseau MF (1977) Diagnostic value of history and maximal exercise electrocardiography in men and women suspected of coronary heart disease. *Circulation* 56:756–761
6. Kwok Y, Kim C, Grady D, Segal M, Redberg R (1999) Meta-analysis of exercise testing to detect coronary artery disease in women. *Am J Cardiol* 83:660–666
7. Sekhri N, Timmis A, Chen R et al (2008) Inequity of access to investigation and effect on clinical outcomes: prognostic study of coronary angiography for suspected stable angina pectoris. *BMJ* 336:1058–1061
8. Johnson BD, Kelsey SF, Bairey Merz CN (2003) Clinical risk assessment in women: chest discomfort. In: Shaw LJ, Redberg RF (eds) *Coronary disease in women: evidence-based diagnosis and treatment*. Humana, Totowa, pp 129–143
9. Patel MR, Peterson ED, Dai D et al (2010) Low diagnostic yield of elective coronary angiography. *N Engl J Med* 362:886–895
10. Shaw LJ, Shaw RE, Merz CN et al (2008) Impact of ethnicity and gender differences on angiographic coronary artery disease prevalence and in-hospital mortality in the American College of Cardiology-National Cardiovascular Data Registry. *Circulation* 117:1787–1801
11. Maas AH, van der Schouw YT, Regitz-Zagrosek V et al (2011) Red alert for women's heart: the urgent need for more research and knowledge on cardiovascular disease in women: proceedings of the workshop held in Brussels on gender differences in cardiovascular disease, 29 September 2010. *Eur Heart J* 32:1362–1368
12. Chow BJ, Abraham A, Wells GA et al (2009) Diagnostic accuracy and impact of computed tomographic coronary angiography on utilization of invasive coronary angiography. *Circ Cardiovasc Imaging* 2:16–23
13. Budoff MJ, Dowe D, Jollis JG et al (2008) Diagnostic performance of 64-multidetector row coronary computed tomographic angiography for evaluation of coronary artery stenosis in individuals without known coronary artery disease: results from the prospective multicenter ACCURACY (Assessment by Coronary Computed Tomographic Angiography of Individuals Undergoing Invasive Coronary Angiography) trial. *J Am Coll Cardiol* 52:1724–1732
14. Meijboom WB, Meijis MF, Schuijff JD et al (2008) Diagnostic accuracy of 64-slice computed tomography coronary angiography: a prospective, multicenter, multivendor study. *J Am Coll Cardiol* 52:2135–2144
15. Mowatt G, Cummins E, Waugh N et al (2008) Systematic review of the clinical effectiveness and cost-effectiveness of 64-slice or higher computed tomography angiography as an alternative to invasive coronary angiography in the investigation of coronary artery disease. *Health Technol Assess* 12:iii–iv, ix–143
16. Meijboom WB, Weustink AC, Pugliese F et al (2007) Comparison of diagnostic accuracy of 64-slice computed tomography coronary angiography in women versus men with angina pectoris. *Am J Cardiol* 100:1532–1537
17. Miller JM, Rochitte CE, Dewey M et al (2008) Diagnostic performance of coronary angiography by 64-row CT. *N Engl J Med* 359:2324–2336
18. Pryor DB, Shaw L, McCants CB et al (1993) Value of the history and physical in identifying patients at increased risk for coronary artery disease. *Ann Intern Med* 118:81–90
19. Agatston AS, Janowitz WR, Hildner FJ, Zusmer NR, Viamonte M Jr, Detrano R (1990) Quantification of coronary artery calcium using ultrafast computed tomography. *J Am Coll Cardiol* 15:827–832
20. Austen WG, Edwards JE, Frye RL et al (1975) A reporting system on patients evaluated for coronary artery disease. Report of the Ad Hoc Committee for Grading of Coronary Artery Disease, Council on Cardiovascular Surgery, American Heart Association. *Circulation* 51:5–40
21. Skinner JS, Smeeth L, Kendall JM, Adams PC, Timmis A, Chest Pain Guideline Development Group (2010) NICE guidance. Chest pain of recent onset: assessment and diagnosis of recent onset chest pain or discomfort of suspected cardiac origin. *Heart* 96:974–978
22. Meijboom WB, van Mieghem CA, Mollet NR et al (2007) 64-slice computed tomography coronary angiography in patients with high, intermediate, or low pretest probability of significant coronary artery disease. *J Am Coll Cardiol* 50:1469–1475
23. Dharampal AS, Rossi A, Papadopoulou SL et al (2011) Is there a difference in the diagnostic accuracy of computed tomography coronary angiography between women and men? *Coron Artery Dis* 22:421–427
24. Wilson EB (1927) Probable inference, law of succession, and statistical inference. *J Am Stat Assoc* 22:209–212
25. Diamond GA (1991) Affirmative actions: can the discriminant accuracy of a test be determined in the face of selection bias? *Med Decis Making* 11:48–56
26. Fischer JE, Bachmann LM, Jaeschke R (2003) A readers' guide to the interpretation of diagnostic test properties: clinical example of sepsis. *Intensive Care Med* 29:1043–1051
27. Weustink AC, Mollet NR, Neeffjes LA et al (2010) Diagnostic accuracy and clinical utility of noninvasive testing for coronary artery disease. *Ann Intern Med* 152:630–639
28. Bossuyt PM, Reitsma JB, Bruns DE et al (2003) Towards complete and accurate reporting of studies of diagnostic accuracy: the STARD initiative. *Clin Radiol* 58:575–580
29. Pundziute G, Schuijff JD, Jukema JW et al (2008) Gender influence on the diagnostic accuracy of 64-slice multislice computed tomography coronary angiography for detection of obstructive coronary artery disease. *Heart* 94:48–52
30. Grady D, Chaput L, Kristof M (2003) Diagnosis and treatment of coronary heart disease in women: systematic reviews of evidence on selected topics. Evidence report/technology assessment 81. Agency for Healthcare Research and Quality, Rockville
31. Wijns W, Kolh P, Danchin N et al (2010) Guidelines on myocardial revascularization. *Eur Heart J* 31:2501–2555
32. Anderson JL, Adams CD, Antman EM et al (2011) 2011 ACCF/AHA focused update incorporated into the ACC/AHA 2007 guidelines for the management of patients with unstable angina/non-ST-elevation myocardial infarction: a report of the American College of Cardiology Foundation/American Heart Association Task Force on Practice Guidelines. *Circulation* 123:e426–579
33. Min JK, Dunning A, Lin FY et al (2011) Age- and sex-related differences in all-cause mortality risk based on coronary computed tomography angiography findings results from the International Multicenter CONFIRM (Coronary CT Angiography Evaluation for Clinical Outcomes: an International Multicenter Registry) of 23,854 patients without known coronary artery disease. *J Am Coll Cardiol* 58:849–860
34. Ostrom MP, Gopal A, Ahmadi N et al (2008) Mortality incidence and the severity of coronary atherosclerosis assessed by computed tomography angiography. *J Am Coll Cardiol* 52:1335–1343
35. Johnson BD, Shaw LJ, Pepine CJ et al (2006) Persistent chest pain predicts cardiovascular events in women without obstructive coronary artery disease: results from the NIH-NHLBI-sponsored Women's Ischaemia Syndrome Evaluation (WISE) study. *Eur Heart J* 27:1408–1415

36. Reis SE, Holubkov R, Conrad Smith AJ et al (2001) Coronary microvascular dysfunction is highly prevalent in women with chest pain in the absence of coronary artery disease: results from the NHLBI WISE study. *Am Heart J* 141:735–741
37. Weustink AC, Mollet NR, Pugliese F et al (2008) Optimal electrocardiographic pulsing windows and heart rate: effect on image quality and radiation exposure at dual-source coronary CT angiography. *Radiology* 248:792–798
38. Neefjes LA, Dharampal AS, Rossi A et al (2011) Image quality and radiation exposure using different low-dose scan protocols in dual-source CT coronary angiography: randomized study. *Radiology* 261:779–786

Chapter 11

Is there a difference in the diagnostic accuracy of computed tomography coronary angiography between women and men?

Coronary Artery Disease. 22(6):421-7 (2011)

A.S. Dharampal, A. Rossi, **S.L. Papadopoulou**, A.C. Weustink, E. Boersma, K. Nieman, C-H Chen, M. Dijkshoorn, N.R. Mollet, G.P. Krestin, P.J. de Feyter

Is there a difference in the diagnostic accuracy of computed tomography coronary angiography between women and men?

Anoeshka S. Dharampal^{a,b}, Alexia Rossi^{a,b}, Stella L. Papadopoulou^{a,b}, Annick C. Weustink^a, Eric Boersma^b, Koen Nieman^{a,b}, Chia-Hui Chen^a, Marcel Dijkshoorn^a, Nico R. Mollet^a, Gabriel P. Krestin^a and Pim J. de Feyter^{a,b}

Objective To assess the influence of sex on the diagnostic performance of computed tomography coronary angiography (CTCA).

Methods A total of 916 symptomatic patients (30.5% women) without earlier history of coronary artery intervention underwent both CTCA and invasive coronary angiography. Descriptive diagnostic parameters, to detect obstructive coronary artery disease (CAD; $\geq 50\%$ lumen diameter narrowing) on CTCA, were compared between women and men on a per-patient, per-vessel, and per-segment level. Adjusted values were calculated for clustered segments and differences in sex variables using logistic multivariate regression models in general estimated equations.

Results Women were older, had less typical chest complaints, and had a lower prevalence, extent, and severity of CAD compared with men. Multivariate analysis on a per-patient level revealed no difference in sensitivity (98 vs. 99%, $P=0.15$), specificity (78 vs. 82%, $P=0.65$), positive predictive value (PPV; 87 vs. 95%, $P=0.10$), negative predictive value (NPV; 97 vs. 98%, $P=0.63$), and diagnostic odds ratio (DOR; 198 vs. 721, $P=0.07$). No difference was found on per-vessel level analysis

(sensitivity 95 vs. 97%, $P=0.14$; specificity 89 vs. 87%, $P=0.93$; PPV 73 vs. 79%, $P=0.06$; NPV 98 vs. 98%, $P=0.72$; and DOR 143 vs. 240, $P=0.08$). Per-segment analysis revealed a lower sensitivity (88 vs. 94%, $P<0.001$) and DOR (163 vs. 302, $P=0.002$) in women compared with men, without a difference in specificity (96 vs. 95%, $P=0.19$), PPV (64 vs. 69%, $P=0.07$), and NPV (99 vs. 99%, $P=0.08$).

Conclusion CTCA can accurately rule out obstructive CAD in both women and men. CTCA is less accurate in women to detect individual obstructive disease. *Coron Artery Dis* 00:000–000 © 2011 Wolters Kluwer Health | Lippincott Williams & Wilkins.

Coronary Artery Disease 2011, 00:000–000

Keywords: coronary artery disease, diagnostic accuracy, multislice computed tomography, multivariate analyses, patient, segment, sex, vessel

Departments of ^aRadiology and ^bCardiology, Erasmus MC, Rotterdam, The Netherlands

Correspondence to Anoeshka S. Dharampal, MD, Department of Radiology, Erasmus MC, Room Ca 207a, 's-Gravendijkwal 230, PO Box 2040, Rotterdam 3015 CE, The Netherlands
Tel: +31 10 7033558; fax: +31 10 7034033;
e-mail: a.dharampal@erasmusmc.nl

Received 21 Jan 2011 Accepted 26 March 2011

Introduction

Coronary artery disease (CAD) remains one of the leading causes of death in the western world in both women and men. A larger number of cardiac deaths are reported in women compared with men [1,2]. The cardiovascular mortality was 55% in women compared with 43% in men in Europe (2007) [3]. In women, the identification of CAD is challenged by the fact that perception and reporting of symptoms is different compared with men, with poorer correlation between symptoms and angiographic coronary obstruction. In addition, diagnostic performance of many commonly used noninvasive tests, such as electrocardiographic (ECG) exercise testing, myocardial perfusion imaging, or stress echocardiography seems to be lower in women compared with men [4–6].

Direct visualization of obstructive CAD by multislice CT (MSCT) has been shown very accurate in comparison with invasive coronary angiography [7–9], although

concerns have been raised regarding its diagnostic performance in women [10]. The few published MSCT diagnostic performance studies presented conflicting data for women [10,11]. These data, regarding the diagnostic accuracy in women, have not been detailed in recently reported multicenter studies [7–9,12].

The purpose of this study was to compare, within a large population, the diagnostic performance of MSCT coronary angiography between women and men, using invasive coronary angiography as reference.

Methods

General study design

The study is a continuation of the research reported in 2007 by Meijboom *et al.* [10]. It is designed as a comparison between women and men with regard to the diagnostic performance of MSCT for the detection of obstructive CAD, using invasive quantitative coronary

angiography as reference [13–15]. Patients were enrolled in previously published study protocols [15,16], which were approved by our institutional review board. The study is performed according to the criteria as set forth in the Standards for Reporting of Diagnostic Accuracy initiative [17].

Patient selection

Between July 2004 and June 2009, 1575 symptomatic patients underwent computed tomography coronary angiography (CTCA) and invasive coronary angiography (ICA) within 2 weeks. Patients with a history of percutaneous coronary intervention or coronary artery bypass grafting ($n = 659$) were excluded. The final study sample comprised a total of 916 symptomatic patients.

Scan protocol and image reconstruction

A total of 385 patients were scanned using a single-source CT (SSCT) from July 2004 to March 2006. The following 531 patients were scanned using a dual-source CT (DSCT) from April 2006 to April 2009.

Beta-adrenergic blocking agents (Metoprolol, Seloken, Astra Zeneca, Zoetermeer, The Netherlands) were administered in the absence of contraindications to patients with high heart rates ($> 65/\text{min}$) before the SSCT scan, but not to the patients scanned by the DSCT. For vasodilation of the coronary arteries, sublingual nitroglycerin (Nitrolingual, Nitroglycerin Pumpspray, G. Pohl-Boskamp, Itohenlockstedt, Germany) was administered before the scan when no contraindications were present.

The scan settings are described in Table 1. All patients received an unenhanced CT scan to calculate the calcium score using the Agatston method [18]. Subsequently a bolus tracking technique was used to synchronize the start of image acquisition with the arrival of the iodinated contrast agent [Iomeprol, iomeron (400 mgI/ml), Bracco, Milan, Italy; and Ultravist, iopromide (370 mgI/ml), Schering, Berlin, Germany] in the coronary arteries. The SSCT used a full-dose spiral scan technique with retrospective ECG-gated image reconstruction. In the DSCT, the tube current modulation was introduced to reduce the effective radiation dose. Datasets with motion-free images were reconstructed in the systolic and diastolic phases for the analysis of high and low heart rates, respectively. Both systolic and diastolic phases were used in medium heart rates. Images were analyzed using medium-to-smooth and sharp convolution kernels as described in previous studies [14,16].

Computed tomography image evaluation

The total calcium score was calculated using a multi-modality workstation with dedicated software (Siemens, Erlangen, Germany). Experienced observers, blinded for the ICA result, independently evaluated all CT coronary angiograms for the presence of CAD, using axial source

Table 1 Computed tomography coronary angiography protocol

	SSCT	DSCT
β -blocker ^a	Yes	No
Nitroglycerine ^a	No	Yes
Slices	64	64
Collimation	32×0.6 (Z-FFS)	32×0.6 (Z-FFS)
Gantry rotation time (ms)	330	330
Temporal resolution (ms)	165	83
Spatial resolution (mm)	$0.4 \times 0.4 \times 0.4$	$0.4 \times 0.4 \times 0.4$
Pitch	0.20	0.2–0.53
Unenhanced scan		
Tube voltage (kV)	120	120
Tube current	200–150 effective mAs	75 mAs/rot
Contrast enhanced scan		
Tube voltage (kV)	120	120
Tube current	850–960 effective mAs	320–412 mAs/rot
ECG-triggered tube current modulation	No	Yes
Effective radiation dose (mSv)	16.3	14.9

DSCT, dual-source CT; ECG, electrocardiogram; mAs/rot (mAs per rotation) = total mA \times rotation time; mSv (millisievert) = dose length product \times 0.017; SSCT, single-source CT; Z-FFS, Z-flying focal spot.

^aWhen no contraindication was present.

images, multiplanar, curved reformatted reconstructions, and thin-slab maximum-intensity projections on a multi-modality workstation. Interobserver disagreements were resolved by a joint consensus reading. The κ statistic for interobserver–intraobserver agreement in SSCT and DSCT were 0.70, 0.72 [10] and 0.73, 0.81 [14], respectively.

The 17-segment American Heart Association model was used to classify each segment [19]. Each segment was visually scored as obstructive in the presence of 50% or more lumen diameter narrowing and nonobstructive when the lumen diameter narrowing was less than 50% in comparison with the proximal and distal lumen. All anatomically available segments, irrespective of image quality or calcification, were included and scored. Poor quality segments that were not evaluable due to calcification, stack, or movement artifacts were classified as obstructive. Coronary segments distal to a chronic total occlusion were excluded from the analysis.

Quantitative coronary angiography

Experienced cardiologists, blinded toward the CT results, visually assessed each coronary segment (American Heart Association model) for the presence of luminal narrowing in two orthogonal planes. Stenoses scored as having more than 20% narrowing on visual assessment were quantified using a validated quantitative coronary artery algorithm (Cardiovascular Angiography Analysis System II; Pie Medical Imaging, Maastricht, The Netherlands). The segments were considered obstructed when the quantified lumen diameter narrowing in the two planes was more than or equal to 50%.

Statistical analyses

The statistical analysis was performed using a dedicated statistical software program (SPSS, version 16.0, IMB,

Chicago, Illinois, USA). Categorical variables are expressed as percentages and numbers. Continuous variables are expressed as mean values \pm standard deviation and continuous variables with a skewed distribution as median with 25th and 75th percentiles.

The clinical characteristics between women and men were compared using the two-sided independent Student *t*-test. The χ^2 -test was used for independent nonparametric comparison of categorical variables.

Lesions on CTCA and ICA were compared on a per-segment level (Fig. 1). Obstructive lesions on both CTCA and ICA were classified as true-positive results. Non-obstructive lesions on both CTCA and ICA were classified as true-negative results. Obstructive lesions on CTCA that were nonobstructive on ICA were classified as false-positive results. Nonobstructive lesions on CTCA that were obstructive on ICA were classified as false negative.

The sensitivity, specificity, positive predictive value (PPV), negative predictive value (NPV), and diagnostic odds ratio (DOR) were calculated with 95% confidence intervals on a per-patient, per-vessel, and per-segment level for women and men using a 2×2 table. The DOR is used as a measure of the discriminatory power of the CTCA and represents the odds of an obstructive result among diseased persons relative to the odds of an obstructive result among nondiseased persons.

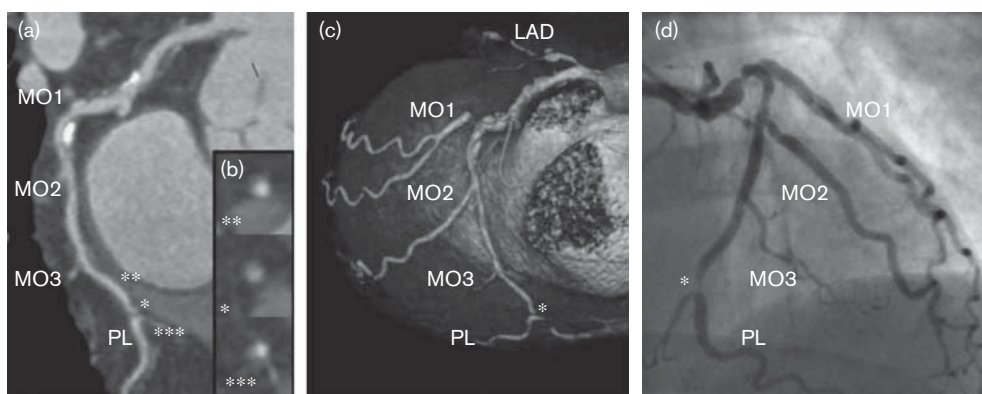
To investigate whether sex had an influence on sensitivity, specificity, PPV, NPV, and DOR, analyses were performed on a per-patient, per-vessel, and per-segment level through a binary logistic regression. Subanalysis of the segments was performed dividing the segments into proximal, mid, distal, and branches. In the awareness that multiple segments from one patient cannot be considered as independent

values, the binary logistic regression in Generalized Estimation Equation was used to fit model parameters. Sex, smoking, diabetes, family history of cardiovascular disease, age, hypertension, hypercholesterolemia, clinical presentation of chest complaints, BMI, average heart rate during enhanced scan, calcium score, and the type of scanner were imported as variables in the multivariate model. The backward elimination technique was used to remove variables from the model based on the probability of the Wald statistics. Variables were reentered in the model when a significant influence on sex was seen in terms of significant change in β -coefficient and/or a *P* value. Sex was kept in the multivariate model even when the β -coefficient did not show a significant additive value to the model. Adjusted sensitivity, specificity, positive predictive, and NPVs were calculated using multivariate models. The adjusted DOR was calculated using the adjusted sensitivity and specificity. The adjusted values were reported along with the sex-associated β -coefficients and corresponding *P* value for their influence on the multivariate model. A *P* value of less than 0.05 was considered significant.

Results

A total of 280 (30.6%) women and 636 (69.4%) men with symptoms suspected or known CAD were evaluated. The sex-specific population characteristics and CT findings are described in Table 2. The women in our population presented more often with non-anginal chest complaints (30 vs. 18%, *P* < 0.001). They were slightly older (63 ± 11.1 vs. 60 ± 10.4 years, *P* < 0.001) and had higher heart rates during image acquisition in comparison with men (67/min vs. 63/min, *P* < 0.001). The prevalence of obstructive disease was higher in men (60 vs. 76%, *P* < 0.001) accompanied by a higher calcium score (143

Fig. 1



A male patient (50 years) with typical complaints had computed tomography coronary angiography (CTCA; a–c) and invasive coronary angiography (ICA; d). There was a total occlusion of the left anterior descending and an obstructive lesion at the origin of the first obtuse marginal branch (MO1), which can be observed in the volume-rendering image (c). The distal circumflex (CX) demonstrates a missed lesion (*) on CTCA demonstrated with the curved multiplanar reconstruction (a) and detailed in the axial images (b). (**) Proximal to the lesion (distal CX); (*) missed lesion; and (***) in the posterolateral branch, distal to the lesion. The lesion was missed by CTCA but was acknowledged by ICA (d).

Table 2 Patient characteristics and computed tomography coronary angiography findings

	Women	Men	<i>P</i>
Total patients (%) ^{a,f}	30.6 (280/916)	69.4 (636/916)	
Age (years) ^g	63 (11.1)	60 (10.4)	<0.001
BMI (kg/m ²) ^e	26.8 (4.4)	26.9 (3.6)	0.84
Clinical presentation (%) ^{a,f}			
Typical angina	34 (93/277)	52 (319/616)	<0.001
Atypical angina	36 (101/277)	30 (187/620)	0.06
Non-anginal chest pain	30 (83/277)	18 (112/617)	<0.001
Risk factor (%) ^{a,f}			
Current smoker	23 (65/277)	31 (195/626)	0.019
Diabetes ^g	17 (46/277)	16 (103/625)	0.96
Family history of cardiovascular disease	54 (150/277)	44 (278/626)	0.007
Hypercholesterolemia (%) ^h	57 (159/277)	55 (344/627)	0.50
Hypertension (%) ⁱ	52 (145/277)	47 (294/617)	0.13
Average heart rate (/min) ^{b,e}	67 (11.7)	63 (11.8)	<0.001
Effective radiation dose (mSv)			
SSCT	16.0 (1.3)	16.4 (1.1)	0.002
DSCT	14.4 (4.6)	15.2 (4.8)	0.10
Calcium score ^{d,e}	143 (5–446)	268 (61–689)	<0.001
Prevalence of disease on ICA (%)			
Patients ^{a,f}	60 (169/280)	76 (485/636)	<0.001
Vessel ^{c,e}	24 (0.24)	34 (0.25)	<0.001
Segment ^{c,e}	8 (0.10)	13 (0.12)	<0.001
Prevalence of total obstructions	13 (35/280)	22 (141/636)	<0.001
Single-vessel disease (%)	33 (77/280)	32 (206/636)	0.81
Multivessel disease (%)	28 (77/280)	44 (280/636)	<0.001

BMI, body mass index; CX, circumflex; DSCT, dual-source CT; ICA, invasive coronary angiography; LAD, left anterior descending; LM, left main; RCA, right coronary artery; SSCT, single-source CT.

mSv (millisievert) = dose length product × 0.0017.

Prevalence of disease was calculated per patient as:

[(Patients with disease × 100%)/(total number of patients)] on patient level.

[[Diseased vessels × 100%]/[4 vessels(LM, RCA, LAD, CX)]] per patient on vessel level.

[(Number diseased segments × 100%)/(total of number segments)] per patient on segment level.

^aPercentage (number/total number).

^bMean (standard deviation).

^cPercentage (standard deviation).

^dMedian with (25th–75th percentile).

^eIndependent Student *t*-test.

^fChi-square test.

^gTreatment with oral antidiabetic medication of insulin.

^hTotal cholesterol > 180 mg/dl or treatment for hypercholesterolemia.

ⁱBlood pressure ≥ 140/90 mmHg or treatment for hypertension.

vs. 268, *P* < 0.001) and higher prevalence of total occlusions (13 vs. 22%, *P* < 0.001; Table 2).

Unadjusted diagnostic accuracy analyses

The unadjusted diagnostic performances of CTCA for the detection of obstructive lesions on a per-patient, per-vessel, and per-segment level are detailed in Table 3. On a per-patient level, there was a lower PPV in women compared with men (87 vs. 95%, *P* = 0.005). This difference was also present on a per-vessel level (PPV, 74 vs. 79%, *P* = 0.031). On a per-segment level, the PPV was not significantly different; however, there was a lower sensitivity (88 vs. 94%, *P* < 0.001) in women accompanied by a higher specificity (96 vs. 95%, *P* < 0.001) and lower DOR (171 vs. 298, *P* < 0.001).

Adjusted diagnostic accuracy analyses

After adjusting for clustering of segments and clinical variables that were different between women and men, the adjusted and unadjusted values were similar on each level.

Adjusted analyses on a per-patient and per-vessel levels did no longer show significant differences in terms of sensitivity, specificity, PPV, NPV, and DOR between women and men (Table 4).

On a per-segment level, the lower sensitivity (88 vs. 94%, *P* < 0.001) and DOR (163 vs. 302 *P* = 0.002) in women remained present in the adjusted analysis, whereas the adjusted specificity no longer showed a difference (96 vs. 95%, *P* = 0.43).

In the subanalysis on a per-segment level (proximal, mid, distal segments, and branches), the sensitivity remained significantly different between women and men. The sensitivity for women versus men in the proximal and mid segments was 91 versus 96% (*P* < 0.05) and 93 versus 98% (*P* < 0.01), respectively. A decline in the sensitivity was observed for both women and men in distal segments (76 vs. 89%, *P* 0.03) and branches (77 vs. 90%, *P* = 0.09).

Discussion

This study demonstrated that the diagnostic performance of CTCA was equally reliable to exclude obstructive CAD

Table 3 Unadjusted diagnostic performance of computed tomography coronary angiography for women and men

	Women				Men				P
	TP	TN	FP	FN	TP	TN	FP	FN	
Patient level	166	87	24	3	482	124	27	3	
Sensitivity		98				99			(99–100) 0.28
Specificity		78				82			(76–88) 0.34
PPV		87				95			(93–97) 0.005
NPV		97				98			(95–100) 0.68
DOR		201				738			(220–2472) 0.07
Vessel level	262	752	94	14	840	1464	219	27	
Sensitivity		95				97			(96–98) 0.18
Specificity		89				87			(85–89) 0.08
PPV		74				79			(77–82) 0.031
NPV		98				98			(98–99) 0.98
DOR		150				208			(138–313) 0.18
Segment level	319	4221	175	45	1134	9117	510	68	
Sensitivity		88				94			(93–96) <0.001
Specificity		96				95			(94–95) <0.001
PPV		65				69			(67–71) 0.07
NPV		99				99			(99–100) 0.08
DOR		171				298			(230–387) 0.006

Sensitivity = TP/(TP + FN), Specificity = TN/(FP + FN), PPV = TP/(TP + FP), NPV = TN/(TN + FN), are presented as %. DOR = (TP × TN)/(FN × FP). Numbers in square brackets are the 95% confidence intervals. P values are calculated using the independent Student t-test. CI, confidence interval; DOR, diagnostic odds ratio; FN, false negative; FP, false positive; NPV, negative predictive value; PPV, positive predictive value; TN, true negative; TP, true positive.

Table 4 Adjusted diagnostic performance of computed tomography coronary angiography on patient, vessel, and segment level

	Women	Men	β-coefficient	P
Patient level				
Sensitivity (%)	98	99	-1.32	0.15
Specificity (%)	78	82	0.16	0.65
PPV (%)	87	95	-0.50	0.10
NPV (%)	97	98	-0.52	0.63
DOR	198	721		0.07
Vessel level				
Sensitivity (%)	95	97	-0.52	0.14
Specificity (%)	89	87	0.14	0.93
PPV (%)	73	79	-0.28	0.06
NPV (%)	98	98	-0.12	0.72
DOR	143	240		0.08
Segment level				
Sensitivity (%)	88	94	-0.84	<0.001
Specificity (%)	96	95	0.16	0.19
PPV (%)	64	69	-0.24	0.07
NPV (%)	99	99	-0.41	0.08
DOR	163	302		0.002

Adjusted sensitivity, specificity, PPV, and NPV calculated using binary logistic regression analyses (generalized estimation equation). Clustering for 17 segments. Input variables: sex, smoking, diabetes, family history of cardiovascular disease, age, hypertension and hypercholesterolemia, type of chest complaints, BMI, heart rate, and calcium score. Backward elimination technique removed nonpredicting variables from the model. Sex influence on this model is demonstrated as β-coefficient with corresponding P value. DOR calculated with adjusted sensitivity and specificity: [(sensitivity/(1-sensitivity))/((1-specificity)/specificity)]. DOR, diagnostic odds ratio; NPV, negative predictive value; PPV, positive predictive value.

both in women and men. The diagnostic performance of CTCA to detect individual coronary obstructions was good, but lower in women compared with men. This is in line with other noninvasive diagnostic studies, demonstrating lower accuracy in women in exercise-ECG testing, stress-echocardiography, and myocardial perfusion imaging (single photon emission computed tomography) [2,4,20]. This

may be related to sex-varying factors such as the presence of risk factors, presentation of symptoms, prevalence, extent and severity of CAD all of which may influence noninvasive CAD ischemia test outcomes [2,4].

Previous comparisons of the diagnostic performance of CTCA between men and women were in disagreement. Meijboom *et al.* [10] reported a lower diagnostic accuracy on a per-segment level in women, which was not confirmed in another study by Pundziute *et al.* [11]. In contrast with the two former studies in our diagnostic accuracy study we were able to collect a large number of women, which allowed adjustment of sex-varying factors that could have an influence on CT-diagnostic performance. After adjusting for the sex-varying factors by multivariate analyses, we found similar results in women and men except for the sensitivity on a per-segment level. This difference in sensitivity can be explained by the presence of more severe and extensive CAD in men. In addition, the prevalence of total occlusions (13 vs. 22%, $P < 0.001$) was higher in men, which may have positively affected the sensitivity in men because these lesions are detected with an almost 100% sensitivity.

Traditionally, exercise ECG testing, stress echocardiography, or single photon emission computed tomography have been used as a first-line diagnostic test in patients with suspected CAD to serve as gatekeeper for ICA [21]. The rather modest diagnostic performance of these tests and relative under use particularly in women may have contributed to the high percent of nonobstructive CAD by ICA. The absence of obstructive CAD in women undergoing elective diagnostic ICA was approximately 51.2–72.6%, which was much higher than the 33.3–52.8% in men [22,23].

Although the sensitivity to detect individual obstructions was lower in women (88 vs. 94%, $P < 0.001$), this did not affect the ability to exclude CAD because the NPV on a per-patient level was similar between women and men (97 vs. 98%, $P = 0.63$). This suggests that CTCA in women can be used as a first-line noninvasive diagnostic test to serve as an effective gatekeeper for ICA, which may result in significant reduction in normal ICAs compared with other first-line noninvasive tests.

Study limitations

The ionizing radiation inherent to CTCA remains of concern. Especially, women have higher lifetime that was attributable for breast and lung cancer at all ages compared with men. This risk decreases with age because of decrease of radiosensitivity of involved organs at an increasing age. Women with symptoms suggestive of CAD are generally older and thereby fall in a relatively favorable range. Our reported radiation exposure was rather high, which was due to the fact that this study was initiated in 2004 when we had access to CT scanners, which then used a full-dose spiral scan protocol, resulting in a relatively high effective radiation dose. Since then gradually, by introducing radiation exposure reduction techniques, the radiation exposure has decreased first after use of wide window tube current modulation and subsequently further decreased by use of a narrow window tube current modulation (Table 2). The estimated risk of cancer has been decreased by approximately 60% by the introduction of radiation reduction techniques [24,25]. With the current optimized scan protocols this radiation dose has decreased even more, to less than 5 mSv [26–28].

The study group consisted of patients with stable angina pectoris referred for ICA who have a high prevalence of CAD. Therefore, the results may not be extrapolated to patients with unstable CAD or patients with low prevalence of CAD.

Furthermore, the retrospective study design and the inclusion of patients referred for ICA may have caused selection and verification bias, which may have resulted in a relative higher sensitivity and lower specificity of CTCA. However, this would be similar for women and men.

Conclusion

CTCA can accurately rule out obstructive CAD in both women and men. CTCA is less accurate in women to detect individual obstructive disease.

References

- 1 Thom T, Haase N, Rosamond W, Howard VJ, Rumsfeld J, Manolio T, et al. Heart disease and stroke statistics, 2004 update: a report from the American Heart Association Statistics Committee and Stroke Statistics Subcommittee. *Circulation* 2006; **113**:e85–e151.
- 2 Shaw LJ, Bairey Merz CN, Pepine CJ, Reis SE, Bittner V, Kelsey SF, et al. Insights from the NHLBI-Sponsored Women's Ischemia Syndrome Evaluation (WISE) study: part I: gender differences in traditional and novel

risk factors, symptom evaluation, and gender-optimized diagnostic strategies. *J Am Coll Cardiol* 2006; **47** (Suppl 3):S4–S20.

- 3 Rayner M, Allender S, Scarborough P; British Heart Foundation Health Promotion Research Group. Cardiovascular disease in Europe. *Eur J Cardiovasc Prev Rehabil* 2009; **16** (Suppl 2):S43–S47.
- 4 Mieres JH, Shaw LJ, Arai A, Budoff MJ, Flamm SD, Hundley WG, et al. Role of noninvasive testing in the clinical evaluation of women with suspected coronary artery disease: consensus statement from the Cardiac Imaging Committee, Council on Clinical Cardiology, and the Cardiovascular Imaging and Intervention Committee, Council on Cardiovascular Radiology and Intervention, American Heart Association. *Circulation* 2005; **111**:682–696.
- 5 Bairey Merz CN, Shaw LJ, Reis SE, Bittner V, Kelsey SF, Olson M, et al. Insights from the NHLBI-Sponsored Women's Ischemia Syndrome Evaluation (WISE) study: part II: gender differences in presentation, diagnosis, and outcome with regard to gender-based pathophysiology of atherosclerosis and macrovascular and microvascular coronary disease. *J Am Coll Cardiol* 2006; **47** (Suppl 3):S21–S29.
- 6 Shaw LJ, Bugiardini R, Merz CN. Women and ischemic heart disease: evolving knowledge. *J Am Coll Cardiol* 2009; **54**:1561–1575.
- 7 Meijboom WB, Meijs MF, Schuijff JD, Cramer MJ, Mollet NR, van Mieghem CA, et al. Diagnostic accuracy of 64-slice computed tomography coronary angiography: a prospective, multicenter, multivendor study. *J Am Coll Cardiol* 2008; **52**:2135–2144.
- 8 Miller JM, Rochitte CE, Dewey M, Arbab-Zadeh A, Niinuma H, Gottlieb I, et al. Diagnostic performance of coronary angiography by 64-row CT. *N Engl J Med* 2008; **359**:2324–2336.
- 9 Budoff MJ, Dowe D, Jollis JG, Gitter M, Sutherland J, Halamert E, et al. Diagnostic performance of 64-multidetector row coronary computed tomographic angiography for evaluation of coronary artery stenosis in individuals without known coronary artery disease: results from the prospective multicenter ACCURACY (Assessment by Coronary Computed Tomographic Angiography of Individuals Undergoing Invasive Coronary Angiography) trial. *J Am Coll Cardiol* 2008; **52**:1724–1732.
- 10 Meijboom WB, Weustink AC, Pugliese F, van Mieghem CA, Mollet NR, van Pelt N, et al. Comparison of diagnostic accuracy of 64-slice computed tomography coronary angiography in women versus men with angina pectoris. *Am J Cardiol* 2007; **100**:1532–1537.
- 11 Pundziute G, Schuijff JD, Jukema JW, van Werkhoven JM, Boersma E, de Roos A, et al. Gender influence on the diagnostic accuracy of 64-slice multislice computed tomography coronary angiography for detection of obstructive coronary artery disease. *Heart* 2008; **94**:48–52.
- 12 Maffei E, Palumbo A, Martini C, Meijboom W, Tedeschi C, Spagnolo P, et al. Diagnostic accuracy of 64-slice computed tomography coronary angiography in a large population of patients without revascularisation: registry data and review of multicentre trials. *Radiol Med* 2009; **115**:368–384.
- 13 Pugliese F, Mollet NR, Hunink MG, Cademartiri F, Nieman K, van Domburg RT, et al. Diagnostic performance of coronary CT angiography by using different generations of multislice scanners: single-center experience. *Radiology* 2008; **246**:384–393.
- 14 Weustink AC, Mollet NR, Pugliese F, Meijboom WB, Nieman K, Heijnenbroek-Kal MH, et al. Optimal electrocardiographic pulsing windows and heart rate: effect on image quality and radiation exposure at dual-source coronary CT angiography. *Radiology* 2008; **248**:792–798.
- 15 Weustink AC, Neeffjes LA, Kyrzopoulos S, van Straten M, Neoh Eu R, Meijboom WB, et al. Impact of heart rate frequency and variability on radiation exposure, image quality, and diagnostic performance in dual-source spiral CT coronary angiography. *Radiology* 2009; **253**:672–680.
- 16 Meijboom WB, Mollet NR, van Mieghem CA, Weustink AC, Pugliese F, van Pelt N, et al. 64-Slice CT coronary angiography in patients with non-ST elevation acute coronary syndrome. *Heart* 2007; **93**:1386–1392.
- 17 Bossuyt PM, Reitsma JB, Bruns DE, Gatsonis CA, Glasziou PP, Irwig LM, et al. Towards complete and accurate reporting of studies of diagnostic accuracy: the STARD initiative. *Clin Radiol* 2003; **58**:575–580.
- 18 Agatston AS, Janowitz WR, Hildner FJ, Zusmer NR, Viamonte M Jr, Detrano R. Quantification of coronary artery calcium using ultrafast computed tomography. *J Am Coll Cardiol* 1990; **15**:827–832.
- 19 Austen WG, Edwards JE, Frye RL, Gensini GG, Gott VL, Griffith LS, et al. A reporting system on patients evaluated for coronary artery disease: report of the Ad Hoc Committee for grading of coronary artery disease, Council on Cardiovascular Surgery, American Heart Association. *Circulation* 1975; **51** (Suppl 4):5–40.
- 20 Kwok Y, Kim C, Grady D, Segal M, Redberg R. Meta-analysis of exercise testing to detect coronary artery disease in women. *Am J Cardiol* 1999; **83**:660–666.

- 21 Bassand JP, Hamm CW, Ardissino D, Boersma E, Budaj A, Fernandez-Aviles F, *et al.*; Task Force for D, Treatment of Non STSEACSoESoC. Guidelines for the diagnosis and treatment of non-ST-segment elevation acute coronary syndromes. *Eur Heart J* 2007; **28**:1598–1660.
- 22 Patel MR, Peterson ED, Dai D, Brennan JM, Redberg RF, Anderson HV, *et al.* Low diagnostic yield of elective coronary angiography. *N Engl J Med* 2010; **362**:886–895.
- 23 Shaw LJ, Shaw RE, Merz CN, Brindis RG, Klein LW, Nallamothu B, *et al.* Impact of ethnicity and gender differences on angiographic coronary artery disease prevalence and in-hospital mortality in the American College of Cardiology-National Cardiovascular Data Registry. *Circulation* 2008; **117**:1787–1801.
- 24 Einstein AJ, Henzlova MJ, Rajagopalan S. Estimating risk of cancer associated with radiation exposure from 64-slice computed tomography coronary angiography. *JAMA* 2007; **298**:317–323.
- 25 Weustink AC, Mollet NR, Neefjes LA, van Straten M, Neoh E, Kyrzopoulos S, *et al.* Preserved diagnostic performance of dual-source CT coronary angiography with reduced radiation exposure and cancer risk. *Radiology* 2009; **252**:53–60.
- 26 Achenbach S, Ropers D, Kuettner A, Flohr T, Ohnesorge B, Bruder H, *et al.* Contrast-enhanced coronary artery visualization by dual-source computed tomography: initial experience. *Eur J Radiol* 2006; **57**:331–335.
- 27 Earls JP, Berman EL, Urban BA, Curry CA, Lane JL, Jennings RS, *et al.* Prospectively gated transverse coronary CT angiography versus retrospectively gated helical technique: improved image quality and reduced radiation dose. *Radiology* 2008; **246**:742–753.
- 28 Tatsugami F, Husmann L, Herzog BA, Burkhard N, Valenta I, Gaemperli O, *et al.* Evaluation of a body mass index-adapted protocol for low-dose 64-MDCT coronary angiography with prospective ECG triggering. *AJR Am J Roentgenol* 2009; **192**:635–638.

PART V

Summary and conclusions

Chapter 12

Summary and conclusions

CT coronary angiography for the assessment of atherosclerotic plaque

Chapter 2

We evaluated the ability of 64-slice CT coronary angiography (CTCA)-derived plaque parameters to detect and quantify coronary atherosclerosis, using intravascular ultrasound (IVUS) as the reference standard. We analyzed 1364 co-registered 1-mm coronary cross-sections and 255 segments of 5-mm length. Compared with IVUS, CTCA demonstrated 86% sensitivity and 71% specificity for the detection of plaque on cross-sectional level; on a per segment basis we observed 96% sensitivity and 88% specificity. The sensitivity of CTCA to detect plaque decreased with smaller plaque size and with the distance from the coronary ostium. Correlation for vessel plaque volumes measured by CTCA and IVUS was high. Bland–Altman analysis showed a slight underestimation of any plaque volume by CTCA, with a trend to underestimate non-calcified and overestimate mixed/calcified plaque volumes. In conclusion, CTCA is able to detect and quantify atherosclerotic plaque, but further improvement in CT resolution is necessary for more reliable assessment of very small and distal coronary plaques.

Chapter 3

Reproducibility of the quantitative assessment of atherosclerosis by CTCA is paramount for the design of longitudinal studies. We assessed the inter- and intra-observer reproducibility using semiautomated CT plaque analysis software in symptomatic patients who underwent CTCA at baseline and after 3 years. The plaque quantitative analysis was performed in untreated vessels with mild-to-moderate atherosclerosis and included geometrical and compositional characteristics. Our results suggest that the geometrical assessment of coronary atherosclerosis by CTCA is highly reproducible using semiautomated quantification software and that serial plaque changes can be detected beyond observer variability. The compositional measurements are more variable between observers than geometrical measurements.

Chapter 4

We assessed the serial changes in coronary plaque burden, lumen dimensions and arterial remodeling in patients with acute coronary syndromes who underwent 64-slice CTCA after percutaneous coronary intervention at baseline and after a median of 39 months. All patients received contemporary medical treatment. Clinical events at follow-up were documented. Our findings showed that despite standard-of-care treatment, the atheroma size in untreated non-culprit lesions increased over 3 years, compensated for by an increase in the vessel size (positive expansive remodeling) and without compromising the lumen. Patients with clinical events had a larger plaque volume at baseline. We concluded that CTCA can assess the progression of coronary atherosclerosis and may be used for noninvasive monitoring of pharmacologic interventions in coronary artery disease.

Chapter 5

We compared the diagnostic performance of quantitative CTCA with visual CTCA for the detection of flow-limiting coronary lesions using fractional flow reserve (FFR) as reference standard. CTCA and FFR measurements were obtained in 99 symptomatic patients. In total, 144 coronary lesions detected on CTCA were visually graded for stenosis severity. Quantitative CTCA measurements included lesion length, minimal area diameter, % area stenosis, minimal lumen diameter, % diameter stenosis, and plaque burden $[(\text{vessel area} - \text{lumen area}) / \text{vessel area} \times 100]$. Optimal cutoff values of CTCA-derived parameters were determined, and their diagnostic accuracy for the detection of flow-limiting coronary lesions ($\text{FFR} \leq 0.80$) was compared with visual CTCA. Our findings demonstrated that CTCA cross-sectional quantitative parameters improve the prediction of flow-limiting lesions, compared to visual assessment, but remain insufficient and functional assessment is still needed for lesions of moderate severity to guide patient's management.

CT coronary angiography for the assessment of coronary bifurcations

Chapter 6

We evaluated the distribution and composition of atherosclerotic plaques at bifurcations with intravascular ultrasound-virtual histology (IVUS-VH) and CTCA in relation to the bifurcation angle (BA). Thirty-three bifurcations were matched and studied with both modalities; the analyzed main vessel was divided into a 5-mm proximal segment, the in-bifurcation segment, and a 5-mm distal segment. Our findings demonstrated that the proximal segment has a more extensive plaque burden with more lipid content. The plaques with high-risk features on IVUS-VH and the non-calcified plaques on CTCA both show a differential distribution along the bifurcation being more frequent in the proximal segment, and are associated with higher BA values.

Chapter 7

We evaluated the distribution of atherosclerosis at bifurcations with CTCA and proposed a novel CT-Medina classification for bifurcation lesions. We quantified plaque in 39 bifurcations; the analysis included the proximal main vessel, the distal main vessel and the side branch (SB). The carina cross-sections were divided into four equal parts according to the expected wall shear stress (WSS) to assess circumferential plaque distribution. All the bifurcation lesions were classified using the Medina classification and a novel CT-Medina classification combining lumen narrowing and plaque burden $\geq 70\%$. Our investigation demonstrated that atherosclerotic plaque is widely present in all bifurcation segments, even in the absence of coronary lumen stenosis. The plaque is more often located opposite to the flow divider, whereas the carina is rarely affected. Characterization of bifurcation lesions using the new CT-Medina classification provided additional information in 18% of cases compared to the Medina classification, indicating that a CT-Medina classification scheme combining lumen stenosis and plaque severity is more informative than angiographic classification of bifurcation lesions.

CT coronary angiography for risk stratification of coronary atherosclerotic disease

Chapter 8

The invasive coronary angiography SYNTAX score (ICA SXscore) is an important prognostic tool in risk stratifying patients undergoing revascularisation, as well as an independent predictor of adverse cardiac events. We investigated the feasibility and reproducibility of the CTCA-derived SYNTAX score. The SXscore of 80 symptomatic patients who underwent ICA and CTCA was retrospectively calculated for both modalities by 2 independent teams of experienced reviewers. The CTCA SXscore was recalculated after two months in 40 random patients to assess intra-observer variability. We found a good correlation between the ICA SXscore and the CTCA SXscore ($r_s=0.76$, $p<0.001$), whereas the median CTCA SXscore was higher compared to the median ICA SXscore. Kappa statistics indicated a substantial intra-observer agreement for CTCA SXscore tertiles and the correlation between the two rounds of analyses was high ($r=0.95$, $p<0.001$). We concluded that the calculation of the SXscore by CTCA in symptomatic patients appeared feasible and reproducible. The long-term prognostic role of this scoring methodology should be further investigated.

Chapter 9

Detection of patients with LM and/or 3VD (so-called “high risk CAD”) is important because optimal medical treatment combined with revascularization has shown to improve prognosis in these patients. We investigated the diagnostic performance of CTCA to rule in/out “high risk CAD” in 1136 symptomatic patients using invasive coronary angiography (ICA) as the reference standard. Vessels were considered obstructive in the presence of $\geq 50\%$ lumen diameter stenosis. We compared the discriminatory value of CTCA to detect “high risk CAD” to the Duke risk score and calcium score. The sensitivity of CTCA to detect these patients was 95%; the specificity was 83%; the positive predictive value was 54% and the negative predictive value was 99%. CTCA provided incremental value in the discrimination of “high risk CAD” with an area under the receiver operating characteristic curve of 0.90 for CTCA separately. We

concluded that CTCA accurately rules out “high risk CAD” in patients with suggestive symptoms. However, the performance of CTCA to rule in “high risk CAD” is suboptimal, due to the high number of false positive observations by overestimating severity of stenosis. CTCA provides incremental value in the discrimination of “high risk CAD” compared to the Duke risk score and calcium score.

Chapter 10

We investigated the diagnostic accuracy of CTCA in women at low to intermediate pre-test probability of coronary artery disease (CAD) compared with men. We included 570 symptomatic patients who underwent both invasive coronary angiography (reference standard) and CTCA and were stratified as low (women 73%) and intermediate risk (women 39%). The pre-test probability of CAD was estimated using the Duke risk score. Thresholds of less than 30% and 30–90% were used for determining low and intermediate risk, respectively. We found that sensitivity, specificity, positive predictive value and negative predictive value were not significantly different in and between women and men at low and intermediate risk.

Chapter 11

We assessed the influence of gender on the diagnostic performance of CTCA. A total of 916 symptomatic patients (30.5% women) without earlier history of coronary artery intervention underwent both CTCA and invasive coronary angiography. Descriptive diagnostic parameters, to detect obstructive CAD ($\geq 50\%$ lumen diameter narrowing) on CTCA, were compared between women and men on a per-patient, per-vessel, and per-segment level. Our analysis showed that women were older, had less typical chest complaints, and had a lower prevalence, extent, and severity of CAD compared with men. Multivariate analysis on a per-patient level revealed no difference in sensitivity, specificity, positive predictive value, negative predictive value, and diagnostic odds ratio (DOR). No difference was found on per-vessel level analysis. Per-segment analysis revealed a lower sensitivity (88% vs. 94%) and DOR (163 vs. 302) in women compared with men, without a difference in specificity (96% vs. 95%), PPV (64% vs. 69%), and NPV (99% vs. 99%). We concluded that CTCA can accurately rule out obstructive CAD in

both women and men. CTCA is less accurate in women to detect individual obstructive disease.

Samenvatting en conclusies

CT coronaire angiografie voor de beoordeling van coronaire atherosclerose

Hoofdstuk 2

We hebben de mogelijkheid onderzocht om met 64-slice CT coronaire angiografie (CTCA)-afgeleide plaque parameters coronaire atherosclerose op te sporen en te kwantificeren, met intravasculair ultrageluid (IVUS) als referentiestandaard. We analyseerden 1364 gecorreleerde 1-mm coronaire doorsneden en 255 segmenten met een lengte van 5 mm. Vergeleken met IVUS, CTCA toonde 86% sensitiviteit en 71% specificiteit voor de detectie van plaque op transversaal niveau; per segment zagen we 96% sensitiviteit en 88% specificiteit. De sensitiviteit van CTCA voor de detectie van plaque nam af naarmate de plaque kleiner werd en de afstand van het coronaire ostium langer werd. De correlatie voor het coronaire plaque volume gemeten met CTCA en IVUS was hoog. Bland-Altman-analyse toonde een lichte onderschatting van elk plaque volume door CTCA, met een trend voor onderschatting van niet-verkalkte en overschatting van gemengde/verkalkte plaque volumes. Concluderend, CTCA is geschikt voor het detecteren en kwantificeren van atherosclerotische plaque, maar verdere verbetering van de CT resolutie is noodzakelijk voor een meer betrouwbare beoordeling van zeer kleine en distale coronaire plaques.

Hoofdstuk 3

Reproduceerbaarheid van de kwantitatieve beoordeling van atherosclerose door CTCA is van groot belang voor het ontwerpen van longitudinale studies. Wij hebben daarom de inter- en intra-observer reproduceerbaarheid beoordeeld met behulp van semi-automatische CT plaque analyse software bij symptomatische patiënten die CTCA ondergingen op baseline en na 3 jaar. De kwantitatieve plaque analyse werd uitgevoerd in onbehandelde coronairen met milde tot matige atherosclerose, en bestond uit geometrische en compositorische kenmerken. Onze resultaten suggereren dat de geometrische beoordeling van coronaire atherosclerose door CTCA zeer reproduceerbaar is middels semi-automatische kwantificering software, en dat seriële

plaque veranderingen nauwkeuriger kunnen worden gedetecteerd ondanks observer variabiliteit. De compositorische metingen zijn meer variabel tussen observers dan geometrische metingen.

Hoofdstuk 4

Wij hebben de seriële veranderingen onderzocht in coronaire plaque burden, lumen afmetingen en arteriële remodeling bij patiënten met acuut coronair syndroom die 64-slice CTCA ondergingen na percutane coronaire interventie op baseline en na een mediaan van 39 maanden. Alle patiënten kregen de hedendaagse medische behandeling. Klinische events bij follow-up werden gedocumenteerd. Onze bevindingen toonden aan dat ondanks de standard-of-care behandeling de atheroma grootte in onbehandelde non-culprit laesies was gestegen na 3 jaar, gecompenseerd voor een toename van de grootte van het vat (positive expansive remodeling) en zonder afbreuk te doen aan het lumen. Patiënten met klinische events hadden een groter plaque volume op baseline. Wij concludeerden dat CTCA de progressie van coronaire atherosclerose kan beoordelen en kan worden gebruikt voor non-invasieve bewaking van farmacologische interventies bij coronaire hartziekte.

Hoofdstuk 5

We vergeleken de diagnostische waarde van kwantitatieve CTCA in vergelijking met visuele CTCA voor de detectie van flow-limiting coronaire laesies middels fractionele flow reserve (FFR) als referentiestandaard. CTCA en FFR metingen werden verzameld bij 99 symptomatische patiënten. In totaal werden 144 coronaire laesies gevonden op CTCA visueel beoordeeld op ernst van de stenose. Kwantitatieve CTCA metingen bestonden uit laesie lengte, minimale oppervlakte diameter, percentage oppervlakte stenose, minimale lumen diameter, percentage diameter stenose, en plaque burden $[(\text{vessel area} - \text{lumen area}) / \text{vessel area} \times 100]$. Optimale cutoff waarden van CTCA-afgeleide parameters werden bepaald, en de diagnostische nauwkeurigheid voor het detecteren van flow-limiting coronaire laesies ($\text{FFR} \leq 0.80$) werd vergeleken met visuele CTCA. Onze bevindingen laten zien dat CTCA cross-sectionele kwantitatieve parameters de voorspelling van flow-limiting laesies verbeteren, vergeleken met visuele

beoordeling, maar onvoldoende blijven en dat daarom een functionele beoordeling nog steeds nodig is voor laesies van matige ernst om de behandeling van patiënten te ondersteunen.

CT coronaire angiografie voor de beoordeling van coronaire bifurcaties

Hoofdstuk 6

We evalueerden de distributie en samenstelling van atherosclerotische plaques bij vertakkingen met intravascular ultrasound-virtual histology (IVUS-VH) en CTCA met betrekking tot de hoek van de bifurcatie (BA). Drieëndertig vertakkingen werden gevonden en bestudeerd met beide modaliteiten; de geanalyseerde main vessel werd verdeeld in een 5-mm proximaal segment, een segment in de aftakking, en een 5-mm distaal segment. Onze bevindingen laten zien dat het proximale segment een uitgebreidere plaque burden heeft met een hoger lipidegehalte. De plaques met hoog-risico eigenschappen op IVUS-VH en de niet-gecalcificeerde plaques op CTCA tonen een verschillende verdeling over de vertakking, met name vaker in het proximale segment, en worden geassocieerd met hogere BA waarden.

Hoofdstuk 7

We hebben de verdeling van atherosclerose bij vertakkingen met CTCA beoordeeld en stellen een nieuwe CT-Medina classificatie bij bifurcatie laesies voor. We kwantificeerden plaque in 39 vertakkingen; de analyse omvatte de proximale main vessel, de distale main vessel en de zijtak (SB). De carina doorsneden werden verdeeld in vier gelijke delen volgens de verwachte wand shear stress (WSS) om zo de circumferentiële plaque distributie te beoordelen. Alle bifurcatie laesies werden ingedeeld aan de hand van de Medina classificatie en een nieuwe CT-Medina classificatie die lumen vernauwing en plaque burden $\geq 70\%$ combineert. Ons onderzoek heeft aangetoond dat atherosclerotische plaque wijdverspreid is in elke segment van de bifurcatie, zelfs bij afwezigheid van vernauwingen in het coronaire lumen. De plaque is

vaker tegenover de stroomverdeler gelokaliseerd, terwijl de carina zelden is aangedaan. Karakterisering van bifurcatie laesies met behulp van de nieuwe CT-Medina classificatie leverde aanvullende informatie op in 18% van de gevallen in vergelijking met de Medina classificatie, wat aangeeft dat een CT-Medina classificatieschema die lumen vernauwing en plaque ernst combineert informatiever is dan een angiografische classificatie van bifurcatie laesies.

CT coronaire angiografie voor risicostratificatie van coronaire atherosclerose

Hoofdstuk 8

De invasieve coronaire angiografie SYNTAX score (ICA SXscore) is een belangrijk prognostisch instrument voor het stratificeren van patiënten die revascularisatie ondergaan, alsook een onafhankelijke voorspeller van ongewenste cardiale events. We onderzochten de haalbaarheid en de reproduceerbaarheid van de CTCA-afgeleide SYNTAX score. De SXscore van 80 symptomatische patiënten die ICA en CTCA ondergingen werd retrospectief berekend voor beide modaliteiten door 2 onafhankelijke teams van ervaren beoordelaars. De CTCA SXscore werd opnieuw berekend na twee maanden bij 40 willekeurig gekozen patiënten om de intra-observer variabiliteit te evalueren. We vonden een goede correlatie tussen de ICA SXscore en de CTCA SXscore ($r_s=0,76$, $p < 0.001$), terwijl de mediane CTCA SXscore hoger was in vergelijking met de mediane ICA SXscore. De Kappa waarden lieten een aanzienlijke intra-observer overeenkomst zien voor CTCA SXscore tertiles en de correlatie tussen de twee analyserondes was hoog ($r=0.95$, $p < 0.001$). We concludeerden dat de berekening van de SXscore met CTCA bij symptomatische patiënten zowel haalbaar als reproduceerbaar bleek. De lange termijn prognostische rol van deze scoring methode moet verder worden onderzocht.

Hoofdstuk 9

Detectie van patiënten met LM en/of 3VD (zogenaamde "hoog-risico CAD") is belangrijk omdat optimale medische behandeling in combinatie met revascularisatie de prognose bij deze patiënten blijkt te verbeteren. We onderzochten de diagnostische waarde van CTCA om "hoog-risico CAD" in- of uit te sluiten in 1136 symptomatische patiënten met behulp van invasieve coronaire angiografie (ICA) als referentie standaard. Coronairen werden als vernauwd gezien bij aanwezigheid van $\geq 50\%$ lumen diameter stenose. We vergeleken de discriminerende waarde van CTCA om "hoog-risico CAD" te detecteren ten opzichte van de Duke risk score en calcium score. De sensitiviteit van CTCA om deze patiënten te detecteren was 95%; de specificiteit was 83%; de positief voorspellende waarde was 54% en de negatieve voorspellende waarde was 99%. CTCA levert een zeer belangrijke meerwaarde bij het identificeren van "hoog-risico CAD" patiënten, met een receiver operating characteristic curve van 0.90 voor CTCA afzonderlijk. We concludeerden dat CTCA nauwkeurig "hoog-risico CAD" kan uitsluiten bij patiënten met suggestieve symptomen. Echter, de mogelijkheid van CTCA om "hoog-risico CAD" aan te tonen is suboptimaal, met name door het grote aantal vals-positieve bevindingen door overschatting van de ernst van de stenose. CTCA biedt een belangrijke meerwaarde in het maken van onderscheid in "hoog-risico CAD" in vergelijking met de Duke risico score en calcium score.

Hoofdstuk 10

We onderzochten de diagnostische nauwkeurigheid van CTCA bij vrouwen met een laag tot intermediaire a priori kans op coronaire hartziekte (CAD) in vergelijking met mannen. We includeerden 570 symptomatische patiënten die zowel invasieve coronaire angiografie (referentie standaard) als CTCA ondergingen, en die werden gestratificeerd als laag (vrouwen 73%) en intermediair risico (vrouwen 39%). De pre-test probability van CAD werd geschat met behulp van de Duke risico score. Drempels van minder dan 30% en 30-90% werden gebruikt voor het bepalen van respectievelijk laag en gemiddeld risico. We vonden dat de sensitiviteit, specificiteit, positief voorspellende waarde en negatief voorspellende waarde niet significant verschillend waren bij en tussen mannen en vrouwen met een laag en gemiddeld risico.

Hoofdstuk 11

We onderzochten de invloed van geslacht op de diagnostische prestaties van CTCA. Een totaal aantal van 916 symptomatische patiënten (30.5% vrouwen) zonder een voorgeschiedenis van coronaire interventie ondergingen zowel CTCA als invasieve coronaire angiografie. Beschrijvende diagnostische parameters, om obstructieve CAD ($\geq 50\%$ lumen diameter vernauwing) te detecteren op CTCA, werden vergeleken tussen vrouwen en mannen op patiënt-, coronair- en segment niveau. Onze analyse toonde aan dat vrouwen ouder waren, minder typische angina klachten hadden alsook een lagere prevalentie, mate en ernst van CAD in vergelijking met mannen. Multivariate analyse op een per-patiënt niveau toonde geen verschil in sensitiviteit, specificiteit, positief voorspellende waarde, negatief voorspellende waarde en diagnostische odds ratio (DOR). Er werd geen verschil gevonden op per-coronair niveau analyse. Per-segment analyse toonde een lagere sensitiviteit (88% vs. 94%) en DOR (163 versus 302) bij vrouwen in vergelijking met mannen, zonder een verschil in specificiteit (96% vs. 95%), PPV (64% vs. 69%) en NPV (99% vs. 99%). We concludeerden dat CTCA nauwkeurig obstructieve CAD kan uitsluiten bij zowel vrouwen als mannen. CTCA is bij vrouwen minder nauwkeurig om individuele obstructieve ziekte op te sporen.

General discussion and future directions

In the final part of this thesis book we will discuss the results of our main studies regarding the ability of CTCA to detect, assess and monitor coronary atherosclerotic plaque.

CT coronary angiography for the assessment of atherosclerotic plaque

CTCA vs. IVUS for plaque detection and quantification: are they comparable?

Computed Tomography Coronary Angiography (CTCA) has the potential to become a non-invasive alternative to IVUS for plaque quantification and to be used for risk stratification of asymptomatic individuals or the assessment of atherosclerosis progression/regression. Previous studies (1-4) have focused on the comparison of CTCA- and IVUS-derived quantitative parameters, such as plaque area or plaque burden, showing moderate to good correlation. In our study (*Chapter 2*), we used a CTCA-derived quantitative parameter (wall thickness) to assess diagnostic accuracy on a slice-by-slice and segmental basis. Our data demonstrated that the detection of atherosclerotic plaque based on CTCA-derived quantitative parameters in a similar fashion to IVUS was feasible. Plaques located within the proximal 40mm were detected with very high sensitivity (88–100%) and as invasive imaging studies have shown, the most clinically relevant lesions are highly clustered within the proximal sections of the coronaries (5-7). Moreover, the very good diagnostic accuracy obtained at segmental level is promising for the potential development of prediction models based on plaque presence on a per-segment basis. Nevertheless, it is important to keep in mind that the clinical use of CTCA for detection of early atherosclerosis is still limited by the current spatial and temporal resolution of the technique. Further technical improvements of the acquisition and reconstruction techniques will enable more reliable visualisation of the coronary arteries with better signal-to-noise ratio and decrease of partial voluming and motion artifacts.

Regarding the quantification of plaque volume by CTCA, our results add to the existing literature which only deals with stable angina patients. Several researchers compared

plaque volumes derived from CTCA with corresponding IVUS data and reported strong correlation and moderate agreement (8-13). The differences between CTCA and IVUS volumetric measurements, which were also observed in our analysis, could be attributed to several technical and methodological factors. The spatial resolution of 64-slice CT may still be inadequate for accurate edge discrimination of CTCA images. The smaller coronary plaques, in particular non-calcified plaques, cannot be well defined and may occasionally not be detected, resulting in underestimation of plaque volume. Moreover, the real size of calcified plaque is overestimated by CTCA due to the blooming effects. Quantification of calcified plaque by IVUS can also be imprecise, because the acoustic shadowing in areas of calcification blocks the view of the outer vessel borders. In addition, on IVUS the outer boundaries were defined by the external elastic membrane (EEM), whereas on CTCA the outer vessel border was annotated at the adventitia-fat boundary, which may also have accounted for the discrepancies in the measurements. Furthermore, the IVUS images are not strictly perpendicular to the centerline, depending on the catheter position and vessel tortuosity. In the real life of clinical practice, there is no imaging technique without limitations.

Assessment of atherosclerotic plaque by CTCA: what about reproducibility?

Over the recent few years, CTCA has been more commonly used as a tool to non-invasively assess the temporal effect of medical therapies on coronary plaque size in longitudinal studies (14-20). Moreover, this method has the potential to assess plaque composition and therefore to assess the effect of drug therapies on the phenotype of coronary atherosclerosis. As the impact of medical treatment on the atherosclerotic plaque size and composition over time is relatively small, highly reproducible CTCA quantitative measurements are pivotal. In our investigation (*Chapter 3*), using semiautomated plaque quantification software, the CTCA geometrical measurements were highly reproducible in both intra- and inter-observer comparisons. Furthermore, in comparison with IVUS studies, the CTCA reproducibility appeared to be comparable or better. This observation could be partly attributed to the methodology for the actual analysis, since in CTCA all frames were analyzed in a stepwise approach; first the lumen

and vessel wall borders were delineated as continuous lines in the longitudinal view (L-view). These contour positions functioned as landmarks for the automated contour detection in the individual cross sections; a visual inspection was performed in every cross-section and a manual correction was applied if necessary. In contrast, in IVUS only the individual cross-sections are drawn without the first step (i.e. longitudinal drawing). Regarding the plaque composition, overall the differences of the average plaque attenuation between observers were very small on the cross-sectional and segment level analyses. Despite this finding, the presumably lipid-rich content [the % Low Attenuation Plaque – LAP (<30 HU)] showed a relatively high inter-observer variability of 12%, which is of major significance since the temporal change of such component could potentially become an imaging endpoint of longitudinal studies. The LAP is probably the most clinically relevant component of coronary plaques as it has been shown to correlate closely with plaques of low echogenicity (presumably lipid-rich) on IVUS (21) and to have prognostic value for the development of acute coronary syndromes (22). On the other hand, the intra-observer variability for %LAP was low (median 3% approximately), which underlines the fact that the position of the plaque contours can play a detrimental role in the distribution of attenuation values. Small differences in the lumen or vessel wall delineation would not dramatically influence the geometrical measurements, but they could result in much bigger differences in the compositional measurements due to partial volume, i.e. in case part of the lumen or the pericoronary fat is incorrectly included in the plaque area.

Implications for the design of longitudinal studies

In our study (*Chapter 3*), the observer variability was lower than the temporal changes in plaque burden - the most common endpoint in IVUS progression/regression studies. This finding suggests that CTCA data analysis using semiautomated software can detect changes in atherosclerotic plaque size beyond the observer bias. Certainly, the best approach is that the same analyst analyzes in a blind fashion both the baseline and follow-up CTCA images, since the difference is much lower in the intra-observer comparison for both the cross-sectional and segment based analyses than in the inter-observer comparison; more importantly, for the compositional measurements only the

intra-observer variability was below the generally acceptable threshold of 10%. It should be noted that our study was conducted on a population with mild-to-moderately diseased arteries receiving contemporary medical therapy. This was driven by the intention to study the reproducibility of this quantitative method on patients that would be the most suitable candidates for serial assessment of atherosclerosis in the “real life”; since the severe lesions would have been treated with percutaneous coronary intervention, the efficacy of the statin therapy would be monitored mainly in the untreated, mild-to-moderately diseased atherosclerotic arteries.

CTCA for the serial assessment of atherosclerosis: is it possible in “real world”?

Previous IVUS studies (23) have demonstrated that there is a direct association between the burden of coronary atherosclerosis, its progression, and the presence of clinical events at follow-up. Similarly, in the main PROSPECT study, lesions with plaque burden >70% were shown to be strongly associated with future clinical events (24). Our data (*Chapter 4*) are in accordance with these findings, because the patients presenting with clinical events had greater amount of plaque at baseline. This observation could contribute to the potential development of prediction models based on atherosclerotic plaque burden.

Motoyama et al. (22) and Hoffmann et al. (25) described that the plaques in patients with ACS have positive remodeling and are associated with events. Consistent with the original description by Glagov et al. (26), our investigation showed that arteries enlarge as atherosclerosis progresses. Previous serial IVUS reports have demonstrated that atheroma burden does not limit compensatory remodeling (27), whereas there is a broad spectrum of serial remodeling responses in coronary atherosclerosis (28,29). Importantly, arterial remodeling changes closely relate to changes in Percent Atheroma Volume (PAV), which is the most common primary IVUS endpoint. In the absence of actual change in plaque volume, positive remodeling could reduce PAV, whereas negative remodeling would increase PAV.

Eventually, the greatest strength of CTCA is that it can assess coronary atherosclerosis by combining the 2 “worlds” of QCA-like and IVUS-like parameters. Previous papers

have shown that CTCA is comparable to QCA angiography regarding lumen stenosis assessment (30,31); similarly, IVUS and CTCA comparative studies (4,25) have shown that the CTCA can reasonably evaluate atherosclerotic plaque size, remodeling, eccentricity, and composition, despite the acknowledged limitations of the technique. Voros et al. (4) suggested that quantitative CTCA could be acceptably used in population-based approaches, given the small mean differences between CTCA and IVUS-virtual histology measurements. Interestingly, our results closely fit the regression line in the classical graph depicting the relation between mean LDL levels and median change in PAV for several previous IVUS progression/regression studies. Most prior IVUS studies have used PAV as the primary endpoint; however, the percentage change in TAV may be more suitable for CTCA studies, because not only 1 coronary segment can be imaged, but the full coronary tree can be assessed. Conversely, considering the resolution and reproducibility of CTCA, the minute changes in PAV observed in IVUS studies may be more difficult to detect.

CT coronary angiography for the assessment of coronary bifurcations

Comprehensive assessment of coronary bifurcations by CTCA: what is the role of anatomy?

The complex three-dimensional (3D) geometry of coronary artery bifurcations can affect the local haemodynamic conditions and thereby the plaque distribution and composition. This plausible effect mediated by the bifurcation angle (BA) can only be studied in vivo by means of imaging modalities that provide a 3D reconstruction of the bifurcation, such as multidetector computed tomography (MDCT).

Our study (*Chapter 6*) corroborates earlier findings on plaque volumetric and compositional characteristics at bifurcation sites: the plaque burden and the percentage of the NC were significantly larger in the proximal segment of the non-left main bifurcations. The differential distribution of the NC and the high-risk plaques along the

coronary tree could be attributed to the influence of local haemodynamic factors altered at bifurcation sites.

Our data also demonstrated that predominantly non-calcified plaque type by MDCT corresponded to the IVUS-VH high-risk phenotype. This finding is in agreement with histopathology studies (32) and with previous greyscale IVUS studies showing that plaques with low echogenicity (presumably lipid rich) are mainly soft (noncalcified) by MDCT (10,33,34).

Notably, the present study (*Chapter 6*) emphasizes the added value of MDCT as 3D imaging modality by integrating the MDCT-based BA measurements to the bifurcation assessment. Our *in vivo* data showed that the presence and phenotype of atherosclerotic plaque in the proximal bifurcation segment is related to the BA size. This finding could be supported by computational fluid dynamics (35-37) and histopathology (38) studies demonstrating that the haemodynamic phenomena important in atherogenesis are more pronounced in widely angulated bifurcations. Moreover, the BA size has been described as a determinant of treatment strategy in bifurcation lesions (39). In numerous bench and clinical studies (40-44) a wide BA has been associated with a greater risk for suboptimal post-procedural result and long-term adverse clinical events. Additionally, our data demonstrated that a wide BA is associated with a greater plaque burden and a high-risk phenotype of bifurcation lesions, which make us speculate that NC-rich plaques could be related to the higher restenosis and thrombosis rates (45-47). Eventually, a comprehensive assessment of bifurcation lesions including plaque characterization and BA measurements could lead to optimized interventional strategies and improved long-term clinical outcomes.

A CT-based Medina classification in coronary bifurcations: does the lumen assessment provide sufficient information?

Currently, angiographic classification of bifurcations is widely accepted in clinical practice; nevertheless conventional angiography is an imperfect tool, which considerably underestimates the extent of atherosclerotic lesions when compensatory positive remodeling is present (48-50). In addition, the angiographic assessment of coronary bifurcations is limited by vessel foreshortening and overlap. In a previous

IVUS study, Oviedo et al. (51) reported the distribution of plaque at the LM bifurcation, and proposed an IVUS classification of plaque morphology which was compared with the commonly used Medina system. The authors concluded that there was no relation between the Medina angiographic classification and IVUS plaque distribution. Similarly to IVUS, imaging by CTCA goes beyond lumenography and enables the assessment of atherosclerotic lesions that are angiographically “silent”. In our investigation (Chapter 7), we propose a simple modification of the Medina classification to incorporate plaque severity, by adding an asterisk (*) as a superscript to the existing segments’ score for $\geq 70\%$ plaque burden; this CT-Medina classification scheme combining lumen stenosis and plaque severity is more informative than angiographic classification of bifurcation lesions and could potentially facilitate the decision-making on the treatment of these lesions.

As CTCA is becoming widely available and its value in detecting significant lumen narrowing has been robustly established, many patients are being brought into the cathlab based on the CTCA findings. Percutaneous treatment of coronary bifurcation lesions has been associated with worse acute and late outcomes due to higher restenosis and stent thrombosis rates (52-54). Comprehensive pre-interventional assessment of both lumen stenosis and plaque severity of a diseased coronary bifurcation may be important to better plan a percutaneous strategy. Although carina shift is suggested to be the predominant mechanism of side branch (SB) lumen loss after main vessel (MV) stent implantation, plaque shift from the MV also contributes to the aggravation of an SB ostial lesion and was more frequently observed in hemodynamically significant SB lesions (55,56). Therefore, we envision that a CT-based Medina classification of bifurcation lesions may assist the preparation for the bifurcation stent implantation, regarding for example the location of the stent or even the need for a second stent, whereas the prevailing technique is the provisional stenting. Especially the presence of 0* at the side branch ostium in a case of 1, 0, 0* classification, could herald acute SB occlusion after provisional stenting, which could necessitate a 2-stent strategy from the beginning or the use of dedicated bifurcation stent. Although novel, this classification was based on an analysis of a small number of patients, thus it must be considered work in progress. Larger studies with procedural and clinical outcomes are warranted to examine the value of the newly introduced CT-Medina classification.

CT coronary angiography for risk stratification of coronary atherosclerotic disease

The CTCA-derived SYNTAX Score: is it feasible and reproducible?

Our report (*Chapter 8*) investigates for the first time the feasibility of the MSCT SXscore and shows that it is comparable to the conventional ICA SXscore. For the purpose of this study, we reviewed all the definitions from the ICA SXscore and adapted them to the MSCT capabilities. Of note, in our study the absolute difference between MSCT and ICA SXscores per patient did not correlate with the Ca Score. Although it can be hypothesized that extreme calcification, which is making the assessment of the coronary lumen more difficult, is responsible for the overestimation of SXscore by MSCT, it appears that the presence of high amount of calcium does not account for the difference between the SXscore calculation with the 2 modalities. Not unexpectedly, the median Ca score in each MSCT SXscore tertile increased gradually and proportionally with the increase of the MSCT SXscore value; conversely, this was not the case with the ICA SXscore, as in the two lower tertiles, the median Ca score was similar. This finding suggests that the stratification based on the MSCT SXscore tertiles reflects better the overall burden of the disease.

It is important for a diagnostic tool to be easy to perform and to analyze, accessible and reproducible. Generally speaking, both SXscores share the first qualities, but the MSCT SXscore as investigated by our group appears to have better reproducibility considering historical data (57-61). The general correlation of MSCT SXscore values between the first and second rounds of analysis was high, and so was the intra-observer agreement of the MSCT SXscore tertiles (weighted kappa 0.80). The latter has been reported to be lower in all previous studies using conventional angiography (57,59-61), except for a study by Genereux et al. (58) reporting a kappa value of 0.88 for one of the reviewers. One important consideration is the fact that these reports have mean ICA SXcores ranging from 16.2 to 34.1 while our overall ICA SXscore was much lower (median 10.5, mean 13.05). We acknowledge that the extent and complexity of the disease may affect the reproducibility. Nevertheless, the ICA SXscores of the cases included in our study

are in the same range of values reported in the SIRTAX (SIRolimus-eluting stent compared with pacliTAXel-eluting stent for coronary revascularization) (62) and the LEADERS (Limus Eluted from A Durable versus ERodable Stent coating) (63) all-comers trials; to put our results in perspective, we envision that the MSCT SXscore could be used in the future in such populations since it has a better precision. Finally, it could be assumed that the MSCT SXscore is in part more reproducible than the ICA SXscore because the coronary bifurcations can be better visualized by MSCT, without the limitations of the vessel foreshortening and overlap that exist in conventional angiography. Indeed the reproducibility of the number of bifurcation/trifurcation lesions in MSCT SXscore is much better than the one reported in the studies using conventional angiography (3,26-29).

The CTCA-derived SYNTAX Score: where do we go from here?

The development of an online algorithm customized for the MSCT SXscore calculation (i.e. incorporating the Ca score values), as is currently available for the conventional SXscore, could be of great interest.

Furthermore, the “functional SYNTAX score” – a fractional flow reserve guided SYNTAX score – has been shown to improve the diagnostic accuracy of the SXscore (64). Recently, the feasibility of non-invasive fractional flow measurements has been demonstrated, by applying computational fluid dynamics to MSCT angiography (65); thus the application of this promising technology to the MSCT SXscore may improve its diagnostic accuracy and reproducibility.

In addition, the angiographic SYNTAX score is lacking the information related to clinical factors which are known to have prognostic value, such as a patients’ age, left ventricular ejection fraction and renal function (66). Integrating the aforementioned variables to the SYNTAX score resulted in the development of the Clinical SYNTAX score, which has shown improved predictive value for adverse clinical events after revascularization (62,67,68). Under this perspective, the ability of MSCT to comprehensively assess the heart can have great potential. Apart from the evaluation of the coronary vessels, MSCT can be used for the evaluation of the left ventricular ejection fraction, the valves and the ischemic myocardium; adding the information from all these

parameters may serve to add incremental value to the prognostic utility of the MSCT SXscore.

Conclusion

CT coronary angiography allows detection of coronary atherosclerosis, as well as characterization of different coronary plaque patterns. The accurate and reproducible assessment of atherosclerotic plaque noninvasively is paramount to monitor the progression of disease and the response to pharmacological therapy and quantitative measurements are more reliable when semiautomated software is used. Moreover, the ability of the technique to appreciate the whole coronary tree and the complex 3D geometry of coronary arteries can facilitate the decision-making on the treatment of coronary bifurcation lesions and the risk stratification of patients. The integration of information such as functional significance to the anatomic evaluation of atherosclerosis may serve to add incremental value to the prognostic utility of CTCA.

References

1. Hur J, Kim YJ, Lee HJ, et al. Quantification and characterization of obstructive coronary plaques using 64-slice computed tomography: a comparison with intravascular ultrasound. *J Comput Assist Tomogr* 2009;33:186-92.
2. Petranovic M, Soni A, Bezzera H, et al. Assessment of nonstenotic coronary lesions by 64-slice multidetector computed tomography in comparison to intravascular ultrasound: evaluation of nonculprit coronary lesions. *J Cardiovasc Comput Tomogr* 2009;3:24-31.
3. Sun J, Zhang Z, Lu B, et al. Identification and quantification of coronary atherosclerotic plaques: a comparison of 64-MDCT and intravascular ultrasound. *AJR Am J Roentgenol* 2008;190:748-54.
4. Voros S, Rinehart S, Qian Z, et al. Prospective validation of standardized, 3-dimensional, quantitative coronary computed tomographic plaque measurements using radiofrequency backscatter intravascular ultrasound as reference standard in intermediate coronary arterial lesions: results from the ATLANTA (assessment of tissue characteristics, lesion morphology, and hemodynamics by angiography with fractional flow reserve, intravascular ultrasound and virtual histology, and noninvasive computed tomography in atherosclerotic plaques) I study. *JACC Cardiovasc Interv* 2011;4:198-208.
5. Hong MK, Mintz GS, Lee CW, et al. A three-vessel virtual histology intravascular ultrasound analysis of frequency and distribution of thin-cap fibroatheromas in patients with acute coronary syndrome or stable angina pectoris. *Am J Cardiol* 2008;101:568-72.
6. Rodriguez-Granillo GA, Garcia-Garcia HM, Mc Fadden EP, et al. In vivo intravascular ultrasound-derived thin-cap fibroatheroma detection using ultrasound radiofrequency data analysis. *J Am Coll Cardiol* 2005;46:2038-42.
7. Wang JC, Normand SL, Mauri L, Kuntz RE. Coronary artery spatial distribution of acute myocardial infarction occlusions. *Circulation* 2004;110:278-84.
8. Achenbach S, Moselewski F, Ropers D, et al. Detection of calcified and noncalcified coronary atherosclerotic plaque by contrast-enhanced, submillimeter multidetector spiral computed tomography: a segment-based comparison with intravascular ultrasound. *Circulation* 2004;109:14-7.

9. Dey D, Schepis T, Marwan M, Slomka PJ, Berman DS, Achenbach S. Automated three-dimensional quantification of noncalcified coronary plaque from coronary CT angiography: comparison with intravascular US. *Radiology* 2010;257:516-22.
10. Leber AW, Becker A, Knez A, et al. Accuracy of 64-slice computed tomography to classify and quantify plaque volumes in the proximal coronary system: a comparative study using intravascular ultrasound. *J Am Coll Cardiol* 2006;47:672-7.
11. Otsuka M, Bruining N, Van Pelt NC, et al. Quantification of coronary plaque by 64-slice computed tomography: a comparison with quantitative intracoronary ultrasound. *Invest Radiol* 2008;43:314-21.
12. Schepis T, Marwan M, Pflederer T, et al. Quantification of non-calcified coronary atherosclerotic plaques with dual-source computed tomography: comparison with intravascular ultrasound. *Heart* 2010;96:610-5.
13. Ugolini P, Pressacco J, Lesperance J, et al. Evaluation of coronary atheroma by 64-slice multidetector computed tomography: Comparison with intravascular ultrasound and angiography. *Can J Cardiol* 2009;25:641-7.
14. Burgstahler C, Reimann A, Beck T, et al. Influence of a lipid-lowering therapy on calcified and noncalcified coronary plaques monitored by multislice detector computed tomography: results of the New Age II Pilot Study. *Invest Radiol* 2007;42:189-95.
15. Hoffmann H, Frieler K, Schlattmann P, Hamm B, Dewey M. Influence of statin treatment on coronary atherosclerosis visualised using multidetector computed tomography. *Eur Radiol* 2010;20:2824-33.
16. Inoue K, Motoyama S, Sarai M, et al. Serial coronary CT angiography-verified changes in plaque characteristics as an end point: evaluation of effect of statin intervention. *JACC Cardiovasc Imaging* 2010;3:691-8.
17. Lehman SJ, Schlett CL, Bamberg F, et al. Assessment of coronary plaque progression in coronary computed tomography angiography using a semiquantitative score. *JACC Cardiovasc Imaging* 2009;2:1262-70.
18. Schmid M, Achenbach S, Ropers D, et al. Assessment of changes in non-calcified atherosclerotic plaque volume in the left main and left anterior descending coronary arteries over time by 64-slice computed tomography. *Am J Cardiol* 2008;101:579-84.

19. Tardif JC, L'Allier P L, Ibrahim R, et al. Treatment with 5-lipoxygenase inhibitor VIA-2291 (Atreleuton) in patients with recent acute coronary syndrome. *Circ Cardiovasc Imaging* 2010;3:298-307.
20. Uehara M, Funabashi N, Mikami Y, Shiina Y, Nakamura K, Komuro I. Quantitative effect of atorvastatin on size and content of non-calcified plaques of coronary arteries 1 year after atorvastatin treatment by multislice computed tomography. *Int J Cardiol* 2008;130:269-75.
21. Motoyama S, Kondo T, Anno H, et al. Atherosclerotic plaque characterization by 0.5-mm-slice multislice computed tomographic imaging. *Circ J* 2007;71:363-6.
22. Motoyama S, Sarai M, Harigaya H, et al. Computed tomographic angiography characteristics of atherosclerotic plaques subsequently resulting in acute coronary syndrome. *J Am Coll Cardiol* 2009;54:49-57.
23. Nicholls SJ, Hsu A, Wolski K, et al. Intravascular ultrasound-derived measures of coronary atherosclerotic plaque burden and clinical outcome. *J Am Coll Cardiol* 2010;55:2399-407.
24. Stone GW, Maehara A, Lansky AJ, et al. A prospective natural-history study of coronary atherosclerosis. *N Engl J Med* 2011;364:226-35.
25. Hoffmann U, Moselewski F, Nieman K, et al. Noninvasive assessment of plaque morphology and composition in culprit and stable lesions in acute coronary syndrome and stable lesions in stable angina by multidetector computed tomography. *J Am Coll Cardiol* 2006;47:1655-62.
26. Glagov S, Weisenberg E, Zarins CK, Stankunavicius R, Kolettis GJ. Compensatory enlargement of human atherosclerotic coronary arteries. *N Engl J Med* 1987;316:1371-5.
27. Sipahi I, Tuzcu EM, Schoenhagen P, et al. Compensatory enlargement of human coronary arteries during progression of atherosclerosis is unrelated to atheroma burden: serial intravascular ultrasound observations from the REVERSAL trial. *Eur Heart J* 2006;27:1664-70.
28. Van Mieghem CA, Bruining N, Schaar JA, et al. Rationale and methods of the integrated biomarker and imaging study (IBIS): combining invasive and non-invasive imaging with biomarkers to detect subclinical atherosclerosis and assess coronary lesion biology. *Int J Cardiovasc Imaging* 2005;21:425-41.

29. Von Birgelen C, Hartmann M, Mintz GS, et al. Spectrum of remodeling behavior observed with serial long-term (≥ 12 months) follow-up intravascular ultrasound studies in left main coronary arteries. *Am J Cardiol* 2004;93:1107-13.
30. Miller JM, Rochitte CE, Dewey M, et al. Diagnostic performance of coronary angiography by 64-row CT. *N Engl J Med* 2008;359:2324-36.
31. Weustink AC, Mollet NR, Neefjes LA, et al. Diagnostic accuracy and clinical utility of noninvasive testing for coronary artery disease. *Ann Intern Med* 2010;152:630-9.
32. Virmani R, Kolodgie FD, Burke AP, Farb A, Schwartz SM. Lessons from sudden coronary death: a comprehensive morphological classification scheme for atherosclerotic lesions. *Arterioscler Thromb Vasc Biol* 2000;20:1262-75.
33. Leber AW, Knez A, Becker A, et al. Accuracy of multidetector spiral computed tomography in identifying and differentiating the composition of coronary atherosclerotic plaques: a comparative study with intracoronary ultrasound. *J Am Coll Cardiol* 2004;43:1241-7.
34. Schroeder S, Kopp AF, Baumbach A, et al. Noninvasive detection and evaluation of atherosclerotic coronary plaques with multislice computed tomography. *J Am Coll Cardiol* 2001;37:1430-5.
35. Markl M, Wegent F, Zech T, et al. In vivo wall shear stress distribution in the carotid artery: effect of bifurcation geometry, internal carotid artery stenosis, and recanalization therapy. *Circ Cardiovasc Imaging* 2010;3:647-55.
36. Moore JE, Jr., Timmins LH, Ladisa JF, Jr. Coronary artery bifurcation biomechanics and implications for interventional strategies. *Catheter Cardiovasc Interv* 2010;76:836-43.
37. Perktold K, Resch M, Florian H. Pulsatile non-Newtonian flow characteristics in a three-dimensional human carotid bifurcation model. *J Biomech Eng* 1991;113:464-75.
38. Friedman MH, Ding Z. Relation between the structural asymmetry of coronary branch vessels and the angle at their origin. *J Biomech* 1998;31:273-8.
39. Hildick-Smith D, Lassen JF, Albiero R, et al. Consensus from the 5th European Bifurcation Club meeting. *EuroIntervention* 2010;6:34-8.
40. Adriaenssens T, Byrne RA, Dibra A, et al. Culotte stenting technique in coronary bifurcation disease: angiographic follow-up using dedicated quantitative

- coronary angiographic analysis and 12-month clinical outcomes. *Eur Heart J* 2008;29:2868-76.
41. Collins N, Seidelin PH, Daly P, et al. Long-term outcomes after percutaneous coronary intervention of bifurcation narrowings. *Am J Cardiol* 2008;102:404-10.
 42. Dzavik V, Kharbanda R, Ivanov J, et al. Predictors of long-term outcome after crush stenting of coronary bifurcation lesions: importance of the bifurcation angle. *Am Heart J* 2006;152:762-9.
 43. Murasato Y. Impact of three-dimensional characteristics of the left main coronary artery bifurcation on outcome of crush stenting. *Catheter Cardiovasc Interv* 2007;69:248-56.
 44. Ormiston JA, Currie E, Webster MW, et al. Drug-eluting stents for coronary bifurcations: insights into the crush technique. *Catheter Cardiovasc Interv* 2004;63:332-6.
 45. Joner M, Finn AV, Farb A, et al. Pathology of drug-eluting stents in humans: delayed healing and late thrombotic risk. *J Am Coll Cardiol* 2006;48:193-202.
 46. Kawaguchi R, Oshima S, Jingu M, et al. Usefulness of virtual histology intravascular ultrasound to predict distal embolization for ST-segment elevation myocardial infarction. *J Am Coll Cardiol* 2007;50:1641-6.
 47. Nakazawa G, Yazdani SK, Finn AV, Vorpahl M, Kolodgie FD, Virmani R. Pathological findings at bifurcation lesions: the impact of flow distribution on atherosclerosis and arterial healing after stent implantation. *J Am Coll Cardiol* 2010;55:1679-87.
 48. Alfonso F, Macaya C, Goicolea J, et al. Intravascular ultrasound imaging of angiographically normal coronary segments in patients with coronary artery disease. *Am Heart J* 1994;127:536-44.
 49. Mintz GS, Painter JA, Pichard AD, et al. Atherosclerosis in angiographically "normal" coronary artery reference segments: an intravascular ultrasound study with clinical correlations. *J Am Coll Cardiol* 1995;25:1479-85.
 50. Nakamura Y, Takemori H, Shiraishi K, et al. Compensatory enlargement of angiographically normal coronary segments in patients with coronary artery disease. In vivo documentation using intravascular ultrasound. *Angiology* 1996;47:775-81.

51. Oviedo C, Maehara A, Mintz GS, et al. Intravascular ultrasound classification of plaque distribution in left main coronary artery bifurcations: where is the plaque really located? *Circ Cardiovasc Interv* 2010;3:105-12.
52. Colombo A, Moses JW, Morice MC, et al. Randomized study to evaluate sirolimus-eluting stents implanted at coronary bifurcation lesions. *Circulation* 2004;109:1244-9.
53. Ge L, Airolidi F, Iakovou I, et al. Clinical and angiographic outcome after implantation of drug-eluting stents in bifurcation lesions with the crush stent technique: importance of final kissing balloon post-dilation. *J Am Coll Cardiol* 2005;46:613-20.
54. Routledge HC, Lefevre T, Colombo A, et al. Three-year clinical outcome of percutaneous treatment of bifurcation lesions in multivessel coronary artery disease with the sirolimus-eluting stent: insights from the Arterial Revascularisation Therapies Study, part II (ARTS II). *EuroIntervention* 2009;5:190-6.
55. Kang SJ, Kim WJ, Lee JY, et al. Hemodynamic impact of changes in bifurcation geometry after single-stent cross-over technique assessed by intravascular ultrasound and fractional flow reserve. *Catheter Cardiovasc Interv* 2013.
56. Koo BK, Waseda K, Kang HJ, et al. Anatomic and functional evaluation of bifurcation lesions undergoing percutaneous coronary intervention. *Circ Cardiovasc Interv* 2010;3:113-9.
57. Garg S, Girasis C, Sarno G, et al. The SYNTAX score revisited: a reassessment of the SYNTAX score reproducibility. *Catheter Cardiovasc Interv* 2010;75:946-52.
58. Genereux P, Palmerini T, Caixeta A, et al. SYNTAX score reproducibility and variability between interventional cardiologists, core laboratory technicians, and quantitative coronary measurements. *Circ Cardiovasc Interv* 2011;4:553-61.
59. Serruys PW, Onuma Y, Garg S, et al. Assessment of the SYNTAX score in the Syntax study. *EuroIntervention* 2009;5:50-6.
60. Shiomi H, Tamura T, Niki S, et al. Inter- and intra-observer variability for assessment of the synergy between percutaneous coronary intervention with TAXUS and cardiac surgery (SYNTAX) score and association of the SYNTAX score with clinical outcome in patients undergoing unprotected left main stenting in the real world. *Circ J* 2011;75:1130-7.

61. Tanboga IH, Ekinici M, Isik T, Kurt M, Kaya A, Sevimli S. Reproducibility of syntax score: from core lab to real world. *J Interv Cardiol* 2011;24:302-6.
62. Girasis C, Garg S, Raber L, et al. SYNTAX score and Clinical SYNTAX score as predictors of very long-term clinical outcomes in patients undergoing percutaneous coronary interventions: a substudy of SIRolimus-eluting stent compared with pacliTAXel-eluting stent for coronary revascularization (SIRTAX) trial. *Eur Heart J* 2011;32:3115-27.
63. Wykrzykowska JJ, Garg S, Girasis C, et al. Value of the SYNTAX score for risk assessment in the all-comers population of the randomized multicenter LEADERS (Limus Eluted from A Durable versus ERodable Stent coating) trial. *J Am Coll Cardiol* 2010;56:272-7.
64. Nam CW, Mangiacapra F, Entjes R, et al. Functional SYNTAX score for risk assessment in multivessel coronary artery disease. *J Am Coll Cardiol*;58:1211-8.
65. Koo BK, Erglis A, Doh JH, et al. Diagnosis of ischemia-causing coronary stenoses by noninvasive fractional flow reserve computed from coronary computed tomographic angiograms. Results from the prospective multicenter DISCOVER-FLOW (Diagnosis of Ischemia-Causing Stenoses Obtained Via Noninvasive Fractional Flow Reserve) study. *J Am Coll Cardiol*;58:1989-97.
66. Ranucci M, Castelvechio S, Menicanti L, Frigiola A, Pelissero G. Risk of assessing mortality risk in elective cardiac operations: age, creatinine, ejection fraction, and the law of parsimony. *Circulation* 2009;119:3053-61.
67. Capodanno D, Caggiagi A, Miano M, et al. Global risk classification and clinical SYNTAX (synergy between percutaneous coronary intervention with TAXUS and cardiac surgery) score in patients undergoing percutaneous or surgical left main revascularization. *JACC Cardiovasc Interv* 2011;4:287-97.
68. Garg S, Sarno G, Garcia-Garcia HM, et al. A new tool for the risk stratification of patients with complex coronary artery disease: the Clinical SYNTAX Score. *Circ Cardiovasc Interv* 2010;3:317-26.

PhD Portfolio

Portfolio of awarded ECTS points

Name PhD student: Stella-Lida Papadopoulou

Erasmus MC department: Radiology and Cardiology

Research school: COEUR, Erasmus MC

PhD period: 2009 – 2014

Promotors: Prof. Dr. F. Zijlstra, Prof. Dr. G.P. Krestin

Specific courses offered by COEUR:	Date	ECTS
Pathophysiology of ischemic heart disease	February 2012	1.5
Clinical cardiovascular epidemiology	March 2010	1.5
Congenital heart disease	February 2011	1.5

Erasmus MC courses	Date	ECTS
1. Introduction to clinical research	19-23 January 2009	0.9
2. Biostatistics for clinicians	19-23 January 2009	1.0
3. Photoshop CS3 Workshop for PhD students and other researchers	12 & 14 April 2010	0.25
4. Classical methods for Data Analysis	October 2010	5.7

Other courses followed:	Date and location:	ECTS
Cardiac Cross-Sectional Imaging European School of Radiology GALEN Advanced Course	November 6-7, 2009 Rotterdam, NL	0.6
Radiation Protection Course 5A Stralingsbeschermingsdienst & Opleidingscentrum Erasmus MC	May 2010, Rotterdam, NL	0.6
Advanced Cardiac Life Support (ACLS) course	April 15-17, 2011, Athens, Greece	0.9
ECG & Pharmacology Course Hellenic Society of CPR and American Heart Association	October 30, 2013, Athens, Greece	0.3
ECG & Pharmacology Instructors' Course Hellenic Society of CPR	March 6, 2014, Athens, Greece	0.3

COEUR Research seminars:	Date	ECTS
1. Surgical and percutaneous aortic valve implantation; indications, techniques and follow-up	January 2009	0.4
2. New developments in percutaneous revascularisation	April 2009	0.4
3. Neo-angiogenesis as a treatment of myocardial ischemia	May 2009	0.4
4. Clinical aspects of Heart Failure research	October 2009	0.4
5. Coarctation of the Aorta	November 2010	0.4
6. Imaging of Atherosclerosis	December 2010	0.4
7. Detection of early atherosclerosis	March 2011	0.4
8. Imaging Carotid Arteries: structure and function	December 2011	0.4
9. Endothelin in the Picture	January 2012	0.4
10. Heart Valve Implantation	February 2012	0.4

Lectures/conference presentations:	Date	ECTS
CT detection and quantification of coronary atherosclerosis (COEUR Research Seminar "Detection of early atherosclerosis")	March 2011	0.1
Detection and quantification of coronary atherosclerotic plaque by 64-slice multidetector CT: a systematic head-to-head comparison with Intravascular Ultrasound (RSNA meeting 2011)	November 2011	0.1
Assessment of Temporal Changes in Coronary Atherosclerosis using Multislice Computed Tomography (European Congress of Radiology 2012)	March 2012	0.1
Electrocardiography: Atrioventricular block (ECG & Pharmacology Course, Hellenic Society of CPR and American Heart Association)	April 2014	0.1
Hemodynamic disturbances in STEMI (Educational Programme of department of Cardiology, General Hospital of Katerini, Greece)	February 2016	0.1
Study of the mean platelet volume in hypertensive patients with STEMI (31 st Northern Greece Medical Congress)	April 2016	0.1

Symposia and congresses (0.3 ECTS points/day):	Date, location and number of days:	ECTS
Cardiology and Vascular Medicine – ESC Update and Perspective	11-13/5/2009, Rotterdam (3)	0.9

Translating Coronary Physiology and Biophysics to Clinical Applications	18-19/2/2010, Amsterdam (2)	0.6
5th international symposium on Biomechanics in Vascular Biology and Cardiovascular Disease	15-16/4/2010, Rotterdam (2)	0.6
Acute Myocardial Infarction: the next decade	17/12/2010, Rotterdam (1)	0.3
Cardiology and Vascular Medicine 2011 - An ESC UPDATE programme in Cardiology	23-25/5/2011, Rotterdam (3)	0.9
Radiological Society of North America (RSNA) Annual Meeting 2011	27 Nov - 2 Dec 2011, Chicago, USA (6)	1.8
ESR - European Congress of Radiology 2012	1-5/3/2012, Vienna, Austria (5)	1.5
Patrick Serruys Symposium	19 th May 2012, Rotterdam (1)	0.3
3 rd Educational Seminar on Thrombosis and Antithrombotic Therapy	8-9/2/2013, Athens, Greece (2)	0.6
Symposium on Advanced Imaging in TAVI	15/2/2014, Rome, Italy (1)	0.3
2 nd European Spring School on Pulmonary Circulation and Right Ventricular Function (Center for Thrombosis and Hemostasis Mainz & LUMC)	5-9/5/2015, Sithonia, Greece (5)	1.5
36 th International Congress of Cardiology (Hellenic Society of Cardiology)	29-31/10/2015, Thessaloniki, Greece (3)	0.9
Arrhythmias Update 2016	8-9/4/2016, Thessaloniki, Greece (2 days)	0.6

Teaching	Date, location and number of days:	ECTS
Supervision of medical student on research project	July - October 2010 (4 months)	1.0

Total		31.45
--------------	--	--------------

List of publications

Articles in peer-reviewed journals

1. Sakellarios A, Bourantas CV, **Papadopoulou SL**, Tsirka Z, de Vries T, Kitslaar PH, Girasis C, Naka KK, Fotiadis DI, Veldhof S, Stone GW, Reiber JH, Michalis LK, Serruys PW, de Feyter PJ, Garcia-Garcia HM. Prediction of atherosclerotic disease progression using LDL transport modelling: a serial computed tomographic coronary angiographic study.
Eur Heart J Cardiovasc Imaging. 2016 Mar 16 [Epub ahead of print]
2. Bourantas CV, **Papadopoulou SL**, Serruys PW, Sakellarios A, Kitslaar PH, Bizopoulos P, Girasis C, Zhang YJ, de Vries T, Boersma E, Papafaklis MI, Naka KK, Fotiadis DI, Stone GW, Reiber JH, Michalis LK, de Feyter PJ, Garcia-Garcia HM. Noninvasive Prediction of Atherosclerotic Progression: The PROSPECT-MSCT Study.
JACC Cardiovasc Imaging. 2015 Sep 2. [Epub ahead of print]
3. **Papadopoulou SL**, Girasis C, Gijssen FJ, Rossi A, Ottema J, van der Giessen AG, Schuurbiers JC, Garcia-Garcia HM, de Feyter PJ, Wentzel JJ. A CT-based Medina classification in coronary bifurcations: does the lumen assessment provide sufficient information?
Catheter Cardiovasc Interv. 2014 Sep 1;84(3):445-52.
4. Rossi A, **Papadopoulou SL**, Pugliese F, Russo B, Dharampall AS, Dedic A, Kitslaar PH, Broersen A, Meijboom WB, van Geuns RJ, Wragg A, Ligthart J, Schultz C, Petersen SE, Nieman K, Krestin GP, de Feyter PJ. Quantitative computed tomographic coronary angiography: does it predict functionally significant coronary stenoses?
Circulation Cardiovasc Imaging. 2014 Jan;7(1):43-51.

5. Kirişli HA, Schaap M, Metz CT, Dharampal AS, Meijboom WB, **Papadopoulou SL**, Dedic A, Nieman K, de Graaf MA, Meijs MF, Cramer MJ, Broersen A, Cetin S, Eslami A, Flórez-Valencia L, Lor KL, Matuszewski B, Melki I, Mohr B, Oksüz I, Shahzad R, Wang C, Kitslaar PH, Unal G, Katouzian A, Örkisz M, Chen CM, Precioso F, Najman L, Masood S, Ünay D, van Vliet L, Moreno R, Goldenberg R, Vuçini E, Krestin GP, Niessen WJ, van Walsum T. Standardized evaluation framework for evaluating coronary artery stenosis detection, stenosis quantification and lumen segmentation algorithms in computed tomography angiography. *Med Image Anal.* 2013 Dec;17(8):859-76.
6. Dharampal AS, **Papadopoulou SL**, Rossi A, Meijboom WB, Weustink A, Dijkshoorn M, Nieman K, Boersma EH, de Feijter PJ, Krestin GP. Diagnostic performance of computed tomography coronary angiography to detect and exclude left main and/or three-vessel coronary artery disease. *Eur Radiol.* 2013 Nov;23(11):2934-43.
7. Dharampal AS, Rossi A, Dedic A, Cademartiri F, **Papadopoulou SL**, Weustink AC, Ferket BS, Boersma E, Meijboom WB, Galema TW, Nieman K, de Feyter PJ, Krestin GP. Restriction of the referral of patients with stable angina for CT coronary angiography by clinical evaluation and calcium score: impact on clinical decision making. *Eur Radiol.* 2013 Oct;23(10):2676-86.
8. **Papadopoulou SL**, Girasis C, Dharampal A, Farooq V, Onuma Y, Rossi A, Morel MA, Krestin GP, Serruys PW, de Feyter PJ, Garcia Garcia HM. CT-SYNTAX score: a feasibility and reproducibility Study. *JACC Cardiovasc Imaging.* 2013 Mar;6(3):413-5.

9. **Papadopoulou SL**, Garcia-Garcia HM, Rossi A, Girasis C, Dharampal AS, Kitslaar PH, Krestin GP, de Feyter PJ. Reproducibility of computed tomography angiography data analysis using semiautomated plaque quantification software: implications for the design of longitudinal studies.
Int J Cardiovasc Imaging. 2013 Jun;29(5):1095-104.
10. Neefjes LA, Rossi A, Genders TS, Nieman K, **Papadopoulou SL**, Dharampal AS, Schultz CJ, Weustink AC, Dijkshoorn ML, Ten Kate GJ, Dedic A, van Straten M, Cademartiri F, Hunink MG, Krestin GP, de Feyter PJ, Mollet NR. Diagnostic accuracy of 128-slice dual-source CT coronary angiography: a randomized comparison of different acquisition protocols.
Eur Radiol. 2013 Mar;23(3):614-22.
11. Girasis C, Vassilikos V, Efthimiadis GK, **Papadopoulou SL**, Dakos G, Dalamaga EG, Chouvarda I, Giannakoulas G, Kamperidis V, Paraskevaidis S, Maglaveras N, Karvounis HI, Parcharidis GE, Styliadis IH. Patients with hypertrophic cardiomyopathy at risk for paroxysmal atrial fibrillation: advanced echocardiographic evaluation of the left atrium combined with non-invasive P-wave analysis.
Eur Heart J Cardiovasc Imaging. 2013 May;14(5):425-34.
12. Dharampal AS, **Papadopoulou SL**, Rossi A, Weustink AC, Mollet NR, Meijboom WB, Neefjes LA, Nieman K, Boersma E, de Feijter PJ, Krestin GP. Computed tomography coronary angiography accuracy in women and men at low to intermediate risk of coronary artery disease.
Eur Radiol. 2012 Nov;22(11):2415-23.

13. Serruys PW, Girasis C, **Papadopoulou SL**, Onuma Y. Non-invasive fractional flow reserve: scientific basis, methods and perspectives.
EuroIntervention. 2012 Aug;8(4):511-9.
14. **S.L. Papadopoulou**, S. Brugaletta, H.M. Garcia-Garcia, A. Rossi, C. Girasis, A. S. Dharampal, L. A. Neefjes, J. Ligthart, K. Nieman, G.P. Krestin, P.W. Serruys, P. J. de Feyter. Assessment of Atherosclerotic Plaques at Coronary Bifurcations with Multidetector Computed Tomography Angiography and Intravascular Ultrasound –Virtual Histology.
Eur Heart J Cardiovasc Imaging. 2012 Aug;13(8):635-42.
15. **S-L Papadopoulou**, L.A. Neefjes, H.M. Garcia-Garcia, W-J Flu, A. Rossi, A.S. Dharampal, P.H. Kitslaar, N.R. Mollet, S. Veldhof, K. Nieman, G.W. Stone, P.W. Serruys, G.P. Krestin, P.J. de Feyter. Natural History of Coronary Atherosclerosis by Multislice Computed Tomography: the PROSPECT study.
JACC Cardiovasc Imaging. 2012 Mar;5(3 Suppl):S28-37.
16. LA Neefjes, AS Dharampal, A Rossi, K Nieman, AC Weustink, ML Dijkshoorn, G-J R ten Kate, A Dedic, **SL Papadopoulou**, M van Straten, F Cademartiri, GP Krestin, PJ de Feyter, NR Mollet. Image Quality and Radiation Exposure Using Different Low-Dose Scan Protocols in Dual-Source CT Coronary Angiography: Randomized Study.
Radiology. 2011 Dec;261(3):779-86.

17. **Papadopoulou SL**, Neefjes LA, Schaap M, Li HL, Capuano E, van der Giessen AG, Schuurbiens JC, Gijzen FJ, Dharampal AS, Nieman K, van Geuns RJ, Mollet NR, de Feyter PJ. Detection and quantification of coronary atherosclerotic plaque by 64-slice multidetector CT: A systematic head-to-head comparison with intravascular ultrasound.
Atherosclerosis 2011; 219(1):163-170.
18. Schultz C, Rossi A, Van Mieghem N, Van Der Boon R, **Papadopoulou S-L**, van Domburg R, Moelker A, Mollet N, Krestin G, van Geuns R-J, Nieman K, de Feyter P, Serruys PW, de Jaegere P. Aortic annulus dimensions and leaflet calcification from contrast MSCT predict the need for balloon post-dilatation after TAVI with the Medtronic CoreValve prosthesis.
EuroIntervention. 2011 Sep;7(5):564-72.
19. Schultz CJ, **Papadopoulou SL**, Moelker A, Nuis RJ, ten Kate GJR, Mollet NR, Geleijnse ML, de Feyter P, de Jaegere P, Serruys PW. Transaortic flow velocity from dual source MDCT for the diagnosis of aortic stenosis severity.
Catheter Cardiovasc Interv. Jul 1;78(1):127-35. (2011)
20. Dharampal AS, Rossi A, **Papadopoulou SL**, Weustink AC, Boersma E, Nieman K, Chen CH, Dijkshoorn M, Mollet NR, Krestin GP, de Feyter PJ. Is there a difference in the diagnostic accuracy of computed tomography coronary angiography between women and men?
Coron Artery Dis. 2011;22(6):421-7.
21. H. A. Kirisli, M. Schaap, S. Klein, **S.L. Papadopoulou**, M. Bonardi, C. H. Chen, A.C. Weustink, N.R. Mollet, E.J. Vonken, R.J. van der Geest, T. van Walsum, W.J. Niessen. Evaluation of a multi-atlas based method for

segmentation of cardiac CTA data: a large-scale, multicenter, and multivendor study.

Med Phys. Dec;37(12):6279-91. (2010)

22. **Papadopoulou SL**, Girasis C. Invasive functional testing.

EuroIntervention. May;6 Suppl G:79-86. Review (2010)

Oral and poster presentations at international meetings

1. A. Rossi, F. Pugliese, **SL Papadopoulou**, B. Russo, AS Dharampal, P. Kitslar, RJ Van Geuns, SE Petersen, PJ De Feyter, Gabriel P Krestin. Quantitative CT Coronary Angiography: Does It Predict Functionally Significant Coronary Lesions?

Presented at Radiological Society of North America (RSNA) Annual Meeting 2013, Chicago, USA

2. **S-L Papadopoulou**, L.A. Neefjes, A. Rossi, P.H. Kitslaar, P.J. de Feyter, G.P. Krestin. Assessment of Temporal Changes in Coronary Atherosclerosis using Multislice Computed Tomography.

Presented at European congress of Radiology 2012, Vienna, Austria (Poster)

3. **S-L Papadopoulou**, S Brugaletta, HM Garcia-Garcia, PJ de Feyter, PW Serruys. Assessment of Atherosclerosis at Coronary Bifurcations with Multislice Computed Tomography and Intravascular Ultrasound–Virtual Histology.

Presented at Transcatheter Cardiovascular Therapeutics 2011, San Francisco, USA. JACC Volume 58, Issue 20, Supplement, Pages B176

4. C.J. Schultz, **S.L. Papadopoulou**, A. Moelker, A. Tzikas, R.J. Nuis, G.J.R. Ten Kate, M.L. Geleijnse, P. De Feyter, P.P.T. De Jaegere, P.W. Serruys. Transaortic flow velocity can be calculated from dual source MDCT for diagnosis of aortic stenosis. Proof of concept.

Presented at ESC 2011. European Heart Journal (2011) 32 (Abstract Supplement), 765

5. A.S. Dharampal, A.C. Weustink, A. Rossi, L.A.E. Neefjes, **S.L. Papadopoulou**, C. Chen, N.R.A. Mollet, E.H. Boersma, G.P. Krestin, P.J. De Feyter. Diagnostic accuracy of multi slice CT coronary angiography in males and females for the detection of obstructive coronary artery disease.

Presented at ESC 2011. European Heart Journal (2011) 13 (Supplement A) A44

6. **SL Papadopoulou**, LA Neefjes, M Schaap, H Li, GP Krestin, NR Mollet Detection and quantification of coronary atherosclerotic plaque by 64-slice multidetector CT: a systematic head-to-head comparison with Intravascular Ultrasound.

Presented at Radiological Society of North America (RSNA) Annual Meeting 2011, Chicago, USA

7. A Rossi, **SL Papadopoulou**, LA Neefjes, PJ De Feyter, GP Krestin, NR Mollet. Myocardial Perfusion Imaging Using Dual Source Computed Tomography

Presented at Radiological Society of North America (RSNA) Annual Meeting 2009, Chicago, USA (Poster)

Acknowledgements





I thought writing this part would be simple, but it is actually difficult to put 3.5 years of one's life down on a couple of pages. Looking back at these years, they were all about hard work, meeting wonderful people, learning new things, getting enthusiastic (often), getting frustrated (more often!), but most of all, they were about becoming a stronger person and a better researcher.

At the end of this fascinating journey, the time has come to express my gratitude to all the people who contributed to this thesis and affected my life in Rotterdam.

Dear Professor de Feyter, beste Pim, I am really grateful that I had the opportunity to meet you. You are a top researcher, a great teacher, and most importantly a person to look up to. Your ability to look at a research project in a critical way would sometimes make my life difficult, but it would always result in a better project. I learned from you how to write a paper and most importantly, how to appreciate good quality research: beauty is in simplicity.

Dear Professor Krestin, I would like to thank you for being my promoter and for the great privilege to work in your department, one of the best in Europe and worldwide. You gave us the opportunity to have access to leading-edge technology and to be able to present our work in high-profile international congresses; these should be never taken for granted!

Dear Professor Zijlstra, I would like to thank you for being my promoter. It is really a great honor for me; you are a leader with true impact in the field of cardiovascular medicine in Europe.

Dear Hector, my co-promoter, I dare to say that all this effort would not have been successful without you. Your expertise on intravascular imaging and your practical mind made our collaboration the most fruitful period for me in Rotterdam; it was the "glue" between invasive and non-invasive imaging. There were lots of brainstorming and research ideas: some of them blossomed, others never came to reality, but that is how research (and life) is. It was great meeting also your family; I wish you all the best!

Dear Professor Serruys, I would like to thank you for the opportunity to work with you, a world-famous cardiologist. Even though I was not under your direct supervision, you were

always willing to read a manuscript and give your valuable feedback. You have a keen eye for the details, which can really make the difference for a paper.

I would also like to thank all the committee members for taking the time to read and evaluate my manuscript: Professor Reiber, Professor Prokop, Professor Niessen and Dr. Nieman. Dear Koen, thank you for all your help and your valuable feedback. Good luck with your new life in the USA!

Dear Alexia, my dear friend, I cannot find the words to thank you: you were like family to me during my stay in the Netherlands. You are one of the most hard-working, talented and kind persons I have met in my life - you should never forget that. I am honored that you are my paranymph. I am looking forward to seeing you again in Italy or Greece!

Dear Anoeshka, it was really great meeting you and working with you! I will always remember our trip to Chicago for RSNA 2011: you were a great companion and you guided me through the city - the pictures we took are really wonderful! I also enjoyed your cooking and I hope you will have success and happiness in your life.

Dear Tirza, it was really nice knowing you! You gave me one of my favorite moments in the Netherlands, the Sinterklaas dinner in your house: it was a wonderful evening, with a lot of fun and the opportunity to appreciate Dutch culture!

Dear Lisan, dear Admir, dear Gert-Jan: it was a pleasure to work with you in the Cardiac CT imaging group. We didn't share only the same office, but also the same concerns and troubles as young researchers. You showed me the Dutch culture and I still remember fondly our borrels after work!

I would also like to thank all the people I met in the radiology department: Marcel Dijkshoorn, Ronald Booij and Marcel van Straten, who were always available to answer our silly questions. I would like to make a special mention for Mohamed and Vini, who were there whenever I needed them. I would also like to thank Linda Everse for her assistance and Ton for the last-minute printing of posters! I am sorry if I am forgetting someone.

All the people from Cardialysis and cardiology research fellows: Marie-Angele, Hanny, Salvatore, Yoshi, Roberto, Carl, Michael and so many others that I can't remember! Thank you for your friendship and our great international dinners. To our Greek friends Chris & Thekla and Dimitris & Roula: I will always treasure the time we spent together, it made me feel a bit more like home.

Special thanks to my professors' secretaries: Elles Schaap and Annelise Pires Ferreira. Your assistance to organize the final steps of the PhD process from abroad was priceless. Thank you so much!

Finally, I would like to dedicate this thesis to my family.

To my husband Chris: you are my beloved partner and companion in life, you inspired me to try harder, overcome the difficulties and never give up. Living together in the Netherlands was a life-changing experience that I think we will cherish in the years to come.

To my parents, who have always valued education as the highest quality and gave me the opportunity to become the person I am. To my father, my sister and Ioanna, who have supported me in every possible way. And to my mother, who may not be here with me, but she is always in my heart.

«Σα βγεις στον πηγαιμό για την Ιθάκη, να εύχεται νάναι μακρύς ο δρόμος, γεμάτος περιπέτειες, γεμάτος γνώσεις.» (Κ.Π. Καβάφης, *Ιθάκη*)

“As you set out for Ithaca hope the voyage is a long one, full of adventure, full of discovery.”
(K.P. Kavafis, *Ithaca*)

About the author

Curriculum Vitae

Stella-Lida (Elina) Papadopoulou was born in 1980 in Thessaloniki, Greece. She started Medical School in 1999 at the Aristotle University of Thessaloniki. During her studies, she was involved in several public health and medical education projects of the International Federation of Medical Students' Associations (IFMSA). She was elected President of the Hellenic Medical Students' International Committee (HelMSIC) 2002-03 and IFMSA Regional Coordinator for Europe 2003-04. In 2004 she joined the research team of the Cardiovascular Engineering and Atherosclerosis Laboratory (supervisor: Prof. Dr. G. Giannoglou) at the AHEPA University hospital in Thessaloniki and she participated in several clinical and cardiovascular imaging projects. In 2007 she obtained her medical degree. In January 2009, she started a research fellowship on Cardiac CT Imaging at the Erasmus Medical Center in Rotterdam under the supervision of Professor Pim de Feyter (department of Interventional Cardiology and Radiology), Professor Gabriel Krestin (chairman of the department of Radiology) and Professor Felix Zijlstra (chairman of the department of Cardiology). Her research work in the field of imaging of atherosclerosis with CT coronary angiography resulted in this PhD thesis. Currently, she is working as a cardiology resident at General Hospital of Katerini (Greece), after completing 2-year internal medicine training at the AHEPA University hospital in Thessaloniki.

